OBSERVATION AND MODELLING OF URBAN DEW

By

Katrina Richards

B.Sc. University of Otago, 1989

M.Sc. (Hons.) University of Otago, 1991

A THESIS SUBMITTED IN PARTIAL FULFILLMENT

OF THE REQUIREMENTS FOR THE DEGREE OF

DOCTOR OF PHILOSOPHY

in

THE FACULTY OF GRADUATE STUDIES

DEPARTMENT OF GEOGRAPHY

We accept this thesis as conforming

to the required standard

THE UNIVERSITY OF BRITISH COLUMBIA

March 1999

© Katrina Richards, 1999

In presenting this thesis in partial fulfilment of the requirements for an advanced degree at the University of British Columbia, I agree that the Library shall make it freely available for reference and study. I further agree that permission for extensive copying of this thesis for scholarly purposes may be granted by the head of my department or by his or her representatives. It is understood that copying or publication of this thesis for financial gain shall not be allowed without my written permission.

Department of GEOGRAPHY

The University of British Columbia
Vancouver, Canada

Date 26 March 1999

Abstract

Despite its relevance to many aspects of urban climate and to several practical questions, urban dew has largely been ignored. Here, simple observations, an out-of-doors scale model, and numerical simulation are used to investigate patterns of dewfall and surface moisture (dew + guttation) in urban environments. Observations and modelling were undertaken in Vancouver, B.C., primarily during the summers of 1993 and 1996.

Surveys at several scales (0.02–25 km) show that the main controls on dew are weather, location and site configuration (geometry and surface materials). Weather effects are discussed using an empirical factor, Φ_w. Maximum dew accumulation (up to ~0.2 mm per night) is seen on nights with moist air and high Φ_w, i.e., cloudless conditions with light winds. Favoured sites are those with high Ψ_{sky} and surfaces which cool rapidly after sunset, e.g., grass and well insulated roofs.

A 1/8-scale model is designed, constructed, and run at an out-of-doors site to study dew patterns in an urban residential landscape which consists of house lots, a street and an open grassed park. The Internal Thermal Mass (ITM) approach is used to scale the thermal inertia of buildings. The model is validated using data from full-scale sites in Vancouver. Patterns in the model agree with those seen at the full-scale, i.e., dew distribution is governed by weather, site geometry and substrate conditions. Correlation is shown between Ψ_{sky} and surface moisture accumulation.

The feasibility of using a numerical model to simulate urban dew is investigated using a modified version of a rural dew model. Results for simple isolated surfaces—a deciduous tree leaf and an asphalt shingle roof—show promise, especially for built surfaces.

Table of contents

Abstract ii

List of Tables vii

List of Figures x

List of symbols and abbreviations xix

Acknowledgements xxvi

PART I CONTEXT **1**

Chapter 1: Introduction **1**

1.1 Rationale 1
1.2 Theory 3
1.2.1 Definitions 3
1.2.2 Scales and systems of interest 6
1.2.3 Processes and balances 10
1.2.4 Climatology of dew 17
1.3 Thesis outline 19
1.3.1 Research objectives 19
1.3.2 Approaches 21

Chapter 2: Literature review **23**

2.1 Introduction 23
2.2 Measurement of surface wetness and dew 25
2.2.1 Methods to measure dew or surface wetness 27
2.2.2 Methods to measure dewfall 30
2.2.3 Implementation of measurement methods 32
2.3 Dew as a climatic phenomenon 33
2.3.1 Controls on the distribution of dew 33
2.3.2 Dew and plants 39
2.4 Urban environments and dew 41
2.4.1 Urban temperature and wind fields 41
2.4.2 Urban humidity 44
2.4.3 Urban dew 49
2.4.4 Urban dew and atmospheric pollutants 57
2.5 Modelling of dew 59
2.5.1 Scale modelling 60
2.5.2 Numerical modelling of dew 63
2.6 Potential topics of study 67

PART II OBSERVATION **70**

Chapter 3: Spatial and temporal surveys in Vancouver **70**

3.1 Context 70
3.1.2 Objectives 73
3.1.3 Implementation 74
3.2 Urban-rural differences 75
3.2.1 Sites and seasons 75
3.2.2 Data collection and analysis 79
3.2.3 Results 86
3.3 Urban spatial and temporal variations 112
3.3.1 Sites and seasons 112
3.3.2 Data collection and analysis 115
3.3.3 Results 118
3.4 Summary 136

PART III MODELLING **138**

Chapter 4: Physical modelling of urban dew **138**

4.1 Context 138
4.2 The modelling programme 142
4.2.1 Objectives 142
4.2.2 Scaling considerations 143
4.3 Scaling of the physical domain 145
4.3.1 Spatial dimensions 145
4.3.2 Temporal period 145
4.3.3 Temperature fields 146
4.3.4 Environmental gradients 146
4.4 Scaling of physical processes 149
4.4.1 Radiation 149
4.4.2 Convection 150
4.4.3 Combined conduction-convection 153
4.5 Scaling processes of dew formation in real time 156
4.6 The Internal Thermal Mass Approach (ITM) 161
4.6.1 Theory 161
4.6.2 Practical considerations 165

Chapter 5: A scale model to study urban dew **170**

5.1 Scaling considerations 170
5.1.1 Similitude 170
5.1.2 Assumptions 173
5.2 The model 176
5.2.1 Sites and operation 176
5.2.2 Construction 179
5.2.3 Operational considerations 183

5.3 Data collection and analysis..... 184
5.3.1 Surface moisture..... 186
5.3.2 Surface temperature..... 192
5.3.3 Ambient conditions..... 193
5.4 Validation..... 194
5.4.1 Sites..... 195
5.4.2 Data collection and analysis..... 195

Chapter 6: Validation and results of the scale model..... 201

6.1 Overview..... 201
6.2 Validation..... 202
6.2.1 Physical contrasts..... 202
6.2.2 Model: full-scale comparisons..... 206
6.3 Results of the scale model..... 227
6.3.1 Surface temperature in the model..... 228
6.3.2 Surface moisture and dewfall in the model..... 235
6.4 Summary..... 256

Chapter 7: Numerical modelling of urban dewfall..... 258

7.1 Context..... 258
7.2 Objectives..... 258
7.3 An urban dewfall model 259
7.3.1 Context 259
7.3.2 Theory and structure..... 261
7.3.3 Assumptions..... 270
7.4 Implementation..... 271
7.4.1 Overview..... 271
7.4.2 Input data..... 274
7.4.3 Data to validate the model..... 275
7.5 Results..... 276
7.5.1 Energy balances..... 277
7.5.2 Predicted surface temperature..... 278
7.5.3 Simulation of dewfall for an asphalt shingle roof... 280
7.5.4 Simulation of dewfall for a Japanese maple leaf... 285
7.6 Summary..... 285

PART IV CONCLUSION..... 289

Chapter 8: A measurement protocol and conclusions..... 289

8.1 Summary..... 289
8.2 A protocol for measuring urban surface wetness..... 289
8.3 Conclusions..... 291
8.4 Suggestions for future research..... 293

REFERENCES **294**

APPENDICES **310**

Appendix A1: Common definitions and derivations **310**

A1.1 Converting latent heat flux to an equivalent depth water.. 310
A1.2 Corrections to mobile survey data 310
A1.3 Method of blotting 312
A1.4 Humidity relations 313
A1.5 Statistics of comparison 314
A1.6 Estimating sky view factor using site geometry 315
A1.7 Ratio of wind speed at two heights 317

Appendix A2: Derivations in the numerical model **318**

A2.1 Derivation of the sensible heat flux 318
A2.2 Derivation of the latent heat flux 318
A2.3 Estimating surface temperature 320
A2.4 Estimating Γ 324
A2.5 Statistics of model performance 324

Appendix A3: Dew and the Fine Arts **325**

A3.1 Illustrative examples of dew in art and literature 325

List of Tables

2.1 Some implications of the presence of dew..... 24

2.2 Methods to measure or estimate dew or surface moisture status [A = primarily to assess amount, and B = duration of surface wetness].. 26

2.3 Examples of observational studies of dew which focus on climate or weather controls [A = primarily temporal, and B = primarily spatial]..... 34

2.4 Examples of observational studies of dew which focus on plant-soil atmosphere relationships..... 40

2.5 Observational studies of urban humidity which provide data on the absolute moisture content of air. Results from urban-rural comparisons contained in these studies are summarised using: SDD = warm season (summer) daytime urban deficit; SNX = warm season (summer) nighttime urban excess; WDX = cold season (winter) daytime urban excess; WNX = cold season (winter) nighttime urban excess; NX = nighttime excess; and D = deficit..... 45

2.6 Hypothesised causes for patterns of humidity observed in the urban canopy layer of mid-latitude cities..... 46

2.7 Reasons hypothesised in the literature for reduced urban dew..... 51

2.8 Topics of research and summary of results relevant to dew and atmospheric pollutants..... 58

2.9 Examples of hardware models of cities or buildings, or dew deposition on vegetation..... 61

2.10 Examples of numerical models to simulate dew..... 64

3.1 Instruments and methods used to collect data for studies at the meso-scale..... 80

3.2 Summary of statistical indices used to test the similarity between mean hourly weather data for June and July, 1996, and long-term (1961–1990) mean hourly data for Vancouver for the same period (see text for definitions for parameters). 89

3.3 Summary of statistical indices used to test the similarity between data from vehicle surveys and the fixed sites at R1 and U1 (see text for definitions)..... 100

3.4 Comparitive data for dewfall (mm) by mini-lysimeter and surface moisture (mm) from blotting at a rural (R1) and an urban (U1) site in Vancouver during the summer of 1996, for grass at both sites and a roof at U1 107

3.5 Statistics of the presence and amount of surface moisture on grass at dawn at P1, P2, U1 and U2 on rain/fog-free days, as measured by blotting 120

4.1 Geometric and thermal effects of using a strict geometric approach to scaling the thermal state of a box 160

4.2 Geometric and thermal effects of scaling a box under the Internal Thermal Mass approach (ITM) 162

5.1 Specifications for the scale model at M1, where north-south dimensions are given as widths, and east-west dimensions as lengths 181

5.2 Instruments and methods used in the scale model 187

5.3 Description of landscape elements at the full-scale used to validate the results of the model 197

5.4 Instruments and methods to collect data to validate the model 198

6.1 Summary of average characteristic weather conditions on four nights in 1996. 207

6.2 Summary of statistical indices used to test the similarity in ambient weather conditions between the model (M1) and full-scale sites (M3 and U1) 209

6.3 Summary of statistical indices used to test the similarity in surface temperature conditions between the model (M1) and at full-scale sites (M3 and U1) 215

6.4 Summary of statistical indices used to test the similarity in surface moisture conditions between the model (M1) and at the full-scale site at U1 223

6.5 Apparent surface temperature (°C) observed at dawn in the scale model at M1, showing data for selected sites with relatively open exposure ($\Psi \geq 0.70$). Data are apparent surface temperatures measured using a hand-held Omega infrared thermometer (see Table 5.2 for a more detailed description of the instrument) 230

6.6 Summary of average weather conditions on selected nights in 1996.... 230

6.7 Statistics used to compare measured surface moisture (SM) on grass and normalised surface moisture ($\widetilde{SM}$) from the central transect in the scale model (see also Figures 6.20 and 6.23)..... 248

6.8 Statistics of the presence and amount of dewfall in the model at M1 during 1996, measured using mini-lysimeters for days selected for study in 1996 (dates as for Figure 6.15)..... 252

7.1 Input and output data for the numerical model to predict dewfall on urban surfaces, and data used to validate its results..... 273

7.2 Values for radiative and thermal parameters used in the model, for Japanese maple leaves and an asphalt shingle roof, as present at M1. For the roof, these data and Equation 7.17 provide an h_k value of 5.72 W m^{-2} K^{-1}..... 275

7.3 Energy balance components for a roof and leaf surfaces, as computed by the model, for the example of YD 171/172 with nocturnal weather favourable for dewfall (clear with light winds). Data are nightly mean (W m^{-2}) or nightly total (mm per night) values. Q_H is found by residual..... 278

7.4 Observed and predicted dewfall values (mm), and the difference (ΔE_{Pr-Ob}) between these, for roof and leaf surfaces..... 282

7.5 Summary of statistical indices used to test the skill of the 'roof' and 'leaf' dewfall models (see text for definitions)..... 282

List of Figures

1.1 Naturally occurring surface moisture on (a) maple leaves and (b) grass at two of the author's field sites. Moisture in (a) includes water from fog. In (b) the large droplets on leaf tips are almost certainly guttation..... 4

1.2 Schematic depiction of the horizontal layering of an urban area showing urban (UBL) and rural boundary layers, and the urban canopy layer (UCL). Source: Oke (1987). 7

1.3 Schematic depiction of the fluxes of mass (➡) and energy (⇨) involved in the water and energy balance of a surface plane during (a) day, and (b) a night with dewfall..... 12

1.4 Calculated rates of dewfall on a canopy surface, for an assumed surface temperature of 20°C and ambient air temperature of 22.5°C. Curves labelled A, B, C, and D are for humidity deficits of 0, 1, 2, and 5 g kg^{-1}, respectively. Source: Modified from Garratt (1992). 15

1.5 Schematic depiction of the component fluxes involved in the vapour budget of the air volume of an urban canopy layer, and the surface water balance of an urban three-dimensional surface..... 16

2.1 Schematic cross-section showing dew accumulation along a transect from the edge of a wood (the left hand side) to a more open area (right hand side) on three nights (a, b and c) with contrasting weather. Data are the relative intensity of wetting measured using paper 'dew rolls' (see Mattsson, 1962) and have the arbitrary units cm. Source: Mattsson (1971)..... 37

2.2 Observed spatial patterns in a forest clearing. (a) and (b) depict near-surface air temperature (°C) during calm and strong winds, respectively. (d), (e) and (f) show dew data during conditions of light, moderate and strong winds, respectively. (c) is a schematic cross-section depicting air flow during strong winds. (see Figure 2.1 for an explanation of the units of dew measurement). Source: Mattsson (1979)..... 37

2.3 Generalised cross-section of an urban heat island for a North American, mid-latitude city during clear and calm nocturnal weather. Source: Oke (1987)..... 42

2.4 Urban effects on humidity in Edmonton, showing hourly variation of vapour density (ρ_v) at urban and rural stations during 30 cloudless summer days where SS = sunset and SR = sunrise. Source: Oke (1987), from Hage (1975)..... 48

2.5 Temperature and dew conditions along a transect in Skanör, Sweden, during conditions of clear skies and light winds. The transect is from the town square (to the left) to a point outside the built-up area (to the right). (a) is air temperature (°C) at sunset (~7 pm), (b) is the intensity of dew recorded between 7 pm and 9 pm, and (c) is the intensity of dew recorded between 9 pm and 11 pm. Dew data were measured using the method of 'dew rolls' (see Mattsson, 1962) and have the arbitrary units cm. Sources: Mattsson (1971); Mattsson, pers. comm. (1998). 54

2.6 Spatial distribution of dew for Washington, D.C. under a variety of weather conditions in the summer of 1974. Nights are characterised by (a) windy, (b) calm, and (c) cloudy weather, and (d) shows the average of the observed dew distributions for days in July. Dew intensity is on a 6-step scale (from lightest to darkest shade: none, light, light-moderate, moderate, moderate-heavy, heavy) which is present in its entirety in (a). Source: Modified from Myers (1974)..... 56

2.7 Observed and simulated dewfall deposition for an individual apple leaf. (a) is leaf wetness (wet vs dry states) measured using an electronic wetness sensor, and (b) is dewfall (negative evaporation; W m^{-2}) simulated using the Pedro model. Source: Pedro and Gillespie (1982a)..... 66

3.1 Vancouver and its surrounding land-use, including the location of study sites and the route for the mobile survey..... 71

3.2 Views of (a) the rural site, R1, and (b) the urban site (U1)..... 77

3.3 Details of the Kerrisdale site (U1) and its surrounding neighbourhood.. 78

3.4 The street at the urban site, U1. 81

3.5 The method of blotting (as described in Sections 3.2.2 and A1.3)..... 81

3.6 A schematic cross-section of an electronic 'grass' mini-lysimeter, used to sense dewfall..... 83

3.7 The electronic 'roof' mini-lysimeter installed on a house roof at the urban site (U1), showing the device (a) with its load removed and (b) with this in place; a broken line marks the position of the panel which is weighed by the lysimeter..... 84

3.8 Regional weather data measured for YD 154/155, 1996. Data are the fraction of cloud cover (x10) from visual estimates at VIA and incoming shortwave radiation (measured at 0.5 m; see Table 3.1); air temperature and humidity at screen height (1.5 m), and wind speed and direction (10 m) measured at UBC..... 91

3.9 (a) Canopy-level (1.6 m) air temperature (°C) and vapour density (g m^{-3}) along a 25 km route from a rural site (R1) to an urban residential (U1) site in Vancouver, for selected periods during YD 154/155, 1996. (b) Characteristic environmental conditions during the mobile surveys..... 92

3.10 Canopy-level conditions on YD 154/155 as described in Figure 3.9, but showing vapour density deficits (g m^{-3}). 93

3.11 Regional weather data as described in Figure 3.8, but for YD 171/172, 1996. 94

3.12 (a) Canopy-level and (b) environmental conditions as described in Figure 3.9, but for YD 171/172, 1996..... 95

3.13 Canopy-level conditions on YD 171/172 as described in Figure 3.10, but showing vapour density deficit (g m^{-3}) values. 96

3.14 Computed difference between mean hourly air temperature (°C) values measured at 1.5 m at a rural (R1) and an urban residential (U1) site in Vancouver. Data are for 24 selected days during the summer of 1996. The vertical lines indicate the full range of values, 50% of the data fall inside the boxed region, and the horizontal line and circle indicate median and mean values, respectively..... 98

3.15 Computed urban-rural differences as in Figure 3.14, but for vapour density (g m^{-3}). 99

3.16 (a) Agreement between air temperature (°C) and vapour density (g m^{-3}) data measured during the vehicle survey and using instruments installed at R1 and U1 during the summer of 1996. (b) Selected characteristics of instruments used to collect the two data-sets..... 101

3.17 Data for YD 154/155, 1996 showing (a) air temperature (°C) and vapour density (g m^{-3}) and (b) the vapour density deficit (g m^{-3}) at 1.5 m at a rural (R1) and an urban residential (U1) site in Vancouver..... 102

3.18 As for Figure 3.17, but for YD 171/172. 104

3.19 Ensemble data for air temperature (°C) and vapour density (g m^{-3}) differences at 1.5 m for a rural (R1) and an urban residential (U1) site in Vancouver, for 12 summer days during 1996 with light winds and no/few clouds. Standard deviations for these data are large: 2.1–2.2°C and 1.1–1.4 g m^{-3}, respectively, where the higher value is during day..... 105

3.20 Dewfall (mm) data measured by mini-lysimeter at a rural (R1) and an urban (U1) site in Vancouver, during the summer of 1996. Data are for grass at both sites and a roof at U1 (no bar means zero dewfall)..... 108

3.21 The 'suburban' park (Everett; P1) in Vancouver and its neighbourhood 113

3.22 The park (Fairground; P2) on the campus of the University of British Columbia campus in Vancouver. 114

3.23 The urban residential sites in Vancouver, showing lot maps and the transect sampled for (a) U1 (Kerrisdale) and (b) U2 (Sasamat)..... 116

3.24 Amounts of surface moisture collected by blotting at dawn at the open centre of an urban park (P1) during the summer of 1993 (no bar means zero surface moisture). 119

3.25 Scatter plot of the amount of surface moisture (by blotting) present at dawn in the centre of two urban parks (P1 and P2), in relation to the fraction of cloud cover and wind speed, where the preceding night is characterised by (a) clear skies (cloud fraction at VIA is 0.0–0.2), and (b) light winds (wind speed at 10 m at UBC <2.0 m s^{-1}). 124

3.26 Relationship between surface moisture (mm) measured at the centre of P1 and P2, the weather factor (Φ_w), and vapour density deficit (g m^{-3}) measured at UBC. (a) is the amount of surface moisture present at dawn plotted against Φ_w, with labels of vapour density deficit rounded to the nearest 1 g m^{-3}. (b) is the surface moisture data plotted against vapour density deficit (data labelled by YD and the dotted line ρ_{vd} = 6.7 g m^{-3} are discussed in the text)..... 125

3.27 Relationship between the weather factor, Φ_w, and amount of surface moisture at dawn at P1 and P2. The dashed line indicates the line of best fit, this placed by eye. 126

3.28 Relationship between the amount of surface moisture present on grass at U2 at dawn (YD 240, 1993) and location. (a) A schematic cross-section of the transect sampled (see Figure 3.23b), and (b) spatial trends of surface moisture amount (mm) and Ψ_{sky} (see text for definitions of symbols)..... 129

3.29 As for Figure 3.28, but for YD 218 and the eastern transect at P1 (see Figure 3.21)..... 130

3.30 Relationship between the amount of surface moisture (mm) present on grass at U2 at dawn, location, and the weather of the preceding night, for YD 236–240, 1993. The low value at the 5 m distance on YD 239 relates to an encounter with a raccoon, which removed dew at this point on the lawn, while it was shredding one of the sampling pads..... 133

3.31 As for Figure 3.28, but for two days with nocturnal weather that was less favourable for dew accumulation, (a) YD 236 and (b) YD 237, 1993..... 135

4.1 An illustrative example of the geometry of an urban residential landscape in Vancouver. Source: Modified from Voogt (1995)..... 140

4.2 Selected images of the urban residential landscape of Vancouver. (a) Examples of houses of simple form (most houses are more structurally-complex than these) and (b) a residential street and its neighbourhood park (to the right). 141

4.3 Time dependent thermal behaviour of two similar objects of different size, showing typical responses to (a) a step change in ambient temperature, and (b) a periodic forcing wave in ambient temperature... 158

4.4 Box geometry for the example of a cubic box, showing the definition of 'corner' and 'edge'..... 163

4.5 Envelope indicating the relationship between the scaling factor (F) and the ratio of interior thermal masses (C_{Mi}) for buildings with a range of L:W. Data are for buildings approximated by a cube (see Equation 4.13). Insert: Outcome for a range of L:W and if the relationship were approximated using F^2..... 167

5.1 Stereographic depiction of the theoretical hemispheric geometry looking up at the sky zenith from a point in the centre of the urban lawn. In the lower portion of the diagram '1' indicates the theoretical extent of an infinite array of buildings, '2' is the minimum canyon length as dictated by radiative theory, and '3' is the canyon length ultimately simulated in the hardware model..... 174

5.2 Stereographic depiction as shown in Figure 5.1, but for the outer (south) edge of the theoretical urban park. Here, '1' indicates the theoretical extent of an infinite row of trees, '2' is the minimum canyon length as dictated by radiative theory, and '3' is the row of trees ultimately constructed in the hardware model. The dashed lines superimposed on this image indicate an equivalent view, but from a point that is 1.5 m from the north edge of the park. 175

5.3 Sites used in the modelling programme and the periods of observation..... 177

5.4 The scale model at M1. (a) A general view of the model street from the south-west, and (b) the measurement transect, from its southern end; wooden pegs indicate the sample points for blotting. 180

5.5 Diagrammatic representation of the scale model, showing location of instruments and the transect sampled. 185

5.6 The mini-lysimeter used to measure dewfall to the model roof. (b) The lysimeter in place and (b) the weighing platform (white, lower foreground) and the roof panel supported at 45°..... 188

5.7 Apparent surface temperature (°C) in the prototype model sensed using an AGEMA digital thermal imaging system (ε set to 1.00). (a) is an image sensed at dusk on YD 262, 1994, and (b) is that sensed on the following dawn (YD 263). The view is looking along the row of model houses toward the north-west (see accompanying sketches)..... 190

5.8 Data as in Figure 5.7, but for the model lawn at (a) dusk on YD 262, 1994, and (b) dawn on YD 263, 1994. 191

5.9 Buildings used to validate the thermal responses of the model houses. (a) The service building at M3 viewed from the north-west, and (b) the house at U1, viewed from the north. In (b) the wooden box containing the roof lysimeter is visible on the far right portion of the roof-top. 196

6.1 Fish-eye lens photographs looking up at the sky zenith from the surface of the (a) scale model park (M1) and (b) full-scale park at P1 (see text for associated Ψ_{sky}). 203

6.2 Fish-eye lens photographs as in Figure 6.1, but for the (a) model and (b) full-scale street with trees at U1 (see text for Ψ_{sky} values). Note the close agreement between the horizon obstruction due to the model and full-scale trees and houses..... 204

6.3 Agreement between the observed air temperature measured at 1.5 m in the scale model (M1) and air temperature measured at M3 (mid-roof level, 3.6 m) and U1 (mid-roof level (5.3 m) and 1.5 m height). 208

6.4 As for Figure 6.3, but for vapour density. 210

6.5 Comparison between wind conditions at full-scale and scaled sites. (a) Wind speed measured at 1.5 m in the model (M1) and at mid-roof level at M3 (3.6 m) and U1 (5.3 m), and (b) wind direction measured at the Fairground site and U1..... 212

6.6 Agreement between observed nocturnal surface temperatures of full-scale and scaled roof facets on four nights with contrasting weather in 1996. Data are 15 min mean surface temperature (°C) measured by thermocouple on north- and south-facing facets at M1 and U1, and west- and east-facing facets at M1 and M3..... 216

6.7 Agreement between observed nocturnal surface temperature for full-scale and scaled walls for four nights in 1996. Data are 15 min mean surface temperature (°C) measured by thermocouple for north-, south-, west- and east-facing facets at M1 and M3. 217

6.8 Agreement between observed surface temperature at dawn for full-scale and scaled walls for 16 nights in 1996. Data are surface temperature (°C) measured using a hand-held infrared thermometer at U1 and at M1 thermocouples attached to the north-, south-, west- and east-facing walls of the central house in the model..... 218

6.9 Agreement between observed nocturnal surface temperature for grassed surfaces at full-scale and scaled sites for four nights in 1996. Data are surface temperature (°C) measured using Everest infrared thermometers mounted over the model park and lawn at U1. 221

6.10 Agreement between surface temperature at dawn for deciduous and conifer trees, and pavement in the model and at U1, for 8 and 14 nights in 1996, respectively. 222

6.11 Agreement between the observed nocturnal amount of surface moisture accumulated on grass at the full-scale and model sites, for 18 nights in 1996. Data are the maximum amount (mm) measured by blotting at dawn at M1 and U1..... 224

6.12 Agreement between the observed amount of dewfall measured by mini-lysimeters in the model and at the full-scale during the summer of 1996. Two comparisons are made: (a) dewfall for the roof at M1 and U1(15 nights), and (b) dewfall for the most open locations at M1 (park) and U1 (centre of lawn) (14 nights). Data are the maximum accumulated dewfall per night (mm). 226

6.13 Surface temperature (°C) in the model at dawn on two days, both with trees present but contrasting weather: YD 172 (Φ_w = 1.00) and YD 174 (Φ_w = 0.51), 1996. (a) Schematic cross-section of the transect sampled, and (b) spatial trends of surface temperature (°C)..... 233

6.14 Data as in Figure 6.13, but for three days with no model trees: YD 188 (Φ_w = 0.82), 192 (Φ_w = 0.31) and 194 (Φ_w = 0.53), 1996. 234

6.15 Amounts of surface moisture (mm) collected by blotting at dawn at the open model park (M1 which coincides with P2) during the summer of 1996. No bar means zero surface moisture (note that the sequence of days is discontinuous)..... 236

6.16 Relationship between the amount of surface moisture (mm) present on grass in the model at dawn and micro-scale location. Data for YD 172, 1996, with clear skies, light winds, and trees present in the model. (a) Schematic cross-section of the transect sampled, and (b) spatial trends of surface moisture amount (mm) and Ψ_{sky} (subscripts photo and calc indicate Ψ_{sky} determined using fish-eye lens photography and site geometry, respectively). 239

6.17 As for Figure 6.13, but for YD 188, 1996, with clear skies, light winds, and no trees present in the model..... 240

6.18 Relationship between the amount of surface moisture (mm) present on grass in the model at dawn and micro-scale location with trees present in the model. Days are differentiated by the weather of the preceding night (see text). 242

6.19 As for Figure 6.18, but for nights with no trees present in the model..... 243

6.20 Agreement between surface moisture normalised by sky view factor ($\widetilde{SM}$ with units mm; see text for explanation), and the measured surface moisture (mm) on grass at dawn in the model. Data are for two days with trees in the model: (a) YD 172 (Φ_W = 1.00) and (b) YD 174 (Φ_W = 0.51), 1996..... 246

6.21 Surface moisture data for (a) YD 172 and (b) YD 174, 1996, as shown in Figure 6.20 but with $\widetilde{SM}$ plotted against SM (see text for explanation of terms)..... 247

6.22 Data as in Figure 6.20, but for two days with model trees absent: (a) YD 188 and (b) YD 192, 1996..... 249

6.23 Surface moisture data for (a) YD 188 and (b) YD 192, 1996, as shown in Figure 6.22 but with $\widetilde{SM}$ plotted against SM (see text for explanation of terms)..... 250

6.24 Dewfall data measured by mini-lysimeter in the model for selected days during the period YD 155–195, 1996. Data are the maximum accumulated dewfall per night (mm) on grass in the model park and lawn, and on the roof of the model house (no bar means zero dewfall). The dashed line indicates periods with trees present in the model (YD 155–174) and without model trees (YD 187–195). 253

7.1 Schematic summary of the fluxes involved in the radiation budget and energy balance of (a) a leaf underlain by continuous canopy, and (b) the surface of a horizontal roof, for typical day and night conditions..... 264

7.2 Agreement between observed and computed surface temperature for roof (■) and maple leaf (Δ) surfaces, for periods when the model predicts the presence of dewfall. Three days are shown (YD 163/164, 164/165 and 171/172). The dotted line indicates temporal sequences, and shows how the model under-estimates roof surface temperature in early evening and over-estimates this after sunrise. 279

7.3 Agreement between the amount of dewfall predicted by the model and that measured, for a roof (■) and a maple leaf (Δ). Lines shown are for a 1:1 correlation (—) and its ±0.05 mm per night envelope (· · ·). Outliers (labelled by YD) are discussed in the text. Note that some data points represent more than one outcome..... 281

7.4 Examples of the agreement between the amount of dewfall predicted (■) by the model for a roof, and that measured (□) using a mini-lysimeter at M1, for (a) YD 171/172 and (b) 192/193, 1996..... 284

A1.1 Schematic depiction of the geometry used to derive temporal corrections for data measured along the mobile survey (see text). 311

A1.2 Geometry used to compute terrain view factor for an individual (a) wall and (b) sphere for a given point (P) on the surface. Source: Spronken-Smith (1994)..... 316

A2.1 The saturation specific humidity vs temperature curve, illustrating the geometry used to linearise the slope of the curve at mean temperature ($\bar{T} = \frac{T_a + T_l}{2}$) for the case of a leaf..... 322

A3.1 Dew sculpture by Chris Parsons, Shropshire, created in dew on a lawn at dawn, using a wide broom. Source: Anon. (1995)..... 325

List of symbols and abbreviations

Roman letters

- *Upper case*

A	area [m^2]
A	water vapour flux due to advection [kg m^{-2} s^{-1} or mm h^{-1}]
Bi	dimensionless heat transfer coefficient, Biot Number
C	mass flux of condensation; subscripts f and s indicate dewfall and distillation from soil, respectively [kg m^{-2} s^{-1} or mm h^{-1}]
D	drainage [kg m^{-2} s^{-1} or mm h^{-1}]
D	rate of molecular diffusion [m^2 s^{-1}]
E	mass flux density of water; E (evapotranspiration) = E_t (transpiration) + E_e (evaporation) [kg m^{-2} s^{-1} or mm h^{-1}]
F	scaling factor
F	water vapour flux of anthropogenic origin [kg m^{-2} s^{-1} or mm h^{-1}]
Fo	dimensionless time, Fourier Number
FOV	field of view [°]
G	guttation [kg m^{-2} s^{-1} or mm h^{-1}]
H	Thermal Mass Number
H	height [m]
I	irrigation [kg m^{-2} s^{-1} or mm h^{-1}]
I	step rate [h^{-1}]
ID	index of agreement
ITM	Internal Thermal Mass approach
K	shortwave radiation flux density [W m^{-2}]
L	longwave radiation flux density [W m^{-2}]
L	length or thickness [m]

L_v latent heat of vaporisation [J kg^{-1} K^{-1}]

M mass [kg]

M molecular mass [g mol^{-1}]

M water vapour flux due to mixing with air aloft [kg m^{-2} s^{-1} or mm h^{-1}]

MD mean absolute difference [mm]

Nu Nusselt number

Ob observed value

P pressure [Pa]

P precipitation [kg m^{-2} s^{-1} or mm h^{-1}]

Pr Prandtl Number

Pr predicted value

Q energy flux density; Q* is net all-wave radiation, and subscripts E, H, G, M and S indicate convective latent and sensible heat, sub-surface sensible heat, metabolic heat, and heat storage, respectively [W m^{-2}]

Q_{Eq} maximum or potential rate of condensation [W m^{-2} or mm h^{-1}]

R runoff [kg m^{-2} s^{-1} or mm h^{-1}]

R gas constant [J mol^{-1} K^{-1}]

Re Reynolds Number

Ri Richardson Number

RMSD root mean squared difference [mm]

Ro Rossby Number

S storage

Sc Schmidt Number

SD standard deviation

Sh Sherwood Number

SM surface moisture = dew + guttation [mm]

T temperature [K or °C]

UBL urban boundary layer

UHI urban heat island

UCL urban canopy layer

U:V:W dimensionless velocity

V volume [m^3]

V [kg m^{-2} s^{-1} or mm h^{-1}]

W width [m]

X data value

X:Y:Z dimensionless location

• *Lower case*

a absorptivity for shortwave radiation

c specific heat [J kg^{-1} K^{-1}]

c_M thermal mass [J K^{-1}]; where c_M=M x c

d effective leaf length [m]

e water vapour pressure [Pa]

g acceleration due to gravity [m s^{-2}]

h transfer coefficient; subscripts c, v and k indicate convective sensible heat, convective water vapour, and conductive sensible heat, respectively [W m^{-2} K^{-1}]

k thermal conductivity [W m^{-1} K^{-1}]

k cloud height coefficient

n cloud fraction [tenths]

n number

q specific humidity [kg kg^{-1}]

r resistance to transfer [s m^{-1}]

rhs right hand side

s slope of the saturation humidity *vs* temperature curve [Pa K^{-1} or kg m^{-3} K^{-1}]

t time [s]

tr transmissivity

u wind speed [m s^{-1}]

u_* friction velocity [m s^{-1}]

x:y:z orthogonal location [m]

x thickness of substrate layer [m]

z height of measurement [m]

z_0 roughness length [m]

Greek letters

• *Upper case*

Δ change in or difference

Φ_w weather factor

Γ the fraction $\frac{s}{s+\gamma}$

K hydraulic conductivity [m s^{-1}]

Ψ view factor

• *Lower case*

α reflectivity for shortwave radiation

β vapour transfer coefficient modifier

γ psychrometric constant [kg m^{-3} K^{-1}]

δ thickness of the laminar boundary layer [m]

ε surface emissivity for longwave radiation

κ diffusivity; for heat κ_H [$m^2\ s^{-1}$], soil moisture κ_θ [$m^2\ s^{-1}$], and soil temperature κ_T [$m^2\ s^{-1}\ K^{-1}$]

λ surface area to volume ratio [m^{-1}]

ν kinematic viscosity [$m^2\ s^{-1}$]

v_x, v_y, v_z velocity components in the *x*, *y* and *z* directions [$m\ s^{-1}$]

θ volumetric moisture content [-]

ρ density [$kg\ m^{-3}$]

σ Stefan-Bolzmann constant [$5.67 \times 10^{-8}\ W\ m^{-2}\ K^{-1}$]

τ time constant [s]

φ dimensionless temperature

χ corrected data value

Common subscripts and modifiers

• *Roman letters: Upper case*

A start location

B end location

Max maximum

Min minimum

R rural

T temperature

U urban

• *Roman letters: Lower case*

a air

b laminar boundary layer

c	convective
c	canopy
calc	calculated
d	dew-point
f	fluid
h	building at full scale
h	heat
i	initial
i	interior
in	incoming
k	conductive
l	leaf
m	scaled building or model
m	mobile survey
n	final
out	outgoing
photo	photographic
r	roof
s	solid
sky	sky
soil	soil
ter	terrain
u	underside of roof
v	water vapour
vd	water vapour deficit

w wall

wa water

z at height z

- *Greek letters*

Δ change in or difference

θ moisture

- *Miscellaneous*

$\bar{}$ mean quantity

$\tilde{}$ normalised

$\hat{}$ effective or estimated

* saturation (of humidity), or net (of radiation)

1 upper side

1 start time

2 lower side

2 end time

Acknowledgements

By far the greatest thanks goes to my supervisor Tim Oke who provided encouragement and guidance throughout my research. Without his support this study would not have been possible. I would also like to thank my supervisory committee: Andy Black, Mike Church and Douw Steyn for their assistance.

Many thanks go to my field assistants—Don, Jessica, Kathy, Lee and Trevor in 1994, and Andres, Pascal and Ron in 1996—especially to those who were up at dawn to drive the truck and blot dew. I would like to express my appreciation to those who provided access to field sites: Brian Hull and Al Neighbour at the University of British Columbia, Ran Vered at Boundary Bay Airport, and Robert and Margaret North, Wendy Hales and Andres Soux who allowed me to monitor dew in their yards. I also greatly appreciate the lending of field equipment by: Drs Sue Grimmond, Jamie Voogt, Mike Bovis and Douw Steyn.

This research was funded by a grant to Dr T.R. Oke by the Natural Sciences and Engineering Research Council of Canada. Personal funding was provided by University of British Columbia Graduate Fellowships, Teaching and Research Assistantships in the Geography Department, and by my family in New Zealand; to the latter goes my very special thanks.

Finally, my heart-felt thanks go to my friends, who provided sunshine and chocolate when I needed it most.

PART I CONTEXT

Chapter 1: Introduction

1.1 Rationale

Although usually addressed in a rural context, dew occurs in urban environments. Occurrence of urban dew is linked to microclimate, and has a role in determining urban humidity, evaporation rates, and near-surface temperature. Presence of dew has implications for the moisture supply of urban plants, deposition of pollutants from the atmosphere, and chemical damage to plants and materials. Many of the published studies of dew focus on agriculture where dew has economic implications, on the role of dew in plant water-budgets and crop disease, and on practicalities of measurement and forecasting for crops. Agricultural researchers and plant pathologists are able to satisfactorily measure, and sometimes predict, dew on crops. In contrast, dew in urban environments is seldom measured, often dismissed and even with the best available numerical models has not been simulated.

Measurement of dew is associated with certain difficulties in whatever environment it occurs. There are several sources to these difficulties: dew is a small-scale phenomenon, it involves small fluxes of energy and mass, and occurs seasonally, but irregularly. It is nocturnal, but not all nocturnal surface moisture is strictly dew, leading to difficulties of identification and measurement. Dew is not regularly measured, except at agricultural sites, and then only when economic incentives exist. Dew data are not routinely available for cities.

The best available numerical models for microclimate in urban areas rely, in part, on surface wetness to define rates of evapotranspiration (e.g., Grimmond, 1988). Since dew data are not normally available, the alternative is to assume that surfaces are dry whenever wetting by rain is absent. For many days of the year, in mid-latitude cities, this is an erroneous assumption for several surface types, because dew regularly forms. Numerical simulations, therefore, tend to under-estimate evaporation rates during morning hours, when dew is present but is unaccounted for (Grimmond, 1988), and to over-predict rates of warming, during these same periods (Oke, *pers. comm.*, 1992).

As a consequence there is need for methods to accurately assess dew in urban environments, i.e., to measure dew with consistency and accuracy in cities, and to predict dew from standard weather data. If a model were able to accurately predict dew amounts or durations, it could become part of an existing model of urban evaporation and improve its accuracy.

The broad objectives of this thesis are to measure dew in an urban area and to explore the feasibility of modelling dew in urban environments. Since the study of urban dew does not form a coherent body of research, a multi-disciplinary approach is taken, combining aspects of urban climatology, agricultural biometeorology and thermal engineering theory. Several topics are addressed, including the physical processes of dew formation, techniques for dew measurement, observational studies, and both hardware and numerical modelling.

The research is presented as follows. Part I (Chapters 1 and 2) is contextual, and consists of an overview of theories relevant to dew occurrence (Section 1.2),

the specific aims of the thesis and the approaches taken to implement these aims (Section 1.3), and a review of theory and literature relating to dew from an urban perspective (Chapter 2). Part II (Chapter 3) contains observations, i.e., field surveys of naturally occurring dew in an urban area. Part III deals with the modelling of dew in an urban environment using hardware (Chapters 4–6) and numerical models (Chapter 7). Finally, in Part IV, a protocol for measuring dew in urban environments is forwarded and the main conclusions from Parts I to III are summarised (Chapter 8).

1.2 Theory

1.2.1 Definitions

Controversy over the source of water for dew is more than two thousand years old (Monteith, 1963). To some extent, conflicts during the last 100 years derive from semantics since then, as now, 'dew' has a variety of definitions (Simpson, 1929). In the absence of rain, droplets of water that appear overnight on grass and other surfaces tend to be called 'dew'. It would be more rigorous if this were simply called *surface moisture* (Figure 1.1). The two components of surface moisture of interest here are *dewfall* and *distillation*, but surface moisture can also include water from fog and even that exuded from plant tissue (*guttation*). For example, in Figure 1.1a the surface moisture on leaves includes water from fog. In Figure 1.1b, dew (condensation) is present as small droplets, whereas the large droplets on the leaf tips are almost certainly guttation.

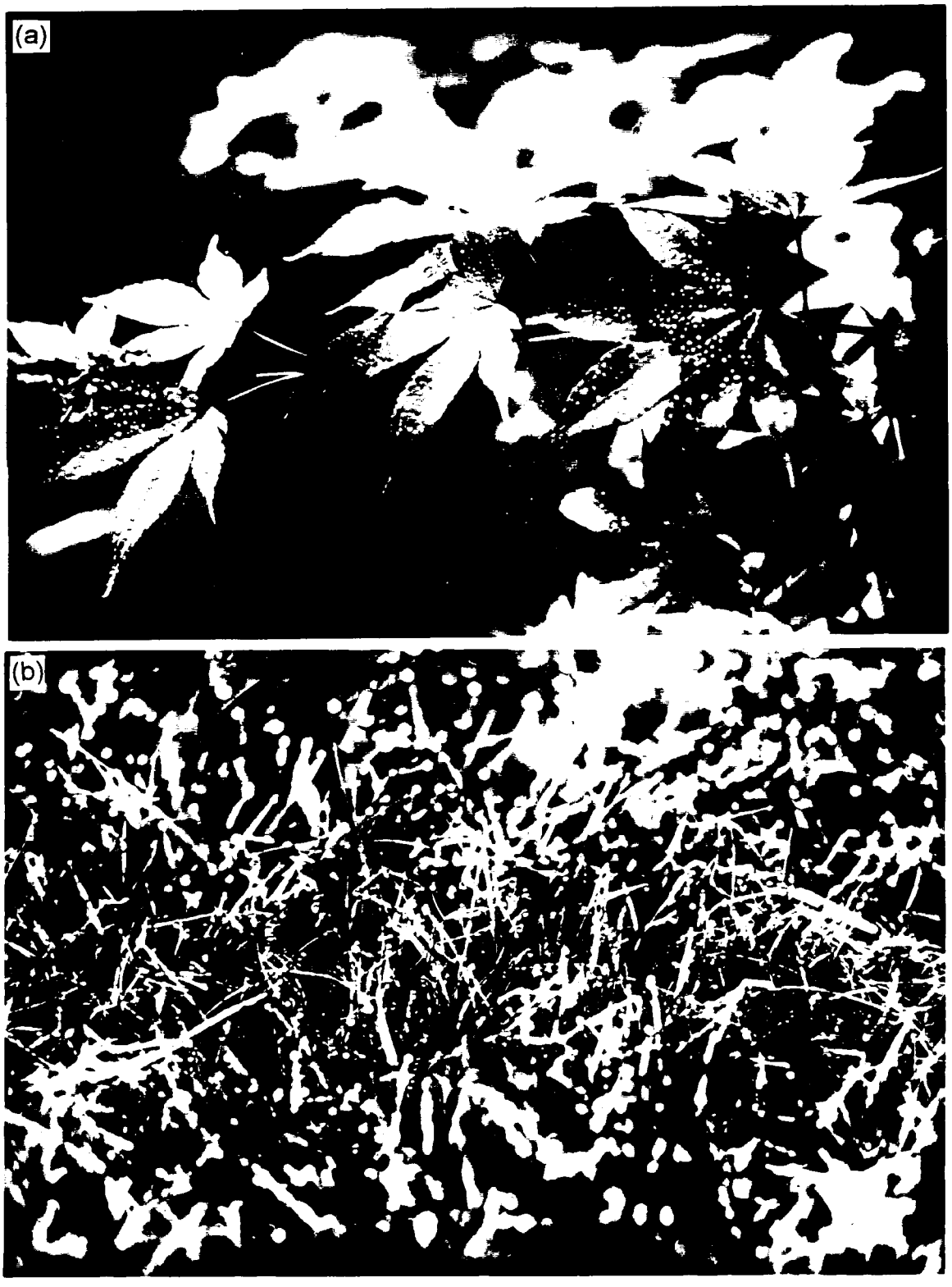

Figure 1.1 Naturally occurring surface moisture on (a) maple leaves and (b) grass at two of the author's field sites. Moisture in (a) includes water from fog. In (b) the large droplets on leaf tips are almost certainly guttation.

Dew, in the strict sense, is surface water solely attributed to condensation. Subdivision of dew is based on the recent origin of the water vapour that is condensed. *Dewfall* is that proportion deposited directly from vapour in the lower atmosphere. It is, therefore, a downwards turbulent or diffusive flux, the rate of which correlates strongly with weather conditions. *Distillation*, or *dewrise*, is also condensed from the atmosphere, but its recent origin is nearby soil moisture or adjacent wetted leaves and, therefore, its rate is largely governed by soil and surface conditions, not weather. The ratio of dewfall to distillation varies greatly and is largely a function of wind speed; in near-calm conditions vapour transport from the overlying atmosphere is inhibited and distillation becomes the dominant flux. Dewfall and distillation cannot be distinguished by appearance; they can only be separated using lysimetry (Section 2.2.2) (Slatyer and McIlroy, 1961). *Guttation*, however, can often be discerned. It is fluid exuded from the leaves of certain plants through pores under internal pressure. It forms distinctive large droplets on the margins and tips of leaves, as illustrated in Figure 1.1b on grass, and its presence tends to coincides with dew. Guttation occurs when leaves are fully turgid, surface air is close to saturation, and the rate of water supply from the roots exceeds losses due to transpiration (Hughes and Brimblecombe, 1994). Leaf water potentials are normally negative and factors controlling guttation are not well understood. Its presence may be linked to the slow adjustment in roots to water potentials in the plant. A continual increase in the solute concentrate in root cells could result in greatly increased pressure inside leaves, sufficient that moisture is exuded from leaf pores.

1.2.2 Scales and systems of interest

To discuss processes relating to dew formation, it is necessary to first define the scales and systems of interest. Climatic phenomena can be divided into categories and assigned characteristic dimensions of horizontal length as follows (Oke, 1987):

Macro-scale: 100 km to 100 000 km

Meso-scale: 10 km to 200 km

Local-scale: 0.1 km to 50 km

Micro-scale: 10 mm to 1000 m

Nano-scale: <1 mm to 10 mm

Similarly, they can be grouped according to their characteristic temporal period (Fitzharris, *pers. comm.*, 1998):

Long-term:	5 years to >50 years
Medium-term:	~1 day to ~5 years
Short-term:	~1 minute to ~1 day
Very short-term:	<1 s to ~12 hours

In the present study, the horizontal length scales of interest range primarily from *meso-scale*, e.g., a city, to *micro-scale,* e.g., a house or a leaf. Temporal scales of interest range mostly from *medium-term* (several years) to *short-term*, i.e., a day or less. It is also possible to study dew at the *nano-scale*, as a single droplet with a

very short-term lifespan (Chameides, 1987), or at the *macro-scale*, across whole regions, using long-term data (Chowdhury *et al.*, 1990).

In the vertical length dimension, characteristic scales are not constant, they are governed by surface-generated heating/cooling, roughness and wind speed (Oke, 1987), and climatic phenomena are best defined with relation to surface systems. At time scales of about a day, an *atmospheric* and a *substrate boundary layer* can be defined where characteristics are governed by the nature of the surface. The atmospheric boundary layer is subdivided into urban (UBL) and rural (non-urban) components (Figure 1.2). Near the rural surface, a *canopy layer* extends from the top of the plant canopy to the soil surface, and in urban areas an *urban canopy layer* (UCL) extends from an imaginary surface above general roof level to the ground surface.

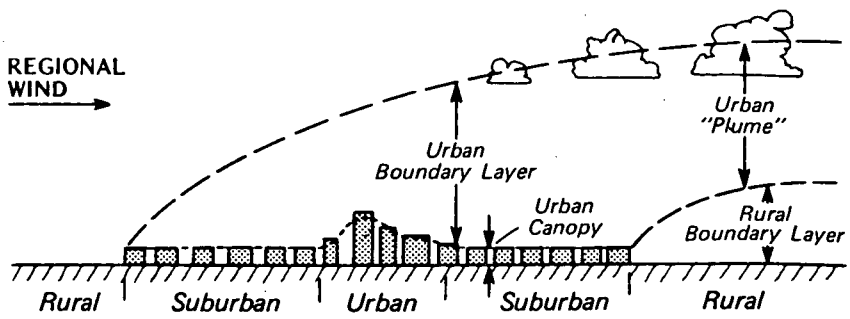

Figure 1.2 Schematic depiction of the horizontal layering of an urban area showing urban (UBL) and rural boundary layers, and the urban canopy layer (UCL). *Source:* Oke (1987).

The atmospheric component of the canopy layer is separated from its substrates by the *three-dimensional surface*, i.e., the combined external surfaces of vegetation, buildings, paving and soil. Since, in theory, dew can be deposited on all of this convoluted surface, it coincides with the *potential active surface* for dew accumulation. However, it is often useful to treat substrates as a unified volume, rather than a series of surfaces, thus a *substrate volume* is defined to include all objects in the canopy layer, extending down to an imaginary plane deep in the soil across which there is no vertical transport (water or heat) over the period considered. This differs from the commonly defined *atmosphere-plant-soil volume* which includes an atmospheric component.

At rural and urban locations, site geometry is commonly expressed by *height to width ratio* (H:W), of the horizon elevation to the opening width, or by the *sky view factor* (Ψ_{sky}) of the surface. The latter is a dimensionless ratio that expresses the fraction of the radiation output from the sky hemisphere which is intercepted by the surface of interest. It is often convenient to think of it as the ratio of the amount of sky hemisphere 'seen' from a given point on the surface compared to that potentially available (Oke, 1987). In open, flat landscapes, such as large playing fields and flat cropland, the sky view approaches the theoretical maximum (1.0) which is seen when the sky hemisphere is entirely unobstructed. However, Ψ_{sky} is severely reduced in forests and at most urban sites because a significant proportion of the sky hemisphere is obscured by trees, buildings and other objects. The exception is sites above general canopy level, where Ψ_{sky} may approach unity. The

complement of Ψ_{sky} is *terrain view factor* (Ψ_{ter}) which expresses the proportion of the sky hemisphere obscured by objects, i.e., $\Psi_{ter} = 1 - \Psi_{sky}$ (Oke, 1987).

For each system it is possible to define balances of heat, mass and momentum so that, in theory, change in storage equals inputs minus outputs. In practice it is often difficult to adequately quantify all components of any particular balance or budget. For fluxes described in this thesis the convention employed is that:

- radiative fluxes directed *towards* a system are positive, while those directed *away from* the system are negative, e.g., incoming solar radiation (K_{in}) is positive, and the proportion of this reflected from the surface (K_{out}) is negative; all components are expressed as flux densities with units W m^{-2},
- non-radiative (mass and energy) fluxes directed *away from* a system are positive, while those directed *towards* a system are negative, e.g., evapotranspiration (E) is positive, and condensation (C) is negative. Both energy (W m^{-2}) and water (kg m^{-2} s^{-1}) components are flux densities, however, the latter is often converted to a mass flux rate (e.g., mm h^{-1}), i.e., an equivalent depth of water per unit time, as if the surface moisture were distributed in a film of constant thickness (Section A1.1), and
- for both energy and mass balances, positive storage indicates a net gain to the system, a negative storage is a loss.

1.2.3 Processes and balances

In essence, formation of dew requires a source of water vapour, eddy or molecular transport, and a sufficiently cool surface, i.e., a surface whose temperature is at or below the ambient dew-point temperature. In detail, the critical ranges of favourable temperature, humidity and wind fields are relatively narrow. Dew is prohibited by freezing temperatures. Although impaction of fog droplets contributes to surface wetness, the formation of near-surface fog inhibits the condensation of vapour onto underlying surfaces (i.e., dewfall). For dewfall (not fog), wind speed must be sufficient to maintain transfer of vapour to the surface. However, wind speed cannot be so rapid that humidity and temperature gradients are destroyed. In practice this means that dewfall is unlikely when near-surface air is motionless or wind speed is greater than about 3.0 m s^{-1}, measured at a height of about 2 m (Monteith, 1963; Garratt and Segal, 1988). Upward movement of water through the soil is governed by soil moisture and temperature gradients, but in the air distillation relies on molecular diffusion of vapour. This means it is deposited only in calm conditions, when near-surface gradients of temperature and humidity favour the upward diffusion of water vapour, and on surfaces close to ground level, e.g., on grass or the under-side of plastic sheeting spread on the ground surface.

Dewfall deposition and subsequent drying involve changes in state from water vapour to liquid, and *vice versa*; thus, dewfall involves fluxes of both mass and energy (Figure 1.3). For a surface plane, moisture can be added or removed by runoff (R), drainage (D) and evapotranspiration (E), where a downward evaporative transfer (Figure 1.3b) is condensation or dewfall. The energy balance of the surface

shown in Figure 1.3 is expressed in terms of net all-wave (Q^*), sub-surface sensible heat (Q_G), convective sensible heat (Q_H), and convective latent heat (Q_E) flux densities [all with units W m^{-2}], where Q_E is the energy equivalent of E.

When dew is present, surfaces are wet, and an appropriate framework for discussion of energy transfers is the Penman combination equation for saturated surfaces (Oke, 1987):

$$Q_E = \Gamma\left(Q^* - Q_G\right) + \frac{h_c\left(\rho^*_v - \rho_v\right)}{s+\gamma} \qquad [1.1]$$

where $\Gamma = \frac{s}{s+\gamma}$

s is the slope of the saturation humidity *vs* temperature curve [kg m^{-3} K^{-1}], γ is the psychrometric constant [kg m^{-3} K^{-1}], h_c is the convective transfer coefficient for sensible heat [W m^{-2} K^{-1}], and ρ^*_v and ρ_v are saturated and ambient water vapour density [kg m^{-3}], respectively. The first term on the right hand side (rhs) of the equation, the 'energy' term, summarises the effects of temperature on potential rates of dewfall deposition (s and γ are temperature dependent), and the energy available to the system (Q^*-Q_G). For isolated thin surfaces, such as leaves, Q_G is omitted, and in some cases anthropogenic heat must be considered (substituting: Q^*-Q_G+Q_F). The second term on the rhs of the equation, the 'vapour deficit' term, accounts for the effects of the drying power of the air (expressed as a vapour density deficit, ρ^*_v-ρ_v), and the effect of near-surface atmospheric turbulence on heat transfer to, and from, the surface.

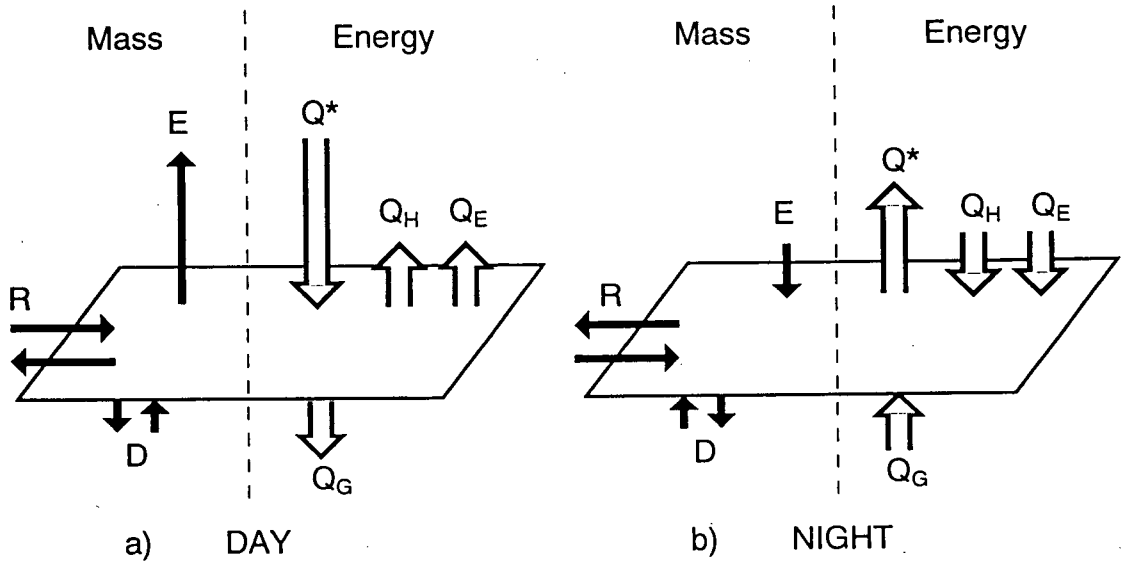

Figure 1.3 Schematic depiction of the fluxes of mass (➡) and energy (⇨) involved in the water and energy balance of a surface plane during (a) day, and (b) a night with dewfall.

This equation predicts dewfall ($-Q_E$) when the energy term is negative, and exceeds the second term in magnitude. Exact values for Q^* and Q_G depend on surface type, its thermal behaviour, and ambient environmental conditions. For most surfaces, Q^* goes negative from around sunset until dawn, due to nocturnal radiative cooling, associated with the heat sink of the cold night sky. Thus, dewfall deposition is predominantly a nocturnal process, is potentially more frequent on objects which cool rapidly at night (e.g., leaves), and occurs seldom on surfaces with a significant Q_G or Q_F, e.g., paving, and poorly insulated, heated buildings.

When the lowest layer of air is saturated, the vapour deficit term goes to zero, and Equation 1.1 reduces to:

$$Q_E = \Gamma\left(Q^* - Q_G\right) \qquad [1.2]$$

This equation is equivalent to that for *potential* or *equilibrium evaporation*, and the term *potential dewfall* (Q_{Eq}) has been coined to describe this state of condensation. Being a function of temperature and available energy, the exact value of Q_{Eq} depends on surface type. For vegetation, Q_{Eq} increases with temperature from 0°C to about 20°C, where it reaches an estimated maximum of ~0.08 mm h^{-1}, but over a wide range of temperatures Q_{Eq} = 0.07 mm h^{-1} ±10% (-47 W m^{-2}) (Hofmann, 1955; Monteith, 1963; Garratt and Segal, 1988). Although theoretically this could result in dewfall accumulations of ~0.7 to ~1.0 mm per night, observed amounts are normally much less because vapour supply is commonly limiting, so condensation seldom reaches its potential maximum rate.

When air is not saturated, Q_E is a function of the humidity deficit and wind speed, because the latter controls the efficiency of transport of heat and mass (water) to, and from, the surface. For vegetation, Q_E is typically less than 0.05 mm h^{-1} (-34 W m^{-2}), so total amounts of dewfall accumulated on vegetation at dawn seldom exceed 0.50 mm. On thin artificial materials which cool rapidly after sunset (e.g., metal car roofs) slightly more dewfall may accumulate. Critical values for wind speed are poorly defined in the published literature. The general consensus is that dewfall changes to evaporation when wind speed near the surface exceeds about 3 m s^{-1}, and ceases when wind speed falls below about 0.5 m s^{-1}, because vapour supply to the surface is impeded (Monteith, 1963; Garratt and Segal, 1988). Theoretical calculations by Garratt and Segal (1988) (Figure 1.4) indicate that, in relatively warm conditions and for short vegetation, dewfall will

change to evaporation at wind speeds of ~1.7 to 2.5 m s^{-1} (measured at 0.5 m), depending on the moisture content of the air.

Distillation may be present with dewfall, or may be the only source of surface moisture on any particular occasion. Its rate is estimated using the moisture diffusivity of the top layer of soil. The transport of liquid plus vapour water in a porous medium, such as soil, is given (Jacobs *et al.*, 1990):

$$E_{soil} = -\rho_{wa}\kappa_{\theta}\frac{d\theta}{dz} - \rho_{wa}\kappa_{T}\frac{dT}{dz} - \rho_{wa}K \qquad [1.3]$$

where E_{soil} is the mass flux density of water from the soil [kg m^{-2} s^{-1}]; κ_T [m^2 s^{-1} K^{-1}] and $\kappa\theta$ [m^2 s^{-1}] are the liquid + vapour diffusivities for temperature (T with units K) and water, expressed as θ, the non-dimensional volumetric moisture content, respectively; K is the hydraulic conductivity of the soil [m s^{-1}]; ρ_{wa} is water density [kg m^{-3}]; and z is depth in the soil [m]. At the surface, if ambient conditions (atmospheric temperature, humidity and wind fields) are favourable, vapour from the soil surface (E_{soil}) moves upwards by diffusion to condense on cooled surfaces, thus creating distillation. In theory, distillation will change to evaporation at higher wind speeds, and if air is relatively warm and dry.

In cities, dew is deposited on the three-dimensional urban surface in locations where substrates cool sufficiently to produce condensation. Processes are the same as those at rural locations, however, the potentially active surface in a city is likely to be more complex in terms of geometry and materials, compared to that typical for rural locations, i.e., agricultural locations characterised by an extensive

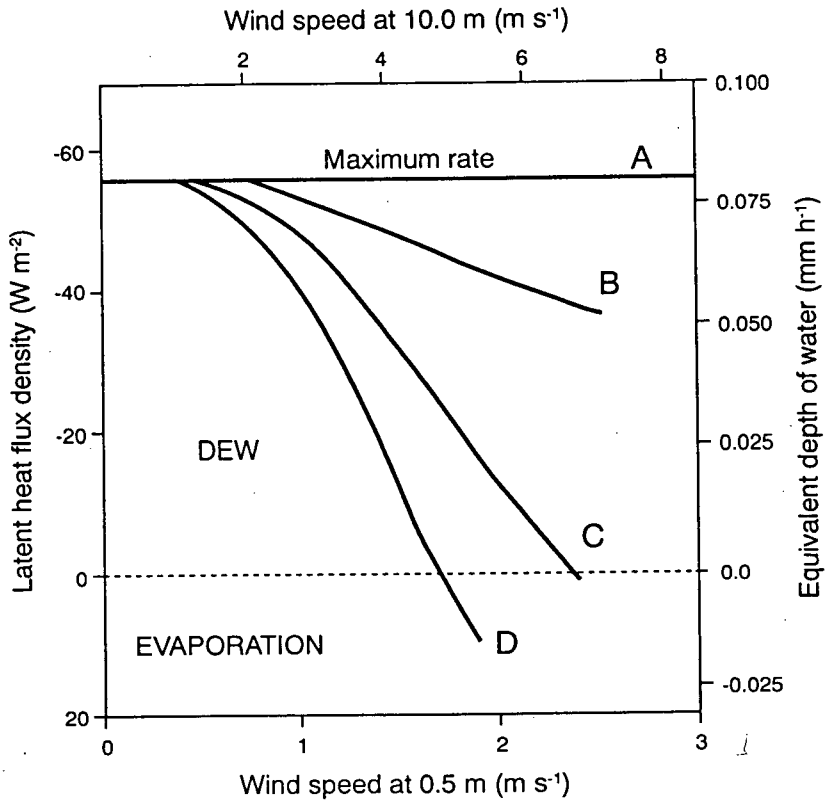

Figure 1.4 Calculated rates of dewfall on a canopy surface, for an assumed surface temperature of 20°C and ambient air temperature of 22.5°C. Curves labelled A, B, C, and D are for humidity deficits of 0, 1, 2, and 5 g kg^{-1}, respectively. *Source*: Modified from Garratt (1992).

and homogeneous pasture or crop canopy. Water can be stored on this convoluted three-dimensional surface (Figure 1.5), as liquid or ice. In the absence of freezing a water balance for the change in storage of liquid water on this surface (ΔS) can be written:

$$\Delta S = P + C_f + C_s + G + I - E_e \pm R \pm D \qquad [1.4]$$

where inputs are precipitation and fog droplets (P), dewfall (C_f), that proportion of distillation originating from within the soil (C_s), guttation from plant tissue (G), and perhaps irrigation (I). Outputs are evaporation (E_e), and moisture can be added or

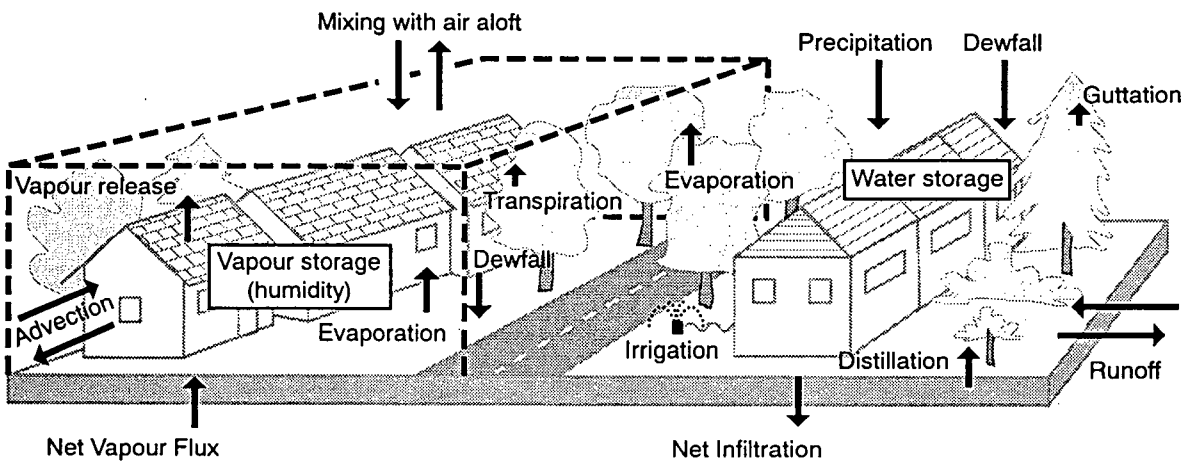

Figure 1.5 Schematic depiction of the component fluxes involved in the vapour budget of the air volume of an urban canopy layer, and the surface water balance of an urban three-dimensional surface.

removed from the surface by surface runoff (R), and infiltration into, or seepage from, underlying substrates (D). Transfers *through* this surface (anthropogenic vapour release and transpiration), and internal transfers (redistribution of pre-existing dew) are not included in the balance.

The balance for the substrate volume differs in detail from that for the three-dimensional surface in that, for the volume guttation and distillation are internal transfers (and are ignored), vapour loss occurs *via* transpiration (E_t), and moisture can be added to or removed from the volume by horizontal sub-surface drainage (D) and irrigation (I); that is:

$$\Delta S = P + C_f - E \pm R \pm D \pm I \qquad [1.5]$$

where E is evapotranspiration, and equals transpiration plus evaporation ($E_t + E_e$).

Processes of dew formation are closely connected to the state of near-surface humidity, because dew is a sink or source for atmospheric water vapour, through evaporation and condensation. At night, when winds are light and skies clear, the lower layers of the atmosphere become stable and dewfall has a significant effect on near-surface humidity, because vertical and horizontal transport of vapour is diminished and the air supply is replenished only slowly. At dawn, evaporation of dew (dewfall and distillation) into these stable layers increases the humidity, although this effect is diluted when the ground surface warms, near-surface air become unstable, and mixing through a deeper layer of the atmosphere occurs. Considering only the air component of the urban canopy layer, a humidity balance for its change of water vapour storage (ΔS) can be written (Figure 1.5):

$$\Delta S = E + F - C_f \pm A \pm M \pm V \qquad [1.6]$$

where inputs to the air layer are E and anthropogenic release of vapour (F). In the absence of fog, the sole output is dewfall (C_f). Moisture may be added or removed from the system by horizontal advection (A), mixing with air aloft (M), and any net flux of soil vapour (V). Since distillation and irrigation are, by definition, deposited on the surface promptly after they enter the atmosphere these are not included in this balance, except that water from distillation contributes to E.

1.2.4 Climatology of dew

Dew is a frequent event in many parts of the world. Its occurrence varies with climate, weather, substrate type, and site geometry. Some regions have climates which favour dew, such as humid areas of the USA, and a dew season can often be

identified, e.g., spring and/or fall for many mid-latitude locations. The presence or absence of dew is only quasi-predictable at time scales of a day, but on average its presence and amount correlate well with weather. *Heavy dew* often occurs on cool nights with clear skies, light winds and/or moist soil, i.e., when radiative cooling is promoted, vapour supply is not limiting, and wind speed lies within acceptable limits, i.e., about 0.5–3.0 m s^{-1} measured at about 2 m above the surface (Monteith, 1963; Garratt and Segal, 1988). The amount of dew that accumulates overnight can be comparable in magnitude to light rainfall. Heavy dewfall may involve 0.3–0.5 mm of water per night, whereas a light rainfall event may involve only 0.2 mm of water (Wisniewski, 1982). However, fluxes of dew are small compared to typical rates of evaporation and, after sunrise, dewy surfaces tend to dry rapidly.

At a given site, observed amounts of dew vary, depending on weather and substrate type, from a trace (0.01 mm) to very heavy (>0.50 mm) but, as discussed above, amounts rarely approach theoretical limits. In general, cooling is strongest for surfaces which are openly exposed to the radiative sink of the cold night sky, and for thin, elevated and unheated objects which have negligible heat storage or external heat fluxes (e.g., from soil or human sources). Thus, in general, good dewfall collectors are thin leaves or insulated roofs at open sites, whereas dew forms less frequently, in smaller amounts or not at all on sheltered undergrowth, warm pavements and heated walls. Dew is often a useful indicator of microclimatic conditions because its presence depends on temperature, humidity and wind conditions at the surface.

In cities, the potential active surface for dew is three-dimensional, consisting of an irregular mosaic of different materials (e.g., soil, leaves, and building materials), each with its own distinctive thermal characteristics. Equally important, patterns of intrinsic thermal behaviour by materials are modified by site geometry and juxtaposition of surfaces, so that, for example, advection and shelter are important. In addition, while cities tend to be warmer than rural areas at night, which tends to inhibit dewfall, they also have significant anthropogenic vapour release, which promotes dew formation. Taken together this means that, at the micro-scale, patterns of dew deposition are likely to be more complex in cities, compared to surfaces typical of rural areas (pasture or crops). At the meso-scale, an urban-rural difference might be anticipated in dew distribution and amount.

1.3 Thesis outline

1.3.1 Research objectives

There is growing interest in the study of urban dew, and its relevance is recognised in fields of research ranging from urban microclimate, to the deposition of pollutants from the lower atmosphere, and the subsequent chemical damage to built materials. Despite its relevance to many components of urban physical systems, the fundamental research needed to adequately describe and explain patterns of urban dew has largely been neglected. Data on dew in cities are rare. Urban dew is seldom measured and cannot be simulated with current numerical models of urban environments—even basic logistical questions concerning dew measurement are unresolved for cities.

The topic of urban dew does not exist as a coherent field of study. It was therefore decided that for the present research the best approach is, first, to address the topic of urban dew as a whole—this required a multi-disciplinary approach—and second, within this broad contextual framework to focus on several selected key issues. Thus, an extensive literature review was undertaken to build up a broad understanding of the dew phenomenon as a whole. This is presented in Chapter 2. Ultimately, the research objectives of the present study (given in this section) are drawn from the findings of the review, as summarised in Section 2.6.

The overall goals of this thesis are to investigate methods appropriate to measuring dew in urban environments, to implement these for a particular urban area, and to investigate the feasibility of modelling urban dew. The specific objectives are to:

1. design, construct and test instruments and other methods of dew measurement, appropriate for use in cities,
2. design and implement appropriate observation programmes to assess dew accumulation in cities on several scales by measuring dew, humidity and other climate variables at urban residential and park sites in Vancouver, and at rural sites,
3. assess the roles of location, weather, and substrate controls on the spatial and temporal patterns of dew in cities,
4. design, construct and test an out-of-doors scale model of a residential lot and urban park to model dew amount and pattern in a city at the micro-scale. This requires:

- establishing the theoretical basis of appropriate scaling laws,
- the design and construction of a hardware prototype, and
- validation using field observations,

5. develop an exploratory numerical model based on the physical processes of dew formation to simulate accumulation of dew on typical urban surfaces, and to validate it using field observations, and
6. develop a protocol for the assessment of dew in cities, based on the results of the above research.

1.3.2 Approaches

The specific objectives set out in Section 1.3.1 are implemented using: (a) an intensive observational programme, (b) detailed consideration of theoretical concerns relevant to scale modelling, and (c) hardware and numerical modelling. All field research was undertaken at selected sites in Vancouver and its rural surroundings. The observational programme consists of four main components, although these are not mutually exclusive:

1. instruments and other methods for measuring dew were field tested at urban sites,
2. dew data and/or accompanying climate data were measured at two urban residential sites and two park sites in Vancouver,
3. humidity and air temperature were measured along a transect route between a rural site and an urban residential site in the Vancouver area, and

4. synchronous measurements of dew and humidity were undertaken at the urban and rural end-points of the route described in 3.

Results of the observational programme are presented in Chapter 3. Field data were also used in the development, validation and/or operation of the scale and numerical models. The scale modelling programme consists of a theoretical investigation of topics relating to out-of-doors scale models (Chapter 4), a field trial during the summer of 1994, and the main model season during the summer of 1996. The scale model and results are presented in Chapters 5 and 6, respectively. Chapter 7 concerns the numerical model, its derivation and results. The main conclusions are summarised in Chapter 8. Formulae used in general data analysis are given in Appendix A1, and additional theoretical details of relevance to the numerical model are given in Appendix A2.

PART I CONTEXT

Chapter 2: Literature review

2.1 Introduction

Dew has obvious relevance to climatology and to the scientific study of surface-atmosphere processes. However, the accumulation of dew on outdoor surfaces has far broader implications in biophysical science, the fine arts, and many human activities. A review of publications concerning dew reveals a wide range of topics including, for example, dew's role as an environmental hazard to insects (Samways, 1989), dew chemistry and the deposition of atmospheric pollutants (Padro, 1994), and, even, dew as a medium for sculpture (see Section A3). A selected list of the implications is presented in Table 2.1.

The study of urban dew does not exist as a coherent field of research. Only rarely is the topic of urban dew mentioned in the literature. However, studies of urban environments and rural dew are numerous and, in theory, information from these studies can help to inform the development of a study of urban dew. In this chapter, the relationship between humanity, physical environments, and dew is explored in some detail to provide context for the study of urban dew and, more specifically, the research in this thesis.

Few publications deal with more than one or two aspects of dew, its measurement, and the implications of its presence. Here, Section 2.2 reviews methods to measure dew; Section 2.3 discusses aspects of the implication of dew as a climatic phenomenon; Section 2.4 addresses the urban physical environment of relevance to dew, and urban dew itself; in Section 2.5 consideration is given to

Table 2.1 Some implications of the presence of dew.

Optical Physics: creates dewbows, heligenschein, sylvanshine[1, 2]

Zoology: provides drinking water for insects, snails, birds, grazing animals; provides bathing water for birds; creates hazard for insects[3, 4, 5]

Botany: provides water for plants; acts as passive buffer to reduce transpiration; activates lichen metabolism [6, 9]

Plant pathology: permits infection of plants by fungal pathogens

Agricultural science: hinders efficiency of fungicides; delays harvest or reduces harvest quality; promotes mould; activates defoliants prior to cotton harvest; causes sunburn on fruit; causes bloating of cattle[12, 13, 29, 30]

Climatology: inhibits radiation fog; provides water for evaporation; alters energy partitioning and Bowen ratio; depletes near-surface humidity; reduces canopy resistance to evapotranspiration; delays morning warming[7, 8, 10, 11]

Geomorphology: enables chemical erosion of rock

Fine Arts and Religion: provides medium for sculpture; conveys meaning in poetry/prose; holds religious value; bestows holy halo (heligenschein)[1, 16, 17, 18]

Human water supply: potentially supplies drinking water or irrigation in dry climates/deserts; supplies soil water in 'cold-water' agriculture[5, 19, 20, 21, 22, 31, 32, 33]

Outdoor human activity: hampers fieldwork, mowing, trekking; reduces wildfire risk, hinders controlled burn-offs; promotes growth of algae on roofs, mildew on outdoor fabrics, rust on outdoor steel; obstructs morning performance of solar panels[15, 23, 24, 25]

Atmospheric pollutants: enhances deposition of pollutants from the atmosphere; facilitates chemical damage of plants and buildings[26, 27, 28]

Sources: 1. Corliss, 1984; 2. Fraser, 1994; 3. Samways, 1989; 4. Woodhouse, 1959; 5. Pereira, 1973; 6. McAneney *et al.*, 1992; 7. Pickering and Jiusto, 1978; 8. Landsberg, 1981; 9. Douglas, 1983; 10. Dirks, 1974; 11. Hage 1975; 12. Barr and Brown, 1995; 13. McCown and Wall, 1981; 14. Bourque and Arp, 1994; 15. Haines, 1979; 16. Anon., 1995; 17. Price, 1967; 18. Judges 6:37, The Bible; 19. Johnson, 1964; 20. Rajvanshi, 1981; 21. Anon., 1993; 22. Parks, 1996; 23. Sadler, 1996; 24. Salau and Lawson, 1986; 25. Haines, 1979; 26. Mulawa *et al.*, 1986; 27. Wagner *et al.*, 1992; 28. Wisniewski, 1982; 29. Myers, 1974; 30. Newton and Riley, 1964; 31. Nikolayev *et al.*, 1996; 32. Monteith, 1963; 33. Jumikis, 1965; and others.

the modelling of dew and/or urban environments by physical and numerical models; and a summary of topics of potential interest is given in Section 2.6.

2.2 Measurement of surface wetness and dew

Dew and surface wetness cannot be measured using regular weather station equipment and there is no standard method to measure these parameters. Dew measurement lacks universal protocols, such as those developed for weather observations (Rodda *et al.*, 1976), and, while in theory techniques used to measure evaporative fluxes can be used to measure condensation (dew), many standard micro-meteorological techniques (eddy correlation, flux-profile, and energy balance-Bowen ratio approaches) are unsuitable for measuring dew at night and in cities. The exception is lysimetry (described below), which can be used to measure the dewfall component of dew.

The vast majority of dew observations are undertaken in rural areas, where surface wetness has important economic implications, and, consequently, methods have been developed to assess surface wetness or dew on crops and pasture. Selected methods are reviewed by Nagel (1962), Noffsinger (1965), Wallin (1967) and, for the specific example of lysimeters, Grimmond *et al.* (1992) and Daamen *et al.* (1993). A comprehensive listing of methods to assess surface wetness or dew is given in Table 2.2. It illustrates the wide variety of approaches taken, ranging from simple, e.g., visual observation of wetness, to those requiring sophisticated electronic equipment such as wetness sensors and weighing lysimeters.

Table 2.2 Methods to measure or estimate dew or surface moisture status [A = primarily to assess amount, and B = duration of surface wetness].

Visual-Tactile[A, B]
Estimate using sight and/or touch (normally on vegetation)[1, 2, 3, 16]
Expose Duvdevani blocks and use calibration photographs[2, 3, 4, 9]

Drosometer or dew gauge[A]
Expose non-hygroscopic[1, 3, 7] or hygroscopic[3, 10] materials and weigh

Blotting (Parchinger's Method)[A]
Blot grassed surface[3, 5] or individual leaves[6, 7] and weigh paper

Mechanical recording gauge[A, B]
Record weight of element (aluminum, nylon mesh or polystyrene)[3, 8, 9]
Record change in length of element (gut, hemp or *Sellotape*)[3, 9]
Use colour intensity of dye on paper, or pencil trace on paper[3, 4, 9, 28]

Change in electrical resistance[B]
Expose electronic mock leaf (plastic, circuit board or cloth)[9, 16, 17, 18, 26, 30]
Use electrodes or grid in contact with leaves[5, 17, 18]

Volumetric measurement[A]
Collect drops, sweep water from vegetation, or clip wet leaves[11, 12, 6, 15]
Expose self-draining collector (aluminum, glass or plastic)[9]
Wipe dew from clean and inert plate (glass or teflon)[12, 13, 14]
Expose pre-moistened tension plate (tensiometer)[27]

Remote sensing (experimental techniques)[A, B]
Use canopy retroreflectance to assess dew intensity[15, 29]
Use infrared thermometry to time onset and drying of dew[25]

Lysimetry (dewfall only)[A, B]
Install lysimeter (>1 m width)[19, 20] or mini-lysimeter (<0.3 m width)[21, 22]
Use manually weighed micro-lysimeters (0.05–0.3 m width)[23, 24]

Sources: 1. Myers, 1974; 2. Haines, 1980; 3. Nagel, 1962; 4. Hsu and Sakanoue, 1980; 5. Collins, 1961; 6. Burrage, 1972; 7. Jacobs *et al.*, 1990, 1994; 8. Lloyd, 1961; 9. Noffsinger, 1965; 10. Wales-Smith, 1983; 11. Hughes and Brimblecombe, 1994; 12. Schroder *et al.*, 1989; 13. Wagner *et al.*, 1992; 14. Mulawa *et al.*, 1986; 15. Pinter, 1986; 16. Pedro, 1980; 17. Gillespie and Duan, 1987; 18. Weiss and Lukens, 1981; 19. Fritschen and Doraiswamy, 1973; 20. Sharma, 1976; 21. Grimmond *et al.*, 1992; 22. Spronken-Smith, 1994; 23. Butler, 1980; 24. Sudmeyer *et al.*, 1994; 25. Sadler, 1996; 26. van Eimern, 1985; 27. Chen and Novak, 1997; 28. Mattsson, 1962; 29. Mattsson and Cavallin, 1972; 30. Collins and Taylor, 1961; and others.

2.2.1 Methods to measure dew or surface wetness

A wide variety of methods exist to assess the presence/duration, relative intensity, and amount of dew and/or surface wetness (Table 2.2); where surface wetness can be from any source, including rain and guttation, but dew (dewfall + distillation) is solely from condensation. Visual assessment of the presence and/or amount of moisture is the least complex and the most subjective. It is included in many studies (Myers, 1974; Sudmeyer *et al.*, 1994) but the method has been shown to lack precision and, often, consistency (Nagel, 1962; Haines, 1980). Some standardisation is provided if dew amount is assessed on Duvdevani blocks, rather than on vegetation, since patterns of droplets on these painted wooden blocks are assessed using a standard set of calibrated photographs (Tuller and Chilton, 1973; McCowan and Wall, 1981; Chowdhury *et al.*, 1990), but the method has never become a universally accepted standard, as was once supposed (Haines, 1980).

Another simple approach is to expose a small artificial surface, or *drosometer* to measure dew amount. Many materials have been tested (Nagel, 1962; Myers, 1974; Wales-Smith, 1983), with poor results. The only drosometer in general use is the Leick plate, which is a non-hygroscopic porcelain disk (Jacobs *et al.*, 1994).

In 1918 Parchinger (see Nagel, 1962) suggested collecting dew directly from grass using blotting paper. Sheets of pre-weighed blotting paper are pressed onto wet leaves; the papers are then weighed to determine the mass of water absorbed. Blotting is a widely accepted method to assess moisture amount and has been used in several studies of dew on pasture (Sudmeyer *et al.*, 1994), mown lawn, (Collins, 1961), and crop leaves (Burrage, 1972; Jacobs *et al.*, 1994). For grass, 'hand-sized'

sheets (0.2 x 0.2 m) are commonly used. Papers can also be cut to fit individual leaves (Jacobs *et al.*, 1994). While blotting does not provide absolute amounts of water, because some droplets inevitably escape capture, blotting remains the best method to assess the total amount of surface moisture present on grass or leaves (Angus, 1958; Slatyer and McIlroy, 1961; Nagel, 1962; Sudmeyer *et al.*, 1994). It is expected that errors in this method will, for the most part, cause surface wetness to be under-recorded. Although difficult to test or quantify, in the published literature it is assumed that for grass errors are systematic, and spatial and temporal trends are conserved (Monteith, 1957; Collins, 1961; Sudmeyer *et al.*, 1994).

During the 1950s and 1960s, numerous mechanical gauges were designed which provided continuous data for surface wetness amount, normally recorded on a paper trace (see review in Noffsinger, 1965). All the devices are relatively bulky, difficult to calibrate, and not very accurate, and no one gauge is universally accepted.

The development of reliable electronic wetness sensors in the 1970s and 1980s provided a dependable and convenient method to continuously monitor the duration of leaf wetness (Mintah, 1977; Pedro, 1980; Gillespie and Duan, 1987). A wetness sensor consists of two sets of fine parallel wires mounted on a flat or cylindrical frame; the latter comprised of a wettable material, e.g., cloth, painted plastic, or a leaf. When the sensor is wet, the change in the surface resistance of the sensor is read electronically, and output is calibrated to delimit wet *vs* dry surface states. Wetness sensors of varying design and sensitivity have been used by several researchers in cities (Spronken-Smith, 1994) and in agriculture, in the

latter case, to forecast wetness-associated diseases of crops (Haines, 1980; Richards, 1991; Hoogenboom, 1996). Although sensors require a data logger (electronic microprocessor) to be read, they are simple to construct, cheap to replicate, and their sensitivity can be altered easily by changing materials or surface treatments. In addition, techniques are transferable to challenging locations and built surfaces, e.g., sensors can be miniaturised and glued to the ceilings of storage buildings, to monitor condensation (Campbell, *pers. comm.*, 1994). In some studies, amount of surface moisture is inferred from its duration, however, calibration can be difficult, and even wet *vs* dry data have to be interpreted carefully, e.g., in vegetation canopies, where leaves dry at different times.

In recent decades, interest has grown in the chemical composition of dew (see Section 2.4.4), and several methods are used to collect dew for chemical analysis. Often dew collection is from a flat surface of glass or teflon (Wagner *et al.*, 1992; Schroder *et al.*, 1989; Janssen and Römer, 1991), and sometimes, if natural dew is absent, condensation is induced using cooling coils (Mulawa *et al.*, 1986).

Dew accumulates on leaves when their surface temperature is at or below dew point temperature, so remotely sensed leaf temperature can be used to time the onset and drying of dew, when near-surface humidity is known (Sadler, 1996). Further, dew often forms spheroidal drops on vegetation. This increases canopy reflectance in the visible wavelengths so, potentially, *retroreflection* (reflection of incident light toward the light source) can also be used to assess relative amounts of dew. Pinter (1986) tested this for wheat, with promising results, and Mattsson (1971; 1979; *et al.*, 1972) used retroreflectance from dewy grass to map dew

intensity around a variety of objects. Techniques are largely experimental, however remote sensing holds great potential for the rapid sampling of spatial and temporal distributions in complex environments (e.g., cities) with minimal site disturbance.

2.2.2 Methods to measure dewfall

Often a researcher is more interested in the amount of moisture transferred from the lower atmosphere (dewfall) than in total amounts of surface wetness from both condensation (dew) and other sources (guttation). In such cases individual fluxes must be differentiated. One method to monitor dewfall directly is lysimetry. In its broadest definition, a lysimeter consists of an appropriately-sized and representative portion of the surface of interest, which can be weighed. The sides and base of the lysimeter are sealed. In the absence of rain and irrigation, changes in mass can then be attributed to fluxes of water to and from the atmosphere, i.e., evaporation and dewfall, respectively. In some cases drainage also needs to be allowed for and measured.

The sophistication, size and design of lysimeters, and the means used to assess their mass, vary greatly (Grimmond *et al.*, 1992; Daamen *et al.*, 1993). The accuracy of a lysimeter depends on how well conditions within the lysimeter mimic those in the surrounding undisturbed surface, normally of soil and vegetation (Slatyer and McIlroy, 1961; Grimmond *et al.*, 1992). To be useful for dewfall measurements, a lysimeter requires an operational resolution of the order of 0.005–0.01 mm equivalent depth of water ($Q_E \approx 3$–7 W m^{-2}). This precision is approached by some of the larger lysimeters installed to monitor rates of evaporation from mown

grass (Brooks and Pruitt, 1966), pasture (Sharma, 1976), and even trees (Fritschen and Doraiswamy, 1973; Oke, 1987).

Lysimeters of smaller size—mini-lysimeters—can also have sufficient resolution to measure dew, provided they possess an appropriately sensitive weighing mechanism and sufficient surface area. For example, if a weighing mechanism has an operational accuracy of 1 g, change in mass can be resolved to 0.01 mm for lysimeters having a surface area of 0.10 m^2, and to 0.005 mm for those with surface areas of 0.20 m^2. Provided they fulfill sensitivity requirements, electronically weighed mini-lysimeters (<1 m diameter) are significantly cheaper and easier to install compared to full size hydraulic lysimeters, and can be installed in patchy environments such as cities (Spronken-Smith, 1994). The useful lifespan of a mini-lysimeter tends to be short, typically of the order of a week. This is because when the monolith dries out (or is flooded by rain) its temperature and moisture characteristics become unrepresentative of its undisturbed surroundings.

Finally, micro-lysimeters are essentially those which are weighed manually and are diminutive (<30 cm) in size, but this classification is not immutable. In several studies of evaporation rates, micro-lysimeters of about 0.05–0.3 m in width and 0.1–0.15 m in depth are used (Nunez, 1974; Daamen *et al.*, 1993; Plauborg, 1995). Micro-lysimeters have been used in bare soil (Daamen *et al.*, 1993; Plauborg, 1995; Ari *et al.*, 1998) and, less commonly, in rural grassland (Sudmeyer *et al.*, 1994), urban lawn (Oke, 1979), and urban gravelled surfaces (Nunez, 1974). Micro-lysimeters in soil have shorter lifespans compared to mini-lysimeters (1–5 days). On the other hand, the techniques used in micro-lysimetry are flexible, and

can be used to determine the amount of dewfall on discrete objects, which are detached for weighing, and then dried and reweighed, e.g., cocoa pods, plant shoots and leaves (Slatyer and McIlroy, 1961; Butler, 1980). Micro-lysimetry has potential for use with built materials, and to sense in challenging locations such as pavement, roofs or walls. To date, techniques have been almost entirely confined to natural and/or horizontal surfaces.

2.2.3 Implementation of measurement methods

Many methods theoretically measure the amount of moisture deposited overnight, but not all measure the same physical phenomenon, or perform consistently. For example, visual techniques assess the total amount of moisture present but are often unreliable; electronic wetness sensors are technically sophisticated, reliable and need minimal maintenance, but give no direct information on dew amount; and mini-lysimeters, while reliable, register dewfall but not distillation.

The methods chosen for any study reflect the needs of the user, whether dewfall, dew (condensation) or surface wetness is required, as well as practicalities, i.e., cost and maintenance. Commonly two or more methods are employed together to assess, say, surface wetness duration and dewfall, or to provide corroboration for data. Visual observation, mechanical dew gauges and Duvdevani blocks are popular choices for simple studies where an index of dew intensity suffices. However, in more rigorous research, blotting, electronic wetness sensors and lysimetry are favoured. The latter three methods were chosen to assess surface moisture and its component fluxes in the present study (see Chapter 3).

Dew distribution at rural sites (pasture and crops) can often be adequately sampled at a single point because vertical variation in the amount of water on leaves exceeds horizontal variability (Jacobs *et al.*, 1994). However, in cities the physical system (materials and geometry) is complex, three-dimensional, and consists of irregular mosaics of different surface types. Each type of surface material has its own distinctive radiative, thermal and hydrological characteristics and, of equal importance, patterns of intrinsic behaviour are overlaid by patterns caused by geometric configuration and juxtaposition. All observational programmes conducted in cities to measure climate related parameters need to address site complexities and practical logistics. Difficulties are magnified, however, when the parameter of interest (dew) cannot be measured using standard meteorological methods. For this reason, measuring dew in cities is difficult for all but the most simple site.

2.3 Dew as a climatic phenomenon

As illustrated in Table 2.1, the presence of dew is linked to many possible topics of study in the natural and applied sciences. Topics which deal with dew and surface wetness as a climatic phenomenon are of interest in the present study, i.e., controls on the distribution of dew and links between dew and plants.

2.3.1 Controls on the distribution of dew

The presence of dew, and how much water accumulates overnight, is greatly dependent on weather conditions. Therefore, not surprisingly, a review of the

literature shows that many observational studies correlate dew behaviour with local climate or weather (Table 2.3 and Chapter 1). Meso-scale studies of the spatial distribution of dew are not common. Observational studies range from spatial surveys at contrasting elevations or locations (Marlatt, 1971) to statistical analyses of dew characteristics for a single site (Baier, 1966). Medium-term temporal studies,

Table 2.3 Examples of observational studies of dew which focus on climate or weather controls [A = primarily temporal, and B = primarily spatial].

Author	*Year*	*Location and/or topic of study*
Meso-scale relationships		
• *Role of climate, season and regional location*		
Padmanabhamurty and Subrahmanyam[A]	1960	Waltair, India
Baier[A]	1966	Potchefstroom, South Africa
Tuller and Chilton[A]	1973	Victoria, BC
Sharma[A]	1976	Deniliquin, NSW
Pindják[A, B]	1980	Bratislava, Czechoslovakia[1]
Wales-Smith[A]	1983	Akrotiri, Cyprus
Salau and Lawson[A]	1986	Port Hartcourt, Nigeria
Buiuc[A, B]	1990	Romania; time-of-year, location
Chowdhury *et al.*[A, B]	1990	India; time-of-year, location
Cuesta *et al.*[A]	1990	Casablanca, Cuba.
Malek[A]	1998	Nevada, USA
Micro-scale relationships		
• *Environmental controls on dew*		
Steubing	1952	Wind shelter
van Eimern	1953/54	Wind shelter
Lloyd[A, B]	1961	Time-of-year, site geometry
Marlatt[B]	1971	Topographic elevation
Mattsson[B]	1971	Rural/woodland geometry, wind shelter
Jacobs *et al.*[B]	1998	Dune geometry, shading
• *Role of dew in microclimate*		
Landsberg	1981	Radiative cooling of grass
Pickering and Jiusto	1978	Radiation fog and dew

1. Research undertaken in the former Czechoslovakia.

consisting of daily data over several seasons or years, are well represented. Only in rare cases is there a macro-scale monitoring network giving long-term records of dew and weather at many sites (Chowdhury *et al.*, 1990; Buiuc, 1990).

In addition to the overview of dew patterns and processes in Chapter 1, several further generalisations can be drawn from medium-term temporal surveys. Dew is strongly governed by regional, seasonal and annual variations in characteristic weather patterns and climate. For example, Tuller and Chilton (1973), working in the summer-dry climate of Victoria, British Columbia, found that during summer months dewfall (2–3 mm per month) normally amounted to 2–14% of rainfall and 2–4% of potential evaporation. In dry years, however, dewfall could exceed rainfall, and amounts equivalent to 154% of monthly rainfall were measured.

At the micro-scale, field data indicate that ambient microclimatic conditions govern patterns of dew deposition. In turn, the formation of dew, and its drying, affect the energy and water budgets of surfaces and the lowest layer of air. Correlations between dew and near-surface humidity, and dew and surface temperature are easily apparent. When dew forms near-surface humidity is depleted, and when dew evaporates vapour is added to the atmosphere. Dew forms when surfaces cool to the dew-point temperature, but during condensation latent heat energy is released, temporarily increasing surface temperature (Landsberg, 1981; Sadler, 1996). Other relationships have been investigated, e.g., Pickering and Jiusto (1978) present field evidence showing that formation of dewfall inhibits, and is inhibited by, the formation of radiation fog. When water vapour close to the ground is directed into condensation on surfaces (dewfall) or in the air (fog),

conditions which favour one will hinder the other. By contrast, surface moisture (water from all sources) is enhanced when near-surface fog is present and air is in motion, because fog droplets contribute to surface wetness when they accumulate on exposed objects.

Relatively few studies of microclimate and dew have been undertaken in patchy landscapes or locations where site geometry is a significant factor. Studies in forest clearings, and near hedges and shelterbelts indicate that, while the maximum amount of dew deposited on any particular night is largely a function of weather, the site geometry (expressed by Ψ_{sky} or H:W) is an important control on the spatial distributions. On nights favourable for dew, more surface moisture accumulates at sites which are exposed to the radiative sink of the cold night sky, compared to sites where objects (trees and hedges) partially obscure the sky view. With moderate wind speed, view factor controls on radiative cooling are weakened and dew deposition is governed, in part, by shelter. Then, more dew is deposited in the lee of trees and hedges where wind speeds are reduced, and it is less or absent at unsheltered sites (Steubing, 1952; van Eimern, 1953/54; Lloyd, 1961; Mattsson, 1971, 1979). After sunrise, surface geometry affects shading patterns and thus dew persistence, e.g., on desert sand dunes (Jacobs *et al.*, 1998).

To illustrate, Lloyd (1961) found that about 50% less dew fell at the centre of large clearings (H:W = 0.5) in pine forest, compared to nearby open meadows. No dew occurred in small gaps (H:W = 2), under closed canopy, or on top of the pine canopy. Mattsson (1971; 1979) investigated spatial distributions of dew at the edge of a wood (Figure 2.1), in a woodland clearing (Figure 2.2), and in fields with

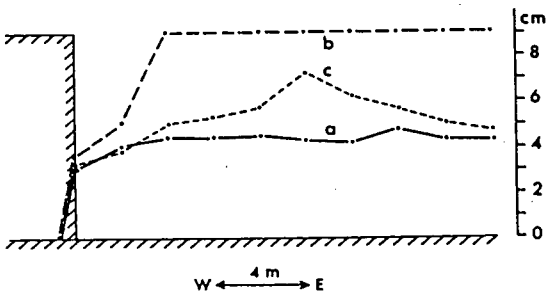

Figure 2.1 Schematic cross-section showing dew accumulation along a transect from the edge of a wood (the left hand side) to a more open area (right hand side) on three nights (a, b and c) with contrasting weather. Data are the relative intensity of wetting measured using paper 'dew rolls' (see Mattsson, 1962) and have the arbitrary units cm. *Source*: Mattsson (1971).

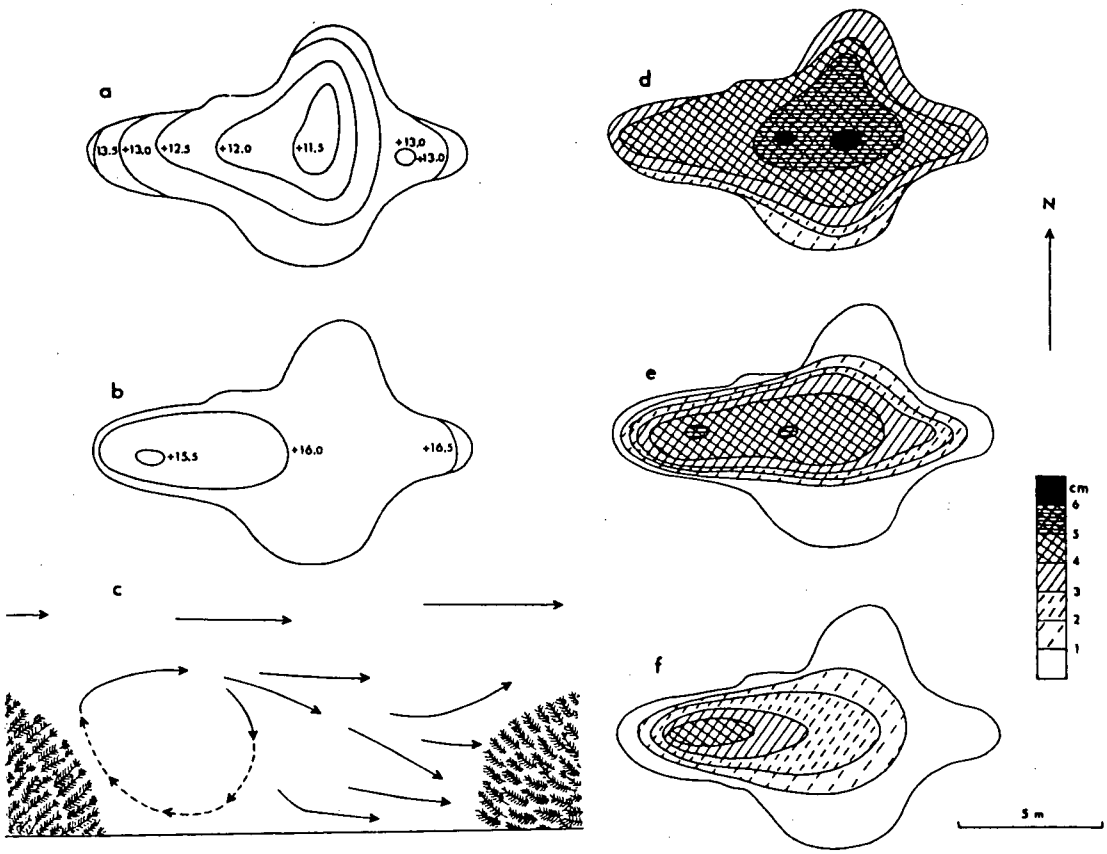

Figure 2.2 Observed spatial patterns in a forest clearing. (a) and (b) depict near-surface air temperature (°C) during calm and strong winds, respectively. (d), (e) and (f) show dew data during conditions of light, moderate and strong winds, respectively. (c) is a schematic cross-section depicting air flow during strong winds. (see Figure 2.1 for an explanation of the units of dew measurement). *Source*: Mattsson (1979).

hedges and shelter belts. Observations show that proximity to objects (trees and hedges), surface temperature, and wind shelter are significant controls on the observed amount of dew. Maximum amounts of dew tended to occur away from hedges and trees (Figures 2.1 and 2.2). On nights with light winds (Figure 2.2a, d) more dew was seen at the centre of the clearing, compared to close to trees where the surface was warmer. When wind speeds were moderate or strong (Figure 2.2b–c, e–f) more dew was deposited at sheltered locations.

Defining the links between weather, site geometry, and dew is further complicated by guttation, which occurs on many common plants, including lawn grasses. Although not dew, guttation is of concern in the present study. There are several reasons for this: on nights with dew, up to 50% of surface moisture may be guttation; estimates of surface moisture based on latent heat flux calculations cannot account for water from guttation, because a phase change is absent; and not all methods to measure surface moisture sense guttation (Section 2.2). Guttation occurs when the rate of water supply from the roots exceeds loss by transpiration. The general consensus is that the rate of guttation is a function of soil moisture and near-surface (-0.1 m) soil temperature, but the linking mechanisms are uncertain. Studies of guttation are rare. Hughes and Brimblecombe (1994), measuring dew- and guttation-drops on grass, showed that on average overnight totals of water from guttation and dew may be of similar magnitude; about 0.10 and 0.14 mm, respectively. However, the actual amount of guttation remaining on blades at dawn is relatively small (~0.02 mm), because pores exude several drops per night, and most of these fall to the ground. Hughes and Brimblecombe conclude that the

contribution of guttation to total surface wetness (leaves and soil) should not be neglected, especially for grass, but this view is not prevalent in the literature.

2.3.2 Dew and plants

In semi-arid climates, where rain is infrequent, dew is a significant source of moisture for plants. On the other hand, in moist climates plants are vulnerable to diseases which thrive on wet leaves. Hence dew monitoring or forecasting can be beneficial for vulnerable and valuable plants. Extensive reviews of these topics are given by Wallin (1967), Myers (1974), and Huber and Gillespie (1992). A list of observational studies is given in Table 2.4.

Several generalisations can be drawn from these studies. Dewfall is commonly only a small input to soil moisture and distillation, when present, depletes the soil water budget. Some species absorb dew directly through their leaves (e.g., Mesambrianthenum cristallinum; Salau and Lawson, 1986), however, the main beneficial role of dew is passive, inasmuch as water loss by evapotranspiration is buffered whenever leaves are wetted by dewfall (Kerr and Beardsell, 1975; Sharma, 1976; McAneney *et al.*, 1992). In arid areas and during drought, dew can exceed rain in amount, frequency and/or number of wetness hours, or be the sole source of liquid water for plants (Tuller and Chilton, 1973; Haines, 1979; Hicks, 1981; Chowdhury *et al.*, 1990; Jacobs *et al.*, 1998). In deserts, radiative cooling is strong after sunset because skies are typically clear. Hence, dewfall may be heavy in coastal deserts when relatively moist maritime air is advected over the land (Mooney *et al.*, 1980; Moomen and Barney, 1981; Subramaniam and Kesava Rao,

Table 2.4 Examples of observational studies of dew which focus on plant-soil-atmosphere relationships.

Author	*Year*	*Topic of study*
Bare soil		
Budagovskii and Nasonova	1991	Dew and soil water budgets
Heusinkveld *et al.*	1998	Dew in the Negev desert
Pasture and Rangeland		
Brooks and Pruitt	1966	Èvaporation from mown grass
Kerr and Beardsell	1975	Water status of pasture
Sharma	1976	Dew on semi-arid grassland
Hicks	1981	Micrometeorology at Wangara
McCown and Wall	1981	Dew and mould on standing hay
Sudmeyer *et al.*	1994	Dewfall on pasture
Crops and Orchards		
Burrage	1972	Dew on wheat
Pinter	1986	Dew and canopy reflectance
Jacobs *et al.*	1990	Dew on maize
McAneney *et al.*	1992	Evaporation in kiwifruit orchards
Wittich	1995	Dew in an orchard canopy
Forest		
Fritschen and Doraiswamy	1973	Water balance of a fir tree
van Eimern	1985	Leaf wetness in a beech forest
Dröscher *et al.*	1989	Dew and fog in forest stands
Skvarenina and Mindas	1998	Dew chemistry in forests

1983; Budagovskii and Nasonova, 1991; Jacobs et al., 1998).

Frequent and persistent dew can be detrimental to plants, because many fungal and bacterial pathogens release spores and infect nearby plants when wetted. Dew reduces the efficiency of some fungicides and, since many crops are damaged if harvested wet, this leads to delay in harvesting (McCown and Wall, 1981; Barr and Brown, 1995). For example, cotton fibres are damaged if harvested when wet with dew, and wetting promotes fungal disease. However, dew is required

to activate defoliants applied to the canopy of cotton before harvest (Newton and Riley, 1964; Myers, 1974). Thus, dew is monitored closely in cotton growing regions such as southeastern USA, where a regional network of electronic wetness sensors is installed (Getz, 1978; Garrard and Griffiths, 1996; Getz and Harker, 1996). Similarly, in market gardens, and in ornamental gardens in cities and their rural surroundings, observations of dew events are used to gauge the time for application of fungicide. Forests are also at risk; for example, Lloyd (1961) correlated the inhomogeneous spatial patterns of dew in pine forests (see Section 2.3.1) with the distribution of blister rust disease (*Cronartium ribicola*).

2.4 Urban environments and dew

Surface wetness is often overlooked in cities, however, Table 2.1 and Chapter 1 suggest several possible topics of study which could be of value and interest in an urban setting. These include urban temperature, wind speed, and humidity fields, urban dew itself, and links between dew and the deposition of pollutants from the lower atmosphere.

2.4.1 Urban temperature and wind fields

When humidity is not limiting, temperature is a fundamental control on the rate of dew accumulation because condensation forms only when surfaces are at or below dew-point. Observational studies show that cities cool relatively slowly after sunset, and at night are often warmer than surrounding rural areas, at the surface and in the UCL. This temperature differential is known as the *urban heat island* (UHI). Its

magnitude (excess or deficit) is often described using an urban-rural difference, ΔT_{U-R}, where 'urban' temperature is commonly measured 'downtown', in the central business district of the city. Reasons for this phenomenon are discussed in Oke (1982). Factors include increased heat storage, anthropogenic heat release, radiation trapping, and increased fluxes of sensible heat, as opposed to latent heat, in cities compared to rural areas.

Meso-scale patterns of near-surface (1–2 m) air temperature have been well documented for several mid-latitude cities, using data collected at fixed sites and mobile vehicle surveys. Observed patterns follow similar spatial and temporal trends. In Vancouver, as in other cities, meso-scale spatial differences in the UCL are small during windy and/or cloudy weather, when regional conditions dominate. In summer, during day, there is often only a small near-surface urban-rural temperature difference (±1°C), in all weather conditions. At night, under conditions of clear skies and light winds, a significant (≤10°C) temperature differential may develop between downtown Vancouver and agricultural rural sites, with a 'cliff' at the major urban-rural boundary (Figure 2.3). Cool temperatures correlate with rural land-use and urban parks, urban residential areas tend to be relatively warm, and

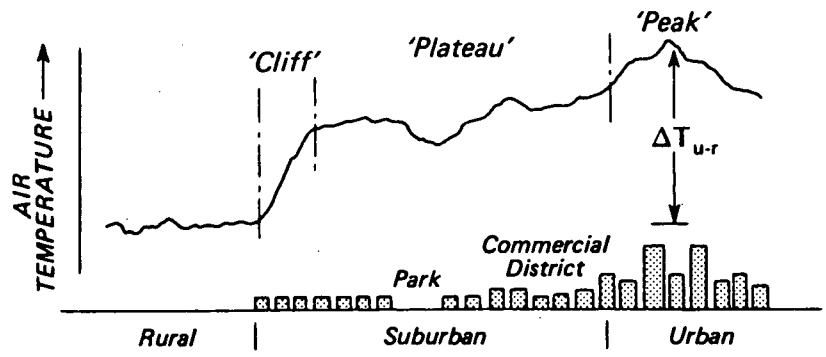

Figure 2.3 Generalised cross-section of an urban heat island for a North American, mid-latitude city during clear and calm nocturnal weather. *Source:* Oke (1987).

the warmest sites (outside of the downtown urban core) are commercial and/or industrial areas (Oke and Maxwell, 1975; Runnalls, 1995).

Urban effects on surface temperature have also been described for several cities, including Vancouver, using data from satellite images, aircraft-mounted thermal imaging systems, and land-based surveys (Roth *et al.*, 1989; Eliasson, 1992; Spronken-Smith, 1994; Voogt, 1995). During fine summer weather, studies show that nocturnal surface temperature varies as a function of meso- and local/micro-scale location, surface materials and site geometry (H:W and Ψ_{sky}). The intrinsic thermal properties, heat storage capacity, and external heat fluxes (Q_G or Q_F) to and from an object are important controls on surface temperature but, for any given material, the warmest sites are those sheltered from the radiative heat sink of the cold night sky by buildings and trees. Eliasson (1990/91; 1992), working in central Göteburg, Sweden, during clear calm nights, found a statistically significant, inverse correlation between nocturnal surface temperature and Ψ_{sky}, i.e., temperatures measured between buildings (small Ψ_{sky}) were higher than those sensed in open squares and urban parks (large Ψ_{sky}). Spronken-Smith (1994) studied temperature patterns in residential areas of Vancouver during fine summer weather. Field surveys and subsequent scale-modelling (Section 2.5.1) showed that open grassed parks, isolated tree-tops, and well-insulated roofs cool rapidly after sunset, because of strong radiative heat loss (Spronken-Smith, 1994).

Urban areas are characterised by a relatively complicated mix of bluff bodies (buildings and trees) and open spaces (streets and parks), and this produces a complex wind field. The speed and direction of flow depends on regional conditions

and the nature of the surface, especially building shape, orientation and spacing. Wind speeds in the urban canopy layer are generally less, compared to those measured in the open countryside, at the same height, because the roughness of the city surface slows regional wind speeds. When regional winds are very light, air between buildings may stagnate, trapping water vapour and air pollutants below roof level. However, when winds aloft are stronger, air is deflected down the face of taller buildings, around corners, or along street canyons, so increasing wind speed at street level in certain areas. At the same time, in the lee of buildings, some sites may enjoy relative calm (Oke, 1987).

2.4.2 Urban humidity

As theory dictates (Chapter 1), near-surface humidity is closely associated with rates of deposition and evaporation of dew. The effects of cities on humidity are reviewed by Oke (1979), Landsberg (1981) and Atkinson (1985). Comprehensive studies of near-surface humidity have been conducted in several mid-latitude cities (Table 2.5). Very little corresponding humidity data exist for cities in deserts or the tropics, e.g., Oke, *et al.* (1998) show that urban-rural differences in naturally arid areas are strongly governed by irrigation. Several generalisations can be made from the studies conducted in mid-latitude cities. During fine summer weather several studies report an absolute deficit of atmospheric moisture in the urban canopy layer during daytime, compared to values in the surrounding countryside. On summer nights, and at all times of day during winter, absolute excesses of humidity have

Table 2.5 Observational studies of urban humidity which provide data on the absolute moisture content of air. Results from urban-rural comparisons contained in these studies are summarised using: SDD = warm season (summer) daytime urban deficit; SNX = warm season (summer) nighttime urban excess; WDX = cold season (winter) daytime urban excess; WNX = cold season (winter) nighttime urban excess; NX = nighttime excess; and D = deficit.

Author	*Year*	*City*	*Observed urban effect on humidity*				
			Summer reversal		*Winter excess*		*Other*
Humidity in the urban canopy layer							
Kratzer	1956	Munich	SDD		WDX		
Chandler	1967	Leicester					NX
Landsberg and Maisel	1972	Columbia					D
Kopec	1973	Chapel Hill	SDD	SNX			
Dirks	1974	St. Louis	SDD				
Goldreich	1974	Johannesburg	SDD	SNX	WDX	WNX	
Hage	1975	Edmonton	SDD	SNX	WDX	WNX	
Hilberg	1978	St. Louis	SDD	SNX			
Ackerman	1987	Chicago	SDD	SNX	WDX	WNX	
Lee	1991	London	SDD	SNX	WDX	WNX	
Eliasson and Holmer	1996	Göteborg	SDD	SNX	WDX	WNX	
Oke, *et al.*	1998	Sacramento	SDD	SNX			
		Sacramento[1]		SNX			SDX
		Tucson[1]		SNX			SDX
Humidity in the urban boundary layer							
Bornstein *et al.*	1972	New York					SDX
Dirks	1974	St. Louis	SDD				
Dzurisin	1978	St. Louis	SDD				
Shea and Auer	1978	St. Louis	SDD				
Sisterson and Dirks	1978	St. Louis	SDD				

1. For a desert rural site.

been observed. During periods with strong winds, overcast skies, or rain, regional conditions dominate and urban-rural differences weaken or disappear.

These observed features have been attributed to several causes including, in part, meso-scale patterns of dewfall (see Table 2.6). Daytime contrasts are primarily attributed to differences in urban and rural evapotranspiration. Cities are often

Table 2.6 Hypothesised causes for patterns of humidity observed in the urban canopy layer of mid-latitude cities.

Summer daytime deficit in urban humidity

- *Enhanced mixing of dry air from aloft in city*
  Urban surface relatively rough and warm

- *Reduced evapotranspiration in city*
  Less open water, vegetation, soil moisture sources
  Sealed artificial surfaces are dry
  Rapid removal of precipitation by drains

- *Absence of evaporation of dew during morning hours*
  Dewfall inhibited by nocturnal urban heat island

Summer nighttime excess in urban humidity

- *Reduced depletion by dewfall in city*
  Dewfall inhibited by nocturnal urban heat island

- *Stagnation of near-surface air*
  Narrow canyon geometry in city

- *Nighttime evapotranspiration*
  Evaporation persists in nocturnal urban heat island

- *Nocturnal anthropogenic water release in city*
  Space heating, industry, vehicles

- *Enhanced mixing of moist air from aloft*
  Urban surface relatively rough and warm

Winter excess in urban humidity

- *Increased anthropogenic vapour release in city*
  Seasonal combustion, space heating, vehicle use

- *Enhanced mixing of moist air from aloft in city*
  Urban surface relatively rough and warm

- *Reduced evapotranspiration in surrounding countryside*
  Dormant vegetation, frozen soil, snow cover

described as relatively dry and lacking in sources of moisture for evapotranspiration (soil, vegetation, bodies of water) compared to rural areas (Table 2.6). In addition, it is commonly held that dew is reduced or absent in cities compared to their surrounding environs, and so cannot contribute to evaporation in cities during the morning hours.

The nocturnal humidity excess in the urban canopy layer, which has been observed in several cities, is attributed to several factors, including a lack of urban dew. When winds are light, narrow canyon geometry favours stagnation of surface air, and this traps vapour near the surface and increases canopy layer humidity. At the same time, urban dewfall is thought to be inhibited by the relatively higher nocturnal temperature associated to the urban heat island, which may even be responsible for continued evapotranspiration at night, thus adding to the urban humidity.

These suppositions may be reasonable for limited areas, but it is misleading to characterise the city surface as entirely lacking in sources of water for evapotranspiration and dewfall. Most mid-latitude cities possess lakes or rivers and substantial areas of vegetation. After rain or irrigation, water absorbed by or deposited on building materials and urban vegetation is a source of water for evapotranspiration (Oke, 1974; Douglas, 1983; Hall and Kalimeris, 1984; Cleugh and Oke, 1986; Grimmond, 1988). Urban gardens and lawns are often vigorously irrigated, so human intervention in the water budget is significant (Grimmond, 1983; Grimmond and Oke, 1991). Hence, while the latent heat flux is often less in a city (Cleugh and Oke, 1986), typically it still utilises 0.25–0.50 of the net radiation in

North American cities (Grimmond and Oke, 1995). In addition, anthropogenic sources of water vapour (industrial cooling, space heating and vehicle emissions) are concentrated in cities. Taken together these sources mean vapour input to the atmosphere of cities may be of significant magnitude and cannot be neglected. It is known that dewfall occurs under some conditions in cities and, when present, contributes to urban evaporation rates during the morning hours (Spronken-Smith, 1994; Grimmond and Oke, 1995). However, direct data are not often available to confirm this source (Cleugh and Oke, 1986).

Hage (1975), working in Edmonton, observed urban-rural differences in humidity during fine summer weather (Figure 2.4) and during winter. At nighttime during summer, rural humidity declined while urban humidity was stable. The result was a relative excess of humidity in the city. After sunrise, humidity at the rural site increased rapidly and a relative deficit in urban humidity resulted. Hage attributed these patterns, in part, to greater depletion by dewfall in the cooler rural area by night, and greater evaporation of dewfall in the countryside after dawn, compared to the relatively dry urban surface. However, dewfall was not measured.

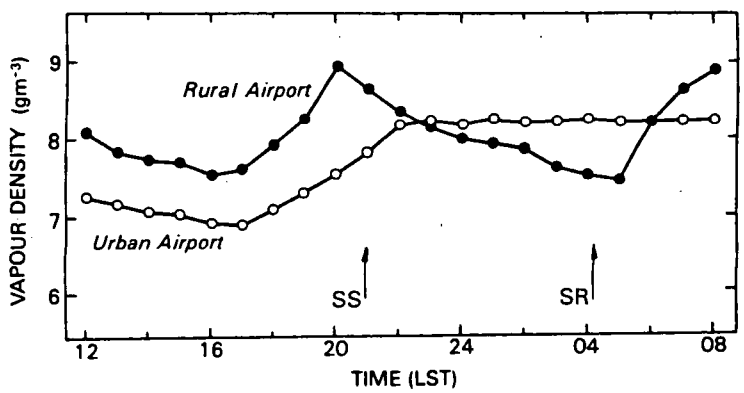

Figure 2.4 Urban effects on humidity in Edmonton, showing hourly variation of vapour density (ρ_v) at urban and rural stations during 30 cloudless summer days where SS = sunset and SR = sunrise. *Source:* Oke (1987), from Hage (1975).

Ackerman (1987), working in Chicago, observed that although at any particular time urban humidity can be greater or less than rural humidity, statistical patterns are present in averaged data. Several observations at a rural site showed a moisture inversion at night, i.e., an increase in humidity with height above the ground. At these times, rural humidity was less than in the city, and it was inferred that dewfall depleted humidity in the lower atmosphere at the rural site. Again, no dewfall data were measured in the study.

There are some similar data for Vancouver. Spronken-Smith (1994) showed that, during fine summer weather, absolute humidity in an urban park in Vancouver exceeded that seen at a rural site during night, but was similar to or less than rural values by day (Spronken-Smith, *unpubl.*). On most mornings, observations show that dew was present until noon in the urban park. Observations summarised by Oke, *et al.* (1998) show that in Vancouver during summer urban-rural differences in humidity are small and change sign often, and they suggest this may reflect the coastal location.

2.4.3 Urban dew

Dew in cities is much less well understood than urban temperatures or dew on rural crops. The study of urban dew has largely been neglected, despite the several observational studies of urban humidity noted above which invoke its difference from rural values. It is not possible to conduct a large scale field experiment to observe the true effect of urbanisation on climatic phenomena such as dew. To paraphrase Lowry (1988): one would need to be able to compare the dew observed

in a city with what would have been observed if the city were not present at the same point on the landscape. The alternative is to compare synchronous observations in an existing city and at a location in its rural surroundings, i.e., urban-rural differences. This approach has two important implications. First, it means that the nature of the surrounding countryside is as important as the nature of the city in generating differences. Second, in all but the most simple landscapes (e.g., an extensive and homogeneous plain) urban-rural contrasts may be created by differences in urban and rural topography, elevation, or proximity to large bodies of water. This can lead to difficulties in identifying and interpreting urban effects.

For a given region, dew, like humidity, reflects the regional climate, time of year, and human influences. However, there is little dew data available to compare cities with their rural surroundings, the only comprehensive observational study being that of Myers (1974), described below. Despite this lack of work, there seems to be a general consensus that dew is absent, reduced or delayed in cities, compared to their rural surroundings. Although this is largely unproven, reasons hypothesised to explain such a pattern have been forwarded (Table 2.7). The urban surface is a relatively convoluted surface composed of a wide range of materials, and this produces a complex set of temperature, moisture and wind fields. Hence, it is suggested that dew distribution in cities has a unique complexity compared to rural areas. My field observations (Chapter 3) support this statement.

At night in fine weather, warmer surface temperatures in cities may prevent or delay the onset of dew. At the micro-scale, urban areas seem to offer few sites favourable for dewfall compared to the vegetation in the countryside, since buildings

Table 2.7 Reasons hypothesised in the literature for reduced urban dew.

Warmer air and surface temperatures
Nocturnal urban heat island
Reduced rates of surface cooling
Less frequent or delayed cooling to dew-point
Reduced sources of moisture
Sealed surface and rapid runoff
Lack of vegetation and exposed soil
Reduced evapotranspiration
Reduced wind speeds
Drag of city reduces wind speed in light winds
Vapour transfer is weak in calm air in the UCL

and pavement retain heat well into the night. However, vegetation is also present in cities. Tree tops and open lawns cool rapidly after sunset, and are potential sites for the formation of dew. In addition, shingle or metal roofs which are well insulated and have, because of their height above surroundings, an unobstructed horizon cool strongly overnight and have the potential to collect significant amounts of dew.

Besides cool surfaces, dew requires a sufficient vapour supply and suitable wind speeds. Reasons proposed in the literature to explain reduced evapotranspiration in cities (Table 2.6) are also used to explain lack of urban dew (Table 2.7), e.g., paving seals off soil moisture exchange, rainfall is quickly removed, and vegetation is scarce. At night, in those weather conditions when dew forms, regional winds are light. It is known that the roughness of the urban surface further reduces wind speeds in the city. Hence, it is argued in the literature that reduced wind speed in cities reduces rates of dewfall deposition because dewfall

ceases when air is motionless (Table 2.7). However, this statement is overly simplistic. It may even be incorrect because urban wind speeds may, at times, enhance rates of urban dewfall. The reduced wind speed in cities may allow dew to form on nights with relatively strong regional winds, which would otherwise prohibit dew. On the other hand, in light winds, the increased roughness of the urban surface may increase dewfall, because increased turbulence increases the vertical transfer of moisture toward the surface.

Although reduction in dew is unproven it is used in turn to explain features of urban climate. Absence of dew is inferred to favour the formation of an UHI during morning hours, since, in the absence of surface water from dew, the available energy is partitioned into sensible (Q_H and ΔQ_S) rather than latent heat (Q_E), and this heats surfaces and air. In rural areas, a rapid increase is seen in evaporative rates immediately after sunrise. This is supplied in part from the drying of dew, so this feature is supposed to be absent in cities where dew is absent (Dirks, 1974; Hage 1975; Landsberg, 1981). During the night, the presumed lack of dewfall in cities is used to explain the excess in humidity which is observed in urban areas at this time of day, compared to the rural surroundings where dewfall depletes near-surface humidity (Hage, 1975). In addition, since transpiration may continue during the night in warm cities, and dew is absent as a buffer to transpiration, it is proposed that there is virtually no break in demands made on the water regime of urban plants and they suffer increased physiologic stress (Potts and Herrington, 1979; Douglas, 1983).

Very few data exist to support or refute these generally held opinions about patterns of urban dew. Some information can be gleaned from urban climate studies, where negative evaporation or dewfall is indicated in observations using mini-lysimeters or wetness sensors (Spronken-Smith, 1994). Several studies (Section 2.4.4) have collected urban dew for purposes of chemical analysis, but urban-rural differences are not investigated, weather conditions are seldom addressed, and the focus is on chemistry, not dew. There exist only two observational studies explicitly dealing with urban dew, i.e., Mattsson (1979) and Myers (1974).

Mattsson (1979; *pers. comm.*, 1998) measured dew and air temperature in Skanör, Sweden, during an August night with clear skies and weak winds (Figure 2.5). Relative dew intensities were measured using exposed paper 'dew rolls' (see Mattsson, 1962). These change colour in the presence of water and give data with units cm, i.e., the length of paper affected by condensation. Gauges were placed over grass at relatively open locations, where longwave radiative fluxes from trees and buildings were minimal. Dew was measured along a transect from the town square ('Torget'; Figure 2.5) to a point outside the built-up area ('Gräsmark'), a distance of about 2 km. Dew rolls were exposed at sunset (~7 pm) and 9 pm, and data were read manually, at 9 pm and 11 pm. To paraphrase Mattsson (*pers. comm.*, 1998): during the early evening, air temperature in the built-up area remained high and dew deposition was prohibited; dew was deposited only in the rapidly cooling area outside the built-up zone (as shown by line 'b' in Figure 2.5). Later in the evening, urban temperatures decreased sufficiently that dew was

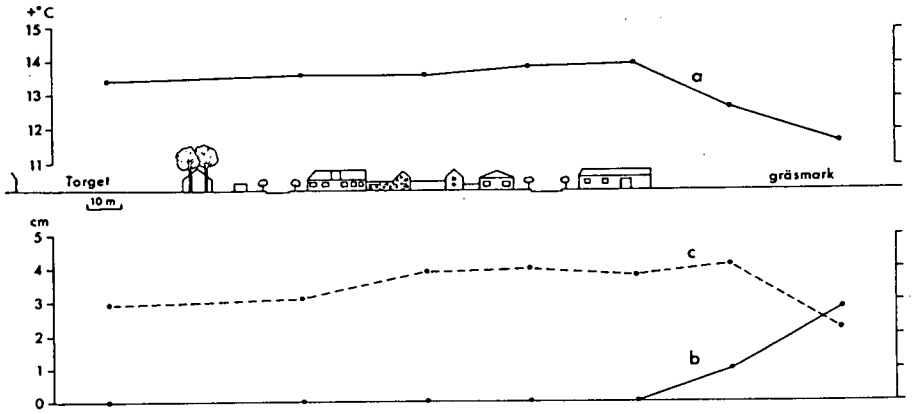

Figure 2.5 Temperature and dew conditions along a transect in Skanör, Sweden, during conditions of clear skies and light winds. The transect is from the town square (to the left) to a point outside the built-up area (to the right). (a) is air temperature (°C) at sunset (~7 pm), (b) is the intensity of dew recorded between 7 pm and 9 pm, and (c) is the intensity of dew recorded between 9 pm and 11 pm. Dew data were measured using the method of 'dew rolls' (see Mattsson, 1962) and have the arbitrary units cm. *Sources:* Mattsson (1971); Mattsson, *pers. comm.* (1998).

present at all locations (line 'c') but, at the same time, conditions promoting higher rates of dew deposition outside the built-up zone seemed to have weakened. When the total amount ('b' + 'c') is considered, dewfall is heavier outside the built-up area than within it. Thus, there is some evidence to support commonly held assumptions about urban dew, that dew is delayed or less in urban areas. However, Mattsson's results have not been published in English translation, and are often overlooked.

The only substantial set of urban observations of dew is that gathered by Myers (1974) in Washington, D.C. Amount of dew at sunrise was simultaneously assessed by members of the pre-existing National Capitol Area Climatological Network at 31 grassed sites across the city, at locations with an open view of the sky. Sites ranged from locations in the urban core, to locations in residential areas

outside the city, surrounded by rural land (Myers, *pers. comm.*, 1997). Dew amount was visually assessed and ranked on a scale from light to heavy dew for eight fine mornings during the summer of 1974. Data were mapped and contour lines drawn to indicate spatial variation of the amount of dew as a function of meso-scale location. A selection of maps is shown in Figure 2.6. In these the central diamond indicates the boundaries of Washington, D.C., the core of urbanisation for the area. The undulating lines depict the west and east banks of the Potomac River in the south and its course (indicated by a single line) to the north-west.

In general, the mapped data show a tendency for dew to be light or absent in the city centre and heavier towards the periphery. This agrees with the expected spatial distribution of the average nocturnal UHI for the city, however, patterns for individual dates vary in detail. Dew is absent at many central sites when wind speeds exceed 1.5 m s^{-1} (e.g., July 12), while on calm nights (e.g., July 13) light dew forms at these locations. There is some evidence that the zone of light or no dew at the centre of the city expands outwards, and urban-rural distinctions break down, on nights which generally hamper heavy dew formation (July 23), i.e., cloudy nights, and, with some exceptions, nights with a less well developed UHI (<3.0°C). During July of 1974, Washington, D.C. received little precipitation and rain that fell was unevenly distributed, with parts of the city remaining dry. Myers found correlation between patterns of dew and antecedent rainfall, and inferred that variations in soil moisture created this effect. Myers' results were summarised, very briefly, by Landsberg (1981), but they have not been widely published, and dew observations of this type have not been duplicated for other cites.

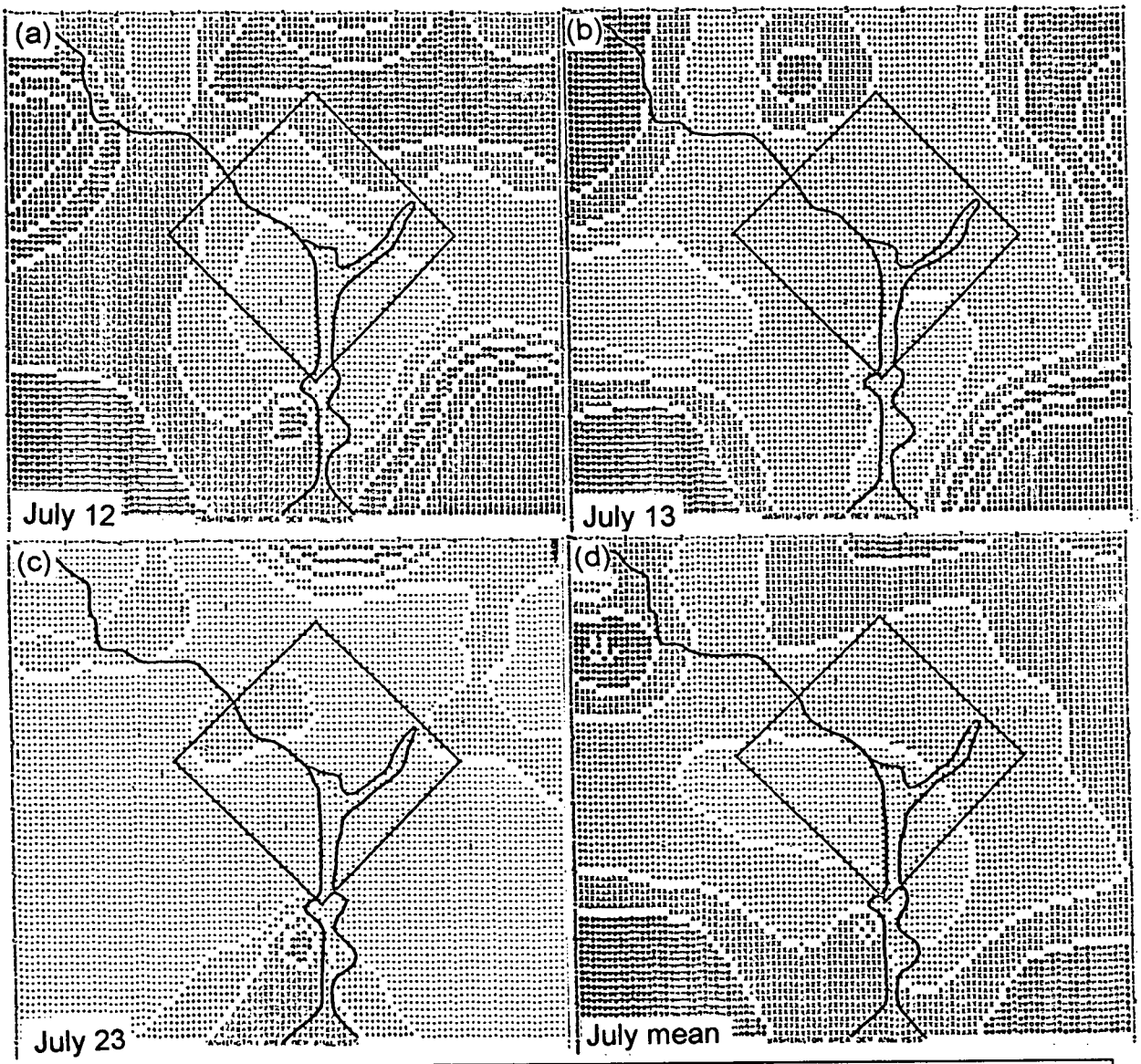

Date, 1974	*Wind speed* ($m\ s^{-1}$)	ΔT_{u-r} (°C)	*Cloud conditions*
July 12	2.5	3.6	some high cloud
July 13	calm	3.4	some high, thin cloud
July 23	1.5	2.8	overcast

Approximate scale: 1: 100 000

Figure 2.6 Spatial distribution of dew for Washington, D.C. under a variety of weather conditions in the summer of 1974. Nights are characterised by (a) windy, (b) calm, and (c) cloudy weather, and (d) shows the average of the observed dew distributions for days in July. Dew intensity is on a 6-step scale (from lightest to darkest shade: none, light, light-moderate, moderate, moderate-heavy, heavy) which is present in its entirety in (a). *Source*: Modified from Myers (1974).

2.4.4 Urban dew and atmospheric pollutants

Concerns about atmospheric pollution created an interest in the potential of dew and guttation as a sink for pollutants in the lower atmosphere. The volume of water involved is small compared to rainfall so the sink is fairly minor (Brimblecombe, 1978) . However, at times wetting by dew can be more frequent than rain and, at the nano-scale, droplets present a large surface area for chemical reactions, e.g., ~10–15 m^2 per m^2 ground for short grass (Hughes and Brimblecombe, 1994). The chemical composition of dew is governed by the composition of the near-surface atmosphere and, to a lesser extent, by the nature of underlying surfaces (Wagner *et al.*, 1992). Since emissions of many air pollutants are concentrated in urban areas it might be expected that urban dew differs in chemical composition from that in rural areas. Although my study does not include the chemistry of dew, this aspect has importance to urban environments. Topics dealing with surface wetness, dew, and the deposition of atmospheric pollutants are reviewed by Fowler (1980) and Wisniewski (1982), and results from a number of observational or theoretical studies are summarised in Table 2.8.

Field evidence and numerical simulations indicate that surface wetness, whether urban or rural, is a site for enhanced deposition of most major ions, with the exception of H^+. For soluble trace gases, such as SO_2 and HNO_3, rates of deposition vary with surface resistance, but for O_3 relationships are poorly understood. There is also uncertainty concerning the frequency of acid dew, or its implications. In theory, formation is favoured by enhanced rates of deposition of acidic gases so urban sites may be favoured locations for acid dew. Field

Table 2.8 Topics of research and summary of results relevant to dew and atmospheric pollutants.

Aerosols: dew compared to dry surface
Minor or major enhanced capture of aerosols (1.1x–2.5x)[8,4]
Seasonal and/or local variations in amount and type of aerosols in dew[8,4]

Chemical composition: dew compared to dry surface
Controls are: near-surface atmosphere composition[6,8], local aerosol sources[9,4,8]
Deposition rates greater for most ions (1.1x–12x)[8,4]
Concentrations of ions greater (2x–20x)[8]

Trace gases: dew compared to dry surface
Rates a function of atmospheric and surface conditions[5,3]
O_3: Effect uncertain, may enhance rates at times[7, 15]
HNO_3: Effect uncertain, may enhance rates (10x)[1,5]
SO_2: Rates high if dew forming or buffered (to 10x)[1,7,10,3]
Rates low if dew acidic or evaporating or static in amount[1,3,4,10]

Acid dew
pH of 2-4 theoretically possible[5,11,10]
pH in field often 6 to 7; values of 3.5 to 8.2 have been reported[2,6,13,11,9]
Alkalines of soil, atmospheric or plant origin reduce acidity[4,10,6]
Dew (pH ≈ c.6.5) is often less acid than rain (pH ≈ 4–5)[8,4,9]

Corrosion of building materials and vehicles
Dew leads to damage, directly (acid dew) or by activating surface chemicals[12,11]
Dew enhances electrochemical corrosion of metals[4,11]

Plants and dew chemistry
Acidic dew leaches leaf nutrients[6,13,10,11]
Guttation adds organic acids to dew[2]
Acid dew can damage leaves and plants[11,4]

Dew as a sink e.g., for annual UK SO_2 emissions
Dew is a negligible sink (0.02–c.0.2%)[10]
Surface wetness is a small sink (0.3–3.6%)[10,1,12]

Sources: 1. Fowler, 1980; 2. Hughes and Brimblecombe, 1994; 3. Fowler, 1992; 4. Mulawa *et al.*, 1986; 5. Chameides, 1987; 6. Brimblecombe and Todd, 1977; 7. Padro, 1994; 8. Wagner *et al.*, 1992; 9. Schroder *et al.*, 1989; 10. Brimblecombe, 1978; 11. Wisniewski, 1982; 12. Harter, 1986; 13. Arends and Eenkhoorn, 1989; 14. Wolff *et al.*, 1990; 15. Fuentes and Gillespie, 1992; and others.

observations suggest that surface wetness in cities tends to be not very acidic (pH 5 to 7), but values down to pH = 3.2 have been reported (Okochi *et al,* 1998).

A small number of observational studies have been conducted in cities to study the chemistry of urban dew (Mulawa *et al.*, 1986; Schroder *et al.*, 1989; Wagner *et al.*, 1992; Okochi *et al.*, 1998). Their results are usually presented as a chemical analysis; dew as a phenomenon and urban effects are rarely addressed. Nevertheless, some urban effects are implied. For example, Wagner *et al.* (1992) correlated the high Cl concentrations observed in Fayetteville in winter with the practice of salting urban streets during cold months. Wolff *et al.* (1990), working in Jacksonville, Florida, showed that urban dewdrops could damage automotive finishes, i.e., when sulphuric acid from the (urban) atmosphere and calcium from soil-derived aerosols were present in sufficient concentrations and dew was evaporating.

2.5 Modelling of dew

When a phenomenon is difficult to measure in its natural state, modelling often provides useful insight. Two types of model are relevant here. One is a scaled, physical model constructed to study a physical system of interest. The other is a numerical model in which the environment and factors governing the processes of interest are simulated mathematically. Hardware models to study dew deposition are rare, those of Mattsson (1971) and Dröscher *et al.* (1989) being exceptions. There are several models which attempt to simulate dew numerically (Section 2.5.2).

2.5.1 Scale modelling

Dew is difficult to create artificially, and few have attempted to do so. Methods are crude, e.g., using outdoor refrigeration (Mulawa *et al.*, 1986), fog droplets in a laboratory chamber (Arends and Eenkhoorn, 1989), or water sprayed onto leaves (Fuentes and Gillespie, 1992). While adequate for investigating the consequences of dew, such as spore germination or droplet chemistry, these approaches provide little information about dew formation. Consequently, hardware models to study dew deposition are rare and must operate in the out-of-doors where dew forms naturally (Table 2.9).

Mattsson (1971; 1979) constructed several small (0.10–0.50 m tall) scaled models of rural windbreaks, some solid and some with less than 100% density, using artificial materials. Models were placed on grass, or a plywood sheet coated with Vaseline (so that dew formed droplets), and exposed out-of-doors in conditions of clear skies and a variety of wind speeds. Dew intensity was recorded using flash-light photography and retroreflectance (Section 2.2.1). Results show that, in moderate winds, shelter plays a role in governing dew distribution in the lee of windbreaks. A cardboard model of forest glades was also constructed.

Dröscher *et al.* (1989), as part of a study of the chemistry of dew and fog, constructed a small artificial spruce tree using chemically inert materials. Deposition on the model tree was measured by lysimetry and data were calibrated using observations collected for a natural tree of similar size. Ultimately, the model was installed at tree-top level (20 m) in a forest to measure water deposition (dew + fog) on the upper canopy.

Table 2.9 Examples of hardware models of cities or buildings, or dew deposition on vegetation.

Author	*Year*	*Topic of Study*	*Scale*
Laboratory Models			
• *City Surface*			
Oke	1981	Urban heat island	~500:1
• *Neighbourhood*			
Spronken-Smith	1994	Park cool island	625:1
• *Building/Buildings*			
Imbabi	1990b	Air conditioning	7:1
Barozzi *et al.*	1992	Solar chimney design	12:1
Out-of-doors Models			
• *City Surface*			
Davis and Pearson	1970	Model of Ft. Wayne	1000:1
• *Neighbourhood*			
Aida	1982	Urban albedo	–
• *Building/Buildings*			
McPherson	1980	Shade and indoor temperature	8:1
McPherson *et al.*	1988	Yard treatments, indoor temperature	4:1
Wegner *et al.*	1988	Solar houses, indoor climate	2:1
Voogt	1989	Urban canyon temperature	~10:1
Discrete Objects			
Mattsson	1971	Dew, windbreaks and forest clearings	–
Dröscher *et al.*	1989	Dew chemistry on conifers	1:1

A model of urban dew must address dew deposition on and around buildings. In cities, investigating how existing buildings interact with their environment is often hindered by site complexity and practical logistics. Prototype buildings, constructed at the full-scale, are costly, time-consuming and difficult to modify (Imbabi, 1990a), and currently available numerical models are restricted to buildings of simple geometry and/or require large amounts of input data (Imbabi, 1990b). Thus, scale

modelling is an attractive option to investigate building-energy processes (Imbabi, 1990b; Voogt, 1989; Wegner *et al.*, 1988).

Hardware models of built systems can be divided into several scales of interest. Models range from small scale replicas of cities in wind tunnels to study dispersion of pollutants in the atmosphere (Hoydysh and Dabberdt, 1988), to apartments constructed at a scale of 2:1, that is, at ½-scale (Wegner *et al.*, 1988). Several models have been constructed out-of-doors, ranging from buildings or built elements that are structurally simple (Voogt, 1989) to ones that are sophisticated (McPherson *et al.*, 1988). A selected list of models of urban areas and buildings is given in Table 2.9. The theoretical criteria which govern the design and scaling of such models are discussed separately in Chapter 4.

To illustrate the range of studies, McPherson (1980) investigated the effect of tree shade using two 8:1 scale model houses. Results showed that shading significantly reduced indoor temperatures during summer and, at the full-scale, savings in air conditioning costs could be expected. At a later date McPherson *et al.* (1988) investigated the effect of more complex yard treatments on indoor temperature, air conditioning costs, and irrigation needs using three detailed 4:1 scale model homes.

Voogt (1989) considered effects of geometry on temperatures in an urban canyon using an outdoor model consisting of two 1 m high concrete block walls of about 10 m in length. Results indicated that daytime wall temperatures were governed by incident short-wave radiation, and nighttime temperatures by radiative heat loss and geometry, expressed as Ψ_{sky} and H:W.

2.5.2 Numerical modelling of dew

For periods when or places where dew data are not directly available, numerical modelling provides a potential means of estimating dew. If a model is able to correctly forecast dew it may also have practical use, for example, in agriculture where diseases are associated with extended periods of leaf wetness and accurate forecasting is of economic benefit (Jones, 1986; Huber and Gillespie, 1992).

Evaporative/latent heat fluxes in cities are difficult to measure or estimate (Oke, 1988). The heterogeneity and roughness of the surface often makes inappropriate the use of traditional flux models developed for extensive, flat and homogeneous surfaces, especially near the ground. At the local- and meso-scale, models that were originally developed to simulate evaporation from forest have gained support. This is the basis of the best available numerical model for estimating evaporation from urban areas (Grimmond, 1988), but even it lacks the resolution needed to simulate dew. Consequently, numerical modelling of dew in urban environments seems to require other approaches.

Numerical models to simulate dew range from simple correlations of dew with climate data (Hutorowicz, 1981), to complex and comprehensive numerical simulations of atmosphere-canopy systems in which amount of dew is a minor output parameter (Thompson, 1981). A selected list of models to simulate dew is given in Table 2.10.

Simple correlation models, which use weather data, lack precision and seldom have much accuracy beyond the data sets used for their calibration

Table 2.10 Examples of numerical models to simulate dew.

Author	*Year*	*Topic of study*
Approaches based on weather conditions		
• *Simple correlation of dew with environmental data*		
Crowe *et al.*	1978	Dew on vegetation
Hutorowicz	1981	Dew on vegetation
• *Simple forecast of dew from weather forecast*		
Hewson and Gait	1992	Hoarfrost and dew on roads
Garrard and Griffiths	1996	Leaf wetness in crops
Getz and Harker	1996	Leaf wetness in crops
Approaches based on micrometeorological conditions		
• *Single-layer or simple object*		
Collins and Taylor	1961	Dewfall on a large leaf
Monteith and Butler	1979	Dewfall on cocoa pods
Butler	1980	Dewfall on cocoa pods
Pedro	1980	Leaf wetness on crop leaves
• *Multiple-layer or canopy volume*		
Thompson	1981	Water balance of a crop canopy
Weiss and Norman	1987	Water balance of a crop canopy
• *Extensive and homogeneous surface*		
Holtslag and de Bruin	1988	Nighttime latent heat fluxes over grass
Janssen and Römer	1991	Deposition of atmospheric pollutants

e.g., the model of Crowe *et al.* (1978) simulated the duration of dew on grass (to ±3 h) with only 60% accuracy, when used at a new site. Simple forecast models, based on local climate and over-night weather forecasts, give better results, to ±1 h, within the region for which they are calibrated (Getz and Harker, 1996). These have some usefulness as agricultural tools, but they lack scientific rigour.

Several comprehensive micrometeorological models have been developed to estimate surface fluxes of heat, water and momentum using profile and other environmental data. Most apply only to daytime. An exception is that of Holtslag and de Bruin (1988), which simulates nighttime fluxes over extensive grass surfaces.

Although otherwise rigorous, their model simplifies the dynamics of dew, e.g., by simulating dewfall, but ignoring its contribution to evaporation. Janssen and Römer (1991) derived a simple scheme from Holtslag and de Bruin's model, and used this to estimate dewfall on glass plates used to sample pollutants deposited from the lower atmosphere. However, such boundary layer models are strictly limited to extensive, homogeneous and flat terrain. Thus, they are invalid in cities, where the necessary fetch requirements cannot be met.

Most authors agree that, while a synoptic model is attractive, an energy balance approach is best for modelling dew at the micro-scale. In addition, although it may be possible to predict presence-absence of dew using simple routines (Mintah, 1977; Getz and Harker, 1996), rigorous simulation of dew amount and duration requires a time-dependent model. The most widespread approach to model dew on crops is a single-layer model, such as that developed by Pedro (1980).

Working in Guelph, Ontario, Pedro developed a numerical model to simulate dew duration for single leaves in crops, specifically, corn, soybean and apple. An energy balance is defined for the leaf, surface wetness duration is inferred from the calculated latent heat flux, and the model is structured so that measurements of leaf temperature are unnecessary. Overall, simulated leaf temperatures were correct to within 1°C, and duration of leaf wetness was simulated to within 30 min for exterior leaves in crop and orchard canopies (Figure 2.7). Accuracy was reduced when environmental parameters were estimated, rather than measured, e.g., for leaves inside canopies (60 min), and when crop conditions were estimated from climate station data, using a number of empirical relationships (60–90 min). Pedro's

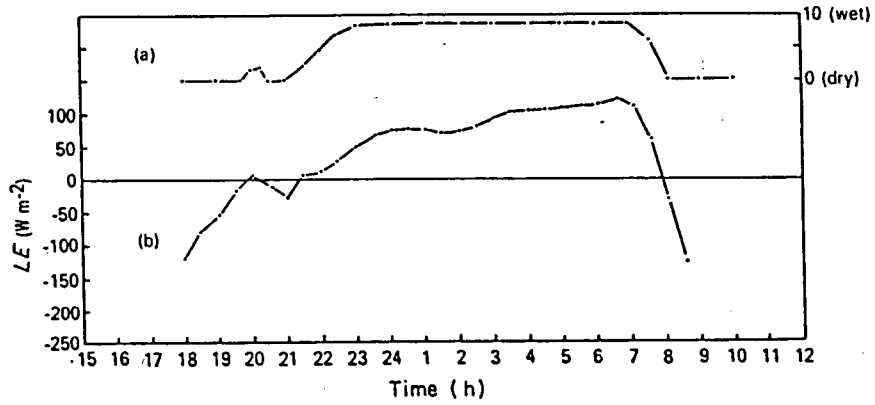

Figure 2.7 Observed and simulated dewfall deposition for an individual apple leaf. (a) is leaf wetness (wet *vs* dry states) measured using an electronic wetness sensor, and (b) is dewfall (negative evaporation; W m^{-2}) simulated using the Pedro model. *Source:* Pedro and Gillespie (1982a).

approach has been validated for a number of different crops and locations: Gillespie and Barr (1984) modelled dew on onion leaves, Scherm and van Bruggen (1993) analysed the climatology of dew in several contrasting climate zones of California, and the approach has been successfully used as a practical tool to schedule agricultural sprays, in lettuce crops where prolonged surface wetness increases risk of fungal infection (Scherm *et al.*, 1995).

Models to simulate dew for surfaces other than leaves could theoretically be extended to simulate dew on built surfaces in cities, but few such models exist. Heusinkveld *et al.* (1998) added a sub-surface sensible heat flux term to Pedro's model (described above) in an attempt to simulate dewfall to the artificial surface of a dew collector. Results were tested using dew data gathered in the Negev desert during 1997. Overall, the outcome was poor. Observed dewfall data were

adequately predicted only when substrate conductivity was artificially inflated by about x15.

Butler and Monteith (1979) and Butler (1980) successfully simulated the formation of dew on cocoa pods using a combined thermal behaviour-energy balance approach. In the plantations, pods remain dry during the night, since their surfaces are warm and dew is inhibited. After sunrise the dew-point temperature (T_d) of surrounding air increases more rapidly than the surface temperature of dry pods (T). When T_d exceeds T condensation occurs, pods become wetted, and the crop is vulnerable to disease. Eventually the temperature lag created by thermal inertia is overcome, pods warm sufficiently that T exceeds T_d, and the dew begins to dry.

Dew also forms on tar-sealed roads in some weather conditions. Hewson and Gait (1992) describe a road surface temperature model which predicts hoarfrost, ice and dew formation on pavement for use in the scheduling of road salting in the UK.

2.6 Potential topics of study

Several of the findings of the studies reviewed in this chapter suggest issues which may be of value and interest in a study of urban dew. These are summarised as follows:

- *What methods should be used to measure dew in a city?*

  A wide variety of methods are potentially available but, even in rural environments, there is no standard method to measure dew (Section 2.2).

- *How does dew deposition vary in a city over time?*

  Patterns of dew formation vary at all temporal scales (Section 2.3) but data for cities are unavailable (Section 2.4.3).

- *How does the deposition of dew vary spatially within a city?*

  Relations between site geometry and dew distribution at rural sites (Section 2.3), combined with knowledge of the intrinsic complexity of urban areas (Section 2.4), suggests that patterns of urban dew will be spatially complex.

- *Does the presence/absence of urban dew affect human activities in cities?*

  In theory, many of the implications of the occurrence of dew (Table 2.1) can be transferred to urban environments, e.g., dew affects on plant health (Section 2.3.2) and links with damage to built materials (Section 2.4.4).

- *Are observed contrasts in urban and rural humidity linked to dewfall?*

  Close links are often postulated between urban-rural contrasts in humidity in mid-latitude cities in summer (Section 2.4.2) and dewfall patterns, but few data are available to test the validity of this supposition (Section 2.4.3).

- *Is there an urban-rural contrast in the frequency and amount of dew?*

  The general consensus is that dew is absent or reduced in cities, compared to their rural surroundings, but very little measured data exist (Section 2.4.3).

- *Are there differences in the chemical compositions of urban and rural dew?*

  Meso-scale contrasts in the lower atmosphere suggest that urban dew should differ in chemical composition from that seen in rural areas (Section 2.4.4).

- *Can patterns of urban dew be studied using a physical, scaled model?*

In theory, existing models of built systems (buildings, cities) can inform the development of a model to study dew deposition in a city (Section 2.5.1).

- *Can patterns of urban dew be simulated using a numerical model?*

  There is no numerical model to predict urban dew but some rural models have potential to be transferred to an urban setting (Section 2.5.2).

In the present study, the main research goals are to investigate methods appropriate to measuring urban dew, to describe the spatial and temporal patterns of dew for an urban area (Vancouver), and to investigate the feasibility of modelling urban dew using a physical, scaled model and a numerical model. Links between urban dew and humidity are also addressed. The specific objectives of the present study are described in detail in Section 1.3. Issues concerning the chemical composition of urban dew and the potential effects of urban dew on human activities are not addressed in this thesis.

PART II OBSERVATION

Chapter 3: Spatial and temporal surveys in Vancouver

3.1 Context

In the present study, surveys of urban dew, surface moisture and near-surface humidity were undertaken to build up an observational understanding of various aspects of the urban dew phenomenon. The observational programme was not intended to be a comprehensive study of urban dew in Vancouver but, rather, an investigation of the controls on dew at various scales. From this, I hoped to formulate hypotheses to inform the development of scale and numerical models (Chapters 4–6 and 7, respectively). Ultimately, a considerable number of surveys were undertaken, at scales ranging from 0.02 to 25 km. Not all results are presented here. Instead, discussion focuses on relatively few days and/or sites which serve to illustrate features of interest. Data are primarily presented for individual nights, rather than as aggregated or multi-occasion statistics.

Vancouver (49°15'N, 123°18'W) is located on the southwest coast of British Columbia. It is bounded to the north by mountains, to the south by the city of Richmond and the farmlands of the Fraser Delta, and to the west by the Strait of Georgia (Figure 3.1). The area is, perhaps, a less than ideal location in which to study urban effects because of the spatial complexity created by contrasts in topography and the presence of water bodies such as the Fraser River and Burrard Inlet (see Figure 3.1). This means that spatial patterns of temperature, humidity and wind speed in Vancouver are potentially more complex than those of an 'ideal' city situated on an extensive and homogeneous plain.

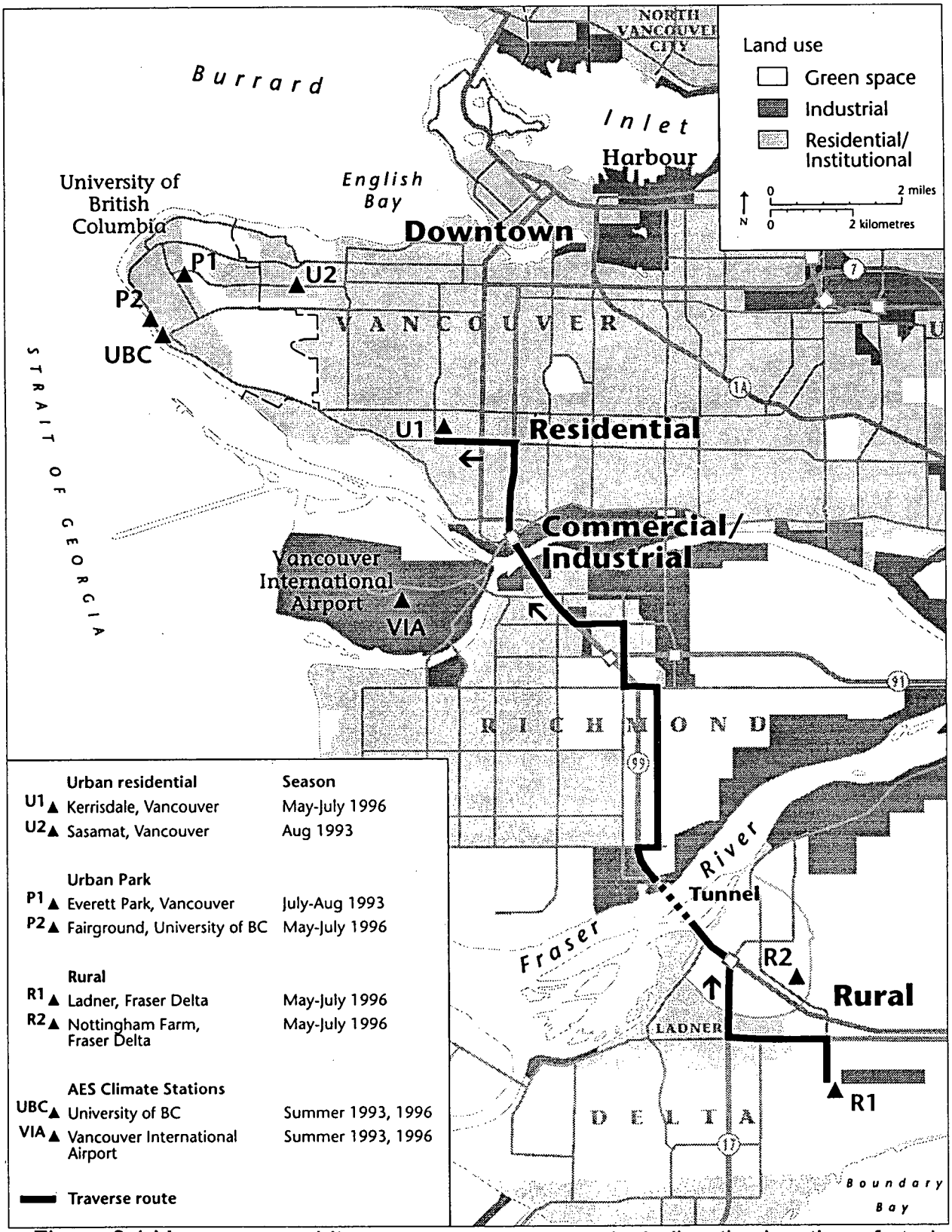

Figure 3.1 Vancouver and its surrounding land-use, including the location of study sites and the route for the mobile survey.

Regional weather tends to be mild, cloudy and rainy during winter, and for many days in spring and fall. During summer (June-August), Vancouver experiences persistent high pressure systems accompanied by settled, clear and warm weather. During these conditions regional winds are light and a land-sea breeze circulation commonly develops, with westerlies by day and weak easterlies or north-easterlies by night. Occasional unsettled periods of cloud and frontal rain occur in summer but these are generally short-lived. Proximity to the ocean and prevailing westerlies ensure that air in Vancouver is relatively moist under most weather conditions (Oke and Hay, 1994).

Few measured dew or surface moisture data exist for the Vancouver region (Spronken-Smith, 1994), but informal observations suggest that dew is frequent in all seasons except winter, whenever rain is absent. During clear weather in spring and fall dew is often heavy when nights are cool and the air is moist. However, the frequency of dew is limited by precluding events such as frost, fog, rain and windiness. During summer, it is hypothesized that the quantity of dew is reduced when the moisture available for condensation is insufficient during periods of drought and at unirrigated locations (Oke, *pers. comm.*, 1992). However, this is unproven. I have observed that, when prompted, Vancouver residents may recall having seen water dripping from house roofs at dawn, in the absence of overnight rain. Although it is difficult to absolutely exclude the presence of water from fog impaction, the source of moisture may be condensation, which suggests that roofs in the city may be a significant site of dewfall deposition. Humidity data for Vancouver provide little evidence to support or refute assumptions concerning dew

behaviour because studies of humidity in Vancouver tend to be limited to short periods and/or few sites.

The need for directly measured data is readily apparent, given the rarity of urban dew data. However, dew measurement lacks universal protocols, and not all methods to measure it are transferrable to urban environments. Thus, my observational study had to also address methods of measurement.

3.1.2 Objectives

The broad objectives of the observational programme are to investigate the spatial and temporal distribution of surface moisture and near-surface humidity for Vancouver, and to provide context for the hardware (Chapters 4-6) and numerical modelling of urban dew (Chapter 7). The study is limited to a selected range of temporal and spatial surveys, to describe several features of urban surface and near-surface (humidity) moisture distributions. The specific objectives are to:

- design and test appropriate instruments and other methods to measure urban surface moisture,
- test whether urban dew is in reality less than rural dew for a particular city,
- investigate the role of weather, time-of-day and meso-scale location as controls on urban-rural differences in near-surface and surface conditions,
- investigate the role of weather, micro-scale location and site geometry as controls on surface conditions at typical urban locations, and
- collect data to validate the results of my scale modelling, and to run and validate the numerical model.

3.1.3 Implementation

The survey programme was undertaken in Vancouver and its rural surrounds (Figure 3.1) during the summers of 1993 and 1996. Some instrument trials were undertaken during 1994. Environmental conditions were investigated at meso- and micro-scales, and the studies focussed on residential neighbourhoods and selected elements of near-surface and surface thermal and moisture environments.

The objectives (Section 3.1.2) were implemented using: (a) surveys of urban-rural environmental differences, undertaken along a rural-to-urban route (Figure 3.1), and at rural and urban sites (U1 and R1, Figure 3.1) at the end-points of the route, and (b) exploratory surveys of surface conditions at the micro-scale, undertaken within the city. There are four main components, although these are not mutually exclusive:

- trials of instruments and methods to measure urban surface moisture and dewfall,
- near-surface humidity and air temperature measured along a rural-to-urban route using vehicle traverses between R1 and U1,
- synchronous measurements of air temperature, humidity, surface moisture and dewfall taken at an urban residential site (U1) and a rural site (R1) in the Vancouver area,
- surface moisture measured at two urban residential sites (U1, U2) and two park sites (P1, P2) in Vancouver, and

- background climate data measured at the sites described above and/or obtained from local Atmospheric Environment Service (AES) climate stations (UBC and VIA).

The location of sites and the seasons of measurement are given in Figure 3.1. Results of spatial and temporal surveys at the meso-scale are described in Section 3.2; Section 3.3 deals with surveys of urban variations at the micro-scale; and a summary in presented in Section 3.4.

3.2 Urban-rural differences

The surveys described in this section look at the effects of broader-scale factors—weather, time and meso-scale location—on patterns of (a) humidity and air temperature data measured along a rural-to-urban transect in Vancouver, and (b) surface and near-surface moisture and temperature conditions at the end-points of the survey route.

3.2.1 Sites and seasons

Seven sets of automobile surveys were conducted along a route from a rural (R1) to an urban residential (U1) site in Vancouver (Figure 3.1) from late May to mid-July, 1996. These were timed to include a variety of weather, and afternoon (~1600 h), night (~2200 h) and dawn (~0400 h) conditions. The 25 km route is from rural land-use in the south, through a zone of mixed land-use, to urban residential land-use in the northwest (Figure 3.1). At night the route took about 0.5 h to traverse. During the day this increased to 0.6–0.8 h when traffic was heavy. Although the route is

essentially rural-to-urban, environmental complexity along the route is increased by the patchiness of intervening land-use, and the presence of specific features, such as a highway tunnel, the Fraser River, and the significant built infrastructure which accompanies major highways. This means that spatial patterns at the urban fringe are more complex than those of an ideal city (Figure 2.3).

In conjunction with these surveys, data were gathered at the rural (R1) and urban (U1) end-points of the vehicle route. In all, 24 days with synchronous urban and rural data, fairly uniform weather, and no rain were selected for study. A variety of weather is included but the data-set is biased toward fine and stable weather. The rural and urban sites were chosen to include an area of mown grass, so that 'grass' mini-lysimeters (Section 2.2.2) could be installed and blotting (Section 2.2.1) undertaken. R1 (Ladner; Figure 3.1) is in a flat area of farmland on the Fraser Delta, amid fairly typical rural surroundings, i.e., crops, pasture and clusters of deciduous trees. The site itself is open grassland (Ψ_{sky} = 0.99), which was roughly mowed during the summer (Figure 3.2a). Although located within the perimeter of Boundary Bay Airport, the site is located well away from paved and built areas. U1 (Kerrisdale; Figure 3.1) is in an urban residential neighbourhood characterised by 1–2 storey houses, interspersed with apartments (Figures 3.2b–3.4). Vegetation of all kinds is relatively abundant, including street and yard trees. Instruments were installed in the back yard of a 1½ storey residential dwelling, where Ψ_{sky} has a maximum value of 0.57, i.e., at the most open location on the back yard lawn. During the period of study, the lot was not irrigated and the back lawn became very dry. Irrigation occurred at other locations in the lot and the neighbourhood.

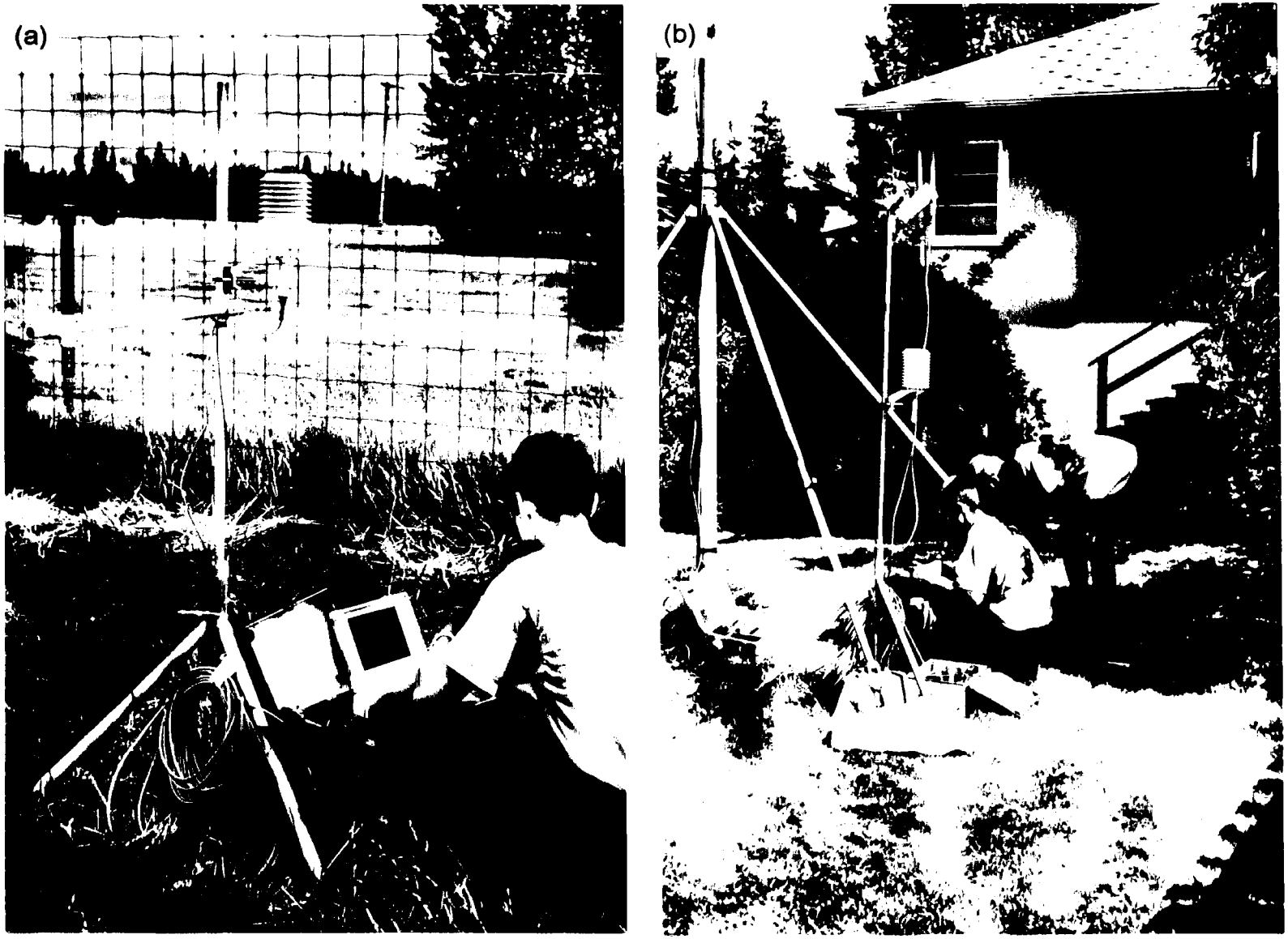

Figure 3.2 Views of (a) the rural site, R1, and (b) the urban site (U1).

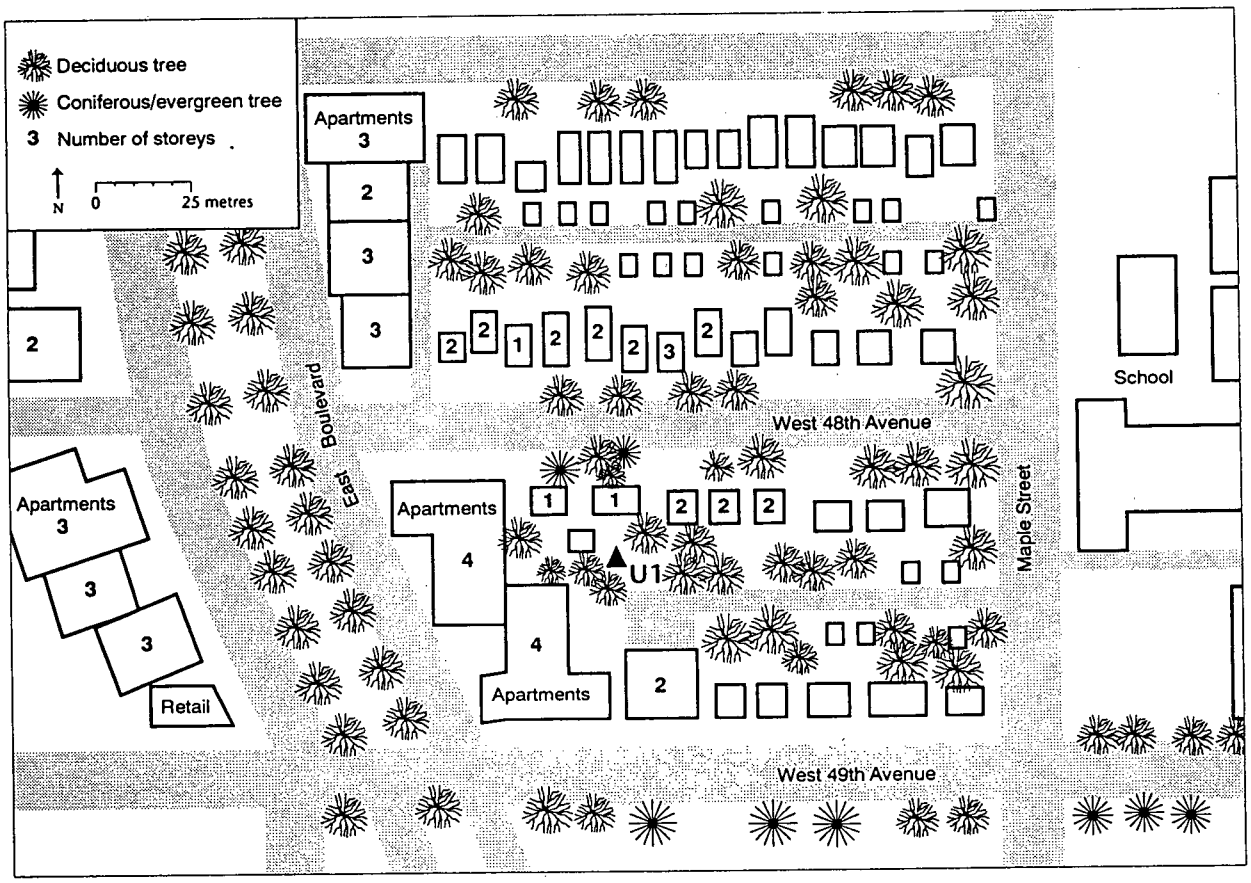

Figure 3.3 Details of the Kerrisdale site (U1) and its surrounding neighbourhood.

Additional data were obtained from two local AES stations—University of British Columbia (UBC) and Vancouver International Airport (VIA)—and at a second rural site, R2 (Figure 3.1). R2 (Nottingham farm) is located in an area of crops and ploughed fields. It is the site of an existing rural climate station ('Delta'; see Spronken-Smith, 1994; Runnalls, 1995), but is unsuitable for comparative measurements of dew, because it lacks a suitable area of managed grass.

3.2.2 Data collection and analysis

Instruments and methods are summarised in Table 3.1. For mobile surveys, data were collected using a pickup truck equipped with air temperature and humidity sensors. Instruments were calibrated to provide a time response of 12–16 s (95% of response), and were mounted together in a radiation shield at the height of 1.6 m, and continuously aspirated by a fan (~4 m s^{-1}). Electronic signals were sampled at 1 s intervals using a *Campbell Scientific* CR21X data logger, and data were stored as 5 s averages. Data were adjusted spatially, according to rates of travel along the route, and corrected for temporal changes during the survey (Section A1.2) so resulting data are equivalent to an instantaneous 'snap-shot' taken at the start time of the survey. The street which is the end-point of the mobile traverse route is shown in Figure 3.4.

Synchronous measurements of surface moisture, dewfall and weather conditions were made at R1 and in the house lot at U1 (Table 3.1). Overall, synchronous urban and rural measurements of dewfall amount/timing and surface wetness duration were collected for 13 days, and the amount of surface moisture on grass at dawn was measured on eight occasions.

Blotting was used to assess the amount of surface moisture (dew + guttation) on mown grass at dawn. The general method is depicted in Figure 3.5, which shows how pads are pressed on the wet grass lightly at first (here using weights), then more firmly. The image shows the relatively small pads which were used in the scale model (Chapter 5); at full scale locations pads 0.2 x 0.2 m were employed. An unknown fraction of the surface water is unmeasured in this method because some

Table 3.1 Instruments and methods used to collect data for studies at the meso-scale.

Parameter	*Instrumentation or method*	*Location*
Mobile surveys		
Humidity	*Vaisala* HMP35C sensor	1.6 m
Air temperature	Thermocouple (Cu-Co, 30 AWG)	1.6 m
Fixed sites		
• *Rural (R1)*		
Surface moisture	Blotting	grass
Wetness duration	Electronic wetness sensor	grass
Dewfall	Weighing mini-lysimeter, 0.11 m^2	grass
Humidity-temperature	*Vaisala* HMP35C sensor	1.5 m
Wind speed	*MetOne* anemometer	1.5 m
Wind direction[1]	*Young Wind Sentry*	1.5 m
• *Urban (U1)*		
Surface moisture	Blotting	grass
Wetness duration	Electronic wetness sensor	grass, roof
Dewfall	Weighing mini-lysimeter, 0.11 m^2	grass
	Weighing mini-lysimeter, 0.156 m^2	roof
Humidity-temperature	*Vaisala* HMP35C sensor	1.5 m, 5.3 m
Wind speed-direction	*Young Wind Sentry*	5.3 m
Background climate data		
Wind speed-direction[2]	*Young* propellor anemometer/vane	10 m
Humidity-air temperature[2]	*Vaisala* HMP35C in *Stevenson* screen	1.5 m
Incoming shortwave radiation[2]	*Kipp and Zonen* pyranometer	0.5 m
Net radiation[2]	*Swissteco* net pyrradiometer	7 m
Soil heat flux[2]	*Middleton* flux plate	-0.08 m
Soil temperature[2]	Thermistor	-0.06 to -0.02 m
Precipitation[1, 2]	Tipping-bucket rain gauge	
Cloud amount and type[3]	Visual estimates	

Measured at: 1. R2; 2. UBC; and 3. VIA.

Figure 3.4 The street at the urban site, U1.

Figure 3.5 The method of blotting (as described in Sections 3.2.2 and A1.3).

droplets run to the ground when the grass is disturbed (Section 2.2.1) so the resulting data systematically under-estimate the total amount of water present on the surface. Prior to the initial set of surveys, several small but careful trials were conducted in an open grassed park (P1; Figure 3.1) to develop a reliable and practical method for blotting on grass. From these tests, protocols were established to maximise droplet capture and minimise changes in mass due to evaporation from, or vapour absorption by, the sampling papers. For example, a pad consisting of three sheets of blotting paper was used to collect each sample. The pads were sealed in plastic bags prior to, and after the act of blotting (see Section A1.3 for more details of the method). Four pads 0.2 x 0.2 m in width were used at each site. These were deployed within about 1 m^2 to sense the maximum amount of surface moisture [g m^{-2}] present at R1 and U1 at dawn. Mass data were later converted to units of mm depth.

Electronic wetness sensors (Section 2.2.1) were used to monitor the duration of surface wetness on grass at both sites and on the roof at U1. Sensors consisted of light-weight cloth mounted on a *perspex* frame (50 x 70 mm in width). Stainless steel wire (AWG = 24) proved the active circuit and signals were sampled at 15 min intervals using a *Campbell Scientific* CR10 or CR21X data logger. Tests showed that the sensors accurately mimicked surface wetness duration for asphalt roof shingle and mown grass surfaces to within about ±15–30 min.

Electronic weighing mini-lysimeters (Section 2.2.2) were installed in grassed surfaces at R1 and U1, and in a false roof at U1 to measure dewfall accumulation. Mini-lysimeter design was based on that described by Grimmond *et al.* (1992) to

measure evaporation from a grassed surface. Weighing platforms were built around an *Interface* SPI50 or SPI7.5 loadcell (sensitivity = 0.001 kg) and surface area was sufficiently large that condensation could be easily resolved. For grass, a lysimeter area of 0.11 m^2 gave a dewfall resolution of 0.009 mm per night (Figure 3.6). Due to mass limits, the soil-grass monolith was shallow (0.10 m) and its useful lifespan was therefore short. In practice, the monolith was replaced every 4–7 days. At U1, a weighing mini-lysimeter (area = 0.156m^2; resolution = 0.006 mm) was designed and installed at 7.0 m above ground on the roof of the dwelling. The weighing platform was enclosed in a purpose-built, wood and asphalt-shingle false roof with a flat upper surface of 1.2 x 1.2 m in width (Figure 3.7). Electronic signals from mini-

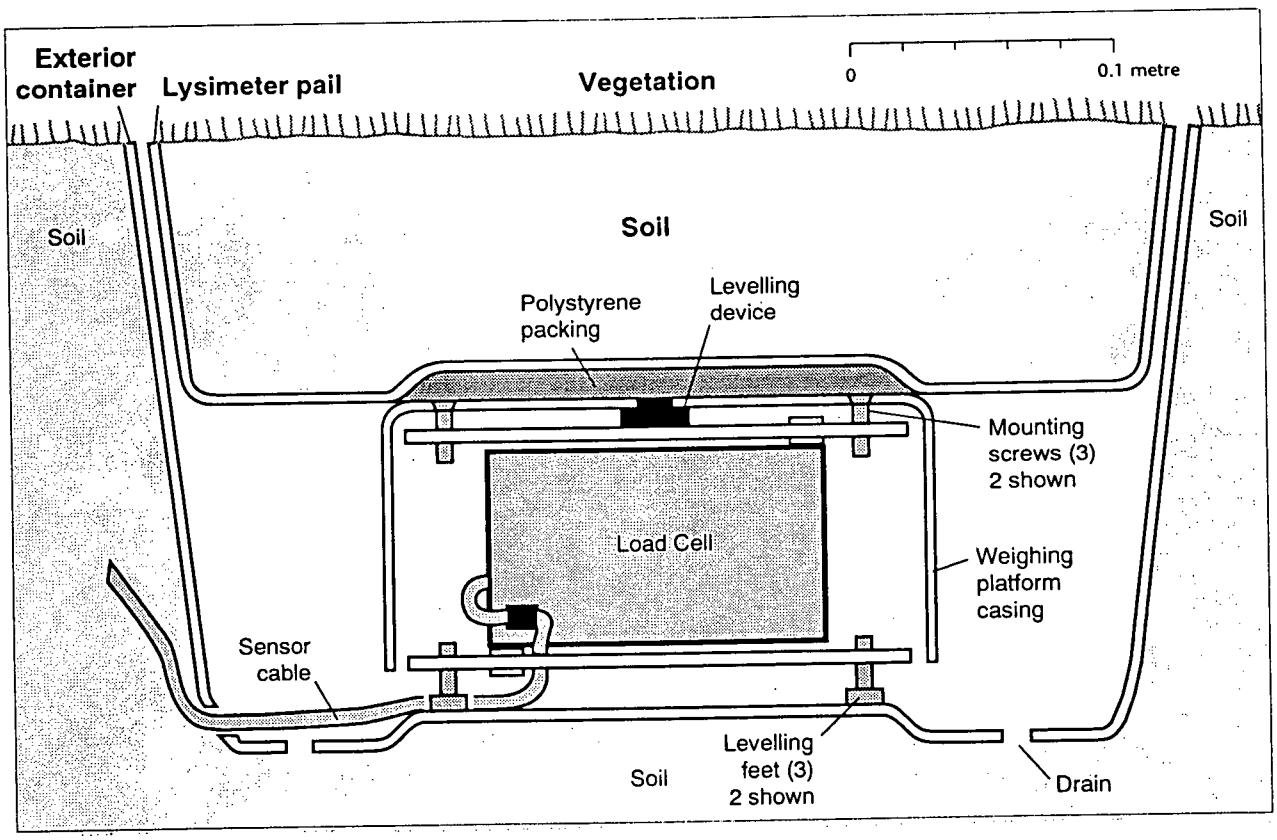

Figure 3.6 A schematic cross-section of an electronic 'grass' mini-lysimeter, used to sense dewfall.

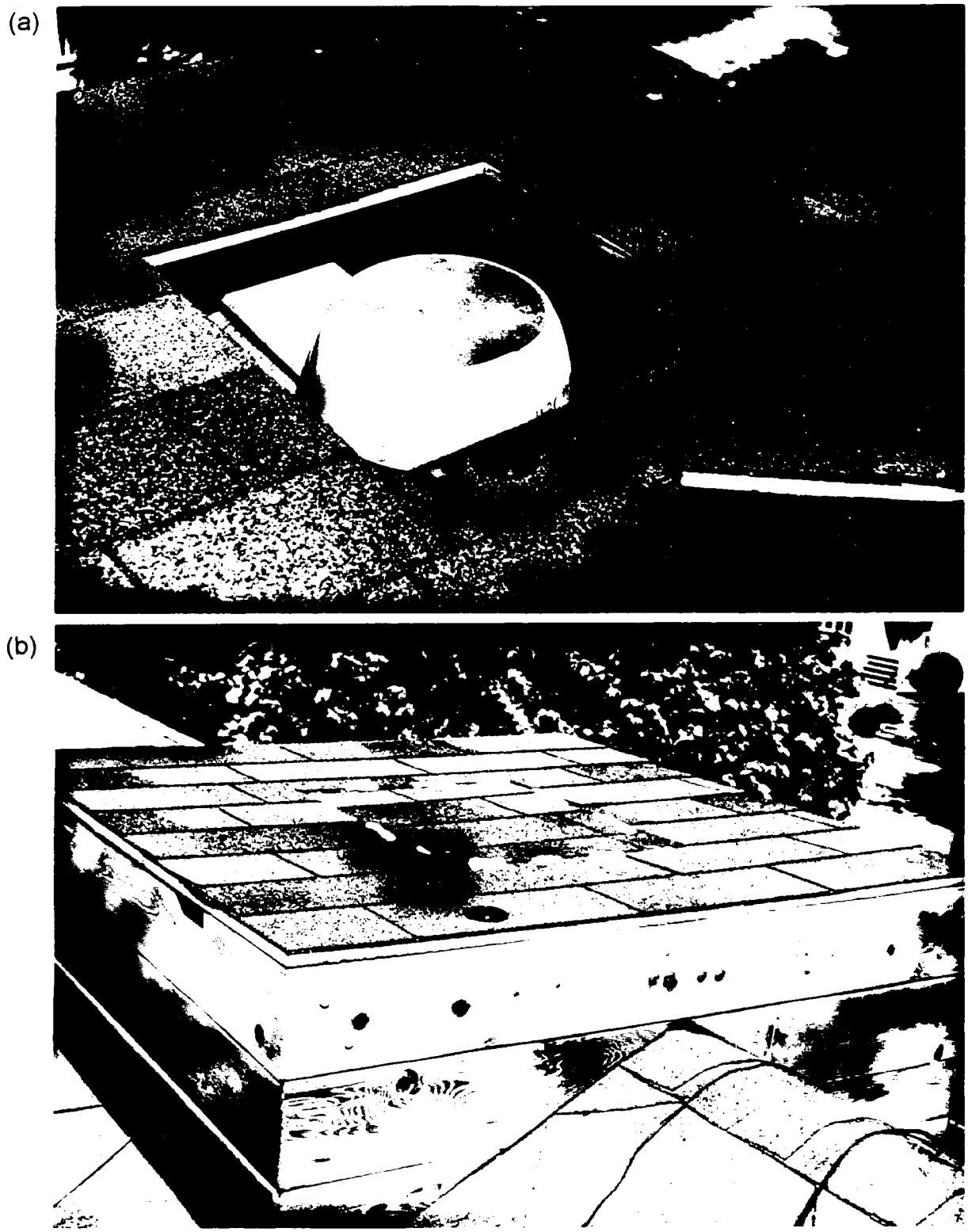

Figure 3.7 The electronic 'roof' mini-lysimeter installed on a house roof at the urban site (U1), showing the device (a) with its load removed and (b) with this in place; a broken line marks the position of the panel which is weighed by the lysimeter.

lysimeters were sampled every 60 s using a *Campbell Scientific* CR10 or CR21X data logger and data were stored as 15 min averages.

Air temperature and relative humidity were measured at 1.5 m above ground at R1 and U1 using a *Vaisala* HMP35C sensor in a *Young* radiation shield, and wind conditions were also monitored (see Table 3.1). Since relative humidity varies as a function of both the actual moisture content and temperature of air, several temperature and humidity related parameters were derived from the primary data, to to describe the moisture content (vapour density ρ_v, g m^{-3}; dew-point T_d, °C) and degree of saturation (vapour density deficit ρ_{vd}, g m^{-3}) of ambient air (Section A1.4).

Sky view factor at R1 and U1 was determined using fish-eye lens photography and a numerical method (Steyn, 1980; Steyn and Lyons, 1985). At each site, a fish-eye lens photograph was taken at ground level looking up at the sky zenith. The resulting image was then projected onto a stereographic grid and distributions of sky and terrain were converted to polar coordinates. From these data, Ψ_{sky} was calculated using the method suggested by Steyn and Lyons (1985), as implemented using a computer programme (SVFPLOT) written in FORTRAN by M. A. McClean (1993).

Background weather data for the region were obtained from UBC and VIA (Figure 3.1). These data were compared to the long-term (1961–1990) mean data for VIA to assess whether weather conditions seen during 1996 were typical for the region. The degree of similarity was tested by comparing means and standard deviations, and by computing the mean absolute difference (MD) and root mean square difference (RMSD) for the data-sets (see Section A1.5 for a description of

these statistical indices). The degree of similarity between air temperature and humidity data from vehicle surveys and fixed sites (Section 3.2.3) was also tested using these statistical indices. MD and RMSD are fundamentally the same as the more commonly employed 'mean absolute error' and 'root mean square error' (Willmott, 1984). In the present study, sets are most often tested for *differences* and seldom for actual *errors*, and the nomenclature (MD and RMSD) is specifically chosen to reflect this.

The relative frequencies of urban and rural dew events were compared (Section 3.2.3) using *comparative amount* as a descriptor. That is, the number of nights when dewfall measured at R1 exceeds that at U1, and *vice versa*, and how often dewfall values at R1 and U1 are equal (to within 0.01 mm) were computed and compared. Since the expected frequency of individual events in each category (e.g., $-E_R > -E_U$) was less than five, statistical tests such as the Chi-squared test could not be used.

3.2.3 Results

In general, the timing and magnitude of heat islands seen in the present study are consistent with those from previously published studies undertaken in Vancouver under similar weather conditions, and for similar times and locations (Oke and Maxwell, 1975; Runnalls, 1995). The present study does not include data for the urban core, so observed UHI values are smaller than in previous studies. Humidity patterns show general agreement with those reported for summer conditions in other mid-latitude cities (Section 2.4) but absolute magnitudes vary.

(a) Weather analysis

The majority of observations undertaken in Vancouver in 1996 were made during June-July (YD 153–213). To assess whether the weather conditions observed in this period were 'typical', data for June-July are compared with the mean conditions for the area, as formalised by the long-term (1961–1990) mean hourly data-set for Vancouver.

The data used in the comparison consist of standard weather observations and parameters derived from them, i.e., air and dew-point temperature (°C) measured at 1.5 m, wind speed (m s^{-1}) at 10 m, the fraction of cloud cover (in tenths), rainfall (mm) and number of raindays (days with rainfall >0.2 mm). The two data-sets are not strictly equivalent because the long-term data are measured at VIA (Figure 3.1), whereas the 1996 data are measured at UBC (except for cloud data, which are from VIA). Nevertheless, observations suggest that weather data gathered at UBC and VIA are fairly similar (Oke, *per. comm.*, 1998) and, therefore, that the two data-sets are comparable. If present, location effects are expected to be greater for wind data because shelter and surface roughness differ at the two sites.

The results of the comparison are presented in Table 3.2. Several measures suggest that mean conditions during June-July, 1996, are similar to the long-term mean conditions for the Vancouver area:

- hourly mean air temperature values for June ($\overline{T}$ = 14.9°C) and July ($\overline{T}$ = 17.5°C), 1996, are similar to their long-term mean values, i.e., 15.1°C and 17.1°C, respectively. For both months MD ≤0.9°C and RMSD ≤1.0°C

(Table 3.2). Hysteresis is evident in the hourly data, i.e., at night, temperature in the 2-month data-set exceeds that in the long-term data-set; during day the converse is true. This is probably a location effect because the two sites are different distances from the sea,

- hourly mean dew-point temperature values for June ($\overline{T}_d$ = 10.4°C) and July ($\overline{T}_d$ = 13.2°C), 1996, are also similar to their long-term mean values ($\overline{T}_d$ = 10.3°C and $\overline{T}_d$ = 12.3, respectively). For both months MD and RMSD values are ≤0.9°C (Table 3.2), and
- there is general agreement between the mean hourly cloud cover observed in June ($\overline{n}$ = 0.64), 1996, and long-term mean values ($\overline{n}$ = 0.65). July, 1996, with a mean cloud cover of $\overline{n}$ = 0.33 is slightly less cloudy than the average ($\overline{n}$ = 0.51). For both June and July, the mean differences (MD and RMSD) between the data-sets are less than 0.2 (Table 3.2).

The greatest difference occurs for rainfall. The number of rain days for June-July, 1996 (10), is less than the long-term mean (17), and rainfall totals for June (2.3 mm) and July (5.8 mm), 1996, are far below the long-term averages for these months (45.7 and 36.1 mm, respectively). Correlation between wind speeds for the two data-sets is weaker than for the other parameters. UBC is known to be more sheltered than VIA. The difference is greater during daytime, whereas at night, the values converge.

Table 3.2 Summary of statistical indices used to test the similarity between mean hourly weather data for June and July, 1996, and long-term (1961–1990) mean hourly data for Vancouver for the same period (see text for definitions of parameters).

	Long-term data-set[1]		**2-month data-set[2]**		**MD**	**RMSD**
	Mean	**SD**	**Mean**	**SD**		
• *Air temperature (°C)*						
June	15.1	2.1	14.9	1.8	0.4	0.5
July	17.1	2.4	17.5	2.0	0.9	1.0
• *Dew-point temperature (°C)*						
June	10.3	0.4	10.4	0.7	0.3	0.3
July	12.3	0.5	13.2	0.4	0.9	0.9
• *Fraction of cloud cover*						
June	0.65	0.05	0.64	0.09	0.04	0.05
July	0.51	0.05	0.33	0.05	0.17	0.17
• *Wind speed ($m\ s^{-1}$)*						
June	3.2	0.6	1.9	0.2	1.3	1.3
July	3.1	0.6	2.6	0.3	0.8	1.0

	Long-term data-set[1] Total	**2-month data-set[2] Total**
• *Raindays (d)*		
June	10	5
July	7	5
• *Rainfall (mm)*		
June	45.7	2.3
July	36.1	5.8

Source: 1. VIA; and 2. UBC.

Taken together these results suggest that the weather conditions during June-July, 1996, were fairly representative of summer conditions in Vancouver, but that rainfall amount was less than average. For the purposes here, this is interpreted to mean that the period was not unusually biased toward weather that either favoured or

inhibited dewfall. However, at unirrigated sites the soil moisture available for distillation may have been reduced compared to normal.

(b) Vehicle surveys

As expected, there is general correlation between urban effects (estimated as urban-rural differences) and local weather. Selected observations for two contrasting days illustrate this:

YD 154/155 is overcast and windy during the daytime, with moderate-light regional winds at night (Figure 3.8). As is expected during windy conditions, when the lower atmosphere is well mixed, day and nighttime temperature and humidity conditions are fairly similar along the survey route (Figure 3.9). At night, vapour density deficits measured at 1.6 m (Figure 3.10) are high at both R1 (2.5 g m^{-3}) and U1 (4.1 g m^{-3}).

YD 171/172 has clear skies and light winds, especially at night (Figure 3.11). In the afternoon, near-surface temperature and humidity conditions are fairly similar across the region (Figure 3.12). Overnight, an UHI of 3.0°C forms between U1 and R1, and there is even greater difference (4°C) between the commercial zone to the north of the Fraser River and R1. U1 is more moist (Figure 3.12), but is characterised by a slightly higher vapour deficit (1.9 g m^{-3}), compared to R1 with a vapour density deficit of 1.3 g m^{-3} (Figure 3.13). On both days, vapour density differences between R1 and U1 are of small absolute size (<1.0 g m^{-3}) at all times (Figures 3.12b and 3.13b).

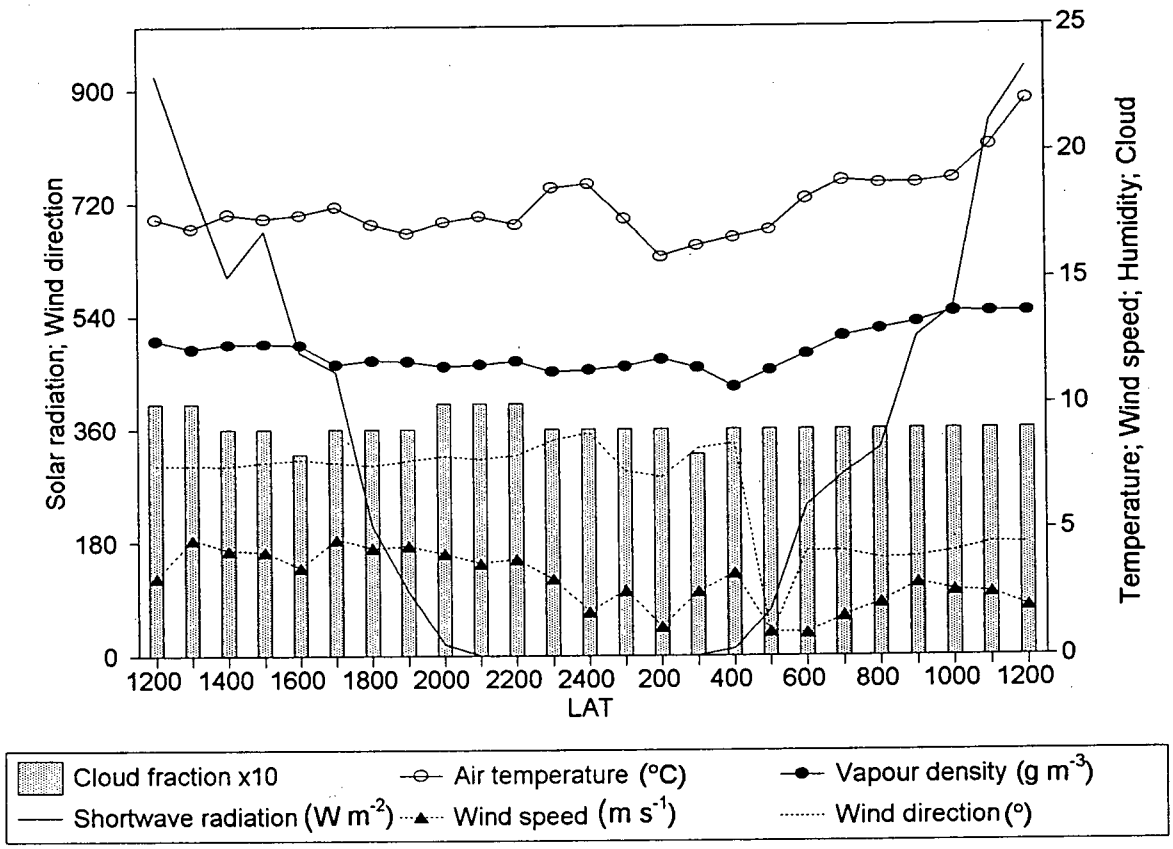

Figure 3.8 Regional weather data measured for YD 154/155, 1996. Data are the fraction of cloud cover (x10) from visual estimates at VIA and incoming shortwave radiation (measured at 0.5 m; see Table 3.1); air temperature and humidity at screen height (1.5 m), and wind speed and direction (10 m) measured at UBC.

(a)

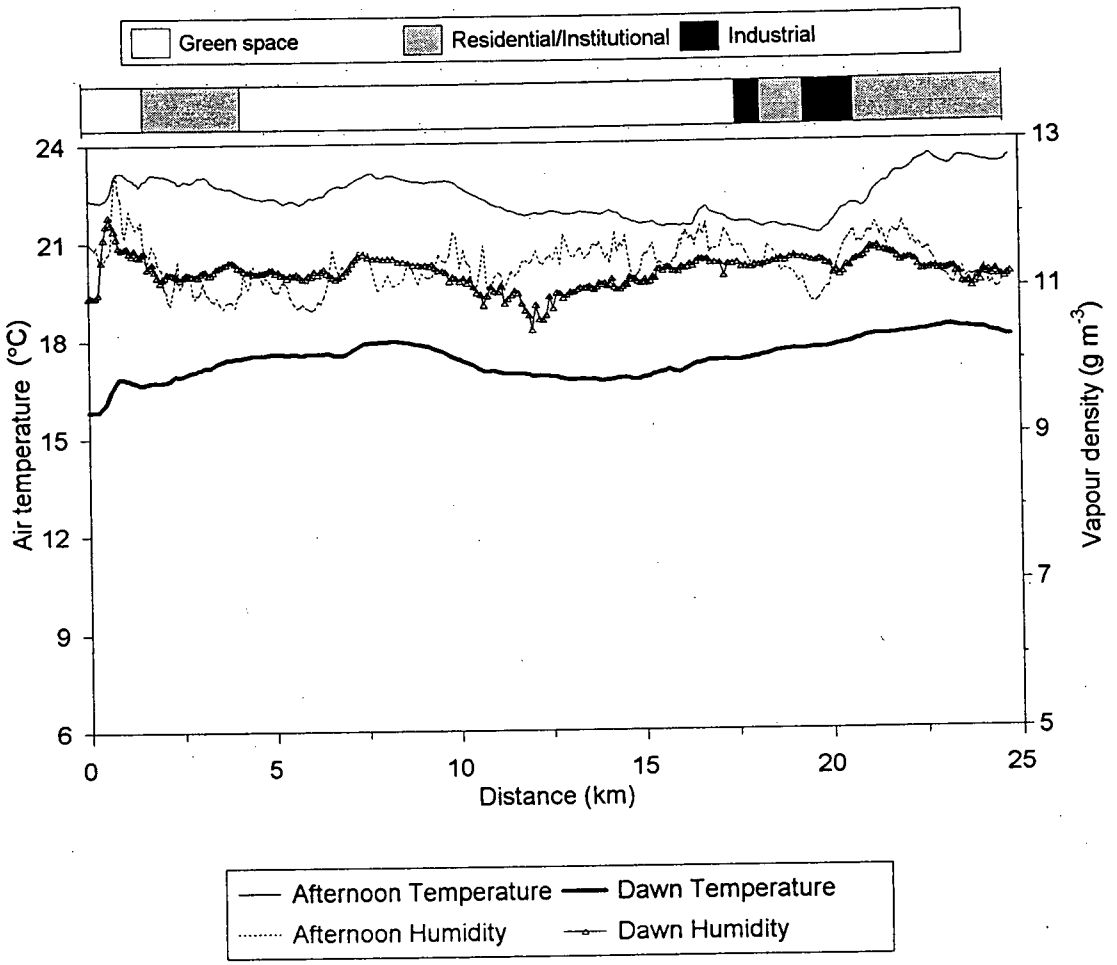

(b)

YD	LAT	Wind conditions at 10 m[1]		Cloud conditions[2]		ΔT_{U-R}	$\Delta \rho_{V\ U-R}$
	(h)	Speed (m s^{-1})	Direction	Cover	Height	(°C)	(g m^{-3})
154	1606	4.0	NW	0.9	Mid	1.1	-0.6
154	2242	3.5	NW	0.9	Mid	0.7	0.0
155	400	2.0	S	0.9	Mid	2.1	0.3

Source: 1. UBC; and 2. VIA.

Figure 3.9 (a) Canopy-level (1.6 m) air temperature (°C) and vapour density (g m^{-3}) along a 25 km route from a rural site (R1) to an urban residential (U1) site in Vancouver, for selected periods during YD 154/155, 1996. (b) Characteristic environmental conditions during the mobile surveys.

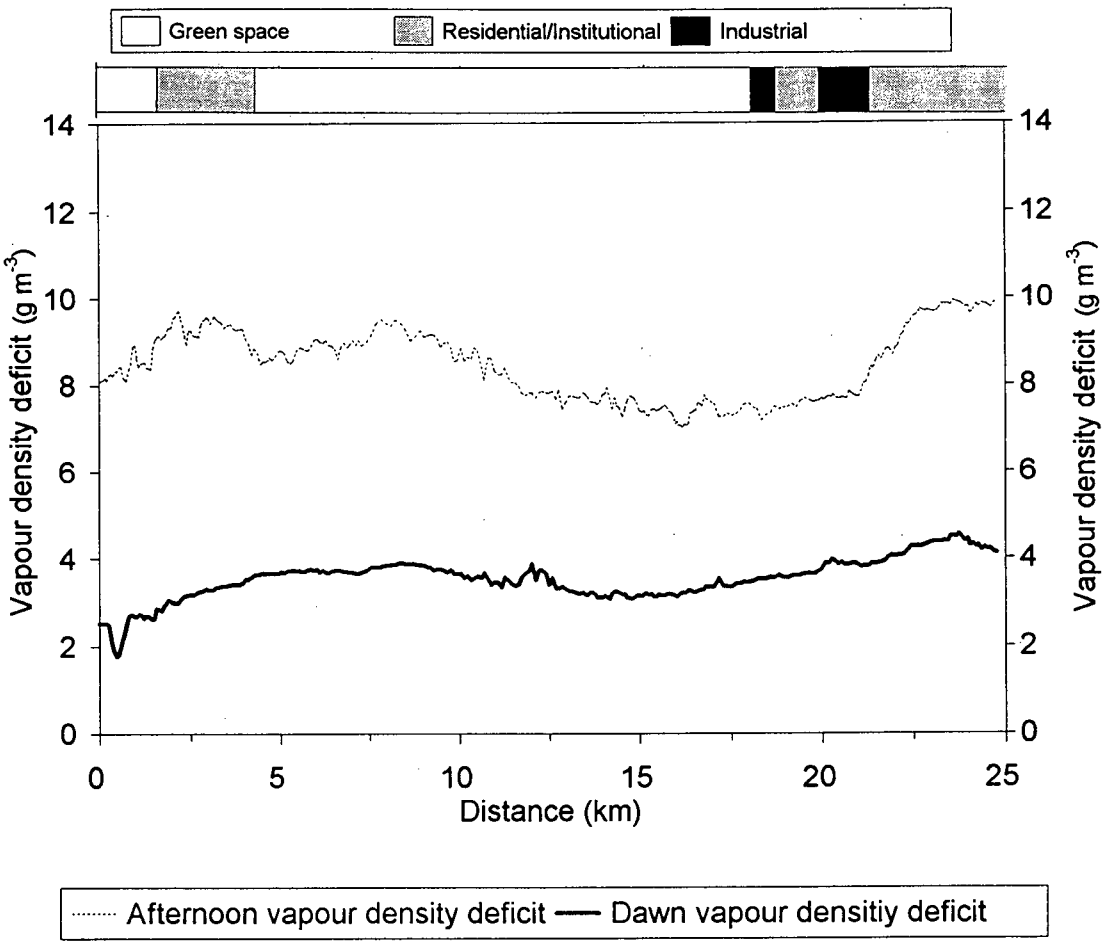

Figure 3.10 Canopy-level conditions on YD 154/155 as described in Figure 3.9, but showing vapour density deficits (g m^{-3}).

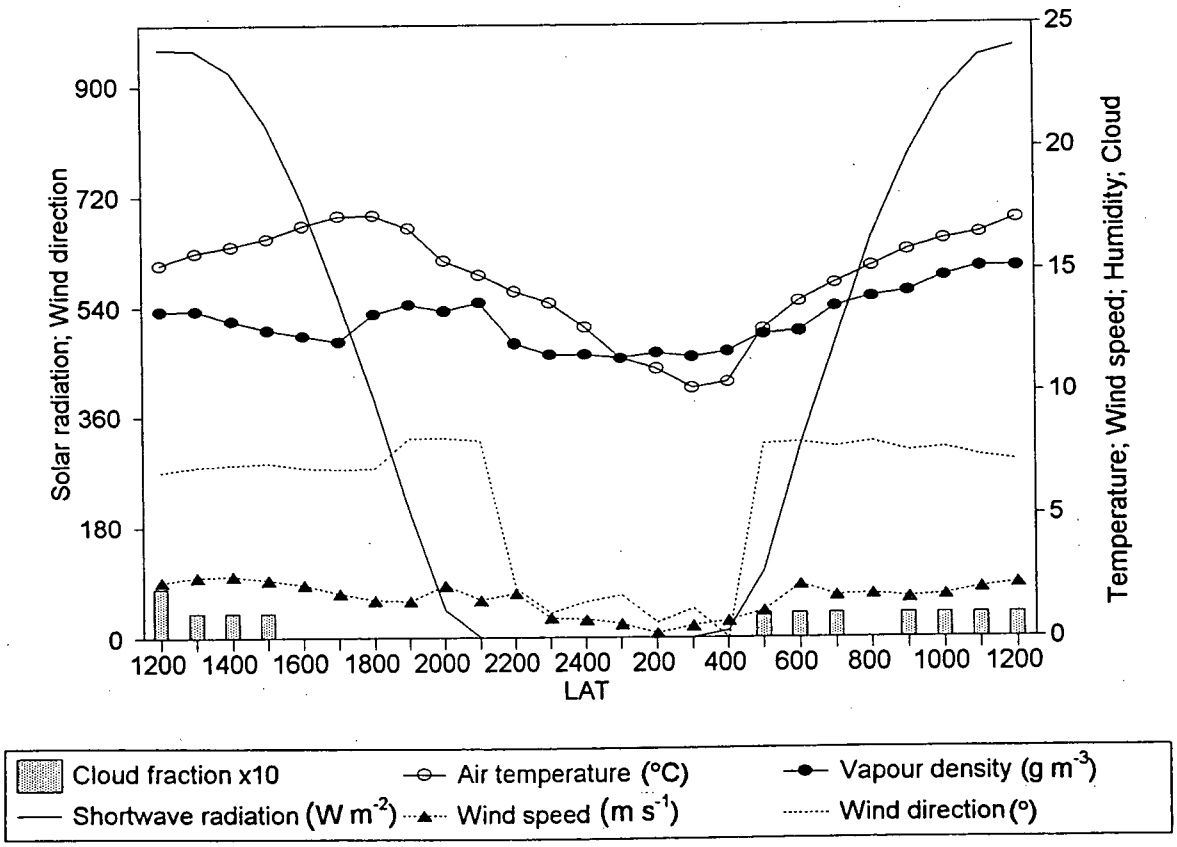

Figure 3.11 Regional weather data as described in Figure 3.8, but for YD 171/172, 1996.

(a)

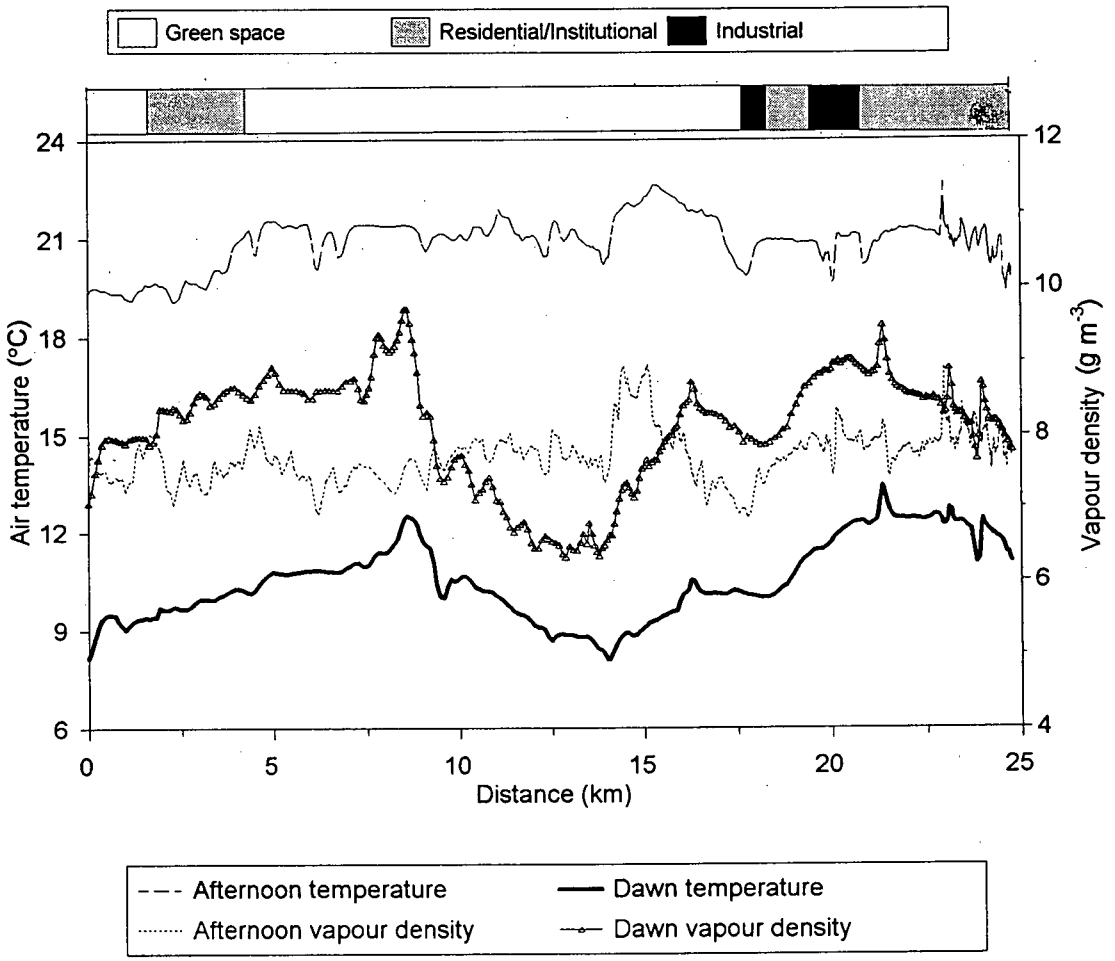

(b)

YD	LAT	Wind conditions at 10 m[1]		Cloud conditions[2]		ΔT_{U-R}	$\Delta \rho_{V\ U-R}$
	(h)	Speed (m s^{-1})	Direction	Cover	Height	(°C)	(g m^{-3})
171	1648	2.0	W	0.0	-	0.7	0.3
171	2236	0.75	NE	0.0	-	2.1	0.5
172	406	0.5	NE	0.0	-	3.0	0.7

Source: 1. UBC; and 2. VIA.

Figure 3.12 (a) Canopy-level and (b) environmental conditions as described in Figure 3.9, but for YD 171/172, 1996.

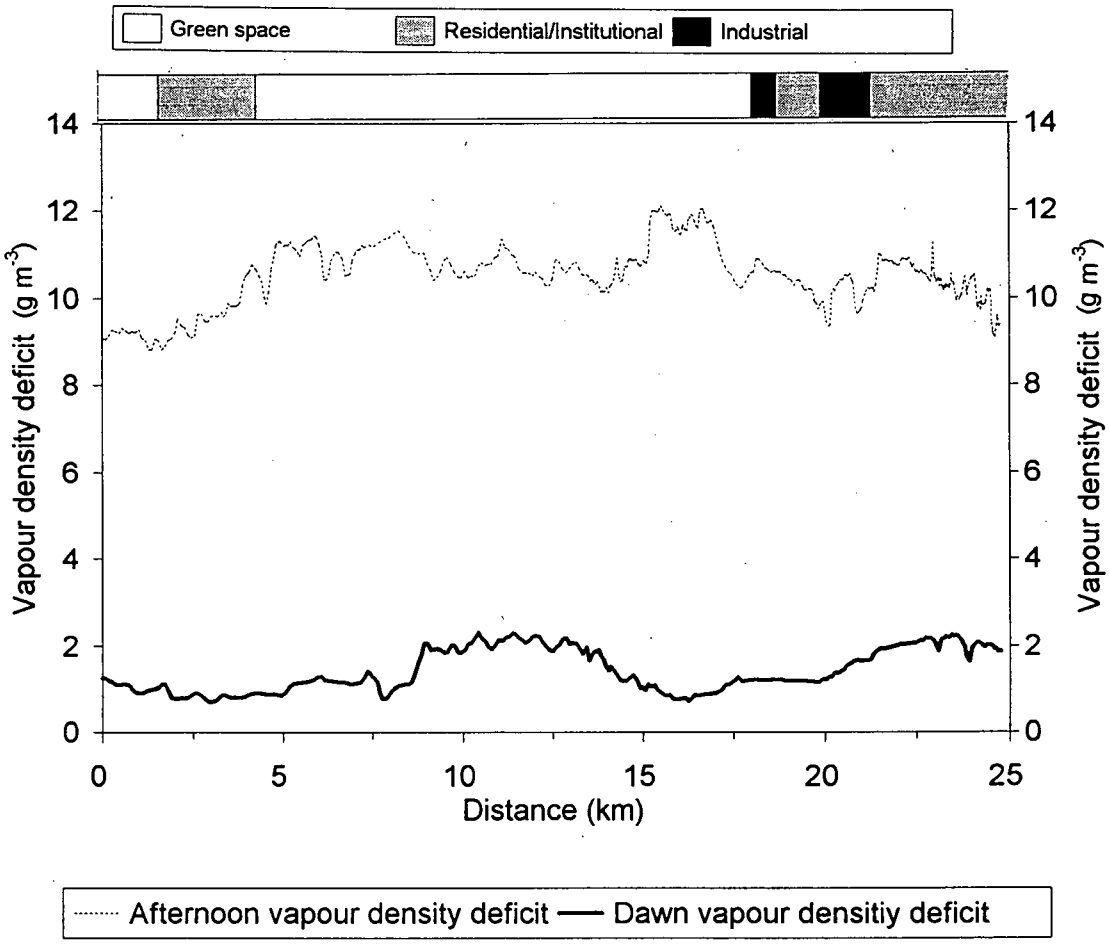

Figure 3.13 Canopy-level conditions on YD 171/172 as described in Figure 3.12, but showing vapour density deficit (g m^{-3}) values.

For nights with clear skies and light winds, coherent spatial patterns are evident at dawn. For example, on YD 171/172 (Figure 3.12), lower temperature tends to correlate with rural (0–2, 10–14 km) and green-space (14–15 km) areas along the route, residential neighbourhoods are relatively warm (2–4, 21–25 km), and the warmest sites are commercial and/or industrial areas (20–21 km). Similarly, lower humidity values are associated with rural land-use and green-space, and higher humidity with built-up areas. Warm, moist anomalies are linked to highway tunnels (8 km) and traffic delays (22 km), where heat and vapour from surrounding vehicles create 'spikes' in sensor readings. General correlation is evident between temperature and humidity, i.e., in warmer areas near-surface air tends to be more moist, whereas cooler areas tend to be drier. Viewed in isolation, this might seem to suggest that in cooler (rural) areas near-surface humidity is depleted by nocturnal dewfall, while at warm (urban) sites dewfall is inhibited.

(c) Fixed sites

Although biased toward fine weather, significant variability is contained in the 24-day data-set gathered at R1 and U1 (Figure 3.14 and 3.15). Based on hourly averages, UCL temperature and humidity can be greater or less than rural values; $\Delta T_{U\text{-}R}$ and $\Delta \rho_{v\,U\text{-}R}$ range from -4 to 6°C, and -3.5 to 2 g m^{-3}, respectively. At night U1 tends to be slightly warmer (~1–2°C; Figure 3.14) than R1, and on average U1 is slightly less humid than R1 at all times (~0.5–1.5 g m^{-3}; Figure 3.15).

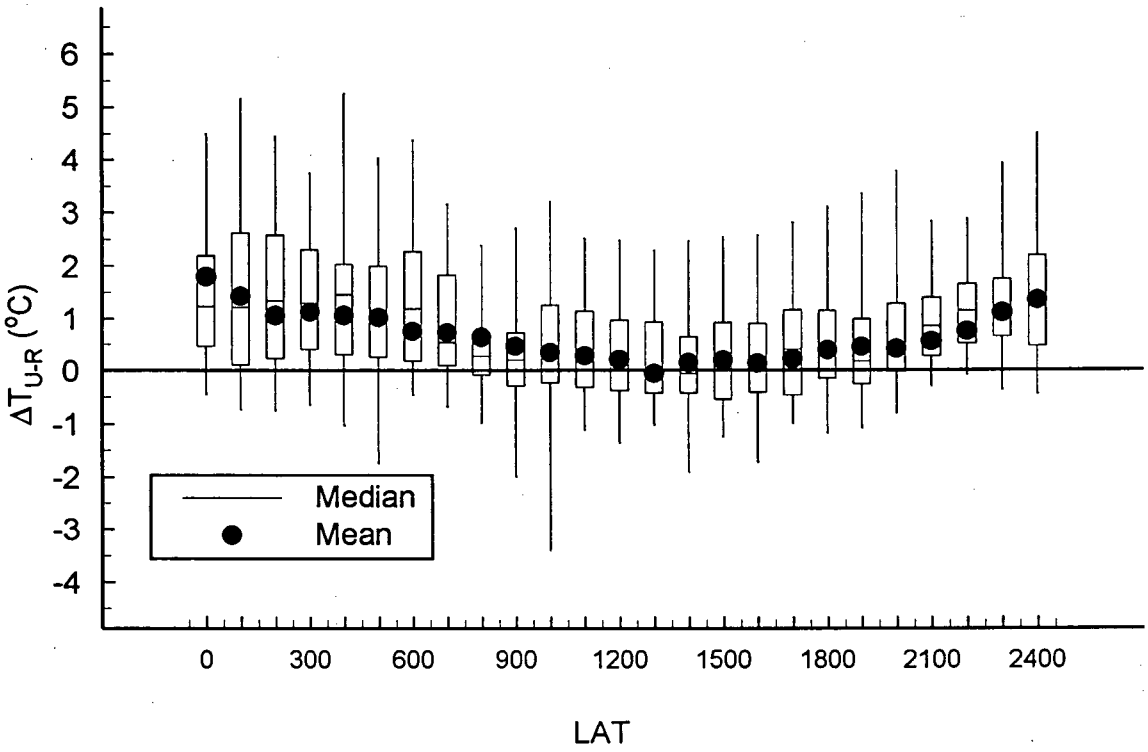

Figure 3.14 Computed difference between mean hourly air temperature (°C) values measured at 1.5 m at a rural (R1) and an urban residential (U1) site in Vancouver. Data are for 24 selected days during the summer of 1996. The vertical lines indicate the full range of values, 50% of the data fall inside the boxed region, and the horizontal line and circle indicate median and mean values, respectively.

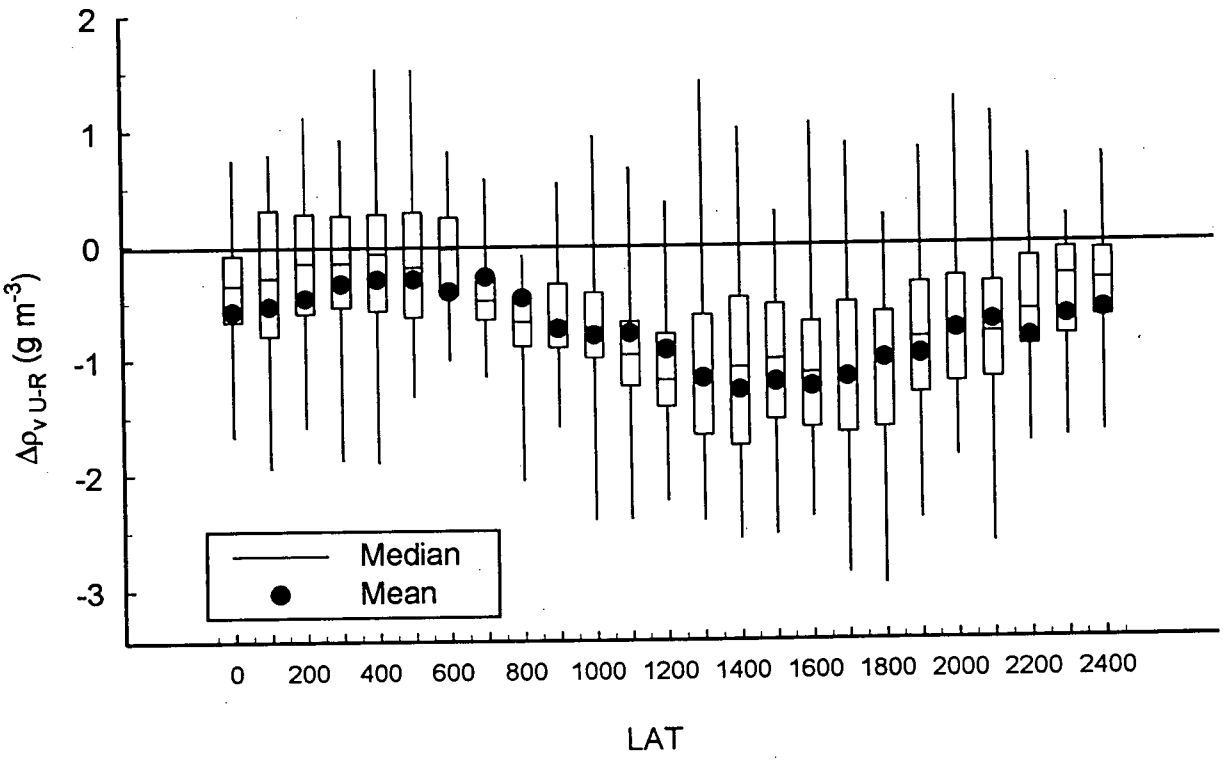

Figure 3.15 Computed urban-rural differences as in Figure 3.14, but for vapour density (g m^{-3}).

The mobile surveys on individual occasions are consistent with the fixed site results (Figure 3.16). There are absolute differences (Table 3.3) but these are small and, on average, they do not exceed 1.3°C and 0.8 g m^{-3} for temperature and humidity, respectively. The observed differences are reasonable because the averaging interval, exact location of instruments—street *vs* back yard at U1 and grassed area at R1—and instrument height differ (Figure 3.16b).

To continue the illustrative example, during YD 154/155 (Figure 3.17a) the urban site is slightly warmer and less moist than R1, except near dawn, when urban and rural humidity values converge. On this day ρ_{vd} values at U1 exceed those at R1 at all times (Figure 3.17b). Overnight, ρ_{vd} at R1 decreases to <1.0 g m^{-3}, but only for 2 h at dawn.

Table 3.3 Summary of statistical indices used to test the similarity between data from vehicle surveys and the fixed sites at R1 and U1 (see text for definitions).

		Vehicle survey		**Fixed sites**			
	n	*Mean*	*SD*	*Mean*	*SD*	*MD*	*RMSD*
• *Air temperature*		*(°C)*	*(°C)*	*(°C)*	*(°C)*	*(°C)*	*(°C)*
Rural (R1)	21	14.7	4.8	14.1	4.9	0.8	1.0
Urban (U1)	21	16.7	4.3	15.6	4.1	1.3	1.6
• *Vapour density*		*(g m^{-3})*	*(g m^{-3})*	*(g m^{-3})*	*(g m^{-3})*	*(g m^{-3})*	*(g m^{-3})*
Rural (R1)	21	8.6	1.4	9.2	1.5	0.8	1.1
Urban (U1)	21	9.0	1.2	9.1	1.3	0.5	0.6

(a)

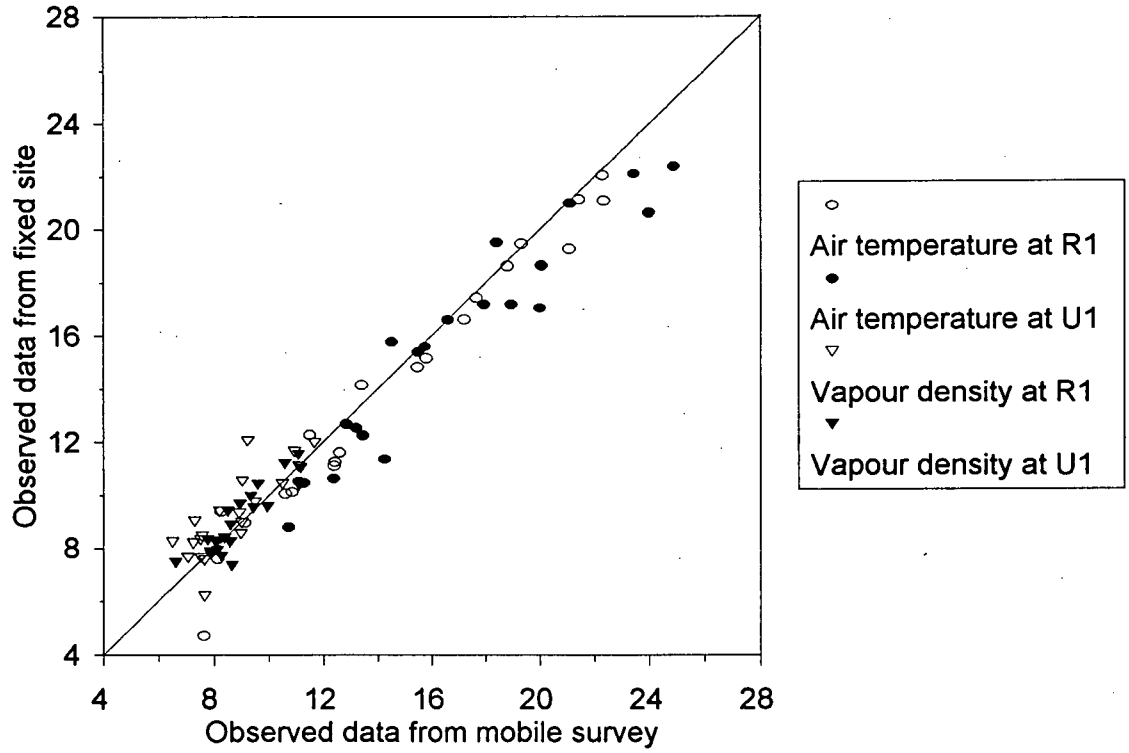

(b)

	Instrument	Averaging interval *(s)*	Instrument location	Measurement height *(m)*
•*Vehicle survey:*	*Vaisala* (ρ_v), thermocouple (T_a)	5	street	1.6 m
•*Fixed instruments:*	*Vaisala* (ρ_v, T_a)	900	back yard (U1)	1.5 m
	Vaisala (ρ_v, T_a)	900	grassed area (R1)	1.5 m

Figure 3.16 (a) Agreement between air temperature (°C) and vapour density (g m^{-3}) data measured during the vehicle survey and using instruments installed at R1 and U1 during the summer of 1996. (b) Selected characteristics of instruments used to collect the two data-sets.

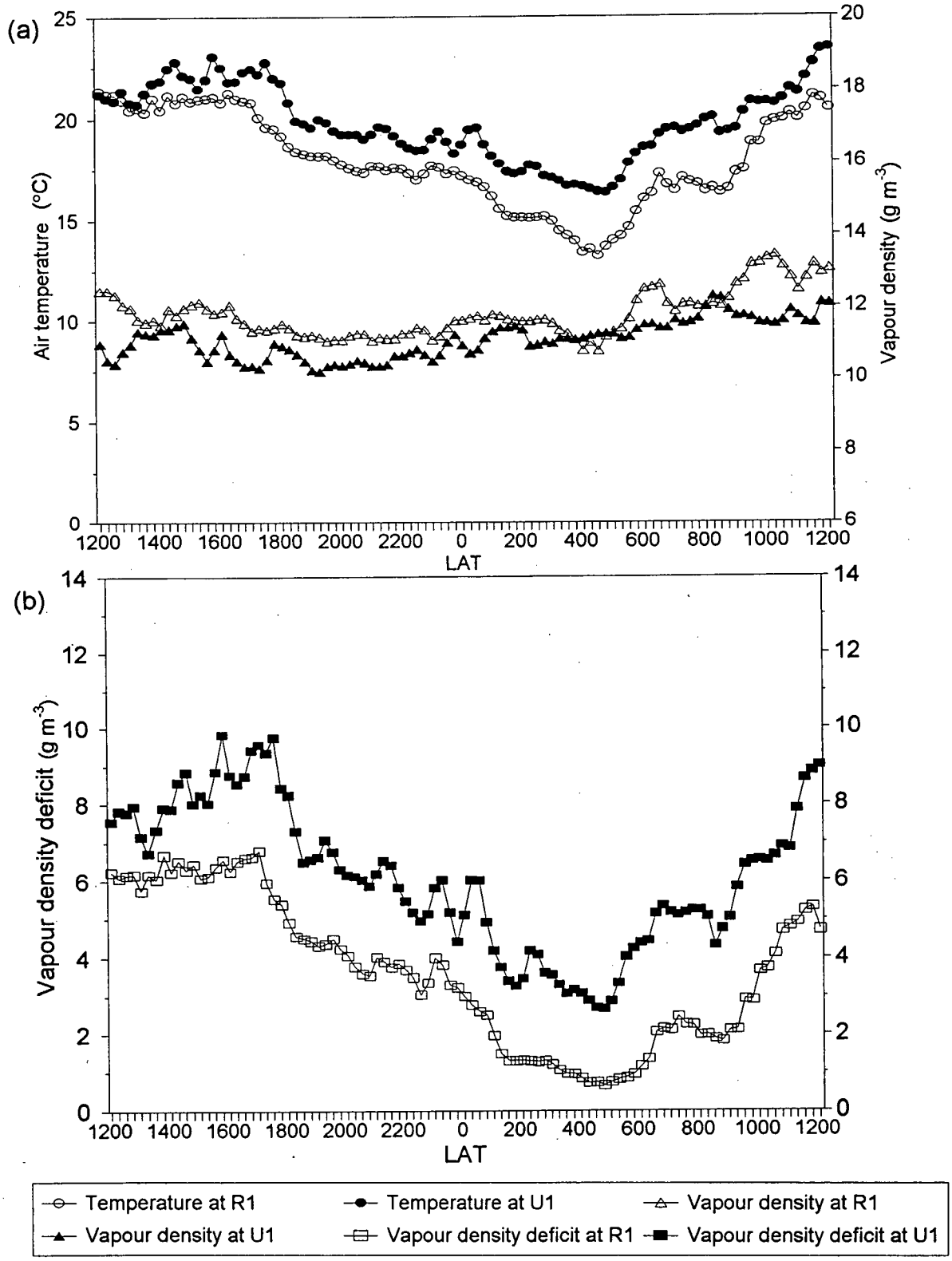

Figure 3.17 Data for YD 154/155, 1996 showing (a) air temperature (°C) and vapour density (g m^{-3}) and (b) the vapour density deficit (g m^{-3}) at 1.5 m at a rural (R1) and an urban residential (U1) site in Vancouver.

On YD 171/172 (Figure 3.18a), UCL humidity is less or similar to rural values by day and up to midnight (0600–2400 h). From about 2100 to 2300 h urban humidity increases and after 2300 h rural humidity declines. The result is greater humidity (up to 0.8 g m^{-3}) at U1, compared to R1. After sunrise, humidity at R1 increases rapidly, urban values more slowly, and the daytime relative urban deficit is reinstated. By day ρ_{vd} values at R1 and U1 are similar but at night they diverge. At R1, ρ_{vd} values are small (<1.0 g m^{-3}) from 2300 to 0545 h, with a minimum value close to saturation (0.3 g m^{-3}) (Figure 3.18b). In contrast, values at U1 are >1.0 g m^{-3} at all times.

A similar temporal pattern to that observed on YD 171/172 (i.e., in Figure 3.18a) is seen for all nights with clear skies and light winds, but there is great variability in the timing and magnitude of the period when an urban excess of humidity is present. Consequently, when data are averaged the urban excess is less evident. This is illustrated in Figure 3.19 for 12 days in 1996 with fine weather. On average, a small nocturnal excess in urban humidity is present between 0200 and 0700 h, but the standard deviations for the data are large and exceed the mean values for ΔT_{U-R} and $\Delta \rho_{v\,U-R}$.

In theory, an excess in urban humidity at night suggests that the vapour storage (humidity) in the rural near-surface layer is depleted by overnight dewfall, whereas in the UCL this process is largely inhibited. Further, although the sharp increase in rural humidity evident after dawn is probably due to the abundant sources (soil and vegetation) of evapotranspiration at rural sites, a small portion

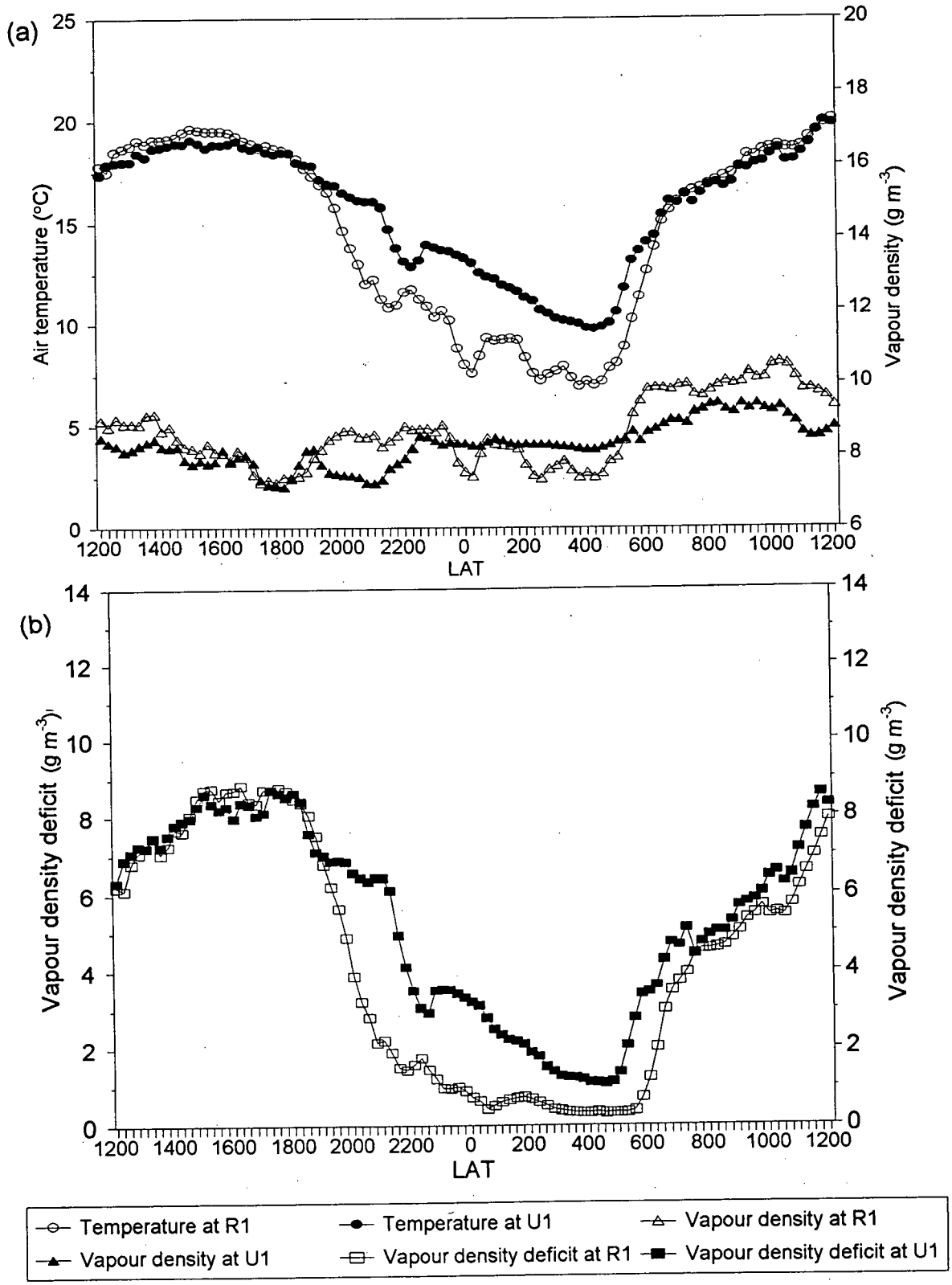

Figure 3.18 As for Figure 3.17, but for YD 171/172.

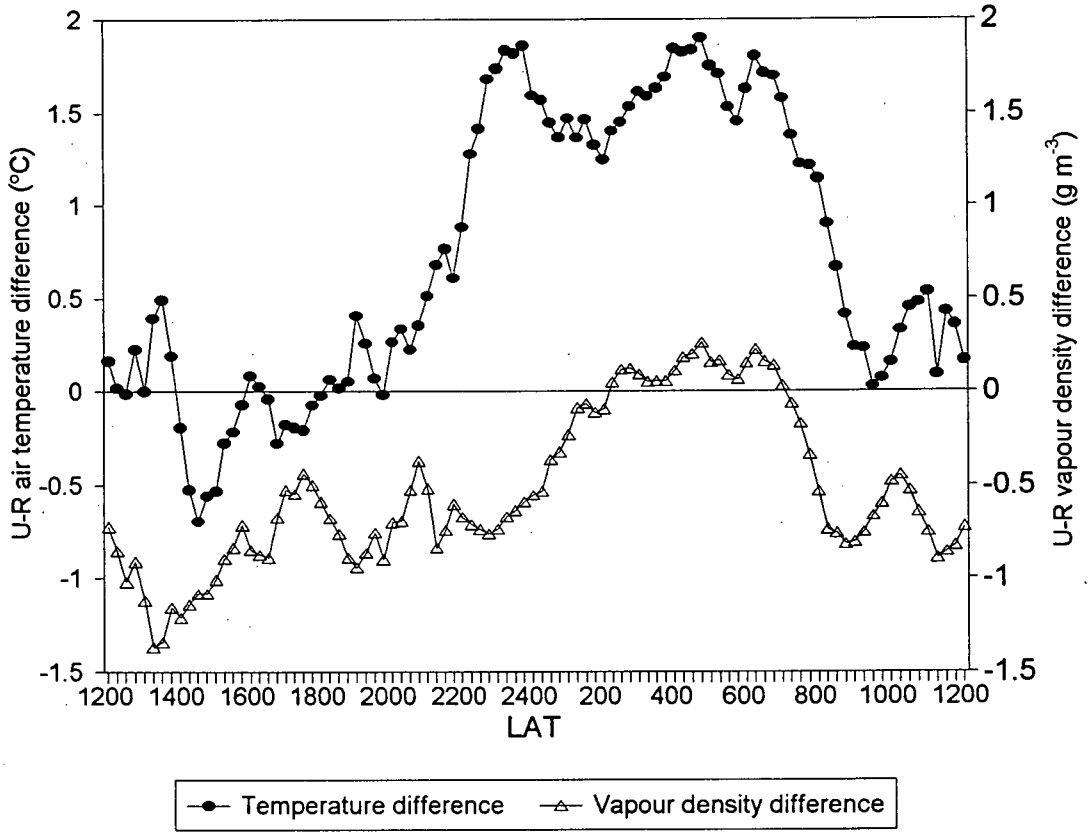

Figure 3.19 Ensemble data for air temperature (°C) and vapour density (g m^{-3}) differences at 1.5 m for a rural (R1) and an urban residential (U1) site in Vancouver, for 12 summer days during 1996 with light winds and no/few clouds. Standard deviations for these data are large: 2.1–2.2°C and 1.1–1.4 g m^{-3}, respectively, where the higher value is during day.

may be derived from evaporation of dew. It might be argued that in the city the evaporative flux in the morning is less strong because in addition to lesser soil moisture and transpiration, dew is absent or reduced. Statements such as these, which attempt to infer causes, can only be speculative, because evidence to support them is circumstantial. However, unlike previous studies of urban humidity, my study includes synchronous measurements of urban and rural surface wetness.

Surface moisture data for grass and, at U1, roof surfaces are available for up to 13 days (Table 3.4). This is a small data-set on which to base conclusions about the general frequency and amount of rural and urban dew in Vancouver during summer. However, weather conditions during the 13 days are fairly typical of conditions seen in Vancouver during summer (Oke, *per. comm.*, 1998) and temperature, humidity and cloud conditions during June–July are similar to the observed long-term (1961–1990) mean values for the Vancouver area (Section 3.2.3). By locating the study days within a long-term framework, a measure of confidence is provided even though the data are too few to provide strict statistical significance.

When data solely for grass are compared (Table 3.4 and Figure 3.20), several measures suggest that there is only a small difference in moisture behaviour at the sites. There is little difference in the *frequency* of surface moisture at the two sites:

- surface moisture measured by blotting at dawn is as frequent at U1 (7 nights) as at R1 (7 nights), and

Table 3.4 Comparitive data for dewfall (mm) by mini-lysimeter and surface moisture (mm) from blotting at a rural (R1) and an urban (U1) site in Vancouver during the summer of 1996, for grass at both sites and a roof at U1.

YD	Surface moisture on grass (blotted)			Dewfall on grass (mini-lysimeter)			Dewfall on roof *vs* on grass (mini-lysimeter)		
	Rural	Urban	ΔSM_{U-R}	Rural	Urban	ΔE_{U-R}	Dewfall on roof	$\Delta E_{roof-grass}$ for rural grass	$\Delta E_{roof-grass}$ for urban grass
	(mm)	(mm)	(mm)	(mm)	(mm)	(mm)	(mm)	(mm)	(mm)
155	0.03	0.03	0.00	0.07	0.00	-0.07	0.06	-0.01	0.06
159	0.05	0.02	-0.03	0.10	0.00	-0.10	0.10	0.00	0.10
164	0.05	0.05	0.00	0.00	0.10	0.10	0.13	0.13	0.03
165	0.03	0.06	0.03	0.00	0.08	0.08	0.13	0.13	0.05
172	0.04	0.02	-0.02	0.10	0.12	0.02	0.16	0.06	0.04
173	0.04	0.02	-0.02	0.00	0.00	0.00	0.11	0.11	0.11
174	0.00	0.00	0.00	0.09	0.00	-0.09	0.06	-0.03	0.06
187	0.01	0.01	0.00	0.08	0.07	-0.01	0.15	0.07	0.08
188	-	-	-	0.27	0.13	-0.14	0.14	-0.13	0.01
189	-	-	-	0.23	0.05	-0.18	0.12	-0.11	0.07
190	-	-	-	0.21	0.10	-0.11	0.13	-0.08	0.03
192	-	-	-	0.10	0.11	0.01	0.11	0.01	0.00
194	-	-	-	0.11	0.12	0.01	0.18	0.07	0.06
Sum	0.25	0.21	-0.04	1.36	0.88	-0.48	1.58	0.22	0.70
Mean	0.03	0.03	-0.01	0.10	0.07	-0.04	0.12	0.02	0.05
SD	0.02	0.02	0.02	0.08	0.05	0.08	0.03	0.08	0.03
Frequ.	7	7	-	10	9	-	13	-	-
U > R			1			5		7	
R > U			3			7		5	
R = U			4			1		1	

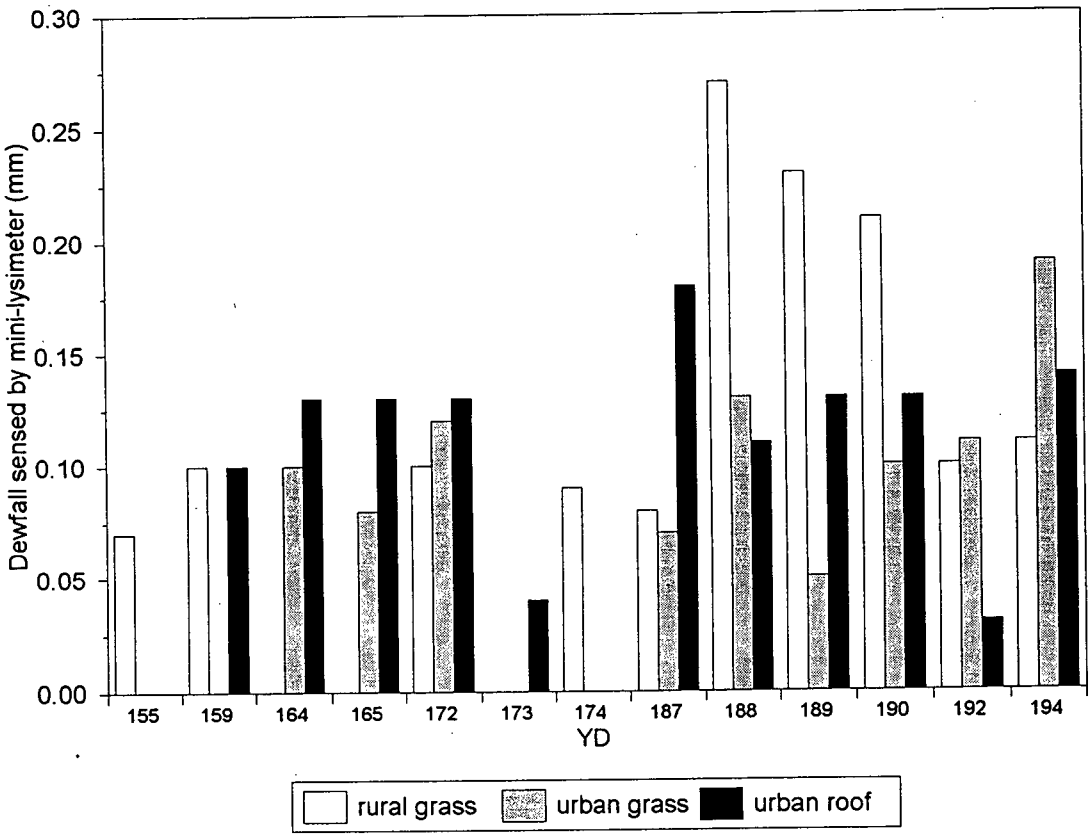

Figure 3.20 Dewfall (mm) data measured by mini-lysimeter at a rural (R1) and an urban (U1) site in Vancouver, during the summer of 1996. Data are for grass at both sites and a roof at U1 (no bar means zero dewfall).

- dewfall is present at the rural site on 10 and at the urban site on 9 of the 13 nights.

Small difference is seen in the *comparative amount* of dewfall for the two sites:

- nights when dewfall at R1 exceeds that at U1 (7 nights) are only slightly more frequent, compared to nights when the converse is true (5 nights),
- blotted surface moisture at R1 equals that seen at U1 (4 nights) more often than it is in excess (3 nights).

On the other hand, there is a marked urban-rural contrast in dewfall *amount*:

- dewfall may be abundant on grass at R1 while on the same night it is absent at the urban residential site, e.g., YD 155 and 159,
- rural dewfall on grass may be much larger, up to 0.27 mm per night, and exceed urban values by up to 0.18 mm (YD 189), and
- the total amount of dewfall measured at R1 for the 13 days of study exceeds that measured at U1 by more than 40%.

At U1, the roof is a surprisingly important site for dewfall accumulation:

- dewfall is sensed by the roof lysimeter on all nights studied,
- dewfall amounts are typically 0.10–0.18 mm per night, and
- the total dewfall to the roof over the study period is much greater in amount (by 80%) and more frequent, compared to that for the urban lawn.

When dewfall data for the rural 'grass' and urban 'roof' lysimeters are compared, the two surfaces show fairly similar overall behaviour. The urban roof is slightly favoured in terms of dewfall frequency and total amount of dewfall over the study period.

However, there are strong contrasts in amount on individual days:

- daily urban-rural differences range from -0.13 to 0.13,
- the largest (>0.20 mm per night) dewfall values are observed for grass at R1 but not for roof and grass at U1, and
- dewfall on the roof is more consistently abundant, compared to that at R1 for grass.

In general, when data for individual days are examined the patterns are explainable. For example, on YD 154/155 only a small amount of surface moisture is present on grass at dawn at U1. This is associated with about 2 h of surface wetness, but dewfall on grass is absent, and the 'grass' lysimeter records evaporation during the night. On the roof, however, up to 0.06 mm dewfall accumulates. In contrast, on the same night at R1 eight hours of surface wetness is sensed on grass, and up to 0.07 mm dewfall accumulates (2400–0800 h), associated with reduced local wind speed (0.0–1.0 m s^{-1} at 1.5 m). These data are consistent with the humidity data shown in Figure 3.17, and suggest: (a) a gradual increase in nocturnal urban ρ_v, associated with ongoing evapotranspiration and absence of dewfall on all but the most favoured (roof) sites; (b) a decrease in nocturnal rural ρ_v (after midnight), associated with the decrease in wind speed and a downward flux of dewfall; and (c) evaporation of dew at the rural site after dawn, contributing a small amount to the sharp increase in rural ρ_v seen at this time. At U1, air at the grass surface fails to reach the dew-point temperature, so no dew forms, despite the low wind speed after 2400 h, whereas the urban roof cooled sufficiently for condensation to proceed.

On YD 171/172 surface moisture began to accumulate at R1 at 2015 h, and up to 0.10 mm of dewfall accumulated overnight, but after dawn this dried relatively quickly. As on YD 154/155, the onset of surface wetness correlates with a drop in wind speed to 0.0–1.0 m s^{-1} at 1.5 m, drying correlates to increased wind speed (> 2.0 m s^{-1} at 1.5 m), and dewfall patterns are consistent with measured humidity data (Figure 3.18). The total accumulation and timing of dewfall on grass at R1 provides good evidence that the nocturnal decrease in ρ_v seen at this site on this night is dewfall related. However, at U1 on the same night relations between canopy level humidity and dewfall data are less straightforward. On this night dewfall is abundant on the house roof (0.16 mm) and grass (0.12 mm) surfaces, and surfaces are wet from 2000 h until 0900 h (roof) or 1030 h (grass). However, nocturnal ρ_v values hardly decrease. Similar patterns are seen at U1 on other fine nights, as summarised in the ensemble data (Figure 3.19). Possible interpretations relate to the areal extent of dew deposition in the city, and sources of water vapour. Surfaces on which dew forms at night at urban sites (roofs, lawns and other vegetation) are only a small fraction of the three-dimensional urban surface, so effects of deposition and drying of urban dew on humidity may be masked. Further, anthropogenic release of water vapour (heating/cooling, cooking and vehicles) into the UCL may tend to offset the removal of water vapour by dewfall.

Taken as a whole, Figure 3.20 suggests that there is a regional weather trend present during the study. In the period YD 155–174 dewfall rarely exceeds 0.13 mm per night at either site. Grass at both sites is without dewfall on several occasions. However, from YD 187 to 194 dewfall is present on all surfaces on each

night, sometimes in large amounts (up to 0.27 mm per night). Examination of the weather conditions for individual nights suggests that the contrast is linked to an increase in nights with clear skies and/or very light winds during the latter half of the study. A measure of corroboration is provided by the mean hourly data presented in Section 3.2.3 which suggests that mean weather conditions during June (YD 153–182, 1996) were similar to the long-term mean values for Vancouver, whereas in July (YD 183–213) cloud amount was slightly less and dew-point temperature was slightly greater than the average. The absolute differences are small but this suggests that conditions promoting dew (moist air and clear skies) may have increased in frequency at about the end of June, 1996.

3.3 Urban spatial and temporal variations

The surveys described in this section investigate the effects of weather, location and site geometry on the amount of surface moisture seen on grass at dawn at urban sites with (a) open exposure, and (b) where sky view factor is progressively reduced by adjacent buildings and vegetation. Temporal and spatial surveys focus on two urban environments which are common in Vancouver (urban parks and residential lots), and grassed surfaces.

3.3.1 Sites and seasons

Observations on the amount of surface moisture present on grass at dawn was collected for two urban parks (P1 and P2) and two residential lots (U1 and U2) in Vancouver, during the summers of 1993 and 1996 (Figure 3.1). P1 (Everett Park;

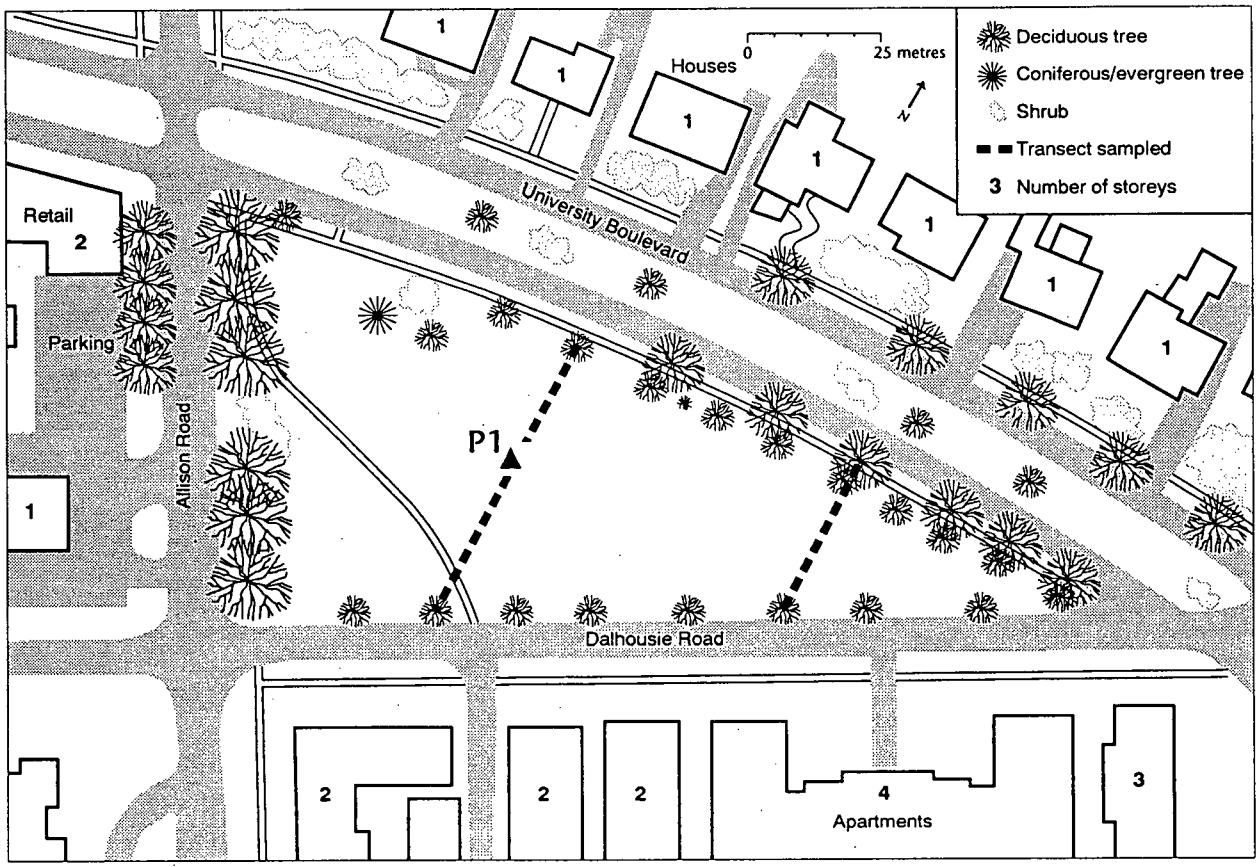

Figure 3.21 The 'suburban' park (Everett; P1) in Vancouver and its neighbourhood.

Figure 3.21) is a small, flat grassed park (0.6 ha), bordered by a regular row of deciduous trees. The centre of the park is open (Ψ_{sky} = 0.93), but sky view factors at the edge of the park under trees are small (0.17). The park is unirrigated, mown at regular intervals, and surrounded by houses, apartments and commercial buildings. P2 (Fairground; Figure 3.22) lies within the Totem Fields Research Area on the campus of the University of British Columbia. Although not located in a residential

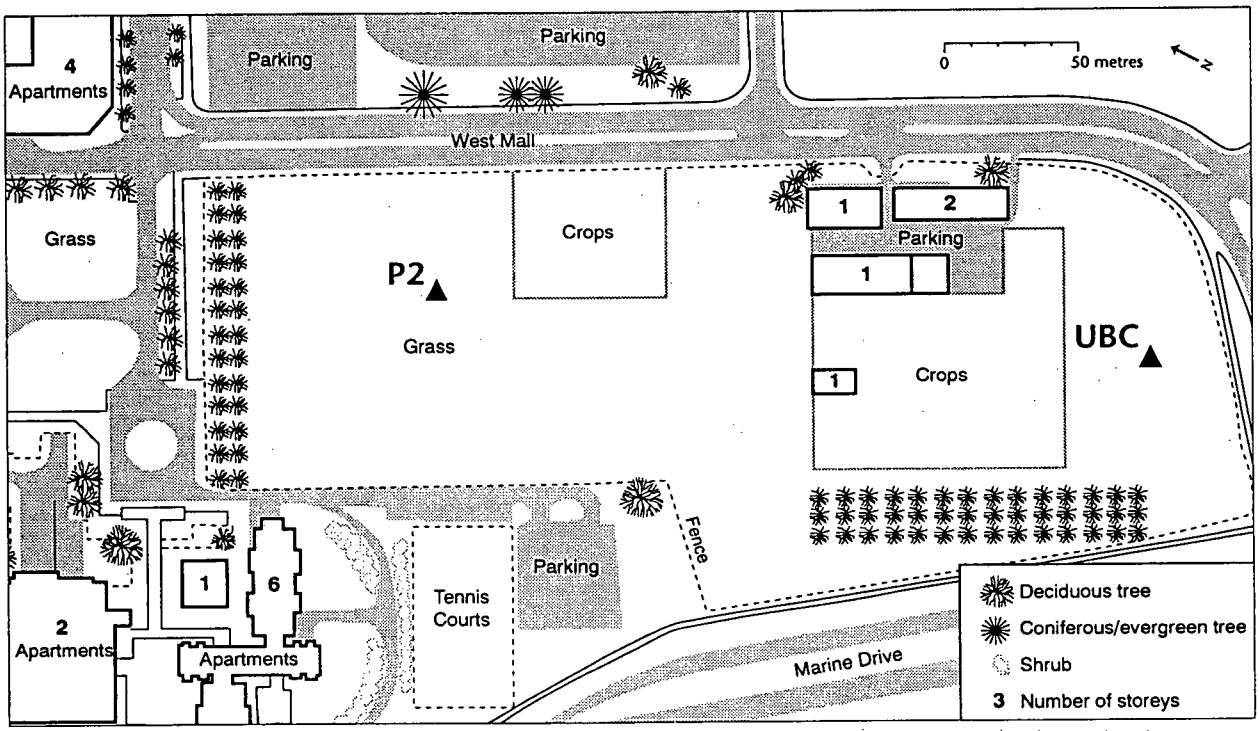

Figure 3.22 The park (Fairground; P2) on the campus of the University of British Columbia campus in Vancouver.

setting, the site is park-like. That is, it is a large, open (Ψ_{sky} = 0.98) and flat grassed area that is bordered by residential apartments, buildings, streets, and a mixture of gardens, lawn and trees. During the summer, the area is well irrigated and mown frequently, to maintain a lush swath of turf (typically 0.05 m high). This location is where the physical scale model was constructed during 1996 (Chapters 4–6). U1 (Kerrisdale) was described earlier (Figures 3.2b–3.4); a lot map is given in

Figure 3.23a. The other urban residential site, U2 (Sasamat; Figure 3.23b) is located in a relatively homogeneous neighbourhood, with 1½–2 storey houses set back from a street bordered with large deciduous trees. The study site is in the backyard of a residential lot, bordered by shrubs and deciduous trees, and, to the south, by large conifers. During the period of study, gardens in the lot were irrigated, however, the lawns were not. The sky view factor of the back lawn is low, with a value of 0.54 near the centre, and 0.29 or less elsewhere.

3.3.2 Data collection and analysis

Data were collected on nights without rain or fog because only then can surface moisture from condensation (dew) be distinguished from that derived from other sources. The amount of surface moisture accumulated on grass at dawn was measured by blotting at the most open (maximum Ψ_{sky}) location of each site. In addition, at all sites except P2 surface moisture at dawn was measured along linear transects on several occasions (their locations are shown in Figures 3.21 and 3.23). Background weather data for each observation season were obtained from UBC and VIA (Figure 3.1).

At the centre of each park and lawn, and at selected locations along transects, Ψ_{sky} was computed using fish-eye lens photography and the numerical method described in Section 3.2.2 (Steyn 1980; Steyn and Lyons, 1985). The method provides an accurate estimate of Ψ_{sky} but is relatively slow to implement. Its main disadvantage is that the polar coordinates necessary for calculations are read

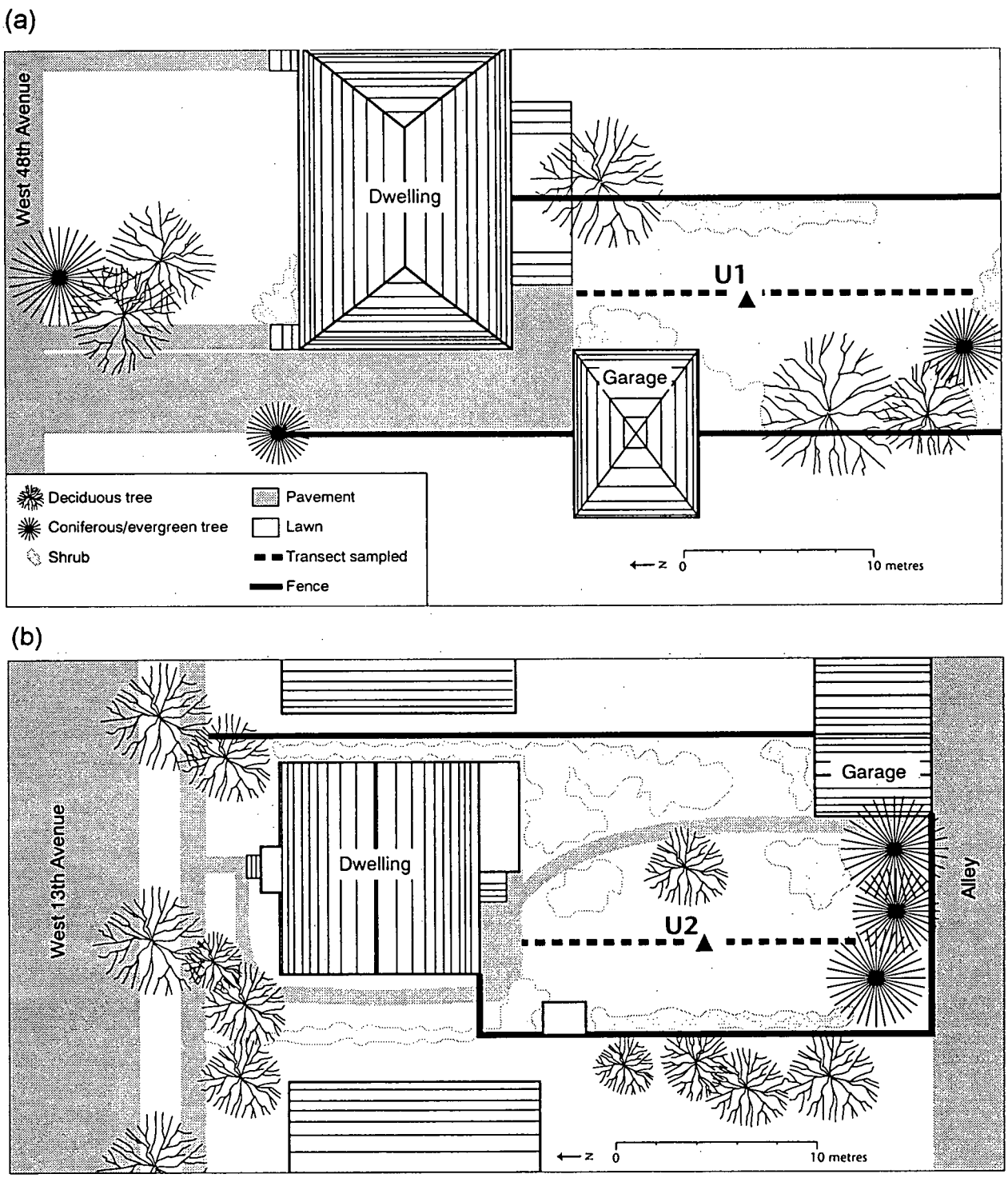

Figure 3.23 The urban residential sites in Vancouver, showing lot maps and the transect sampled for (a) U1 (Kerrisdale) and (b) U2 (Sasamat).

manually from photographic images. Here, a second method was employed to interpolate spatial trends of Ψ_{sky} along transects, i.e., using a simplified representation of site geometry and Ψ_{sky} values previously found using fish-eye lens photographs.

To compute Ψ_{sky} values for house lawns, the shape of the horizon obstruction was approximated using four orthogonal walls, the dimensions of which were determined by lawn length and the mean height of surrounding objects (houses, trees and fences). Close to the house, the apparent height of the 'house' wall was reduced because the roof of the house (the horizon obstruction elsewhere on the lawn) was not visible. For a given point on the lawn surface, Ψ_{ter} was calculated separately for each wall using a formula derived from Steyn and Lyons (1985; Spronken-Smith, 1994) (Section A1.6). The resulting values were summed and Ψ_{sky} found using:

$$\Psi_{sky} = 1 - \sum_{n=4} \Psi_{ter} \qquad [3.1]$$

where n is the number of walls. At P1, spheres were used to approximate the shape of the deciduous trees which border the park and are the primary horizon obstructions at this site (Figure 3.21). Ψ_{ter} for individual trees was found using a formula presented by Howell (1982) (Section A1.6). The effect of several trees was summed and Ψ_{sky} computed using:

$$\Psi_{sky} = 1 - \sum_{i=1}^{n} \Psi_{ter} \qquad [3.2]$$

where n is the number of trees for which Ψ_{ter} is computed; in practice about five per border.

By repeated calculations for points along each lawn and park transect, an estimate of the spatial distribution of Ψ_{sky} was produced. Finally, values were adjusted in magnitude to match the Ψ_{sky} values obtained using the method of fish-eye lens photography. The result is a smooth curve describing the spatial trend of Ψ_{sky} along the transect.

3.3.3 Results

(a) Temporal surveys at relatively open sites

There is considerable day-to-day variation in the maximum amount of surface moisture present on grass at dawn at P1 and P2, as measured by blotting (Table 3.5 and Figure 3.24), but almost all rain/fog-free days, for example 90% at P1, had some surface moisture present at dawn.

Numerous studies of rural dew show a correlation between the amount of surface moisture measured on vegetation at dawn and weather conditions during the preceding night, as measured at a near-by climate station (Chapter 2). Studies report, for example, that more dew accumulates when the preceding night is clear, compared to cloudy, whereas on nights with clear skies more dew is seen when the preceding night is relatively calm. In theory, generalisations to describe relations between rural dew accumulation and weather can be transferred to an urban setting, e.g., a grassed area with large Ψ_{sky} in an urban park.

In the present study, it would be relatively straightforward to perform a multi-variate analysis to define the relationship between, on the one hand, surface moisture measured at dawn at P1 and P2 and, on the other hand, standard weather

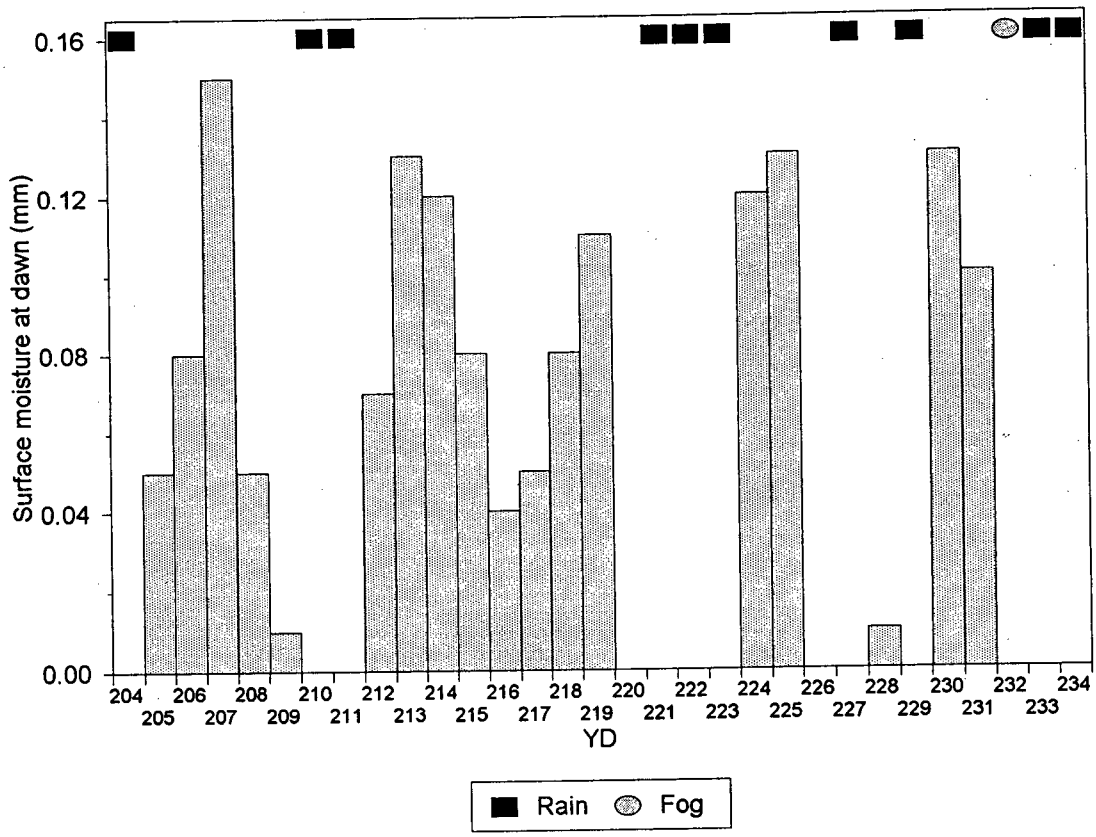

Figure 3.24 Amounts of surface moisture collected by blotting at dawn at the open centre of an urban park (P1) during the summer of 1993 (no bar means zero surface moisture).

Table 3.5 Statistics of the presence and amount of surface moisture on grass at dawn at P1, P2, U1 and U2 on rain/fog-free days, as measured by blotting.

Site	Season	Surface moisture					
	(YD and Year)	*n*	*Present*	*Absent*	*Maximum*	*Mean*	*SD*
		(d)	*(d)*	*(d)*	*(mm)*	*(mm)*	*(mm)*
P1	204–234, 1993[1]	20	18	2	0.15	0.06	0.05
P2	144–196, 1996[2]	22	18	4	0.11	0.05	0.04
U1	155–194, 1993[1]	18	16	2	0.09	0.04	0.03
U2	236–240, 1996[1]	5	5	0	0.11	0.07	0.03

Measured on: 1. Consecutive days; and 2. Days selected for study.

data such as wind speed, air temperature and cloud amount. However, the resulting relation would be based on a fairly small data set and would be specific to the sites and seasons of observation. The approach has been used in several existing models to predict rural dew and few of these find great success (Section 2.5.2). They are particularly handicapped because they lack generality. Here, the feasibility of an alternative approach is explored, this based on a semi-empirical scheme derived from existing studies of urban climate.

Cities tend to cool more slowly after sunset than surrounding rural areas, and this creates an urban-rural temperature differential or nocturnal UHI (Section 2.4.1). The development of this feature is favoured by clear skies and light winds, i.e., weather conditions that promote longwave radiative cooling at the surface. Oke, using data for Vancouver, shows a correlation between nocturnal UCL heat island magnitude and weather expressed as (Oke, 1998):

$$\Phi_w = \left(1 - kn^2\right)u^{-0.5} \qquad [3.3]$$

where k is an empirical coefficient related to cloud type, n is the fraction of cover [tenths], and u is wind speed at 10 m [m s^{-1}] measured at an open location. A large Φ_w value (>1) indicates a cloudless night with little or no wind. Under such conditions radiative cooling at the surface is maximised, meso-scale contrasts in nocturnal air temperature therefore become strong, and a large UHI is expected. Φ_w less than one indicates the presence of cloud and/or wind. As Φ_w decreases, the expected UHI on a given night progressively reduces in magnitude. An UHI of significant magnitude is unlikely when Φ_w approaches zero, its minimum possible value.

The 'weather factor', Φ_w, is empirically derived but its component parts are underpinned by theory relating to known physical processes. That is, it combines the effect of cloud on the longwave radiation balance of the surface, and the influence of wind speed on advection and turbulent mixing. The former portion of the equation is based on the Bolz formula $(1-kn^2)$, which expresses the effectiveness of cloud in reducing net longwave radiation loss from the surface. The empirical coefficient *k* is based on cloud height and therefore accounts for cloud base temperature, classed according to cloud type. This gives emphasis to the importance of warm, low clouds as a control on surface temperatures, compared to equivalent amounts of cold, high cloud, which have little influence. The latter portion of the equation $(u^{-0.5})$ accounts for the non-linear effect of turbulence in homogenising temperature structures at the surface. Here, following Oke (1998), the term $u^{-0.5}$ is used but the exact relation which is chosen is non-critical. In theory, another power or, even, an exponential function would suffice, provided it gives

appropriate emphasis to differences in wind speed when winds are light. At strong wind speeds, temperature structures are broken down, the development of an UHI is then unlikely, and the sensitivity of $u^{-0.5}$ is less important (Oke, 1987; 1998).

Weather conditions which favour the development of a nocturnal, canopy level UHI seem to favour dew accumulation. In other words—and this is the more important link—weather conditions which *promote radiative cooling at the surface* also promote condensation on the cooled surfaces of vegetation and other objects in whatever environment they occur. Hence, it is forwarded that Φ_w has power to describe relations between dew accumulation and weather. More specifically, the scheme predicts that the greatest dew accumulation will be seen on nights with the largest Φ_w values, that dew will be moderate in amount when Φ_w is of intermediate value, and that dew will be absent when Φ_w approaches zero.

In the present study the potential relationship between Φ_w and urban surface moisture accumulation is tested using data collected by blotting on grassed surfaces at P1 (1993) and P2 (1996). Samples were collected at dawn at locations with large Ψ_{sky} (0.93 and 0.98, respectively). The weather data used to solve Equation 3.3 are values measured at UBC, with the exception of cloud data, which are from VIA. Cloud types were converted to *k* using 0.88, 0.73 and 0.24 for low, middle and high cloud, respectively (Oke, 1987). Weighted means of wind speed and cloud cover for the night are used because mean values alone fail to adequately describe characteristic conditions.

Little correlation exists between the observed surface moisture data and wind speed, cloud amount and cloud type when these weather factors are separately

addressed. Even when data are stratified into clear (Figure 3.25a) and calm (Figure 3.25b) nights the scatter is large. Some of the unexplained variability is almost certainly related to the presence of guttation, which is sensed as moisture accumulation but is not directly controlled by weather.

The relationship between Φ_w and surface moisture is presented in Figure 3.26a. There is considerable scatter. However, the accompanying vapour density deficit values (ρ_{vd}; given as data labels in Figure 3.26a) suggest that some of the scatter may be linked to water vapour limitations. Figure 3.26b shows that most days in the combined data set (P1 + P2) have ρ_{vd} values close to the mean (4.63 g m^{-3}). Only one day (YD 216) is strictly an outlier, i.e., its value lies more than three standard deviations away from the mean. However, a total of four days (YD 190, 215, 216 and 217) lie at least one standard deviation away from the mean (see dotted line ρ_{vd} = 6.7 g m^{-3} in Figure 3.26b). Each is characterised by a large vapour density deficit, i.e., 7–14 g m^{-3}, whereas all other days are in the range 2–6 g m^{-3}. Although the threshold is somewhat arbitrary, on this basis I have excluded these four days from the analysis which follows (Figure 3.27).

The relationship shown in Figure 3.27 suggests that there is a general and positive correlation between Φ_w and the amount of surface moisture measured at dawn by blotting. Scatter is still present, but the result is pleasing because Φ_w has not previously been tested against surface moisture accumulation. The contrast between the lack of correlation seen in Figure 3.25 and the correlation evident in Figure 3.27 suggests that the individual roles of wind and cloud are less important than their combined effect as a control on dew accumulation.

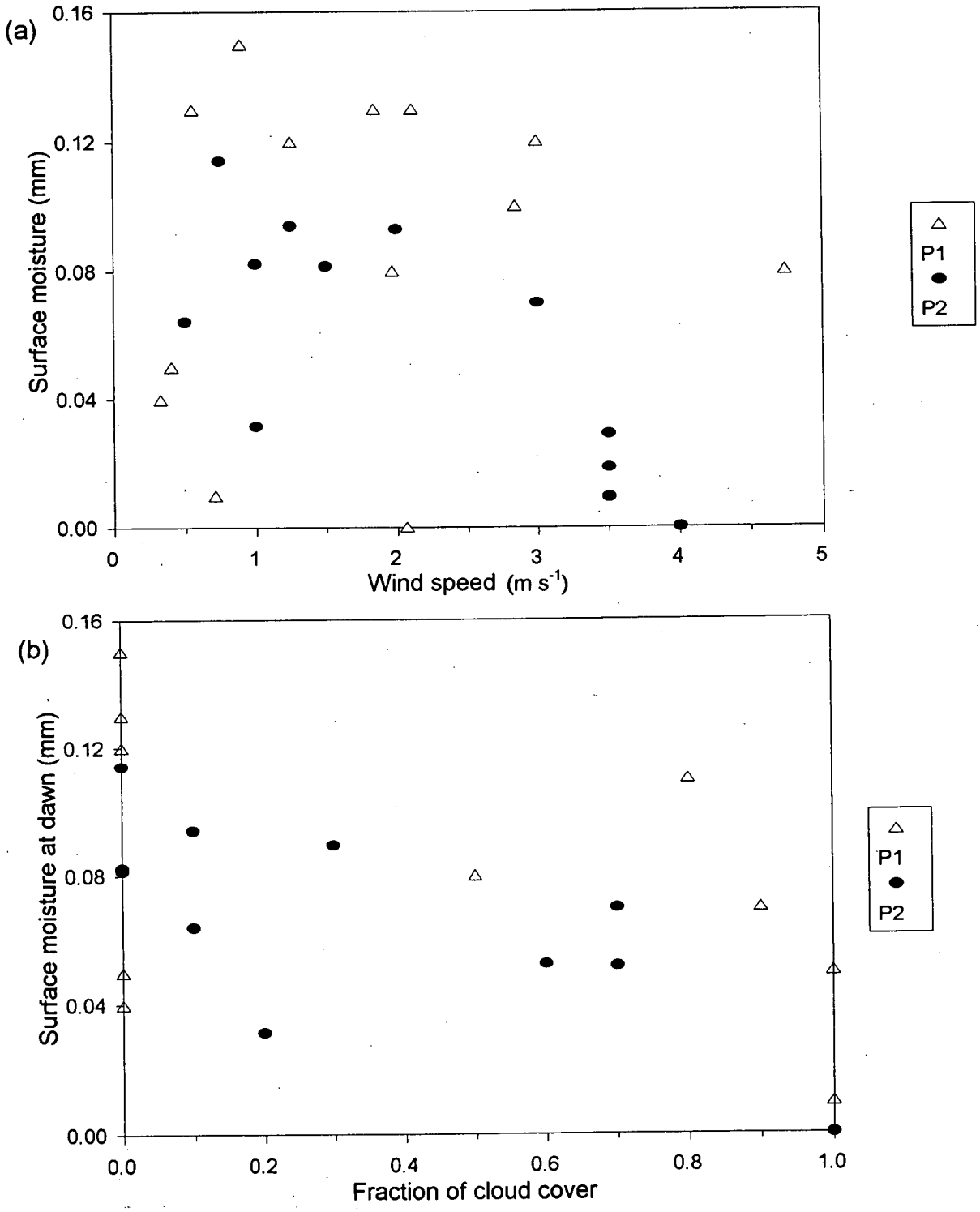

Figure 3.25 Scatter plot of the amount of surface moisture (by blotting) present at dawn in the centre of two urban parks (P1 and P2), in relation to the fraction of cloud cover and wind speed, where the preceding night is characterised by (a) clear skies (cloud fraction at VIA is 0.0–0.2), and (b) light winds (wind speed at 10 m at UBC <2.0 m s^{-1}).

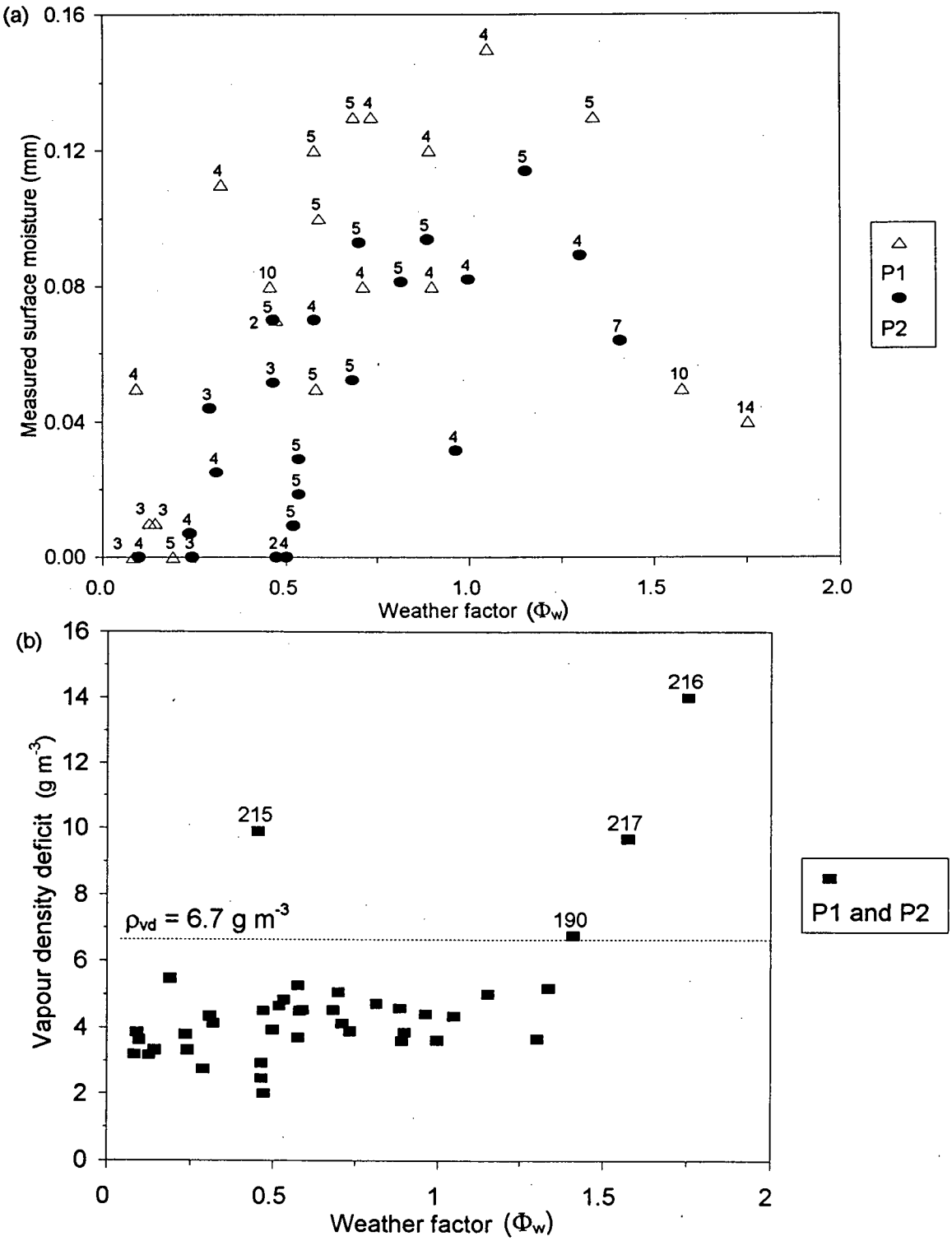

Figure 3.26 Relationship between surface moisture (mm) measured at the centre of P1 and P2, the weather factor (Φ_w), and vapour density deficit (g m^{-3}) measured at UBC. (a) is the amount of surface moisture present at dawn plotted against Φ_w, with labels of vapour density deficit rounded to the nearest 1 g m^{-3}. (b) is the surface moisture data plotted against vapour density deficit (data labelled by YD and the dotted line ρ_{vd} = 6.7 g m^{-3} are discussed in the text).

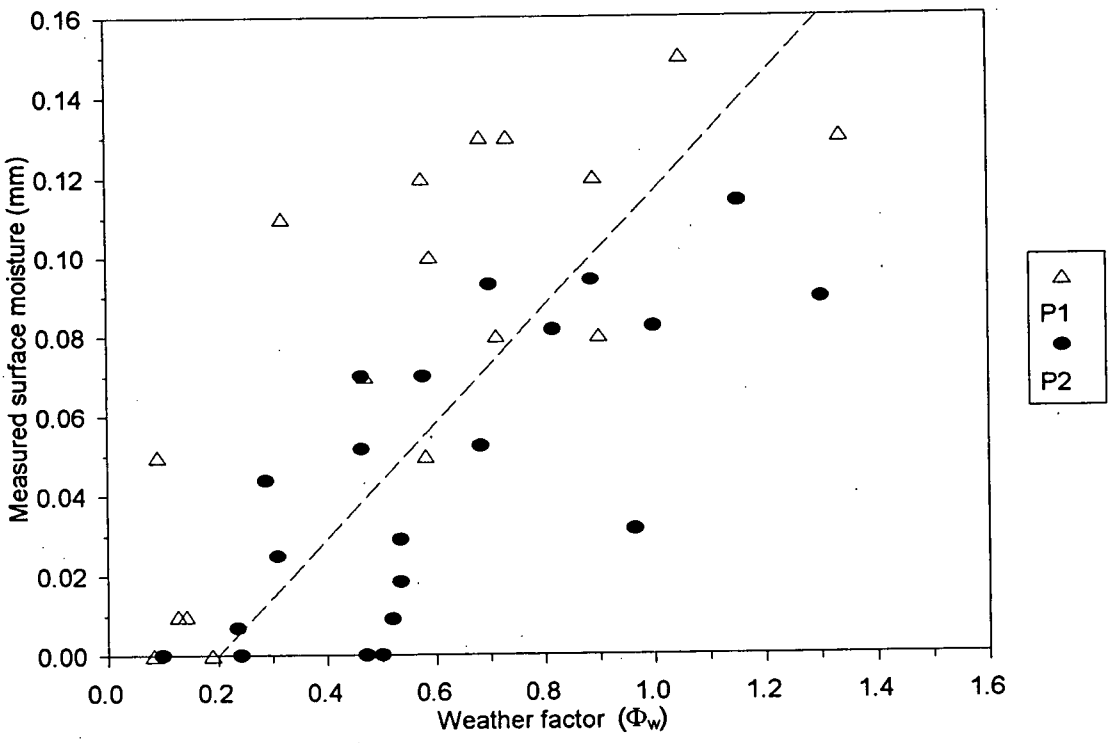

Figure 3.27 Relationship between the weather factor, Φ_w, and amount of surface moisture at dawn at P1and P2. The dashed line indicates the line of best fit, this placed by eye.

It is postulated that some of the scatter in Figure 3.27 is linked to direct physical causes, and that these relate to variations in the supply of moisture, since other major governing factors, wind speed and cloudiness—the latter a surrogate for rates of radiative cooling at the surface—have been taken into account. More than one effect is hypothesized:

- values which plot to the right in Figure 3.27, for which the Φ_w relation over-estimates accumulation, may be linked to the poor transport of vapour to the surface on these dates. $\Phi_w \geq 1.0$ implies clear skies and a wind speed of $\leq$ 1 m s^{-1} at 10m, conditions which may lead to stagnation of air close to the ground surface and reduced dewfall, and
- values which plot further to the left, for which the relation appears to under-estimate accumulation, may signify nights when guttation is present but unaccounted for.

A slight offset may be present in the data (Figure 3.27), i.e., slightly greater amounts of dew tend to be seen at P1 than at P2 for similar Φ_w. The effect may be due to physical differences in the site and/or season of measurement, e.g., night-length, irrigation, soil moisture and/or guttation.

It might be argued that the Φ_w relation points to a useful approach to predicting urban dew. That is, using a scheme based on simple indices of weather and moisture availability, which can be derived from standard weather observations at a local climate station. Adding an appropriately defined humidity term may increase the power of the relations shown in Figure 3.27. Other possible terms could easily be forwarded, such as, for example, antecedent rainfall, sky view factor

and night-length. However, the success of such a scheme rests on its ability to accurately predict absolute amounts of dew. The simple relations discussed here do not do this. A more elaborate scheme based on Φ_w and analogous terms may, eventually, achieve this goal but this is not addressed here. Later I present another numerical method to predict dew is investigated. The approach has the intrinsic advantage that it predicts the absolute amount of moisture accumulation (mm per night), using the energy balance of the object on which dew potentially forms. The model and its results are described in detail in Chapter 7.

(b) Surveys at the micro-scale

Casual observations in urban neighbourhoods (U1, U2 and P1) show that, during conditions favourable for dew, there is significant spatial variation in the amount of water which accumulates overnight. So, for example, dew may be abundant on grassed areas, car roofs and out-door furniture while, on the same night, house walls and pavement remain dry. Substrate type (leaves, wood, plastic, concrete) is clearly a fundamental control. This is because dew deposition is related to rates of cooling, which are strongly governed by the thermal characteristics of each individual surface. Spatial variation may be large on even a single substrate, e.g., mown grass. That is, on lawns, surface moisture may be heavy at open sites and light close to trees, buildings and other horizon obstructions; grass may even be dry among closely-spaced buildings or under tree canopies. This is true at both sites where the area of grass enclosed by trees/buildings is fairly small, e.g., a residential lawn (Figure 3.28), and more open sites such as an urban park (Figure 3.29). In

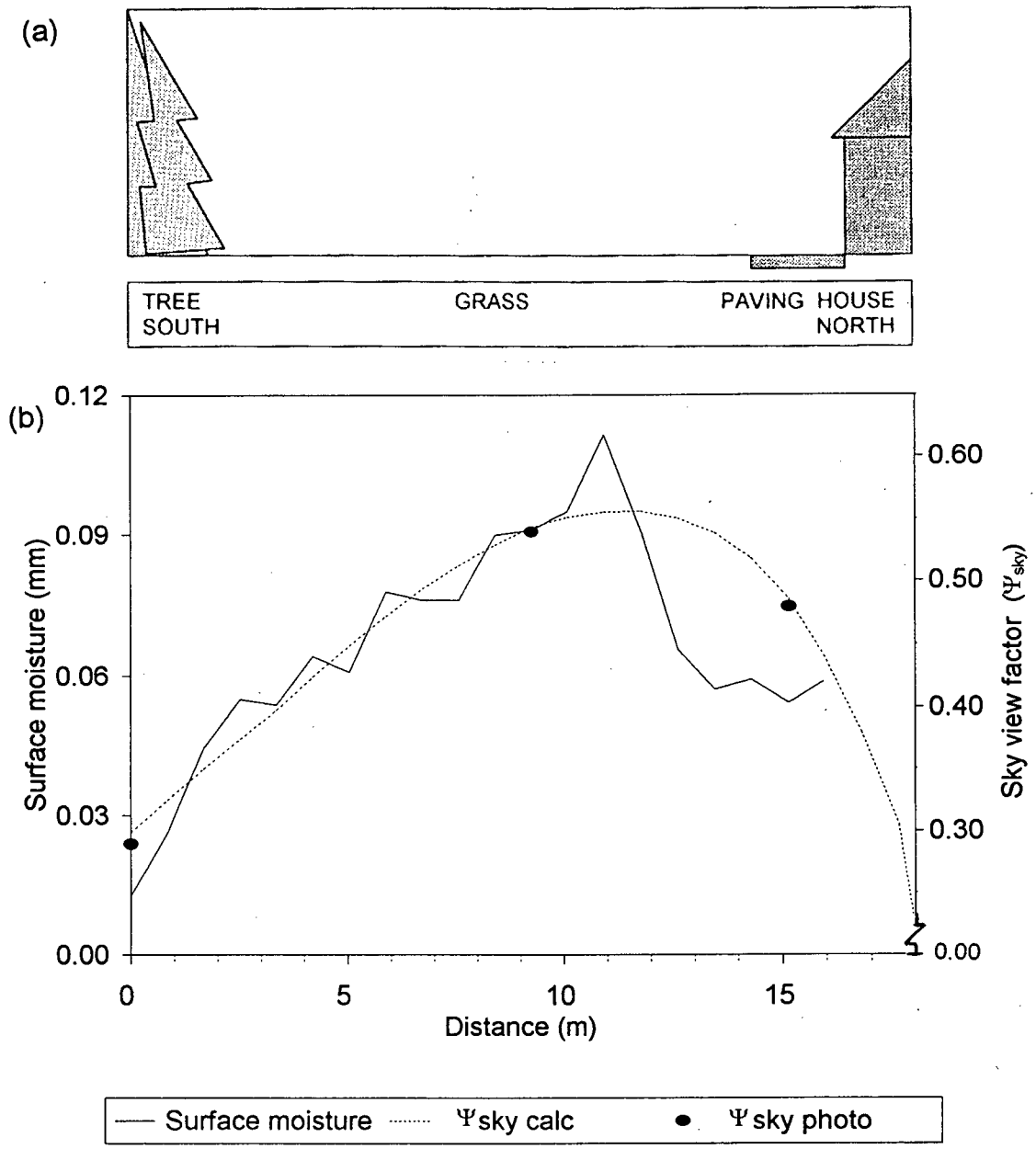

Figure 3.28 Relationship between the amount of surface moisture present on grass at U2 at dawn (YD 240, 1993) and location. (a) A schematic cross-section of the transect sampled (see Figure 3.23b), and (b) spatial trends of surface moisture amount (mm) and Ψ_{sky} (see text for definitions of symbols).

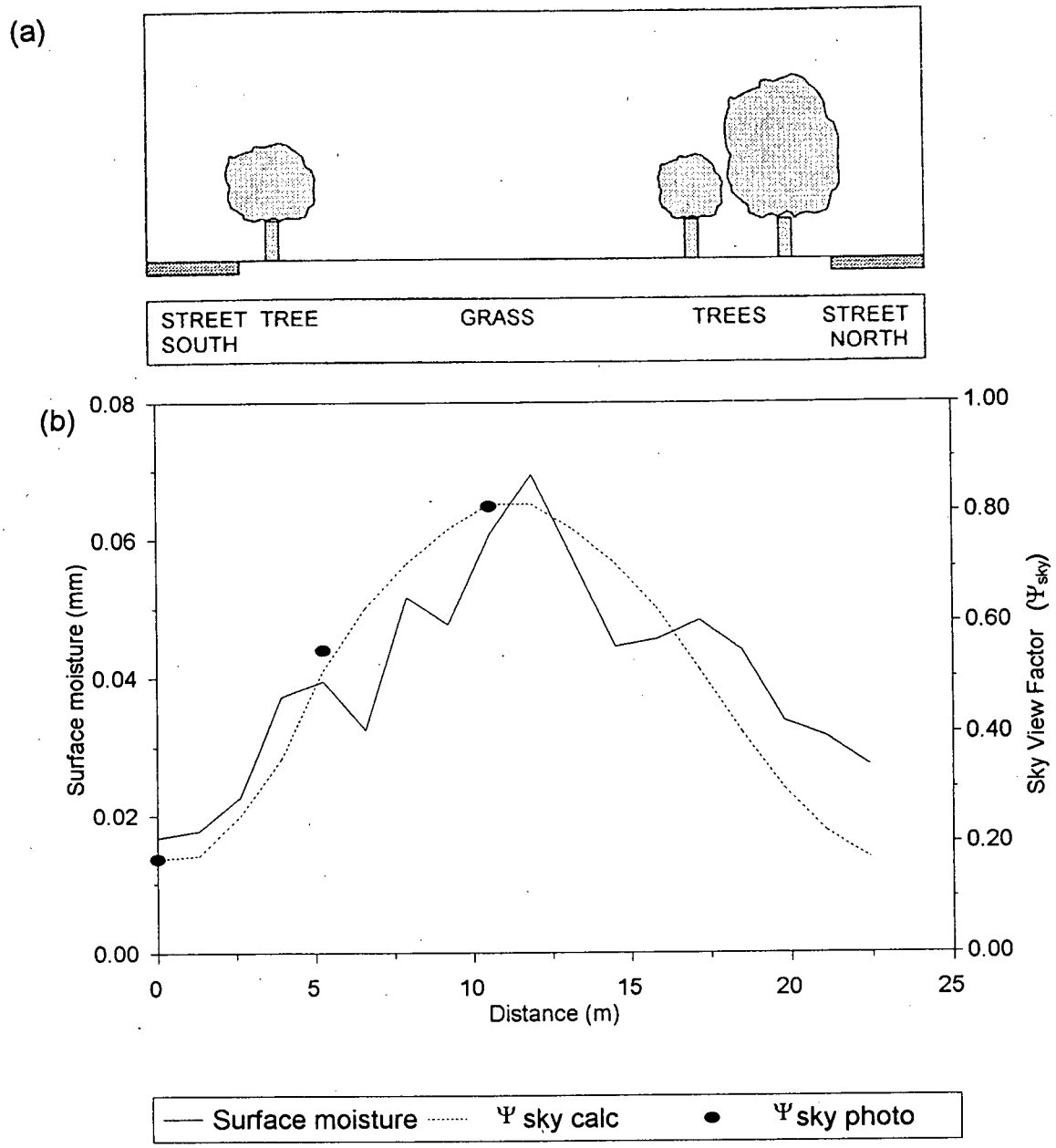

Figure 3.29 As for Figure 3.28, but for YD 218 and the eastern transect at P1 (see Figure 3.21).

these figures, subscripts 'photo' and 'calc' indicate Ψ_{sky} determined using fish-eye lens photography and site geometry, respectively.

Theory and published studies which address spatial patterns of rural dew—these are uncommon (see Chapter 2)—suggest that the primary control is the affect of horizon obstruction on the net radiation budget and therefore energy balance of the surface. At a grassed site with an unobstructed horizon (Ψ_{sky} = 1.00) the energy balance of the surface is expressed:

$$Q^* = L_{in} - L_{out} = \left(\varepsilon_{sky}\sigma T_{sky}^{\ 4}\right) - \left(\varepsilon_c \sigma T_c^{\ 4}\right) \qquad [3.4]$$

where Q^* is net all-wave radiation, L_{in} and L_{out} are incoming and outgoing longwave radiation, respectively (all expressed as flux densities with units W m^{-2}), ε is surface emissivity for longwave radiation, σ is the Stefan-Bolzmann constant (5.67×10^{-8} W m^{-2} K^{-4}), T is temperature in Kelvin, and subscripts sky and c indicate sky and grass canopy, respectively. Equation 3.4 dictates that the value of Q^* is governed by the intrinsic properties (ε) and temperature (T) of both the surface itself (grass) and surrounding objects, in this example, sky. At open grassed sites, Q^* typically has a large negative value because the night sky acts as a strong heat sink for radiation energy, i.e., L_{in} is far less than L_{out}.

At most urban sites L_{in} is associated with two types of source, i.e., the sky and objects in the canopy layer such as trees and buildings. The energy balance for a generic grassed site ($\Psi_{sky} < 1.00$) is therefore written:

$$Q^* = L_{in} - L_{out} = \left(\Psi_{ter} L_{in\,ter} + \Psi_{sky} L_{in\,sky}\right) - \left(\varepsilon_c \sigma T_c^{\ 4}\right) \qquad [3.5]$$

where the subscript ter indicates the surrounding terrain (here, undifferentiated). Subdivision of L_{in} is therefore governed by site geometry expressed as a view

factor. When view of the sky is partially obscured by relatively warm objects the influence of the sky heat sink is reduced, the surface loses less heat, and Q^* has a smaller negative value. This means that the grass canopy remains relatively warm, so dew is inhibited where Ψ_{sky} is reduced.

As a first approximation, moisture accumulation seems to be well described by Ψ_{sky}. That is, similar spatial trends are seen when sky view factor data are graphed with those of surface moisture amount. This is illustrated in Figures 3.28 and 3.29, in which the axes used to plot Ψ_{sky} values are arbitrarily scaled and/or offset to match the observed moisture distribution. The relationships depicted in the two figures are interpreted to mean that dew is most strongly controlled by surface temperature, which on nights favourable to dew (clear skies and light winds) is in turn governed by the net radiation balance of the surface (Q^*), which itself depends on the strength of the environmental heat sink—a parameter which is very strongly dominated by the heat sink that is the night sky. Hence, it can be argued that the proportion of sky 'seen' at a given point on the surface—the sky view factor—has power to explain the spatial distribution of surface moisture on an otherwise uniform surface (lawn or park).

The effect of weather and location at a single site (U2) is clearly shown by the sequence of five days in Figure 3.30. The location effect due to horizon obstruction is best seen during weather favourable for dew, i.e., clear with light winds. When weather is less favourable (overcast and/or windy) amounts of surface moisture are smaller at all locations and the pattern is less evident, but still discernable. The general form of the Ψ_{sky} fit—shown in Figure 3.28 for YD 240 with

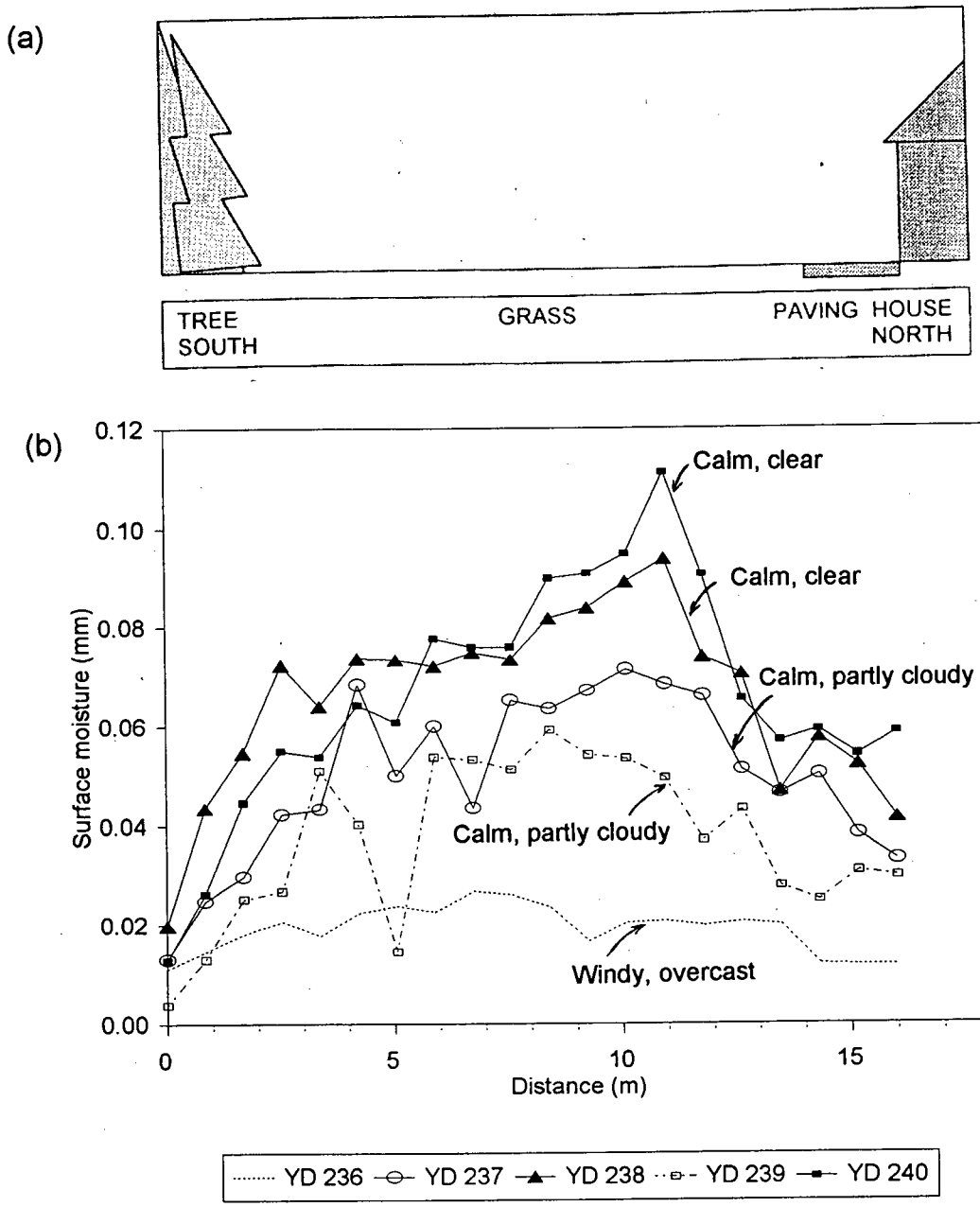

Figure 3.30 Relationship between the amount of surface moisture (mm) present on grass at U2 at dawn, location, and the weather of the preceding night, for YD 236–240, 1993. The low value at the 5 m distance on YD 239 relates to an encounter with a raccoon, which removed dew at this point on the lawn, while it was shredding one of the sampling pads.

favourable weather—is repeated in a more muted form for days with less favourable conditions. To illustrate, data for two days with weather less favourable for dew accumulation are shown in Figure 3.31. As was done previously, the axes used to plot Ψ_{sky} values are scaled by eye to match the observed moisture distributions.

At U2, there appears to be a systematic difference in fit at the north (house) end of the transect, i.e., in Figures 3.28 and 3.31 the moisture seems less than Ψ_{sky} would predict. This may be an advection effect created by differences in moisture sources and air flow close to the building. Alternatively, sensible heat storage in the adjacent paved area may keep the area relatively warm and inhibit dewfall.

The results of these simple surveys suggest that moisture accumulation and Ψ_{sky} are fairly closely linked at grassed sites such as urban lawns and parks. This leads to the possibility that Ψ_{sky} may have potential to predict spatial patterns of surface moisture. The feasibility of such an approach is examined in detail in Chapter 6 using data from the hardware model.

Several small but careful trials were conducted at open locations at P1 to test the spatial variability at small scales (<2 m) of surface moisture on mown grass at dawn. They showed that small-scale variation is present but is relatively small (SD = 0.01–0.02 mm) at locations with consistently large sky view factor and a well maintained turf.

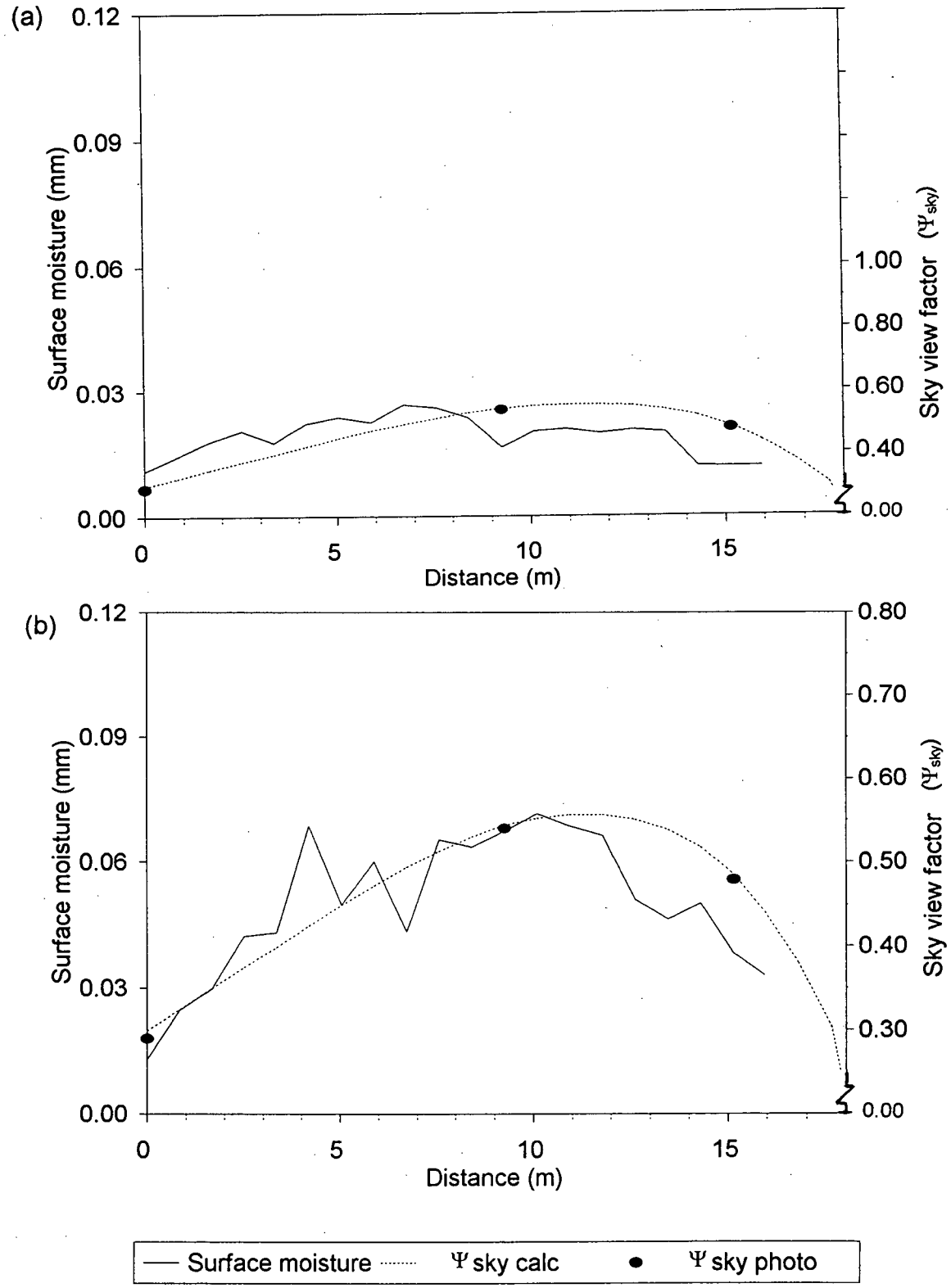

Figure 3.31 As for Figure 3.28, but for two days with nocturnal weather that was less favourable for dew accumulation, (a) YD 236 and (b) YD 237, 1993.

3.4 Summary

The simple surveys described above clearly show that dew distribution in cities is complicated, but that consistent spatial and temporal trends appear to be present. In summary, the main findings are that:

spatial contrasts in canopy layer T_a and ρ_v are most evident on clear nights with light winds. On such nights, residential areas of the city may be warmer, more moist, but have a higher ρ_{vd}, compared to the surrounding countryside,

- as in other mid-latitude cities, humidity data suggest that rural humidity is depleted by dewfall. In the city, the high values of canopy layer humidity which are observed at night seem to be linked to reduced amounts of dew,
- surface moisture data, however, show that urban dew may be as frequent as rural dew. On grass, urban dew tends to be in lesser amount than seen at rural sites, but urban roofs may rival rural grassed surfaces as favoured locations for dewfall accumulation,
- surface moisture amount on grass at dawn at open sites is strongly controlled by weather. Φ_w appears to have power to explain the relationship,
- on any given night, substrate type (leaves, wood, concrete) is a fundamental control on the amount of moisture which accumulates,
- for grassed lawns and parks in the city, similar spatial trends are evident in surface moisture amount at dawn and sky view factor (Ψ_{sky}). The correlation may provide a method to predict spatial patterns of surface moisture, and
- spatial patterns of dew associated with Ψ_{sky} may be modified close to objects with a large sensible heat storage.

In an observational study, a measure of control can be obtained over weather variability by selecting only nights ideal for dew accumulation (clear with light winds). Similarly, site complexity can be simplified by selecting sites with simple geometry and a single substrate material (grass). However, the city is made up of many surface materials beside grass and urban locations are characteristically more complex than the simple lawns and parks discussed above. The potential effects of substrate type and location are difficult to separate, and at most urban sites physical complexity creates problems for interpretation.

A possible alternative is to build a hardware model of the system of interest, wherein the physical environment can be simplified. I decided that this would be a useful approach to studying dew in urban environments. The physical scale model which I designed and constructed is discussed in Chapters 4–6.

PART III MODELLING

Chapter 4: Physical modelling of urban dew

4.1 Context

Several practical difficulties are associated with measuring dew in a city. These range from the logistics of instrumenting a full-sized house, to the time needed to collect data by blotting, to the sheer complexity of the three-dimensional surface on which urban dew may potentially form. For complex environments, physical modelling provides an attractive option to measurement, because models permit the system studied to be simplified and reduced in size. So, in theory, instrumentation and data interpretation are more straightforward. Further, a model is usually easier to modify than a full-scale site. This means that, in a model landscape, building configuration (size, orientation) can be altered radically and elements such as, for example, street trees removed with relative ease.

Most hardware models are laboratory based, but dew is difficult to create artificially, so the only viable approach in this case is to investigate processes in the out-of-doors under conditions where dew forms naturally. Environmental conditions which might otherwise be difficult to duplicate can thus be harnessed. With this advantage comes a loss of control over aspects of the environment, but a measure of passive control can be gained over weather by selecting periods with favourable conditions or stratifying nights according to prevailing conditions.

The urban three-dimensional surface on which dew potentially accumulates is difficult to model in fine detail because it consists of an irregular, three-dimensional mosaic of many different materials. One practical option is to model

urban surfaces in a simple manner by exposing panels of different building materials and measuring differences in the dew deposited overnight. This would provide data for single surface types as if they existed in isolation. However, an essential feature of the urban environment is its three-dimensional nature and the juxtaposition of contrasting materials and vegetation. How then to model this complex environment?

Despite its intrinsic complexity, there is a degree of scale-dependent homogeneity in Vancouver's urban landscape. To summarise observations formalised by Schmid (1988): at the meso-scale, there is a measure of homogeneity within land-use zones; at the micro-scale there are relatively homogeneous surfaces at the scale of a lawn or roof; and at intermediate scales (a neighbourhood) regularity is evident. Many residential neighbourhoods consist of a regular grid of streets, each lined with deciduous street trees (1–2 building heights tall), and rows of similar houses set back from the pavement by an open lawn of about constant width (Figures 4.1 and 4.2). Another landscape element repeated in many Vancouver residential neighbourhoods is the urban park—often a simple rectangle of grass surrounded by a border of regularly-spaced deciduous trees, of few species. In essence, the residential landscape is an ensemble of similar units (streets, lots and parks) which are aggregated to form larger areas. This creates the observed regularity.

Modelling is made more straightforward when the landscape is conceptualised as a sequence of repeating linear units, i.e., semi-infinite 'rows' in parallel, each row an amalgamation of similar objects (houses and trees) or

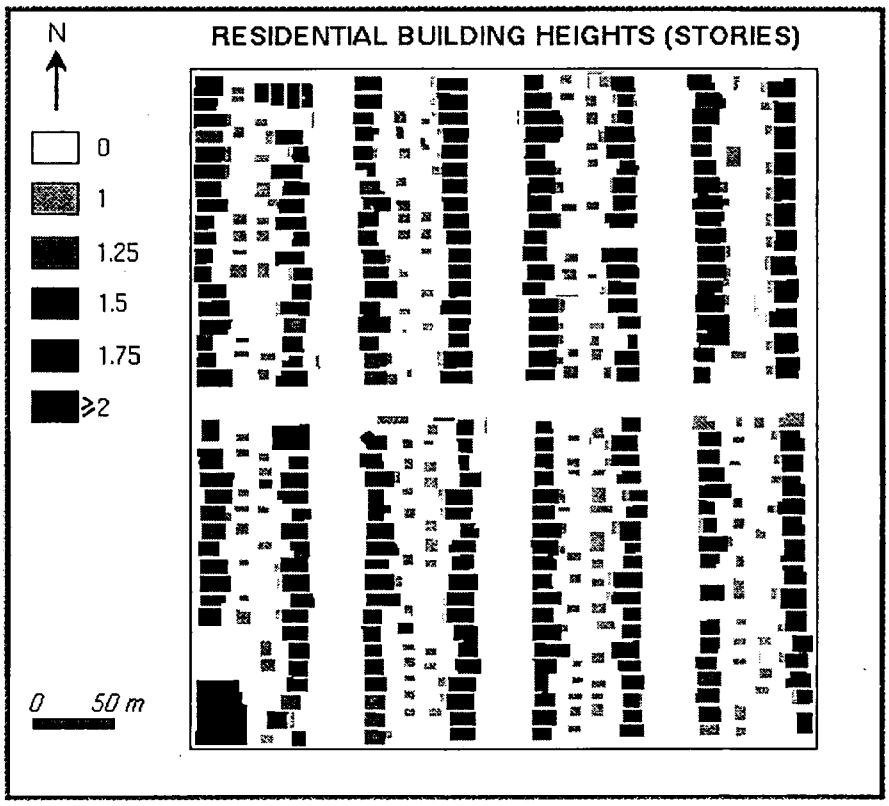

Figure 4.1 An illustrative example of the geometry of an urban residential landscape in Vancouver. *Source*: Modified from Voogt (1995).

(a)

(b)

Figure 4.2 Selected images of the urban residential landscape of Vancouver. (a) Examples of houses of simple form (most houses are more structurally-complex than these) and (b) a residential street and its neighbourhood park (to the right).

surfaces (pavement and grass). In such an array, along-row variation is repetitive at the scale of a lot or tree, thus spatial variation is focussed in a plane at right angles to the direction of linearisation. There are two practical advantages: (a) data measurement can be limited to a vertical cross-section at right angles to street direction, and (b) the landscape can be reduced from a repetitive ensemble of linear units (in an array) to a few representative landscape units of linear structure. These may be, for example, a long residential street bordered by houses and trees, an urban park consisting of an extensive grassed area, or a downtown street *canyon* consisting of a pavement 'floor' for which adjacent buildings create walls.

4.2 The modelling programme

4.2.1 Objectives

The aim of the scale modelling in this study is to investigate the physical processes and spatial patterns of dew and surface moisture occurrence at the micro-scale for a representative section of urban residential land-use. In accordance with the discussion in Chapter 3, the specific objectives of the modelling programme are to investigate the roles of (a) micro-scale location, geometry, and view factors, (b) substrate type, (c) roof and wall orientation, and (d) surface temperature on the amount of dew deposited overnight to surfaces of common urban materials arranged in a representative geometric configuration. The residential landscape has a measure of regularity so can be modelled to a first order using a generic residential lot and a generic urban park, reduced to a relatively small number of physical elements:

- a house,
- lawn,
- back yard trees,
- street pavement,
- an open grassed park, and
- a row of street/park trees.

It is argued that, if dew patterns within such a lot and park can be assessed by hardware modelling, then results can potentially be extrapolated to larger areas of similar geometry. The scaling arguments underlying the design of the model are presented in this chapter; the hardware model itself, its design and operation, is described in Chapter 5; and the results of the model are discussed in Chapter 6.

4.2.2 Scaling considerations

Although a broader definition can be argued, a *scale model* usually implies comparison between objects which have similar geometry, but which differ in size. The model is typically smaller and *scaled* and the prototype is typically larger and is described as *at the full-scale*. If the information from a scale model is to be useful to understand processes at the full-scale, and for the model to have general applicability, formal scaling criteria must be met. If these 'rules' are appropriately implemented *then similitude is achieved, the model's behaviour mirrors that at the full-scale, and mathematical relationships exist between parameters measured at the two scales.* In such cases, results from the model are transferable, and scaled data give direct information about processes at the full-scale.

In nocturnal conditions ideal for cooling (clear skies and light winds), and when air is relatively close to saturation, it is argued that amount of dew is governed largely by surface temperature, because this reflects the energy balance of the surface which governs rates of deposition (see Equation 1.1). Thus, the desired outcome of modelling here is *that surface temperatures in the hardware model are the same as those for a full-scale building at similar locations on its surface and at similar times of day.* The postulate is that, given similar ambient conditions, the model will accumulate similar amounts of dew, compared to its *full-scale* equivalent.

In the present study, it was necessary to consider the theory underlying scaling in some depth. There are several reasons for this. Dew accumulation has not previously been modelled using a scale model; few models operate in the out-of-doors, so well-established scaling 'rules' used in laboratories are not all appropriate; and no one publication summarises the relevant theory in a comprehensive manner.

For discussion purposes it is useful to divide scaling criteria into those dealing with the physical domain of the model (Section 4.3), and those concerned with physical processes (Section 4.4). Each criterion is addressed individually, however, since they are interdependent, a degree of overlap is necessary. This overlap also occurs in practice; conservation of one scaling criterion often conflicts with another and compromise is necessary in the design of a model. Most scaling criteria have been formalised and are expressed as non-dimensional groups or ratios; some are less well developed. Many scaling criteria are discussed in climatological publications, several topics are found only in thermal engineering.

Aspects of scaling are described in Eckert and Drake (1972), Kreith and Black (1980), and Chapman (1984).

4.3 Scaling of the physical domain

4.3.1 Spatial dimensions

In the simplest case, a scale model possesses the same proportions as the object at full-scale, with its geometry scaled by a factor of F (e.g., 0.125). Ratios of proportion (H:W) are the same in the model as at the full-scale, and length scales by F, area by F^2 and volume by F^3 (Imbabi, 1991; Barozzi *et al.*, 1992). However, there is no fundamental law that states a model cannot be scaled by different factors in the horizontal and the vertical, producing a relative elongation (Davis and Pearson, 1970; Wegner *et al.*, 1988), and in exploratory models F may be unspecified or based on mean values observed at the full-scale (Aida, 1982).

Where relevant, surface texture can be scaled, e.g., sand can model gravel, and sandpaper can model an asphalt shingle roof. For vegetation, it is more difficult to conserve geometric proportion because plant form is age, size and species dependent. However, the micro-morphology of a field of wheat can be approximated using grass or artificial materials, and a miniature tree—living or artificial—can model its equivalent at the full-scale.

4.3.2 Temporal period

Out-door models that use natural forcing factors such as diurnal or seasonal patterns of incident radiation operate in real time (McPherson *et al.*, 1989;

Wegner *et al.*, 1988). However, most scale models are constructed indoors and operate in scaled time (Spronken-Smith, 1994), with processes accelerated, often by the same F used to scale geometry (Imbabi, 1991; Barozzi *et al.*, 1992). In such cases, scaling of time is strictly governed by criteria which govern temperature, velocity and geometry. Alternatively, models can operate in equilibrium or steady-state conditions so that, after a period of adjustment, mean behaviour in the model is independent of time (Hoydysh and Dabberdt, 1988).

4.3.3 Temperature fields

Like time, scaling of the temperature field is strictly governed, and criteria scaling temperature and time are often co-dependent. The normal definition for thermal similitude for two geometrically similar objects is *that the ratio of the difference in temperature between any two points in the model to the difference in temperature between corresponding points on the object at the full-scale is constant* (Parczewski and Renzi, 1963). A common outcome is that temperature gradients in the model are greater than those at the full-scale, mean temperature is inflated, and temperature changes are accelerated (Oke, 1981; Spronken-Smith, 1994). This definition differs from that proposed in Section 4.2.2 as more appropriate for the modelling presented in this thesis (that temperatures be the same).

4.3.4 Environmental gradients

Environmental gradients are sometimes specified as boundary conditions for a model; these gradients are deliberate and desired. If gradients exist at the full-scale

then they must undergo some form of scaling to be fitted to the physical and temporal dimensions of the model. Flow models frequently include vertical gradients of turbulence and temperature, thermal models that operate as a transient system may include gradients of temperature that are scaled in both magnitude and time (Spronken-Smith, 1994). The scaling of these gradients is governed by formal criteria appropriate for the physical processes of interest.

In some cases, a scale model is designed to model a body or array that is infinite in some dimension. Similitude requires that the model be also infinite, because the thermal-dynamic/hydrologic behaviour of an isolated object differs from that of a similar object which is fully embedded in a closely-packed array, but practicality means models must be finite in size. In such models elements are often reduced to small scales and/or greatly simplified (Spronken-Smith, 1994). However, if the extent of the model is insufficient then edge effects become pervasive, and this creates gradients in the model that are unintentional and undesirable. Engineering models often model conduction in objects that are infinite in one or two dimensions (Chapman, 1984). The size of model required to avoid edge effects at a central measurement point is formally expressed as a function of the rate of conduction, the dimensions of the body and the time frame (Section 4.4.3). When the primary process is convection, the minimum extent of the model is a function of the speed, turbulence, and buoyancy of the approach flow (Hoydysh and Dabberdt, 1988), and is sufficient when the 'footprint' of the sensor lies within that portion of the model well adjusted to the flow. The exact relationship can be formally

expressed by applying theory developed at the full-scale to describe source areas for measuring convective fluxes over cities (*see* Roth, 1988).

When the primary process is long- or shortwave radiation, the model must be sufficiently large that edges do not act as abnormal sinks or sources, from the point of view of central measurement locations (Aida, 1982; Voogt, 1989). For shortwave radiation, the minimum extent of a three dimensional array is a function how many multiple reflections need be modelled. At certain locations, such as a typical downtown street, patterns of multiple-reflection are more easily determined because the physical structure of the site approximates a *canyon*, i.e., orthogonal walls and floor of finite width/height and infinite length. Walls and floor are barriers to short- and longwave radiation, which enters/exits though the open 'roof'. Canyons may consist of buildings, rock (along a natural canyon) or vegetation, e.g., crops or shelterbelts. In each case, walls may be tilted, translucent or have gaps.

For *full-scale* and scaled orthogonal canyons (e.g., a downtown street), formal relationships derived from numerical modeling (Arnfield, 1976; Voogt, 1989) dictate that canyon length (L) must equal the greater of 8H and 8W for the canyon to act radiatively as if infinite. The relationship is presumed to hold for longwave radiation and thus determines minimum canyon length for scale models of radiative cooling (Voogt, 1989). If this is achieved, measurements in the model may be simplified to a vertical, two-dimensional cross-section at right angles to 'street' direction.

Alternately, the minimum extent of a radiative model can be expressed as a function of preserving Ψ. Similitude of Ψ_{sky} can be assessed numerically, by

calculating Ψ_{sky} based on the geometry of objects surrounding the point of measurement (Howell, 1982; Steyn and Lyons, 1985), or graphically, using stereographic plots of (real or theoretical) full-scale and scaled geometry. If Ψ_{sky} is assessed from a single measurement point, elements can be modelled using distorted geometry, since identical Ψ are produced by more than one geometry. For example, a semi-infinite canyon is modelled over a smaller length if end walls are curved inwards to create a *false perspective*, and elements which are out of view, distant and/or small can be omitted (see Chapter 5).

4.4 Scaling of physical processes

4.4.1 Radiation

In models where flow is absent or slight, radiative processes often dominate, although free convection caused by buoyancy changes may be present. Researchers seem to agree that the characteristic length scale of radiation, presumably wavelength, is negligible when compared to length scales used in even small models. Hence, ratios of, say, building height to radiation wavelength are near-infinite for both *full-scale* buildings and any existing scale model. As well, all radiative transmissions occur at the same speed so processes are internally consistent. Consequently, out-door models make use of natural sunlight with impunity (Voogt, 1989), and radiation is not normally scaled in laboratory models (Oke, 1981). There are exceptions; Barozzi *et al.* (1992) scaled geometry by 0.083 and incident radiation by 0.90 in their model in which time was also scaled.

Geometry and surface properties govern radiative gain to surfaces and radiative cooling rates. Intrinsic surface properties are expressed by the dimensionless ratios emissivity (ε), reflectivity (α), absorptivity (a), and transmissivity (tr). For opaque materials, where tr is zero, these ratios are conserved whenever length is scaled, provided real materials are used in the model (McPherson *et al.*, 1989). For translucent objects, where that proportion of incoming radiation which is not reflected is partitioned into absorbed and transmitted fractions, a and tr are functions of thickness. These ratios therefore scale whenever thickness is scaled.

Parameters associated with geometry and shortwave radiation are conserved whenever H:W and Ψ_{sky} are conserved. 'Structural' reflectivity, which is associated with deeply textured surfaces and trapping of multiple reflections, is conserved when H:W is scaled (Aida, 1982), and shadow patterns are constant when light source-surface orientation is conserved. Factors governing heat loss *via* longwave radiation are scaled when geometry is scaled, since these are functions of H:W and view factors (Oke, 1981), however rates of radiative cooling also depend on substrate materials and temperature gradients. Hence, radiative cooling is normally modelled in scaled time, with surface temperatures determined using formal scaling criteria (Spronken-Smith, 1994).

4.4.2 Convection

Many scale models in wind tunnels, flumes or chambers operate under convective conditions, with the fluid surrounding the model in motion. In such models, the

critical focus is commonly the conservation of thermal-dynamic properties associated with convective or turbulent flow. To paraphrase Chapman (1984), for convective systems the conditions under which two geometrically similar systems have thermal-dynamic similarity can be determined by appropriately non-dimensionalising the equations governing physical processes. Then, the resultant velocity and temperature fields in the model are similar to those at the full-scale, similitude is achieved, and results are transferable. When convective systems are described in the engineering literature, thermal-dynamic response is discussed using three dimensionless parameters:

- Dimensionless location, *X:Y:Z*
- Dimensionless velocity, *U:V:W*, and
- Dimensionless temperature, φ

Dimensionless location (*X:Y:Z*) is familiar. In the form given here, orthogonal location (*x:y:z*) is non-dimensionalised using the characteristic length scale, L, which does not necessarily have the same value for each component direction. That is:

$$X = \frac{x}{L_x}, Y = \frac{y}{L_y}, \text{and } Z = \frac{z}{L_z} \qquad [4.1]$$

where subscripts x, y and z indicate the appropriate length scales for horizontal (x, y) and vertical (z) directions. When the system is non-dimensionalised, then in two geometrically similar cases similar location points result for equal distances *X*, *Y*, and *Z*. L is a function of object shape, and can be for example the thickness of a layer, cylinder radius, and the exterior width or height of a discrete object, such as

a building (Eckert, 1972; Chapman, 1984). Similarly, velocity components in three dimensions (v_x; v_y; v_z) are non-dimensionalised using an appropriately defined $\bar{u}$, the 'free stream' (open system) or mean (enclosed system) velocity of the approach flow (Chapman, 1984):

$$U = \frac{v_x}{\bar{u}_x}, V = \frac{v_y}{\bar{u}_y}, \text{and } W = \frac{v_z}{\bar{u}_z} \qquad [4.2]$$

In two geometrically similar cases, velocities are similar when U, V, and W are similar. Dimensionless temperature is also familiar. The form given here (φ) assumes an initial step-change in fluid temperature. The temperature of the object (T_s) is referenced to that of the fluid (T_f), and non-dimensionalised using the difference between object initial temperature (T_{si}) and fluid temperature:

$$\varphi = \frac{T - T_f}{T_{si} - T_f} \qquad [4.3]$$

It follows that, in two geometrically similar cases, when φ is similar then the ratio of temperatures for two points in the model is similar to the ratio of temperatures at the full-scale, for similar locations (Chapman, 1984).

Once location, velocity, and temperature are appropriately non-dimensionalised, examination of the equations governing processes in the model, and dimensional analysis, leads to the definition of formal scaling criteria. When the characteristics of systems are non-dimensionalised appropriately, they become universal functions of the groups Rossby Number (Ro), Reynolds Number (Re), Richardson Number (Ri), and Prandtl Number (Pr). Briefly, Ro reflects the turning effect on objects in motion due to the Coriolis force; Re describes the importance of turbulence in the flow, because beyond critical values of Re flow alters from laminar

to turbulent; and the relative importance of free and forced convection in the system is contained in Ri. Where convection is the dominant process, similitude for a scale model is achieved by adjusting the fluid type, its velocity and mean temperature, vertical temperature gradients in the fluid, and length scales in the model. Often compromise is necessary to fulfill all formal requirements. In most cases Ro is ignored; in conditions when flow is slight and turbulence minimal, requirements for conservation of Re and Ri are relaxed; and if the model is immersed in the same fluid as at the full-scale then Pr is conserved.

4.4.3 Combined conduction-convection

When fluid motion is present and the focus of the modelling is the thermal behaviour of objects, the system is best characterised as a combined conduction-convection environment. In such a system, the thermal behaviour of an object is a function of its intrinsic properties, its size, and the nature of the fluid which surrounds it. Heat transfer is by conduction in the object, and through the thin laminar boundary layer enveloping it, and by convection in the surrounding fluid; often, radiative processes are also present. When cases of combined conduction-convection are described in the engineering literature, thermal response is discussed using four dimensionless groups:

- Dimensionless location, $X:Y:Z$
- Dimensionless temperature, φ
- Dimensionless time, Fo, and
- Dimensionless heat transfer coefficient, Bi

X:Y:Z is described above, as is φ. Dimensionless time (termed Fourier Number) is the ratio of the rates of heat conductance and heat storage in the object, and is a dimensionless time parameter, since it defines a thermal response time. Fo indicates that large objects and those with low thermal diffusivity respond slowly, compared to small objects and those with high thermal diffusivity:

$$Fo = \frac{\kappa_{Hs} t}{L^2} = \frac{k_s t}{\rho_s c_s L^2} \qquad [4.4]$$

where t is time [s], and κ_{Hs}, k_s, ρ_s and c_s are the thermal diffusivity [$m^2\ s^{-1}$] and conductivity [$W\ m^{-1}\ K^{-1}$], density and specific heat [$J\ kg^{-1}\ K^{-1}$] of the solid, respectively. Fo >1 indicates that edge effects are present, but Fo <1 means the object is semi-infinite with respect to thermal response, i.e., it responds as if infinite, for a given t and k_s. Dimensionless heat transfer coefficient (termed Biot Number) is the ratio of the convective heat transfer coefficient for the fluid, h_{cf} and the conductive heat transfer coefficient for the solid, h_{ks} (these in units $W\ m^{-2}\ K^{-1}$):

$$Bi = \frac{h_{cf}}{h_{ks}} = \frac{R_{ks}}{R_{cf}} = \frac{h_{cf} L}{k_s} \qquad [4.5]$$

where R_{ks} and R_{cf} are heat transfer resistances in the solid and fluid [$K\ m^2\ W^{-1}$], respectively. Large Bi indicates a body that has considerable internal resistance, and thus a delayed thermal response, e.g., a block of masonry. Bi→0 means that a body has negligible internal resistance, a rapid temperature response, and is virtually isothermal (a copper bead). Although Fo and Bi may be unfamiliar, links are evident to the more familiar time constant (τ), which is a measure of how rapidly a body (e.g., a small copper bead) responds to a change in the temperature of its surroundings, and the Nusselt number (Nu), which is commonly used in convection

and turbulence research (Chapman, 1984). Substituting Equations 4.4 and 4.5 into that for τ gives:

$$\varphi = e^{-(A_s ht/V_s \rho c)} = e^{-(Lht/L^2 \rho c)} = e^{-Bi\,Fo} \qquad [4.6]$$

where A_s is the area [m^2] and V_s the volume [m^3] of the solid, and the formula for Nu is similar to that for Bi, except that Nu is concerned with the properties of the fluid, whereas Bi focuses on the solid:

$$Nu = \frac{L}{\delta} = \frac{h_{kb} L}{k_f} \qquad [4.7]$$

where δ is the thickness of the laminar boundary layer [m], h_{kb} is the conductive heat transfer coefficient for this layer [W m^{-2} K^{-1}], and k_f is the thermal conductivity of the fluid [W m^{-1} K^{-1}].

The outcome of appropriately non-dimensionalising the system according to these four groups, is that all geometrically similar objects with the same Bi have the same dimensionless temperature response at *X:Y:Z* according to time measured as Fo. This means that similitude of thermal character is achieved, and the thermal response of two similar objects of different size plot as a single curve (Chapman, 1984). Several engineering researchers have computed and graphed φ for objects of simple form, for ranges of *X:Y:Z*, Fo and Bi. Universal plots, or the mathematical method for their derivation, are available for simple forms under a variety of boundary conditions.

4.5 Scaling processes of dew formation in real time

In the laboratory, where conditions are strictly controlled, similitude for scale models is achieved by applying formal criteria (Sections 4.3 and 4.4). In the out-of-doors, if the model relies on naturally occurring forcing factors (diurnal fluctuations of temperature and solar radiation), then the model must operate in t not Fo. The universal relationships described above are therefore inappropriate.

A scaled object responds more rapidly to changes in temperature, compared to a similar object at the full-scale. Thus, at night the model becomes excessively cool, and by day it is too warm. Conservation of amount of dew per unit area requires that surface temperatures in the model be the same as at the full-scale, for similar locations and similar times of day—so a conflict exists. A review of the literature suggests that there are few approaches available to resolve this conflict. Although Parczewski and Renzi (1963) recognised that it may be useful in a scale model to conserve absolute temperatures, this has seldom been attempted. It is theoretically possible to 'model' at the full-scale, by constructing an out-of-doors, simplified prototype at a scale of 1:1, thus eliminating size effects (Imbabi, 1990a; Barozzi *et al.*, 1992). Alternatively, time can be 'scaled' by, say, alternating shade and exposure, to model a shortened diurnal pattern (Lettau, 1967).

In the present study, the approach taken is to reevaluate geometric scaling from the specific point of view of buildings and other enclosures (furnaces and chambers), and to derive, from this analysis, scaling criteria appropriate to the specific aims discussed above: *to conserve absolute surface temperatures in an out-of-doors model operating in real time.* Houses are essentially box-like

enclosures, consisting of a quasi-solid wall and a largely air-filled interior. Two further scaling criteria are important, besides those discussed in Section 4.4.3 (McPherson, 1980; Imbabi, 1991):

- Surface area to volume ratio, λ, and
- Dimensionless Thermal Mass Number, H

λ is the ratio of the external surface area to overall volume of the object, disregarding any internal voids. In real time, the rate of thermal response of the object is proportional to λ, because smaller objects have proportionately greater surface area, compared to large objects of similar form. Small objects therefore have less thermal inertia, and if two similar objects are exposed to the same step change in ambient temperature (Figure 4.3), the smaller of the two has a faster thermal response, and reaches a new equilibrium in a shorter time. If the forcing factor is a periodic temperature wave, then the smaller body is 'flashy', compared to the larger body—it responds faster and has excessive maxima and minima, compared to the larger object. H specifically concerns box-like objects, for which L is wall thickness. It is the ratio of the thermal mass of the *interior* of the enclosure and anything contained therein (c_{Mi}), to the thermal mass of its *walls* (c_{Mw}). For a building, the wall includes all outer-shell materials, in the walls, roof and floor, and the interior includes inside walls, fittings and an air volume. H is given:

$$H = \frac{c_{Mi}}{c_{Mw}} = \frac{M_i c_i}{M_w c_w} \qquad [4.8]$$

where M is mass [kg], c is specific heat [J kg^{-1} K^{-1}] and subscripts i and w indicate interior and wall, respectively. $H > 1$ indicates a body that has greater thermal mass

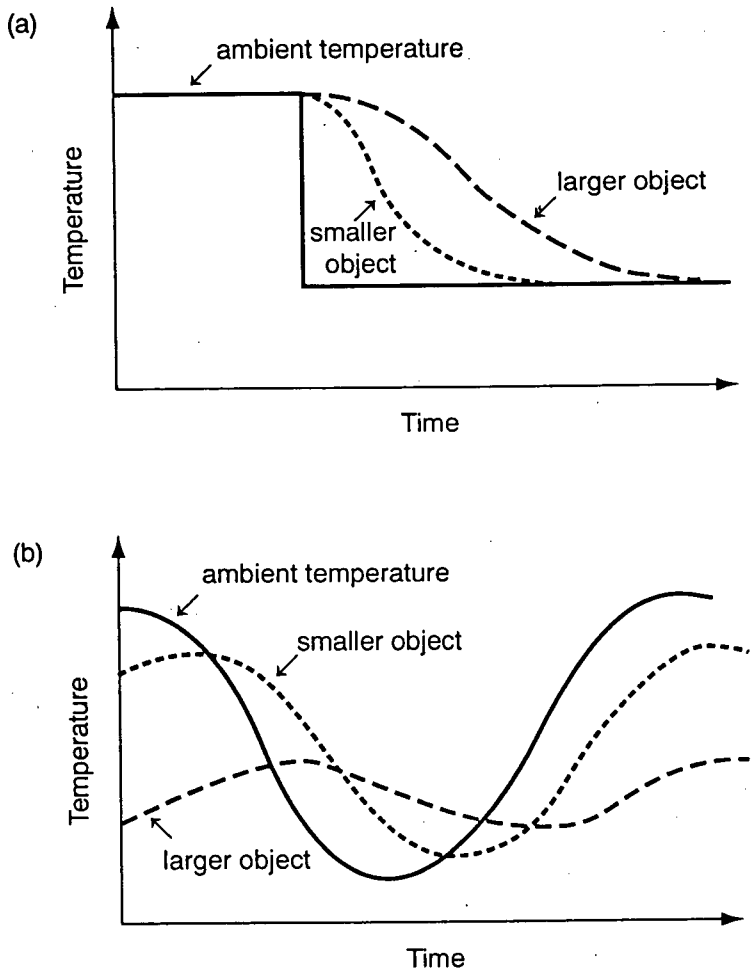

Figure 4.3 Time dependent thermal behaviour of two similar objects of different size, showing typical responses to (a) a step change in ambient temperature, and (b) a periodic forcing wave in ambient temperature.

in its interior compared to that in its walls (e.g., a polystyrene box filled with water), and $H \rightarrow 0$ means a body has little thermal mass in its interior, compared to its walls (e.g., a brick box filled with air).

When an object is scaled in length, width and height by a single $\dot{F}$, this is *strict geometric scaling*. Under this approach thermal characteristics which are length dependent scale by F, those which are area-dependent scale by F^2, and those which are volume-dependent scale by F^3. The effects of strict geometric scaling on geometry and thermal characteristics are summarised in Table 4.1, for the example of a cubic box. Briefly, to preserve similarity of Bi between the model and the *full-scale* building (i.e., $Bi_m = Bi_h$) thermal conductivity (k) scales by F; likewise, to preserve Fo similarity, thermal diffusivity (κ_H) scales by F^2; conservation of H requires that the thermal mass of the interior of the model (c_{Mi}) scales by F^3; and λ scales by F^{-1}, because A_m scales by F^2 and V_m by F^3. Thus, Bi, Fo and H are conserved and the model has the same φ at similar *X:Y:Z* compared to a *full-scale* building, according to time measured as Fo. However, in real time, temperature is distorted.

In the present study, the desired outcome is that absolute surface temperature in the model is the same as temperature at the full-scale, for similar locations, according to time measured as t. A model scaled according to strict geometric scaling cools too fast, and would accumulate too much dew if exposed outside overnight. Consequently, strict geometric scaling is unacceptable.

Table 4.1 Geometric and thermal effects of using a strict geometric approach to scaling the thermal state of a box.

Property	Full-scale	Scale model
	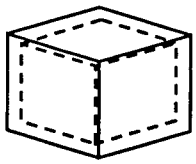	
• *Geometry*		
Wall thickness:	L_h	$L_m = L_h \times F$
Width of box:	W_h	$W_m = W_h \times F$
Surface area of box:	A_h	$A_m = A_h \times F^2$
Overall box volume (ignoring voids):	V_h	$V_m = V_h \times F^3$
Wall volume:	V_{wh}	$V_{wm} = V_{wh} \times F^3$
Ratio of wall thickness to box width:	$(L/W)_h$	$(L/W)_m = (L/W)_h$
• *Thermal character*		
Thermal conductivity:	k_h	$k_m = k_h \times F$
Thermal diffusivity:	κ_{Hh}	$\kappa_{Hm} = \kappa_{Hh} \times F^2$
Interior thermal mass:	c_{Mih}	$c_{Mim} = c_{Mih} \times F^3$
Surface area to volume ratio:	λ_h	$\lambda_m = \lambda_h \times F^{-1}$

4.6 The Internal Thermal Mass Approach (ITM)

4.6.1 Theory

An alternative to strict geometric scaling of box-like enclosures is the *Internal Thermal Mass Approach* (ITM). Aspects of ITM appear, in an intuitive form, in applied engineering, in the modelling of building architecture and human bioclimatology (Mills, *pers. comm.*, 1997). An example of a more rigorous implementation of the approach is given by McPherson (1980) and McPherson *et al.* (1989). ITM consists of scaling overall dimensions geometrically, but controlling thermal behaviour by regulating internal thermal mass, i.e., in the walls, on the one hand, and in the largely air-filled interior space, on the other. The density and thickness of the walls are held constant, by constructing the model walls at full-scale thickness and by using the same materials as at the full-scale (siding, framing, insulation and shingles). When first constructed, the interior of the model is empty; thermal inertia is supplied by adding a calculated mass to the interior of the model, normally bottled water.

Although overall size is scaled geometrically, the effects of scaling under ITM differ from those of strict geometric scaling. When a cubic box is scaled according to ITM, overall width (W) is scaled by F, but wall thickness is not, so the ratio L:W becomes proportionately F^{-1} times greater (Table 4.2). Bi is conserved when k is constant ($k_m = k_h$), and Fo is conserved when κ_H is constant, but detailed geometry is not a simple function of F, and volume is not universally scaled by F^3. To illustrate, the volume of the walls of a cubic box is found by subtracting the volume

Table 4.2 Geometric and thermal effects of scaling a box under the Internal Thermal Mass approach (ITM).

Property	Full-scale	Scale model
	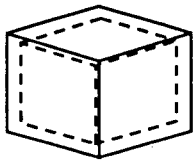	
• *Geometry*		
Wall thickness:	L_h	$L_m = L_h$
Width of box:	W_h	$W_m = W_h \times F$
Surface area of box:	A_h	$A_m = A_h \times F^2$
Overall box volume (ignoring voids):	V_h	$V_m = V_h \times F^3$
Wall volume:	$V_{wh} = 6W_h^2 - 12W_hL + 8L^2$	$V_{wm} = 6F^2W_h^2 - 12FW_hL + 8L^2$
Ratio of wall thickness to box width:	$(L/W)_h$	$(L/W)_m = (L/W)_h \times F^{-1}$
• *Thermal character*		
Thermal conductivity:	k_h	$k_m = k_h$
Thermal diffusivity:	κ_{Hh}	$\kappa_{Hm} = \kappa_{Hh}$
Interior thermal mass:	c_{Mih}	$c_{Mim} = c_{Mih} \times F^2$
Surface area to volume ratio:	λ_h	$\lambda_m = \lambda_h \times F^{-1}$

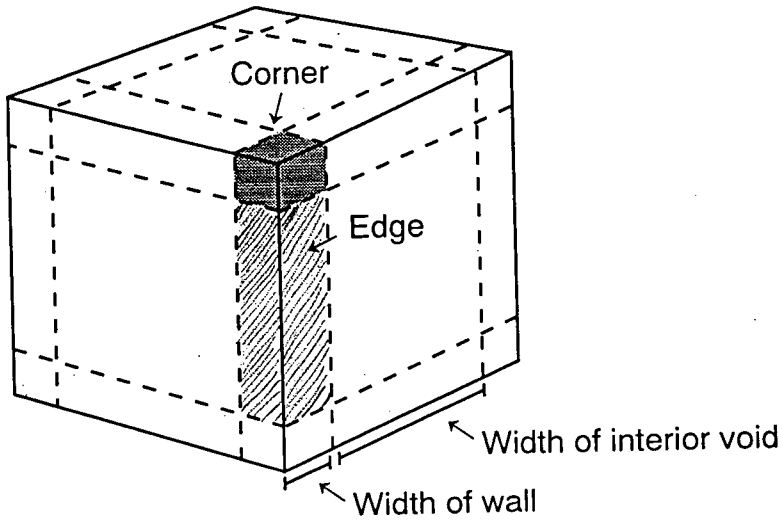

Figure 4.4 Box geometry for the example of a cubic box, showing the definition of 'corner' and 'edge'.

of the interior void, $V_i = (W - 2L)^3$, from the overall volume of the box, $V = W^3$ to give $V_w = 6LW^2 - 12WL^2 + 8L^3$ (see Figure 4.4 for a diagrammatic representation of box geometry). Under ITM, W scales by F but L does not. Consequently, V_w scales as a complex function of F, W and L:

$$V_{wm} = 6LF^2W_h^2 - 12FW_hL^2 + 8L^3 \qquad [4.9]$$

In contrast, V scales by F^3, i.e., $V = FW^3$.

Thermal Mass Number is volume dependent, and scales accordingly. Consequently, to conserve H, so that $H_m = H_h$, the internal thermal mass of the model (c_{Mim}) scales by the ratio of scaled and unscaled wall volume:

$$c_{Mim} = c_{Mih} \frac{V_{wm}}{V_{wh}} \qquad [4.10]$$

For solid objects it is valid to substitute area times length for volume, but for a hollow box care must be taken. Viewed from the exterior, box walls overlap volumetrically at their junctions, i.e., at their 'corners' and 'edges' (Figure 4.4). As a consequence, errors occur if A is used to calculate V_w, because corners and edges (as defined here) are counted not once, but once for each face on which they appear. For a cubic box, the resulting error is equivalent to 12 edges and 16 corners:

$$12\left(WL^2 - 2L^3\right) + 16L^3 = 12WL^2 - 8L^3 \qquad [4.11]$$

The error is less significant for boxes with relatively thin walls, compared to their width, however, the error compounds for models at small scales, because L is held constant. In theory, one solution is to construct corners and edges using alternate materials, for which conductivity has been appropriately scaled (Parczewski and Renzi, 1963), but a more straightforward method is to define an effective wall area ($\hat{A}_w$). This is the area that, when multiplied by L yields V_w, and it is equivalent to the area of an imaginary box located part way through the thickness of the walls. For a cubic box it is given by:

$$\hat{A}_w = \frac{V_w}{L} = 6W^2 - 12WL + 8L^2 \qquad [4.12]$$

Thus, substituting Equation 4.12 into Equation 4.10 gives, for a cubic building scaled by F:

$$c_{Mim} = c_{Mih}\frac{V_{wm}}{V_{wh}} = c_{Mih}\frac{\hat{A}_{wm}L_m}{\hat{A}_{wh}L_h} = c_{Mih}\frac{6F^2W_h^2 - 12FW_hL + 8L^2}{6W_h^2 - 12W_hL + 8L^2} \qquad [4.13]$$

It is assumed that the time scales governing heat exchange inside the model (between the bottled water and walls) are appropriately scaled. However, rates of exchange may be adjusted using fans or by replacing air inside the model with a gas of a suitably scaled conductance (Parczewski and Renzi, 1963; Imbabi, 1990a).

The theoretical outcome of partitioning and scaling the thermal mass of system in this manner is that all similar boxes with the same external geometry (W) will have the same absolute surface temperature response at *X:Y:Z* according to time measured as t. Thus the goal is achieved, the model cools at the same rate as a similar box at the full-scale, and shows similar surface temperature in similar ambient environmental conditions. This means it is theoretically possible to construct a scale model of a building for which surface temperature, and thus dew accumulation, mimics that seen at the full-scale.

4.6.2 Practical considerations

At the full-scale, geometry and materials of construction vary greatly from building to building, but many single-family residential buildings (houses) are of roughly similar geometry. For wooden houses, it is often reasonable to assume that (a) building form is approximated by a cube, (b) L is about the same for roof, floor and walls,

and (c) these have more or less similar thermal properties because artificial insulation dictates their overall thermal character.

These simplifications make computing the amount of thermal inertia required to be placed inside the model far more straightforward since Equation 4.13 can be utilised. Typical values of the ratio c_{Mim}/c_{Mih} are given in Figure 4.5 for a range of building proportions (L:W) and scaling factors (F), for buildings approximated by a cube. In general, buildings at larger scales and/or with relatively thin walls compared to their width (many wooden buildings fall into this category) have larger c_{Mim}/c_{Mih} and thus need proportionately more internal inertia, compared to buildings at smaller scales and/or with proportionately thick walls (brick or concrete). Physical limits are present for each L:W because as $W_m \rightarrow 2L_w$ the volume of the interior void of the model goes to zero, and the required c_{Mim} cannot be installed.

McPherson (1980) estimated that the internal thermal mass for a single-family dwelling is 16.2 MJ K^{-1}, based on a inventory of house contents and internal walls. McPherson *et al.* (1989) cite a similar value (12.8 MJ K^{-1}), and the latter value is used here. Thus, if a building of cubic form with c_{Mih} = 12.8 MJ K^{-1} and L:W = 0.01 (say, L = 0.10 m and W = 10.0 m) is scaled by 0.125, Equation 4.13 shows that c_{Mi} scales by 0.014, to 0.18 MJ K^{-1}. Water is a convenient way to add the required thermal inertia, and provides 4180 J K^{-1} of thermal mass (c_M) per litre, so the thermal mass is supplied by 43.1 litres of water. The amount of water required is scale dependent, so a similar model scaled by 0.25 needs 183.8 litres of water installed, whereas one scaled by 0.10 requires only 31.1 litres.

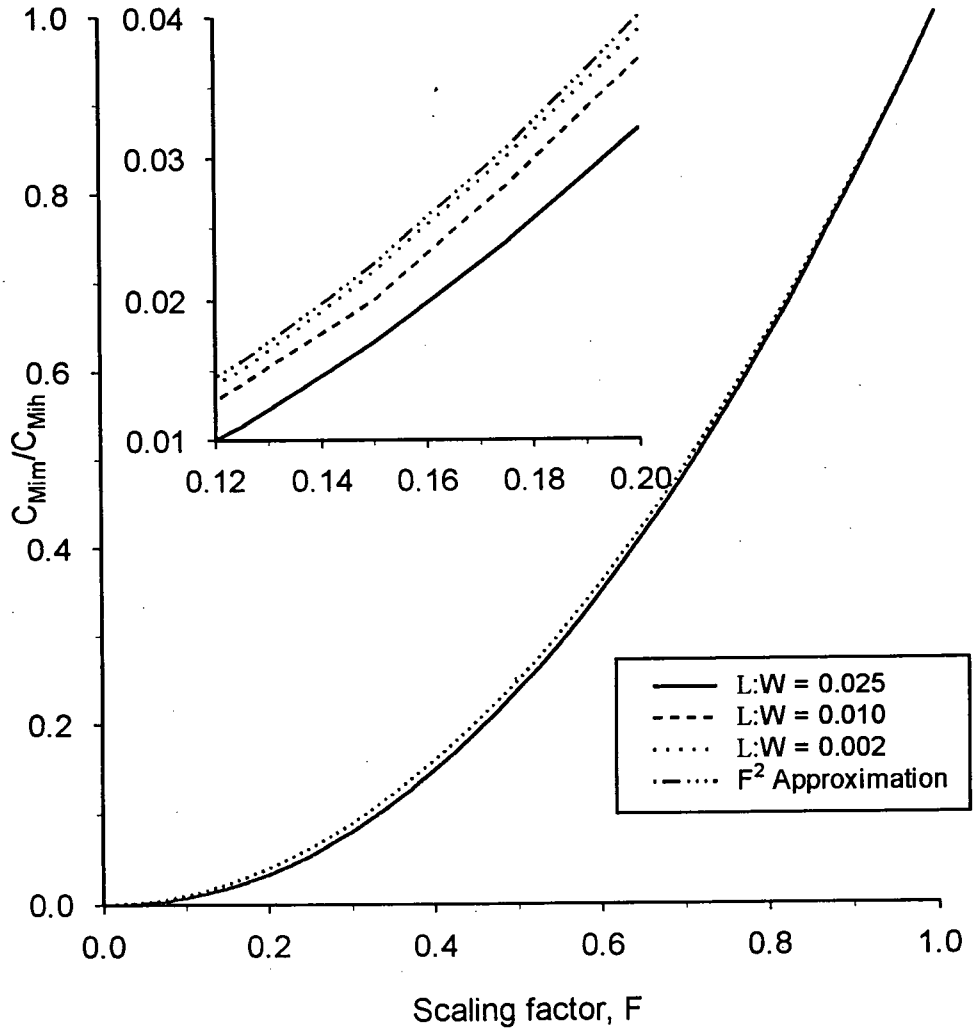

Figure 4.5 Envelope indicating the relationship between the scaling factor (F) and the ratio of interior thermal masses (C_{Mi}) for buildings with a range of L:W. Data are for buildings approximated by a cube (see Equation 4.13). Insert: Outcome for a range of L:W and if the relationship were approximated using F^2.

Equation 4.13 is not difficult to implement, but it lacks intuitive elegance. For many modelling purposes (McPherson, 1980; *et al.*; 1989) a more simple approximation is adequate. For buildings with proportionately thin walls, compared to their width, c_{Mim}/c_{Mih} approaches $F^2 c_{Mih}$ (Figure 4.5). Thus, to continue the example from above, scaling c_{Mi} by F^2 leads to 47.9 litres of water (to give c_{Mi} = 0.20 MJ K^{-1}) being required in the model, similar to that computed using Equation 4.13. The error involved in scaling by F^2 is conservative, because the approximation results in more thermal inertia being added to the model than is strictly required. This means, when modelling dewfall, that the model will cool more slowly after sunset and slightly under-estimate dew accumulation, compared to its *full-scale* equivalent.

For an out-of-doors model, ITM implicitly assumes that vertical environmental gradients are less important than the thermal behaviour of surfaces. Near the ground surface, microclimate (wind speed, air temperature and humidity) varies with elevation and, while model height is scaled by length, the lower atmosphere in which it is immersed is not scaled. Thus, for example, the roof of a scale model house is likely to be exposed to a different wind speed than would be the roof of a full-scale building at the same location. However, vertical gradients observed in the UCL are characteristically smaller than the strong gradients typical of the open countryside (Nakmura and Oke, 1988), and this may mitigate potential errors created by differences in height of exposure.

Under ITM, surface micro-morphology, radiative properties, and water absorptivity of the surface are preserved because real materials are used. This has

immediate advantage in a dew model, where surface characteristics may be critical. ITM explicitly applies to buildings not to vegetation. Nevertheless, in an approach analogous to ITM, canopy micro-morphology (leaf type, size and shape) is conserved by using real grass and foliage, and overall dimensions of plants are scaled geometrically in height and canopy width.

PART III MODELLING

Chapter 5: A scale model to study urban dew

5.1 Scaling considerations

5.1.1 Similitude

Many North American residential areas consist of an ensemble of more or less similar units (house lots, streets and parks), the physical structure of which can be modelled to a first order using relatively few generic landscape elements (Chapter 4). In this study, a generic urban residential neighbourhood is modelled at 1/8th-scale using two landscape units: (a) a 'street' bordered by a row of closely-spaced houses on one side and trees on the other, with lawn and pavement lying between, and (b) an urban park consisting of a grassed surface bordered by trees. The two landscapes are adjacent, with a single row of street/park trees as their common border; the theoretical park is symmetrical, so it is necessary to model only half its width; and park width is chosen to be sufficient that the trees that would have been present on the far edge of the park can be ignored. Hereafter, dimensions parallel to the long-axis of the street are *lengths*, whereas those at right angles to this are *widths*, where *width* (e.g., 'lawn width') means from edge-to-edge, but *half-width* is from edge-to-centre, e.g., of the theoretical park.

Formal scaling criteria (Chapter 4) dictate the dimensions and details of elements in the model so that real world properties are appropriately scaled or conserved. This means the surface thermal behaviour of the model is conserved. Minimum street length is compressed using false perspective techniques, so the

street/park landscape is modelled using few elements. Park half-width was chosen so as to effectively remove any edge effects due to a park border.

The model does not duplicate exactly the conditions at a specific location, but elements in the 1/8th (i.e., 0.125:1) model possess proportions similar to equivalent objects at the full-scale in residential neighbourhoods in Vancouver (Schmid, 1988; Voogt, 1995). Houses in the model are equivalent to real buildings 8.6 m tall (about 1½–2 storeys), the trees are the equivalent of ones 10–12 m tall, lot width is equivalent to 12 m, pavement width to 8 m, and the park has a half-width equivalent to 60 m at the full-scale. Surfaces in the model are constructed using realistic materials (wood, shingles, concrete and living foliage), so surface micro-morphology and intrinsic radiative characteristics (α, tr and ε) are conserved.

For practical reasons, some dimensions in the model are less realistic. Houses were constructed using pre-cut timber, obtained as parts of a kit to build a doghouse, thus are proportionately narrow compared to geometrically-similar full-scale houses; lawn width was exaggerated by a factor of about 1 ½–2 to permit easy access for dew sampling; and the juvenile trees used in the model conform only partially to the morphology of full-grown trees.

Ideally, details of wall construction and c_{Mih} are determined from surveys of real buildings and their contents. In the present case several simplifications were made. Realistic interiors (using drywall, carpets and windows; see McPherson *et al.*, 1989) were not attempted. Expanded polystyrene board and/or air was used as insulation, instead of the glass-fibre batts commonly used at the full-scale in Vancouver, but this seems acceptable since the thermal conductivity of air at 10°C

(0.026 W m^{-1} K^{-1}), expanded polystyrene (0.029 W m^{-1} K^{-1}) and low-density glass-fibre batting (0.037 W m^{-1} K^{-1}) are similar (Oke, 1987; ASHRAE, 1993). These materials therefore provide roughly equivalent insulation, as long as air cavities are sealed and do not experience buoyancy-driven convection, which is unlikely at night. The thickness of insulation used in the model walls (0.09 m) was realistic, but the model floor (with 0.08 m insulation) and ceiling (0.05 m insulation) were under-insulated compared to many homes—insulation 0.15 m in thickness is more common. This means that at night the model may receive an excess flux of sensible heat from the underlying soil and heat loss from the interior to the attic and roof may be too large, making the roof excessively warm. This could lead to under-estimation of dewfall by the model.

The geometry required to conserve Ψ by the model was assessed using a combination of formal criteria (Voogt, 1989) and stereographic plots of equivalent full-scale and scaled theoretical environments. In the theoretical landscape, one wall of the street 'canyon' is formed by the line of houses, the other wall is the outer-edge of the maple tree canopy. The tree canopy is assumed to overhang the entire width of the pavement. Thus, the lawn forms the canyon floor. In a stereographic view an infinitely long street canyon will plot from west to east, i.e., from '1' to '1' in Figure 5.1. Theory (Chapter 4) dictates that street canyon length in the model should be the greater of 8W or 8H, where W is canyon floor width and H is wall height. Here, 8W (8 x 2.5 m) exceeds 8H (8 x 1.08 m) so the model street 'canyon' needs to be 20 m in length to act radiatively as if it were semi-infinite (i.e., from '2' to '2' in Figure 5.1). In practice, similitude is achieved in less than half this length, by

using (a) false walls and inwardly angled panels on the house side of the 'canyon', and slightly broader trees placed at the ends of the row on the tree side, and (b) by ignoring far distant objects at the ends of the street, because they contribute little to Ψ at the centre of the model. In the final decision, radiative similitude for the centre of the lawn was achieved with an 8.5 m length model, as labelled '3' in Figure 5.1.

The view factor environment for the case of the grass in the model park was less accurately conserved (Figure 5.2). The park 'canyon' is 15 m in width (i.e., its half-width = 7.5 m), which suggests its minimum length should be 120 m (from '2' to '2' in Figure 5.2) but the usefulness of applying this rule when W (park width) exceeds H (tree height) by a factor of 10 is questionable. The 7.5 m row of trees used in the model stretches from '3' to '3' in Figure 5.2. In practice, the error incurred in this simplification is small, and Ψ_{sky} increases only slightly more rapidly away from the row in the model, compared to the ideal case with a semi-infinite border of trees. Close to the row of trees, for example at 1.5 m from the north edge of the park (Figure 5.2), tree height (as indicated by the dashed lines) is more important to conserving Ψ_{sky} than the absolute length of the row.

5.1.2 Assumptions

Several assumptions are made concerning conditions in the model. It is assumed that:

- for a single-family wooden dwelling c_{Mih} is about 12.8 MJ K^{-1} (McPherson *et al.*, 1989), L:W (i.e., wall thickness: building width) is relatively small, and the

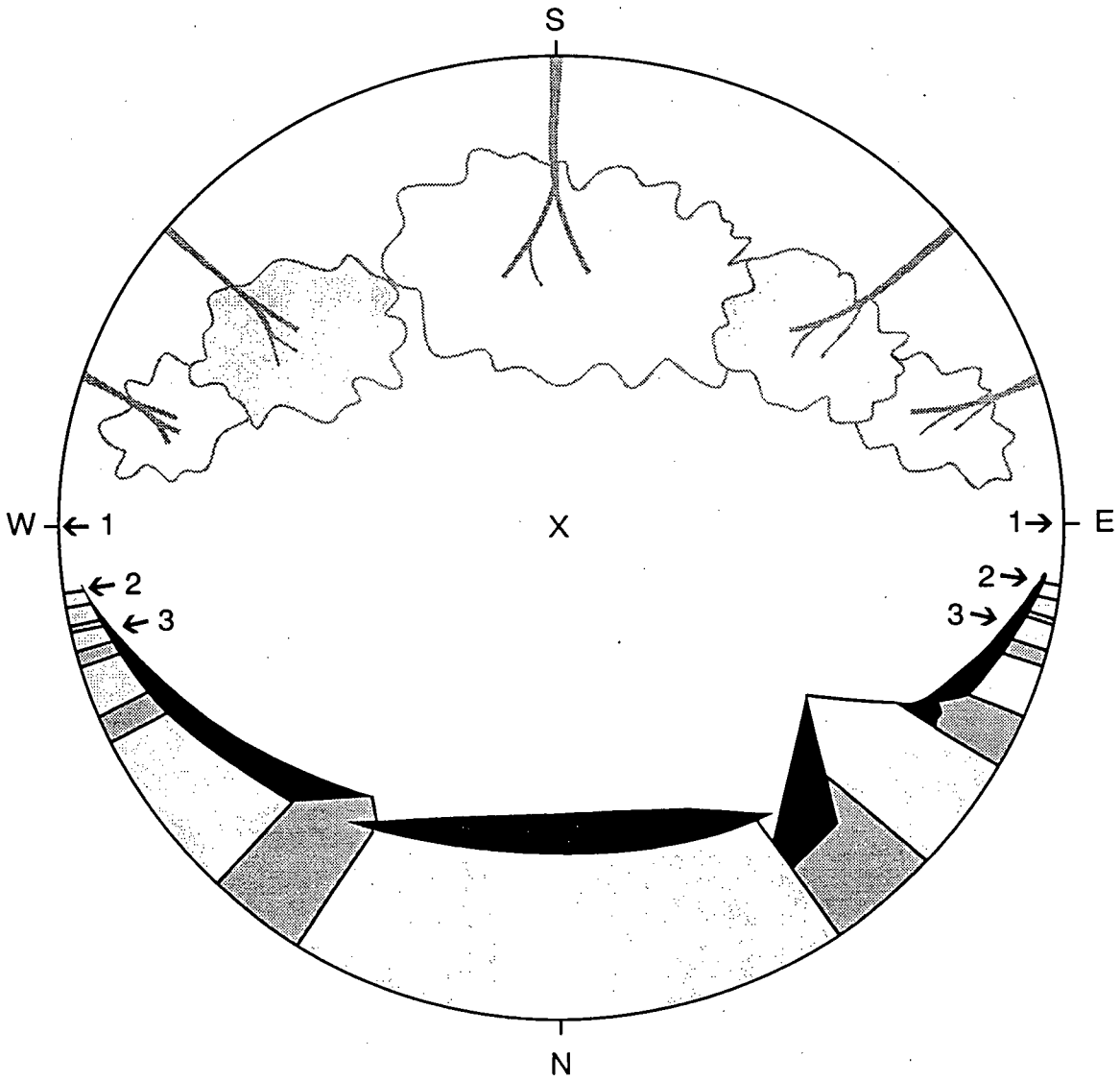

Figure 5.1 Stereographic depiction of the theoretical hemispheric geometry looking up at the sky zenith from a point in the centre of the urban lawn. In the lower portion of the diagram '1' indicates the theoretical extent of an infinite array of buildings, '2' is the minimum canyon length as dictated by radiative theory, and '3' is the canyon length ultimately simulated in the hardware model.

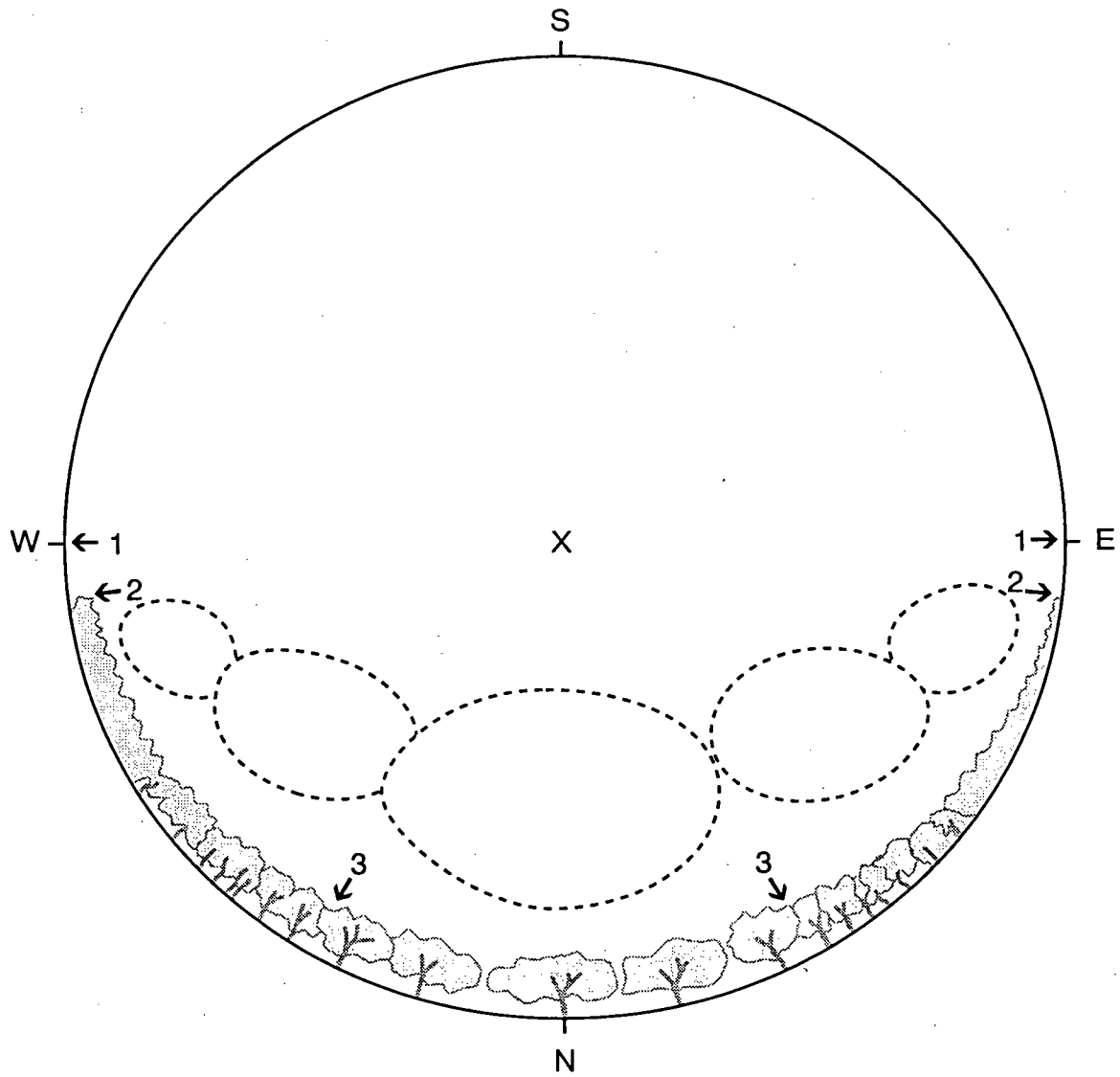

Figure 5.2 Stereographic depiction as shown in Figure 5.1, but for the outer (south) edge of the theoretical urban park. Here, '1' indicates the theoretical extent of an infinite row of trees, '2' is the minimum canyon length as dictated by radiative theory, and '3' is the row of trees ultimately constructed in the hardware model. The dashed lines superimposed on this image indicate an equivalent view, but from a point that is 1.5 m from the north edge of the park.

- building is roughly approximated by a cube. Thus c_{Mim} is $F^2 c_{Mih}$. These assumptions are not always valid.
- the model dwelling has negligible Q_F. Surveys undertaken by the author show that nocturnal heat 'leakage' is significant for many dwellings in Vancouver. Also many attics originally unoccupied are now lived in and so may be artificially heated or cooled which will affect their thermal behaviour at night.
- the model is sufficiently large to produce a local microclimate similar to that in the real world (McPherson *et al.*, 1989). Interest is centred on weather conditions when dew forms (i.e., very light wind speeds and weak turbulence) so that advection is much less important than longwave radiation and heat conduction from the substrate. During periods with stronger wind speeds advection will increase but dewfall becomes small or absent.
- vertical environmental gradients of wind speed, turbulence, temperature and moisture are less important than other controls on dewfall (Chapter 4) and failure to scale them is assumed to be non-critical.

5.2 The model

5.2.1 Sites and operation

Locations where the scale model was tested and operated, and the periods of measurement are shown in Figure 5.3. A trial of the model was conducted at M2 during 1994 (Old Orchard, Figure 5.3), from YD 249 until YD 285. The layout and instrumentation of the model were similar to those described in the following

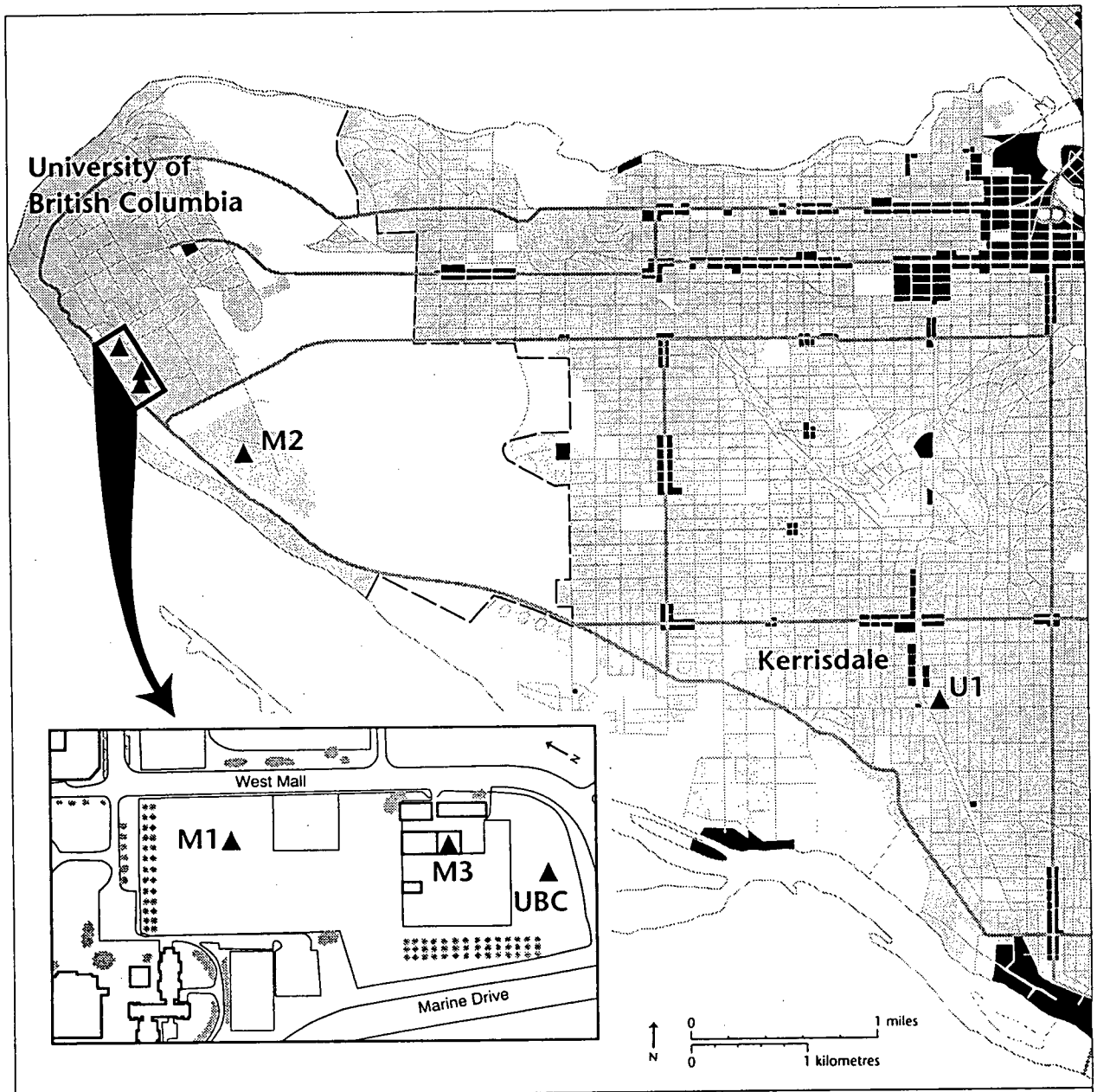

	The Scale Model	Season
M1▲	Fairground, University of BC	June-July 1996
M2▲	Old Orchard, University of BC	Sept-Oct 1994
	Full Scale Sites	
U1▲	Kerrisdale, Vancouver	June-July 1996
M3▲	Totem Building, University of BC	June-July 1996
UBC▲	AES Tower, University of BC	June-July 1996

Land use

- Green space
- Commercial
- Residential/Institutional

Figure 5.3 Sites used in the modelling programme and the periods of observation.

sections (Sections 5.2 and 5.3), but model design was simpler, e.g., only the central house of the three contained an appropriately scaled thermal mass, and several measurement methods were still being refined. Useful information on the design, instrumentation and behaviour of the model were obtained during the trial, but the site itself proved to be less than ideal, because of difficulties with security, irrigation and fog.

In the summer of 1996 the model was re-built at the Fairground site (M1, Figure 5.3). M1 provided a flat, extensive and well-maintained turf surface with a high background Ψ_{sky} (0.98). This site was also used for general observation of dew (see site P2; Figure 3.22) and is described in Section 3.3.1.

At M1 twenty nights covering a variety of weather conditions, but no rain, were selected for intensive study. On each occasion the model was run from dusk until about mid-morning or noon of the next day, by which time dew had evaporated. On two occasions, surface conditions in the model were monitored for a complete day (24 h). During the summer, the model was operated in two configurations: (a) from YD 153 to 182 trees were included, to represent street, park and yard trees, and (b) from YD 183 to 207 trees were absent; otherwise model configuration such as the position of houses and paving was unchanged. Ideally, I would have liked to operate the model for a greater number of nights and, perhaps, to experiment with other configurations. In practice, the number of suitable nights during the study season was relatively small because the out-of-doors model relied on naturally occurring weather and this did not always favour dew.

Hereafter, discussion of the model and its results (Chapter 6) focuses on the primary modelling season conducted at M1. So 'model' means the model constructed at M1 in 1996. Some findings are presented from the 1994 trial, e.g., to illustrate an aspect of instrumentation or some other special feature, but in such instances the model version (1994 *vs* 1996) is clearly indicated.

5.2.2 Construction

The model consists of three similar houses (scaled height 1.08 m tall, i.e., full-scale 8.64 m), a street with scaled trees (1.5 m tall, i.e., full-scale 12 m), and an open grassed park (Figure 5.4). The model was constructed on a 9.0 m x 12.0 m plot of short grass, with the street direction (the short axis of the plot) oriented east-west. Details of the modelled elements are given in Table 5.1.

Houses were closely spaced (0.40 m apart, i.e., full-scale 3.2 m) and placed in a row on the north side of the plot with their front walls aligned parallel (Figure 5.4a); two were placed with their longest wall, and roof ridge, oriented parallel to the street direction, and one normal to it. Two free-standing plywood walls of about house size were installed in line with the houses, smaller panels were attached to these and angled inward (towards the front) by 40°. These contributed to building-like view factors so that from the perspective of a point on the lawn, the model trees, houses and false walls together reproduce a street of significant length.

Scaled houses were of simple form, with a steeply pitched (45°) roof, covered with dark brown asphalt shingles. The houses were constructed from fir framing (0.02 m thick) and cedar (0.018 m thick), and were stained off-white, using acrylic

Figure 5.4
The scale model at M1. (a) A general view of the model street from the south-west, and (b) the measurement transect, from its southern end; wooden pegs indicate the sample points for blotting.

Table 5.1 Specifications for the scale model at M1, where north-south dimensions are given as widths, and east-west dimensions as lengths.

Element	*Description*
Vegetation	
• *Grassed areas*	Lawn = 2.5 m wide; Park = 7.5 m wide Irrigated and mown regularly
• *Trees*	Five Pyramidal cedar (1.2 m tall) = yard trees Five Japanese maple (1.5 m tall) = street/park trees Hand watered daily
Scaled Building	
• *General description*	Height = 1.08 m = 1 storey Plan area = 0.84 m^2 Wooden construction
• *Insulation*	Expanded polystyrene and/or still air Thickness = 9 (wall), 5 (attic), 8 (floor) x 10^{-2} m
• *Wall*	External height = 0.65 m Cedar, stained off-white
• *Roof*	Pitch = 45°; east-west[1] orientated ridge Dark brown asphalt shingles
• *False wall*	Plywood; 0.85 m tall, 1.22 m in length Side panels = 0.5 m long, angled inward by 40°
Pavement	1.0 m wide, 3.75 m long (equivalent to 3 lots) Concrete paving slabs (0.08 m thick)

1. One building is orientated north-south.

paint. Each had an external wall height of 0.65 m (full-scale 5.2 m), with a floor which was 1.10 m x 0.76 m (full-scale 8.8 x 6.1 m). Roofs were slightly larger than this, creating overhangs of 0.15 m on the long sides, and 0.06 m on the short sides of the building (full-scale 1.2 and 0.48 m, respectively). Each model house was elevated 0.05 m above ground level on beams laid length-wise under the floor.

Walls, floor and roof were lined with plastic (of negligible thickness) as a vapour barrier. The walls were insulated with expanded polystyrene board and a sealed cavity loosely packed with expanded polystyrene chips. This gave a total insulation thickness of 0.09 m. The floor was insulated with expanded polystyrene board (0.025 m thick). The 0.055 m sub-floor air-space also provided insulation (giving a total of floor insulation thickness of 0.08 m). An expanded polystyrene board (0.05 m thick) at the top of the walls divided the internal cavity of each house (its *interior*) from the *attic* space, and insulated each from the other. 43 litres of water was placed, in 4-litre plastic containers in the interior of each house. This provided 0.18 M J K^{-1} of interior thermal mass (c_{Mim}) for each house and simulated the existence of otherwise absent internal free-standing walls and the furnishings of the house, the assumed thermal mass of which was scaled according to ITM (Chapter 4). Roofs were removable, to permit access to instruments, but interiors were effectively sealed when the roof was in place. To prevent over-heating of the attic space by day (see McPherson, 1980), attics were passively ventilated, *via* openings in each gable end. No attempt was made to simulate human occupancy or energy use, and buildings were windowless.

Near the centre of the house lots and park, a street pavement (1.0 m wide; full-scale 8 m) was simulated using paving slabs. Thinner slabs (0.04 m thick) were laid in the inner portion of the pavement, compared to those at the outer edge (0.08 m thick); this permitted a weighing mini-lysimeter to be installed. Due to site restrictions, slabs were laid directly on the grass or on a sand-bed, not buried. The street divided the grass in the model into two areas; a 2.5 m (full-scale 20 m) wide

lawn, located between the row of houses and the pavement, and a *park* with a half-width of 7.5 m wide (full-scale 60 m), extending from the pavement to the south boundary of the model. During the study, grassed surfaces were mown and irrigated regularly.

When trees were present, they consisted of a single row of five small (1.5 m tall; full-scale 12 m) Japanese maples, planted at the south edge of the pavement to model street and park trees, and five Pyramidal cedars (1.2 m tall; full-scale 9.6 m), to model yard trees; the latter were placed between the buildings (Figure 5.4). The variety of maple chosen has small leaves, typically 0.06 m in diameter, and the cedar forms a tightly-packed, cone-shaped tree. Trees were planted in plastic containers, for ease of later removal, and were watered daily by hand. The grass under the maple canopy grew faster than in the open park, but there was very little observed lateral spread of water into the upper layers of the surrounding soil as a result of tree watering because the soil was sandy and free draining. The extra growth therefore seems to be due to shading, not differences in irrigation. When trees were removed from the model on YD 182, their locations were filled and re-turfed.

5.2.3 Operational considerations

In 1996, surveys were conducted at M1 prior to the installation of the model to test the homogeneity of surface conditions across the model plot. No apparent spatial trend was seen across the plot for the grass canopy temperature, surface moisture (by blotting) and soil moisture data which was collected at dawn on two occasions.

Spatial variation in these parameters seemed random and of relatively small magnitude. Hence, patterns ultimately seen in the model can reasonably be attributed to model effects.

In theory, differences in night-length may create errors in a dewfall model because water accumulation is potential greater when night-length is greater. However, during the study night-length varied only slightly. In 1996, each night was 8.2 ± 0.3 h in length. Even if the rate of dewfall deposition approached its theoretical maximum (0.07 mm h^{-1}; Equation 1.2), the largest potential error is therefore only ± 0.02 mm per night.

For practical reasons, the model treatments in 1996 were *blocked*, not randomised, i.e., the model was run first in one configuration (with trees) and then in another (without trees). By chance the change-over on YD 182, 1996, coincided with a change in weather trends (see Chapter 3) so that nights favouring heavy dewfall are more frequent during the second treatment than during the first.

5.3 Data collection and analysis

The instruments and methods used to collect data are summarised in Figure 5.5 and Table 5.2. Sampling of dew, surface wetness and surface temperature mainly focus on a north-south transect through the centre of the model, at right angles to the street direction (Figure 5.5). However, data were also collected on other surfaces away from the transect line, e.g., to sample the effect of a specific roof orientation or other special feature. Electronic instrument signals were sampled every 60 s using *Campbell Scientific* data loggers (CR10 or CR21X). Some signals

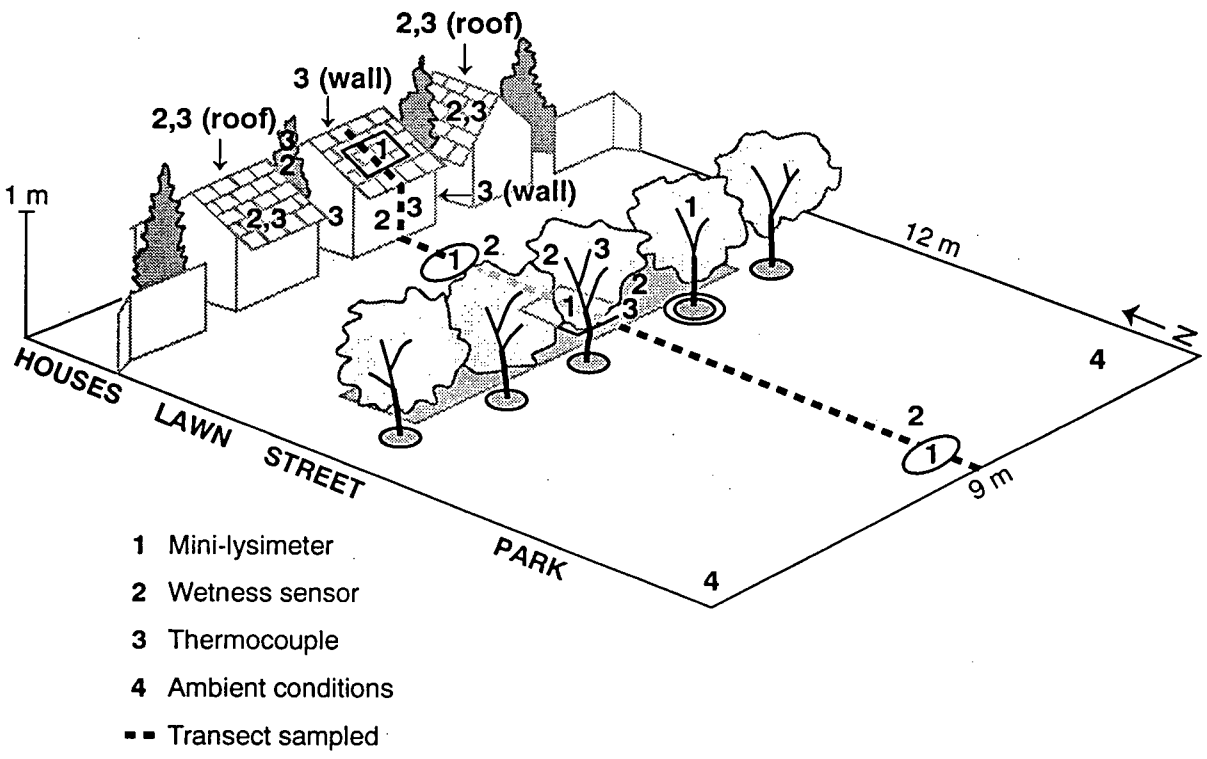

Figure 5.5 Diagrammatic representation of the scale model, showing location of instruments and the transect sampled.

were routed through a *Campbell Scientific* AM32 multiplexer to increase the number of input channels. Data were stored as 15 min averages, except for surface wetness data, which were instantaneous samples at 15 minute intervals.

When the spatial distribution of a particular parameter (e.g., surface moisture) is compared with the distribution of another (e.g., Ψ_{sky}) several statistical indices are used, i.e., mean, standard deviation (SD), mean absolute difference (MD), root mean square difference (RMSD) and Willmott's index of agreement (ID)

(Section A1.5). The latter quantifies the agreement between two data-sets on a scale from 0.0 to 1.0, where 1.0 means perfect one-to-one agreement. ID describes correlation in the data better than other measures such as Pearson's coefficient of determination (r^2), which is insensitive to additive and proportional differences which may be present between the individual data-sets (Willmott, 1984).

5.3.1 Surface moisture

Electronic wetness sensors of the cloth type (Chapter 3) were deployed on built and vegetation surfaces to monitor surface moisture duration (Figure 5.5). On selected days, the amount of surface moisture on grass at dawn was measured by blotting along the central transect, at 0.25 m intervals, using pads of blotting paper 0.20 x 0.10 m in width. Relatively small pads were used so that samples could be placed closer together along the transect (see Figure 3.5). Visual/tactile observations were also made.

Dewfall amount was measured using several electronic weighing mini-lysimeters: one in the model park, one in the house lawn (these as depicted in Figure 3.6), one under a section of pavement, and one under a potted maple (~1.3 m tall), to which quy ropes were attached to reduce wind sensitivity. A fifth mini-lysimeter was designed specifically to measure dewfall on a model house roof. Its weighing platform was installed in the south-facing facet of the roof of the central building, under a rectangular panel of roofing, which was supported at 45° (Figure 5.6). Mass changes were converted to dewfall amount using horizontal

Table 5.2 Instruments and methods used in the scale model.

Parameter	*Method*	*Location*
The model		
• *Surface moisture*		
Surface moisture at dawn	Blotting	park, lawn
Wetness duration	Electronic wetness sensor	park, lawn, tree, roof, wall, paving
Dewfall (electronically sensed)	Mini-lysimeter, 0.11 m^2	park, lawn
	Mini-lysimeter, 0.156 m^2	roof
	Mini-lysimeter, 0.04 m^2	paving
	Mini-lysimeter, ~1 m^2	maple tree
Dewfall (manually weighed)	Micro-lysimeter	roof, leaf
• *Surface temperature*		
Roof, wall, paving	Thermocouple, 30 AWG Cu-Co	on surface
Tree leaves	Thermocouple, 30 AWG Cu-Co	in canopy
Grass canopy[1]	*Everest Interscience* thermometer	park, lawn
Built and vegetation surfaces[2]	Hand-held infrared thermometer	
Ambient conditions		
Wind speed	*Young* Wind Sentry anemometer	1.5 m
Wind direction[3]	*Young* Wind Sentry vane	3.6 m
Humidity-air temperature	*Vaisala* HMP35C in *Young* shield	1.5 m
Incoming longwave radiation	*Eppley* pyrgeometer	0.5 m

1.*Everest Interscience* thermometer (FOV=15°; spectral band = 8-14μm); 2. *Minolta Cyclops* (FOV = 1.7°; ε = 1.00; spectral band 8-14 μm) or *Omega* OS43 (FOV = 60°; ε = 0.98; spectral band 8-14 μm); and 3. At UBC.

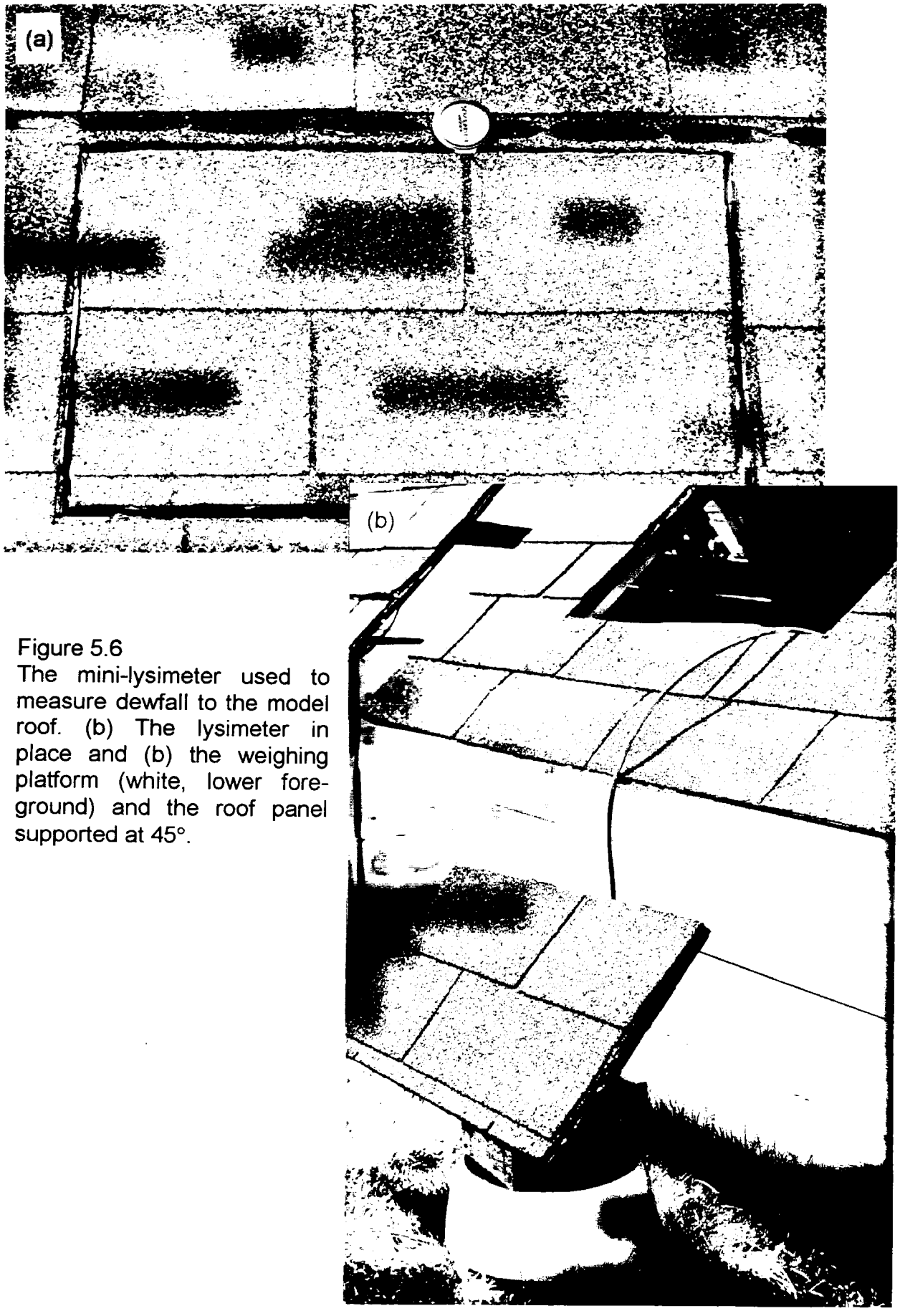

Figure 5.6
The mini-lysimeter used to measure dewfall to the model roof. (b) The lysimeter in place and (b) the weighing platform (white, lower foreground) and the roof panel supported at 45°.

surface area. In the case of the sloping roof the effective horizontal area was 0.11 m^2.

Micro-lysimetry procedures were developed for roof shingles and tree leaves. Removable sections of shingle (area = 0.02 m^2) were laid on north-, south-, west- and east-facing roof facets; these were weighed dry and when dew-wetted, using a field balance. For trees, water accumulation on foliage was measured at dawn by clipping wet leaves from the plant. For the cedars, small branches were clipped. Each wet leaf was placed in a plastic bag and weighed, then wiped dry and re-weighed, so that the mass of water was found by subtraction. Mass was later converted to units of mm depth using leaf area, this found using a planimeter.

Surveys conducted in the model at dawn using hand-held infrared thermometers show general agreement between the surface temperature of wetness sensors and mini-lysimeters and their surroundings. This is most clearly demonstrated using a set of images collected on YD 262/263, 1994. On that occasion an AGEMA digital thermal imaging system was available to sense surface temperature in the prototype model (the system is described in detail in Voogt (1995)). Figure 5.7 clearly illustrates the similarity between the apparent surface temperature of the 'roof' lysimeter and that of the surrounding roof at dusk (Figure 5.7a) and on the following dawn (Figure 5.7b). Similarly, the surface of the 'lawn' lysimeter in the model (Figure 5.8) is similar to that of the undisturbed lawn, except for an edge effect due to the relative warmth of the surrounding soil. Even the thermal signatures of the wetness sensors (e.g., immediately to the left of the roof lysimeter in Figure 5.7) cannot be distinguished. The exception is the paving

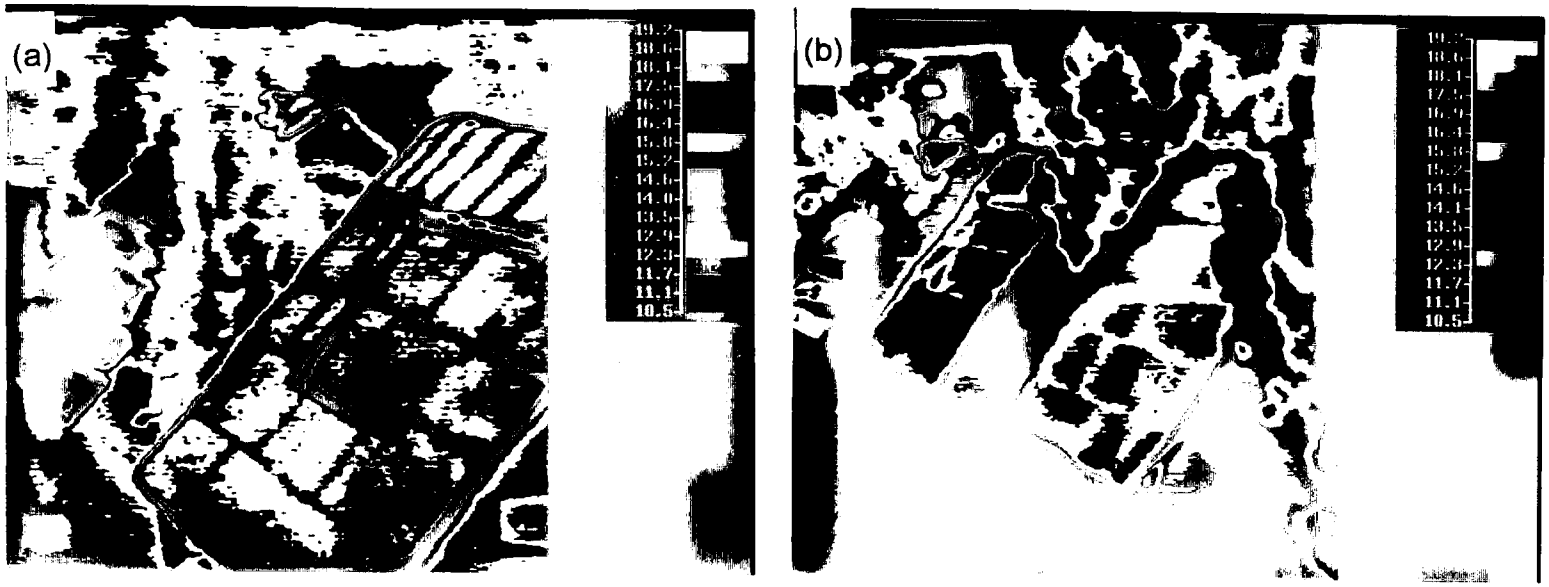

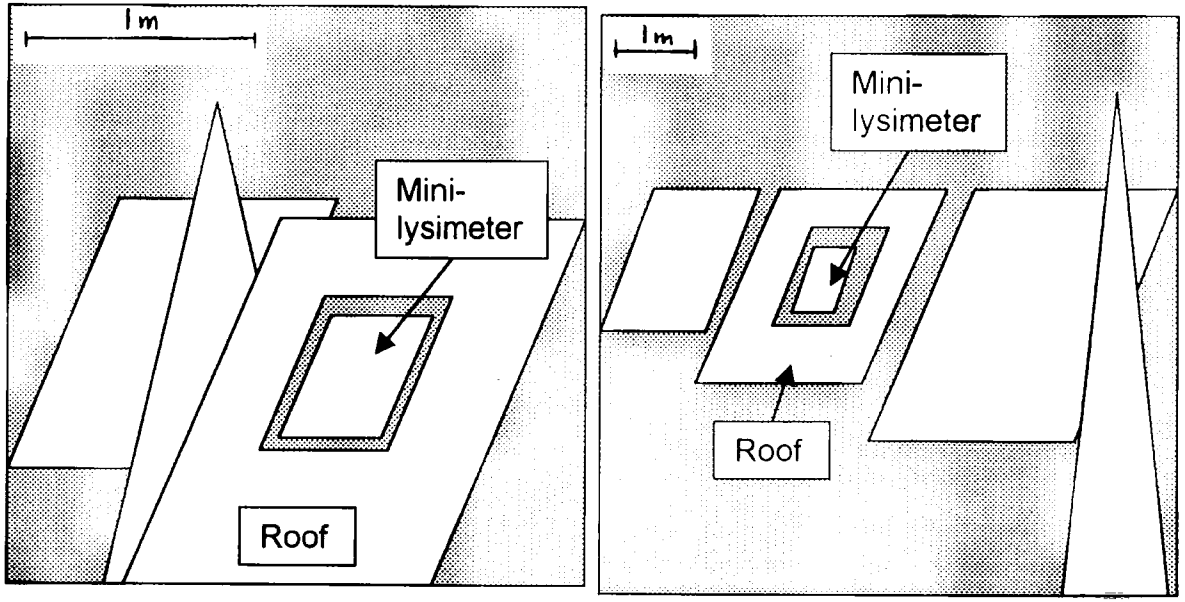

Figure 5.7 Apparent surface temperature (°C) in the prototype model sensed using an AGEMA digital thermal imaging system (ε set to 1.00). (a) is an image sensed at dusk on YD 262, 1994, and (b) is that sensed on the following dawn (YD 263). The view is looking along the row of model houses toward the north-west (see accompanying sketches).

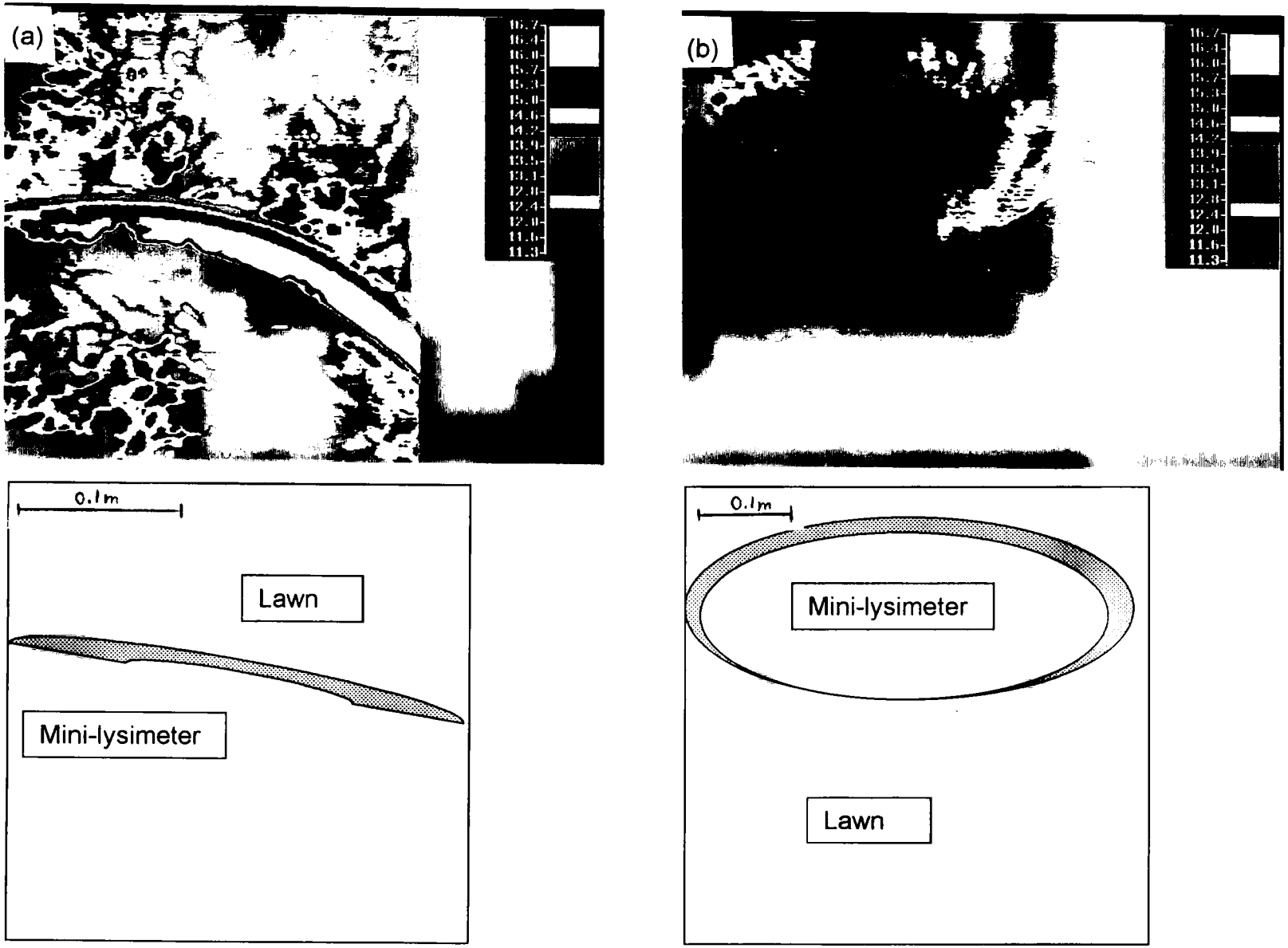

Figure 5.8 Data as in Figure 5.7, but for the **model lawn at (a)** dusk on YD 262, 1994, and (b) dawn on YD **263, 1994.**

lysimeter (not shown) which tends to cool excessively at night. This is non-critical, however, because the paving lysimeter did not accumulate dewfall.

5.3.2 Surface temperature

Thermocouples were used to measured the surface temperature of most surfaces. On artificial materials, thermocouples were glued into a groove on the surface, and coated with a thin layer of the surface material (asphalt, wood or concrete). Single thermocouples were attached to building walls and the pavement slab, and sets of five of thermocouples (attached in a circle of radius = 0.07 m and connected in parallel) were used on north-, south-, east- and west-facing roof facets to provided spatially-averaged data at mid-roof level (0.8 m). Thermocouples were also used to measure the air temperature inside a model house, and surface temperature on the underside of a model roof. For trees, lead wires were secured with adhesive tape and thermocouples themselves were held in contact with the under side of a leaf by wire tension. Three thermocouples (upper, middle and lower canopy level) were installed in a maple, and three in a cedar canopy, to provide an estimate of mean canopy temperature. For grass, which is more difficult to instrument using thermocouples, apparent surface temperature was measured in the model park and lawn using *Everest Interscience* infrared thermometers, with a field of view (FOV) of 15°. They were angled down at 45° to enhance the view of grass blades, rather than the underlying soil. A surface emissivity of 1.00 was assumed; this may introduce errors of the order of 1°C (Oke, 1987).

At dawn, surface temperature was surveyed using a hand-held *Minolta Cyclops* or *Omega* OS43 infrared thermometer, held 0.1 m above the surface of interest. For the former, a surface emissivity of 1.00 was assumed; for the latter, emissivity was set to its highest available value (0.98). This may slightly increase the expected error when temperature data are compared. Data sensed by the former were manually recorded, whereas electronic signals from the latter instrument was sampled every 1 s using a *Campbell Scientific* CR21X data logger. Data sense using the *Omega* thermometer were later adjusted spatially according to rates of travel along the survey route. On YD 164/165 and 174/175 in 1996, temperature surveys were repeated hourly from 1000 h until 2300 h, and from 0400 h until 0900 h; a survey was also undertaken at 0200 h.

5.3.3 Ambient conditions

During periods when dew was present, wind direction at M1 was typically from the east/north-east (by night) or west (by day). Therefore, to ensure the model did not contaminate the assessment of ambient boundary conditions a climate station was installed in the southeast corner of the model (Figure 5.5, Table 5.2). There, wind speed, air temperature and relative humidity were measured at 1.5 m—i.e., at about roof- and tree-top level—using a *Young* Wind Sentry anemometer and a *Vaisala* HMP35C sensor in a *Young* shield. Incoming longwave radiation was measured in the open south-west corner of the model, using an *Eppley* pyrgeometer. Additional environmental data (wind direction, soil temperature, soil heat flux, incoming solar radiation, net radiation and precipitation) were measured at UBC, about 250 m to

the south of the model site (see Table 3.1). A period of calibration showed that wind direction, soil temperature and soil heat flux were similar at M1 and UBC.

View factors (Ψ) along the central transect in the model were determined using fish-eye lens photography (Steyn, 1980; Steyn and Lyons, 1985) and site geometry (Sections 3.3.2 and A1.6). In the latter method, the horizon obstruction ($\Psi_{ter\ wall}$) created by the model houses was approximated using a vertical wall. This was of roof height (1.1 m), except close to the house wall where its height was reduced (to 0.65 m) because the model roof was hidden. Spheres were used to approximate the horizon obstruction ($\Psi_{ter\ trees}$) due to maple trees when these were present. For a given point on the transect, Ψ_{sky} was found using:

$$\Psi_{sky} = 1 - \left(\Psi_{ter\ wall} + \Psi_{ter\ trees}\right) \qquad [5.1]$$

The method slightly over-estimates Ψ_{sky} at M1 because the horizon obstruction due to the surrounding landscape (trees, buildings, topography) is not taken into account. At this site the resulting error is small (~0.01–0.02) and is ignored.

5.4 Validation

The scale model was validated through comparison of synchronous data collected on the model (M1), on a full-scale building located nearby (M3), and on a full-scale residential lot (U1). The three-way comparison permitted conditions at sites with a similar location but at a different scale (M1 and M3), and *vice versa* (M3 and U1) to be compared. Data collected at P1 and U2 during 1993 were also used to test the behaviour of the model. Sites and methods to collect data are described in this

Section. The results of the validation and the modelling programme itself are presented in Chapter 6.

5.4.1 Sites

P1, U1 and U2 were described in Chapter 3 (see Figures 3.21 and 3.23); these are sites where surface moisture was gathered as part of ancillary studies. U1 is approximately 8 km distant from the Fairground site (M1). At U1 the building of interest is a 1 ½ storey (6.8 m tall) wooden dwelling which forms one half of a residential 'duplex' (Table 5.3 and Figure 5.9b). It is simple in form, has an off-white stucco exterior, and a brown asphalt shingle roof (pitch = 35°). The ridge of the roof and the longer wall of the house are orientated east-west, which is parallel to the street direction. At M3, about 200 m from M1, there is a one storey (5.0 m tall), wooden service building (Figure 5.9a). It is simple in form, has a black asphalt shingle roof (pitch = 45°), and the roof ridge is orientated north-south. The building is connected to an equipment barn (to the north) by a wide breeze-way, and is bordered on three sides by open fields and grassed areas; to the east lies a paved area (12 m wide), and beyond this two buildings (7–10 m tall). Although the building is used by day, it is unoccupied at night and is not artificially heated or cooled during the summer.

5.4.2 Data collection and analysis

Instruments and methods used to gather data to validate the model are summarised in Table 5.4. U1 was less intensively instrumented than M1, relatively few electronic

(a)

(b)

Figure 5.9 Buildings used to validate the thermal responses of the model houses. (a) The service building at M3 viewed from the north-west, and (b) the house at U1, viewed from the north. In (b) the wooden box containing the roof lysimeter is visible on the far right portion of the roof-top.

Table 5.3 Description of landscape elements at the full-scale used to validate the results of the model.

Site	*U1*	*M3*	*P1*	*U2*
Vegetation				
• *Grassed areas*				
Area (m^2)	~105[1]	-	~6000	~95
Irrigation	rare	-	unirrigated	often
• *Trees*				
Height (m)	10–16	-	10–20	-
Type	broadleaf, conifers	absent	plum, maple	-
Building				
• *General description*				
Number of storeys	1.5	1		
Height (m)	6.8	5.0		
Plan area (m^2)	88	30		
Construction type	wooden	wooden		
• *Wall*				
External height (m)	4.0	2.6		
Exterior	stucco	wood		
Colour	off-white	pale green		
• *Roof*				
Ridge orientation	east-west	north-south		
Shingle type	asphalt	asphalt		
Pitch	35°	45°		
Colour	brown	black		
Pavement				
Type	tarseal			
Width (m)	9.3			

1. Back yard lawn

instruments were installed at M3, and no instruments were installed at P1 or U2. Data collection on buildings at U1 and M3 focussed on mid-roof (5.3 m and 3.6 m, respectively) and mid-wall (2.0 m at U1, 1.6 m at M3) levels.

The degree of similarity between data collected in the model and at equivalent full-scale sites is assessed using mean ($\overline{m}$, $\overline{h}$) and standard deviation

(SD_m, SD_h) values, and by computing the mean absolute (MD) and root mean square (RMSD) difference for the data-sets (Section A1.5; Willmott, 1984).

(a) Surface moisture

Methods used at U1 were wetness sensors (roof and lawn), mini-lysimeters (roof and lawn) and blotting on grass (see Section 3.2.2). At dawn on selected days moisture samples were collected at 1 m intervals along a central transect on the

Table 5.4 Instruments and methods to collect data to validate the model.

Parameter	*Method*	*Location*
U1		
• *Temperature conditions*		
Roof	Thermocouple (30 AWG, Cu-Con)	5.3 m
Grass canopy	*Everest Interscience* thermometer	lawn
Built and vegetation surfaces[1]	Hand-held infrared thermometer	
• *Surface moisture:*	See Table 3.1	
• *Ambient conditions*:	See Table 3.1	
M3		
• *Surface conditions*		
Wetness duration	Electronic wetness sensor	roof (3.6 m)
Surface temperature	Thermocouple (30 AWG, Cu-Con)	roof, wall
• *Ambient conditions*[2]		
Wind speed-direction	*Young* Wind Sentry anemometer/vane	3.6 m
Humidity-air temperature	*Vaisala* HMP35C in *Young* shield	3.6 m
P1		
Surface moisture at dawn	Blotting	park
U2		
Surface moisture at dawn	Blotting	lawn

1. *Minolta Cyclops* thermometer (see Table 5.2); 2. UBC (also see Table 3.1).

backyard lawn, using pads of blotting paper 0.20 x 0.20 m. At M3 only wetness duration was measured, using sensors placed on the roof at mid-roof level. At P1 and U2 surface moisture was blotted from wet grass at dawn on several occasions along a linear transect, at points with contrasting Ψ_{sky} (Chapter 3).

(b) Surface temperature

Surface temperatures were measured at U1 using three methods: thermocouples on the north- and south-facing roof surfaces (five on each facet, attached in a circle of radius = 0.28 m); an infrared thermometer angled downward at 45° over the backyard lawn; and surveys undertaken at dawn using a hand-held infrared thermometer. On YD 164/165, the latter observations were repeated over a 24 hour period, to coincide with analogous ones made at M1.

At M3 three methods were used: thermocouples on west- and east-facing roof surfaces at mid-roof level (five per facet, attached in a circle of radius = 0.28 m); thermocouples attached to the south-, west- and east-facing walls at mid-wall level; and for the north-facing wall, the internal (reference) thermometer of a *Campbell Scientific* data logger which was mounted on that wall. For the latter, data were offset by -1.0 h and -0.66°C to compensate for differences in thermal lag and minimum nocturnal temperature; these were observed during a calibration period, when a thermocouple was attached to the north-facing wall.

(c) Ambient conditions

At U1 and M3, ambient conditions were monitored at mid-roof level to characterise the nature of the air mass at this level (as done for the scale model at M1). At U1 wind speed and direction, air temperature and relative humidity were measured at 5.3 m on a pneumatic tower installed in the backyard of the lot. At M3 equivalent instruments were mounted at 3.6 m on the UBC AES tower, about 70 m to the south-west of M3. Additional environmental data were also gathered at U1 and UBC (see Table 3.1).

PART III MODELLING

Chapter 6: Validation and results of the scale model

6.1 Overview

This chapter addresses: (a) validation of the hardware model, and (b) presentation and discussion of the results obtained using the scale model. The validation study consists of a comparison between surface temperature and moisture observations from the model and full-scale sites in Vancouver. The model does not attempt to simulate an exact location so one-to-one similitude of an environment is not expected. Rather, a general comparison is undertaken to assess whether aspects of the model behave qualitatively and quantitatively in a 'realistic' manner. That is, the validation question is: are surface conditions of component surfaces (roof, walls, grass, leaves, pavement) in the model similar to those seen at the full-scale, and do the component surfaces relate to each other similarly at both scales? If they behave similarly, generalisations drawn from the model are potentially transferrable and, hence, able to provide insight into processes of dew formation at the full-scale.

The results of the modelling programme are organised around features of particular interest and elaborated using examples from individual nights, rather than data averaged over several occasions. This approach is adopted because the events studied are singular. Conditions on any given night are not replicated on any other night and events occupy a continuum rather than clear categories of, for example, dew intensity.

The outcome of the validation exercise is described in Section 6.2; results from the model are discussed in Section 6.3; and findings are summarised in Section 6.4.

6.2 Validation

6.2.1 Physical contrasts

The landscape simulated in the model has no exact equivalent at the full-scale but approximate equivalents exist for each of its key structural elements, i.e., park, street, building and lawn. Validation is thus provided using a composite comprising of selected data from an urban park (P1), a street with trees (U1), two buildings with simple geometry (U1 and M3), and two residential lawns (U1 and U2).

The degree of geometric similarity between the model and full-scale landscapes can be illustrated using sky view factor information from fish-eye lens photographs and site geometry. Figure 6.1 shows fish-eye lens images from which Ψ_{sky} values were derived, i.e., at the south edge of the model park (Figure 5.5) and the centre of the full-scale park at P1 (Figure 3.21). There is relatively good agreement between values for the most open site in the model park ($\Psi_{sky} = 0.98$) and a full-scale park (P1; $\Psi_{sky} = 0.93$). Similarly, Figure 6.2 illustrates the close similarity between the model ($\Psi_{sky} = 0.74$) and full-scale (U1; $\Psi_{sky} = 0.72$) street-with-trees environments. The images are for the centre of the model street (Figure 5.5) and the north side of the street at U1 (Figure 3.4). Even the extent of horizon obstruction due to a single tree or house is remarkably similar for the full-scale and scaled sites.

(a)

(b)

Figure 6.1 Fish-eye lens photographs looking up at the sky zenith from the surface of the (a) scale model park (M1) and (b) full-scale park at P1 (see text for associated Ψ_{sky}).

(a)

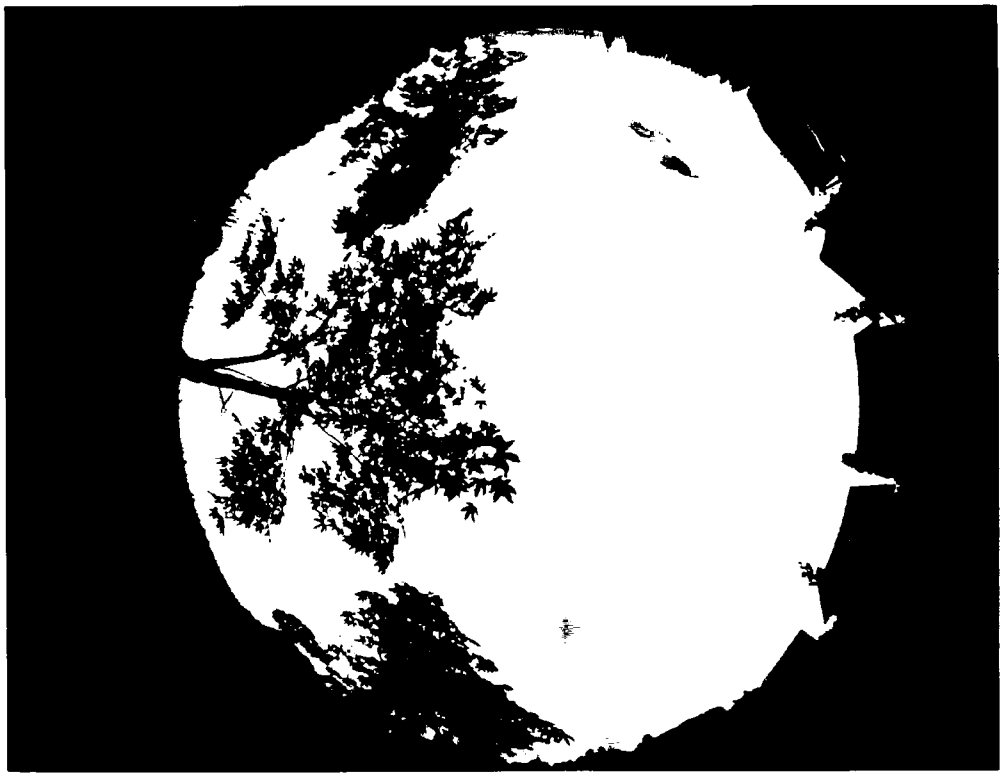

(b)

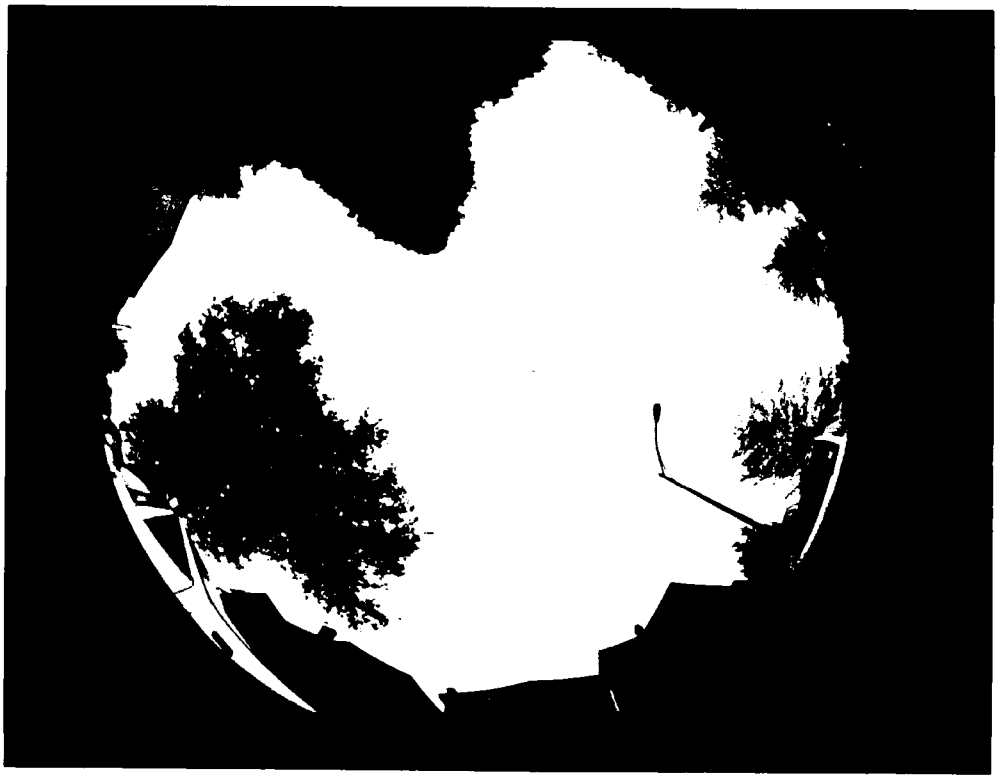

Figure 6.2 Fish-eye lens photographs as in Figure 6.1, but for the (a) model and (b) full-scale street with trees at U1 (see text for Ψ_{sky} values). Note the close agreement between the horizon obstruction due to the model and full-scale trees and houses.

The agreement is less close for the model and full-scale lawns because the geometry of their surroundings (local horizons) differs. The model lawn is bounded by houses and trees on two sides, but horizon obstruction to the east and west are largely absent (Figure 5.4). This means the model lawn has relatively larger Ψ_{sky} values. When street trees are present in the model, Ψ_{sky} values along the transect which is shown in Figure 5.5 range from 0.49 next to the house wall, to 0.89 at the centre of the model lawn, and 0.87 at its south edge. When trees are absent, these values increase to 0.50, 0.92 and 0.96, respectively. In contrast, the full-scale lawns at U1 and U2 are enclosed on four sides by trees, fences and/or buildings (Figure 3.23). This gives lower Ψ_{sky} values, i.e., for the transects shown in Figure 3.23, 0.22–0.66 at U1 and 0.28–0.55 at U2.

The structural details of individual scaled and full-scale elements are summarised in Tables 5.1 and 5.3, respectively. There is general similarity between the elements but physical correspondence is not exact. For example, the buildings studied (M1, M3 and U1) all have simple form, wooden framing and an asphalt shingle roof. However, the type of siding (wood, stucco) and its colour (off-white, green), and roof pitch (35°, 45°), colour (brown, black) and orientation (east-west, north-south) were different.

These differences have potentially important implications for the temperature and energy balances of the surfaces. By day, surface temperature is strongly controlled by local shading regimes and the intrinsic radiative and thermal characteristics of the materials. So, for example, east-facing surfaces may be warmest during morning when they are in full-sun, but the timing and magnitude of

actual temperatures vary from site to site. Residual effects of differences in shortwave radiation loading (e.g., due to the slope, aspect and albedo of surfaces) during the daytime may also be evident during early evening. Especially at night, differences in sources of sensible heat (ΔQ_S, Q_G and Q_F) and of longwave radiation exchange with surrounding objects become important. Further, since the model and full-scale sites are at different locations (Figure 5.3), ambient weather conditions (air temperature, humidity and wind speed) cannot be expected to be the same for otherwise equivalent surfaces.

These physical differences between the sites contributes to increased scatter and the possibility of an absolute offset when model and full-scale data are compared. Nevertheless, there is sufficient similarity between sites to assert that the hardware model can be validated to a first approximation.

6.2.2 Model: full-scale comparisons

(a) Nocturnal ambient conditions

Ambient conditions in the model (M1) and full-scale sites (M3 and U1) are compared using synchronous data collected during four nights in 1996. The nights are selected to provide a range of surface moisture and weather conditions. As summarised in Table 6.1, both YD 171/172 and 187/188 have clear skies and light winds—giving Φ_w values of $\geq$0.82 (Chapter 3)—and moderate amounts of surface moisture (0.08 mm per night), as measured by blotting at dawn at P1. In contrast, YD 173/174 and 191/192 have windy and/or cloudy conditions, $\Phi_w \leq$0.51, and little surface moisture accumulation ($\leq$0.03 mm per night).

Table 6.1 Summary of average characteristic weather conditions on four nights in 1996.

YD	Wind conditions at 10 m[1]		Cloud conditions[2]		Φ_w[1,2]	Surface moisture[3]
	Speed ($m\ s^{-1}$)	Direction	Cover	Height		(mm)
171/172	1.0	NE	0.0	-	1.00	0.08
173/174	3.5	E	0.2	mid	0.51	0.01
187/188	1.5	NE	0.0	-	0.82	0.08
191/192	2.0	E	0.8	low	0.31	0.03

Source: 1. UBC; 2. VIA; and 3. P2 (=M1).

When compared (Table 6.2), results show that nocturnal air temperature data (15 min averages) at M1 are similar to those observed at M3 (0.2 km distant) and U1 (8 km distant) on the same night (Figure 6.3):

- there is close similarity between the air temperature measured at roof/tree height in the model (M1) (1.5 m) and that measured at mid-roof level at M3 (5.3 m). Comparison of the two data-sets gives MD = 0.2°C and RMSD = 0.3°C,
- air temperature measured at 1.5 m in the model and at mid-roof level at M3 (3.6 m) are similar (MD = 0.4°C; RMSD = 0.7°C),
- the greatest contrast is between data measured at 1.5 m at both M1 and U1, but even then differences are of small absolute magnitude (MD = 0.9°C; RMSD = 1.1°C), and
- the means for the sets are fairly similar, i.e., 14.0, 14.1, 13.2–13.9°C for M1, M3 and U1, respectively.

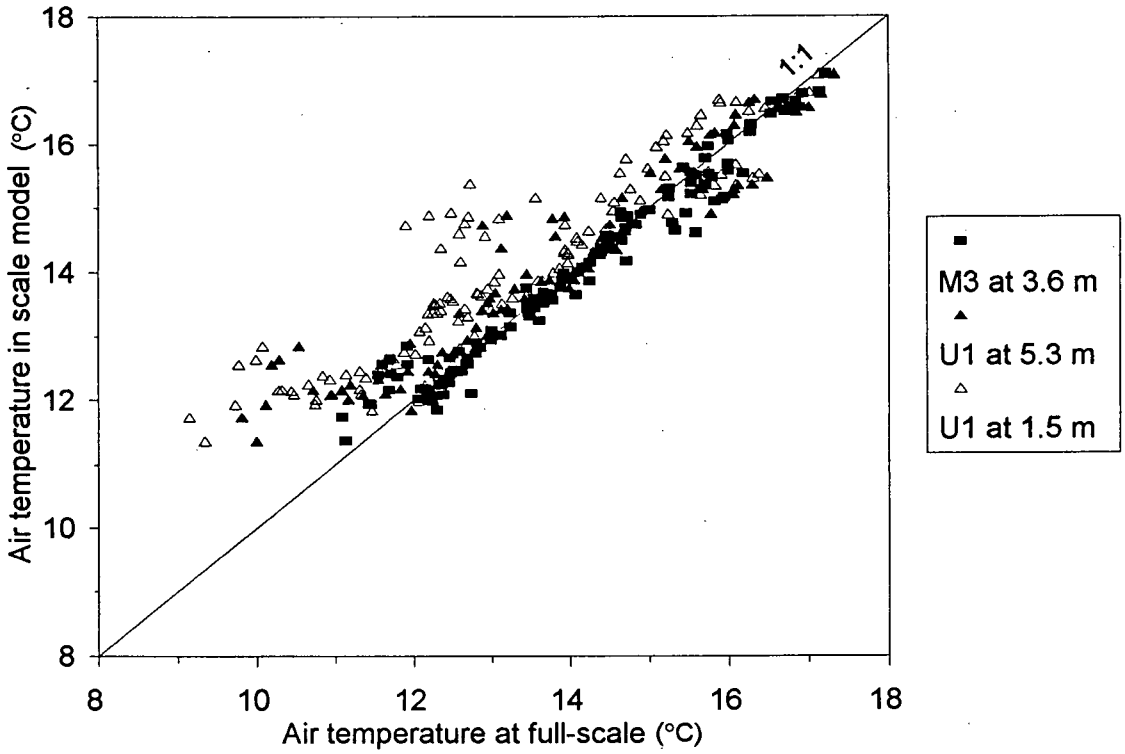

Figure 6.3 Agreement between the observed air temperature measured at 1.5 m in the scale model (M1) and air temperature measured at M3 (mid-roof level, 3.6 m) and U1 (mid-roof level (5.3 m) and 1.5 m height).

Table 6.2 Summary of statistical indices used to test the similarity in ambient weather conditions between the model (M1) and full-scale sites (M3 and U1). .

		Scale model		Full-scale			
	n (d)	*Mean*	*SD*	*Mean*	*SD*	*MAD*	*RMSD*
•*Air temperature (°C)*							
$M1_{1.5}$ *vs* $M3_{3.6}$*	4	14.0	1.5	14.1	1.6	0.2	0.3
$M1_{1.5}$ *vs* $U1_{5.3}$	4	14.0	1.5	13.9	1.8	0.4	0.7
$M1_{1.5}$ *vs* $U1_{1.5}$	4	14.0	1.5	13.2	1.9	0.9	1.1
•*Vapour density (g m^{-3})*							
$M1_{1.5}$ *vs* $M3_{3.6}$	4	9.2	0.6	9.3	0.6	0.1	0.2
$M1_{1.5}$ *vs* $U1_{5.3}$	4	9.2	0.6	9.1	0.7	0.3	0.6
$M1_{1.5}$ *vs* $U1_{1.5}$	4	9.2	0.6	9.0	0.6	0.4	0.6
•*Wind speed (m s^{-1})*							
$M1_{1.5}$ *vs* $M3_{3.6}$	4	1.0	0.7	1.6	1.1	0.6	0.7
$M1_{1.5}$ *vs* $U1_{5.3}$	4	1.0	0.7	0.8	0.7	0.6	0.8
•*Wind direction (°)*							
$M1_{1.5}$ *vs* $U1_{5.3}$	4	120	68	161	89	47	97

* Subscripts indicate height of measurement (m).

Similarly, Figure 6.4 shows that vapour density is also fairly similar at the three sites:

- nocturnal vapour density measured in the model (at 1.5 m height) is most similar to that measured at mid-roof level (3.6 m) at M3 (MD = 0.1 g m^{-3}; RMSD = 0.2 g m^{-3}),
- more scatter is present when data from the model are compared to data measured at U1 (MD = 0.3–0.4 g m^{-3} and RMSD = 0.6 g m^{-3}), but
- the three data-sets show a similar central tendency. Mean values are close, i.e., 9.2, 9.3 and 9.0–9.1 g m^{-3} for M1, M3 and U1, respectively (Table 6.2).

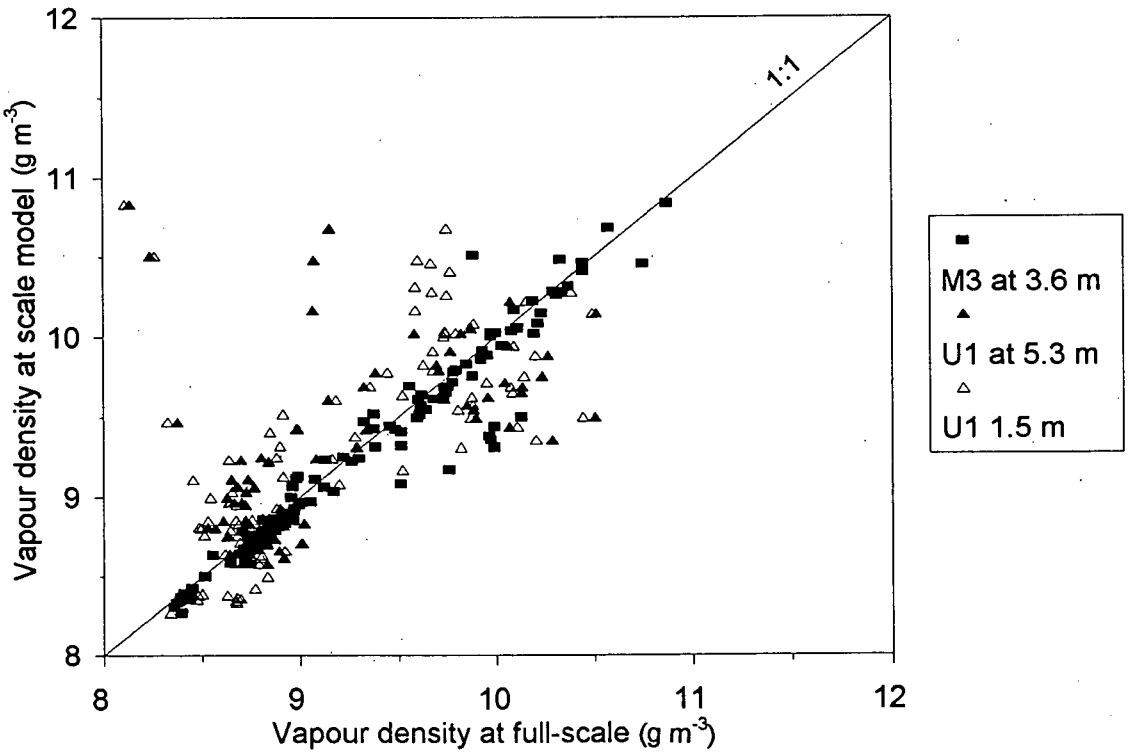

Figure 6.4 As for Figure 6.3, but for vapour density.

Strong contrasts are seen when nocturnal wind speed data are compared (Figure 6.5a):

- when winds are light, wind speed is small at all locations, but
- when winds are stronger, the wind speed at M1 measured at roof/tree level (1.5 m) is about 67% (u_{M1}:$u_{M3} \approx 0.67$) of that observed at mid-roof level (3.6 m) at M3. Since M1 and M3 are at the same location (see Figure 5.3) it is possible to predict that in neutral stability the ratio u_{M1}:u_{M3} is about 0.85 due to height differences (see Section A1.7 for the derivation of this value). In stable conditions the ratio should be smaller and this is in agreement with the observations, and
- wind speed at M1 (1.5 m) is about 330% of that measured at U1 at mid-roof level (5.3 m) when winds are moderately strong. The much larger ratio u_{M1}:u_{U1} is not easily predictable since not only is the roughness length of U1 greater it also needs a zero-plane displacement. The easterly flow at U1 is over tens of kilometers of rough urban terrain, whereas much of the terrain immediately to the east of M1 is relatively smooth car parks and sport fields.

Several features of interest are evident when wind direction at M1 and U1 are compared (Figure 6.5b):

- at night, on the four nights studied, winds at M1 are almost uni-directional, i.e., most are from the east (centred on 90°) quadrant,
- wind direction at U1 is more variable but is often from the east (90°) or north-west (315°) quadrant, and

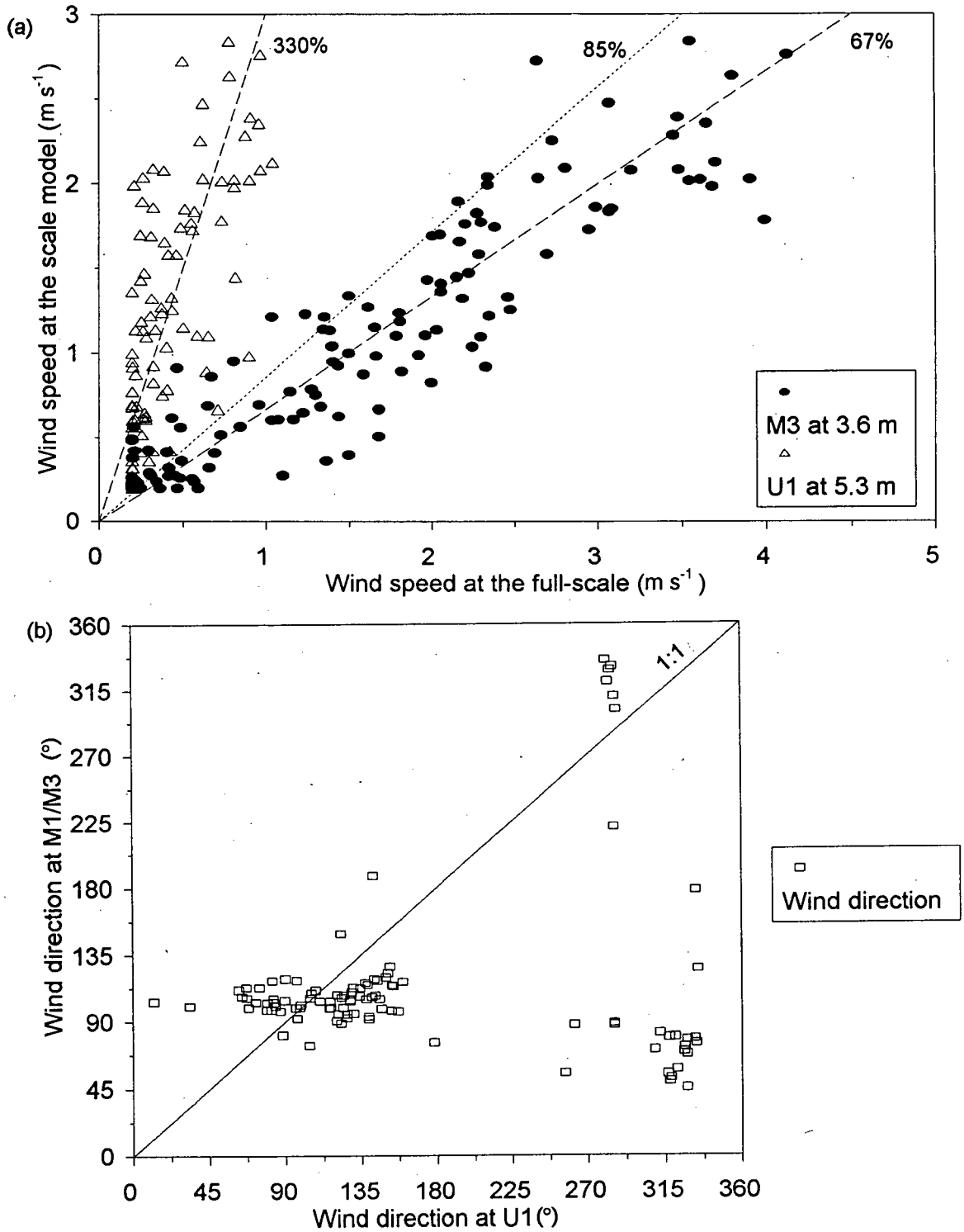

Figure 6.5 Comparison between wind conditions at full-scale and scaled sites. (a) Wind speed measured at 1.5 m in the model (M1) and at mid-roof level at M3 (3.6 m) and U1 (5.3 m), and (b) wind direction measured at the Fairground site and U1. Percentage lines are derived from ratios of wind speed at model *vs* full scale locations (see text for details).

on a few occasions during four the nights studied, wind direction at both M1 and U1 is from the west/north-west (270°/315°).

The easterly dominance is probably associated with the nocturnal land breeze. The greater variability at U1 is understandable given the presence of large roughness elements (buildings and trees) and the fact that, in light wind conditions, this suburban location may experience urban/country breezes as well as land/sea breezes.

From these comparisons it can be concluded that inter-site air temperature and water vapour differences are relatively small and unsystematic. Therefore, they are not likely to have a significant impact on inter-site surface temperature and surface moisture differences. Dewfall is inhibited by stronger wind speeds (see Figure 1.4). Hence, it is speculated, wind speed differences between M1 and M3 may contribute slightly greater dewfall at M1, whereas those between M1 and U1 may lead to smaller contributions at M1.

(b) Surface temperature

Two types of observation are used when surface temperature data are compared. These are synchronous data consisting of (a) 15 min mean values collected at M1, M3 and U1 using thermocouples attached to surfaces or, for grass, using infrared thermometers, and (b) instantaneous data collected at U1 at dawn using hand-held infrared thermometers. Several of the comparitive exercises involve data from only type (a) sets. These data are not always available. Hence, for certain sites and surfaces instantaneous data from (b) are compared to 15 min mean data from (a). It

is assumed that the two sets are comparable and that differences due to surface conditions exceed those created by differences in measurement techniques.

In general, absolute differences are small when nocturnal surface temperature in the model and at the full-scale are compared (Table 6.3). Data are 15 min mean values measured by thermocouples attached to the north- and south-facing roof facets at M1 and U1, and east- and west-facing facets at M1 and M3. The combination of facets used is dictated by roof orientation at these sites (see Table 5.3):

- there is close agreement between the nocturnal surface temperature of full-scale ($\overline{T} = 10.7$) and model ($\overline{T} = 10.1$) roof facets (Figure 6.6),
- temperatures are the least similar at higher values. These are data gathered in the first few hours (~1.5–2.5 h) after sunset. This is interpreted to be a residual effect created by differences in roof albedo and orientation to the solar beam (Tables 5.1 and 5.3), which lead to different shortwave radiation loading during daytime, and
- observations at U1, where the building is inhabited, suggest that temperature differences related to nocturnal Q_F are insignificant.

This close similarity in nocturnal roof temperature exists despite physical differences in location (Figure 5.3) and measurement height.

On the other hand, the surface temperature of wall surfaces in the model are consistently cooler at night than the walls at full-scale sites (Figures 6.7 and 6.8).

Table 6.3 Summary of statistical indices used to test the similarity in surface temperature conditions between the model (M1) and at full-scale sites (M3 and U1).

		Scale model		**Full-scale**			
	n (d)	*Mean* (°C)	*SD* (°C)	*Mean* (°C)	*SD* (°C)	*MAD* (°C)	*RMSD* (°C)
•*Roof: M1 vs M3* [1]							
west-facing	4	10.6	2.3	11.4	3.0	1.0	1.2
east-facing	4	10.1	2.1	11.3	2.7	1.2	1.5
south-facing	4	9.8	2.2	10.1	2.8	0.8	1.1
north-facing	4	9.9	2.2	9.8	2.7	0.7	0.9
Average		10.1	2.2	10.7	2.8	0.9	1.2
•*Wall: M1 vs M3* [1]							
west-facing	4	11.9	1.8	13.7	2.6	1.8	2.1
east-facing	4	11.8	1.9	14.6	1.8	2.9	3.0
south-facing	4	10.9	2.0	13.5	2.0	2.6	2.7
north-facing	4	11.1	1.9	15.2	2.1	4.2	4.2
Average		11.4	1.9	14.3	2.1	2.9	3.0
•*Wall: M1 vs U1* [2]							
	16	10.7	2.5	12.0	2.3	1.5	1.8
•*Grass: M1 vs U1* [1]							
Park	4	10.0	2.0	10.9	2.0	1.0	1.3
Lawn	4	10.3	1.7	10.9	2.0	0.8	1.1
•*Tree:*							
M1 vs U1 [2]	8	11.1	1.7	10.4	1.9	1.1	1.3
•*Pavement:*							
M1 vs U1 [2]	14	11.7	1.8	15.2	2.3	3.5	4.5

1. Both sets are 15 min mean data measured using thermocouples; and 2. Data from M1 is as for 1, but at U1 data are instantaneous values measured using a hand-held thermometer.

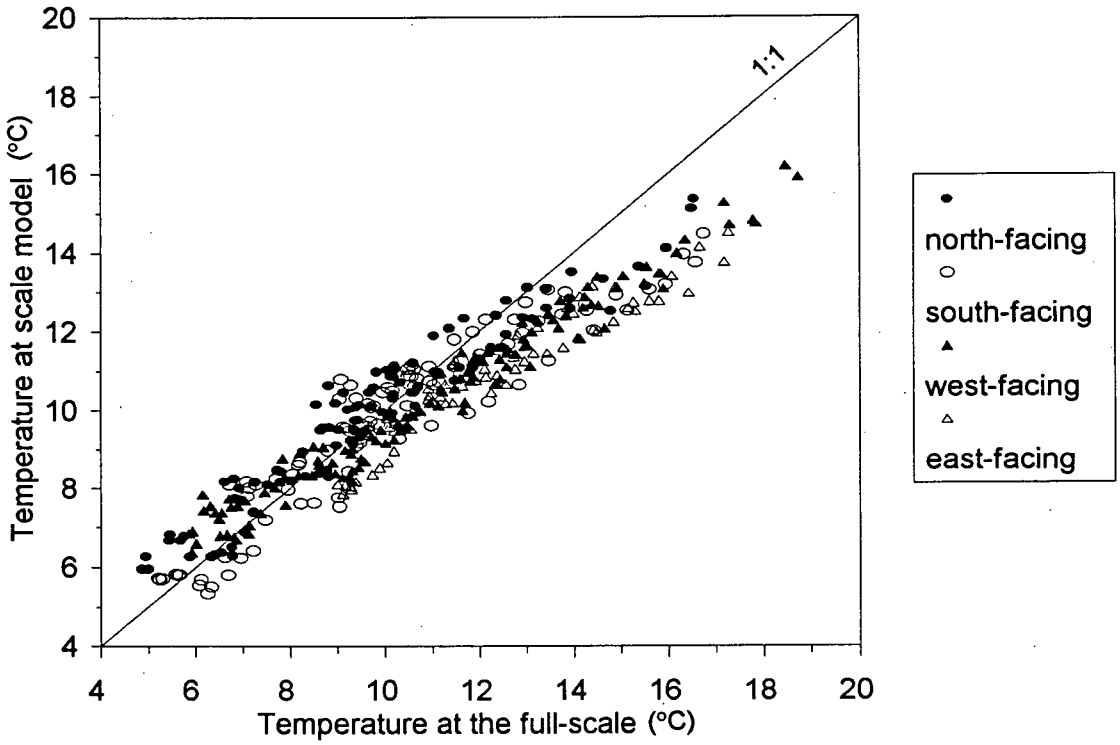

Figure 6.6 Agreement between observed nocturnal surface temperatures of full-scale and scaled roof facets on four nights with contrasting weather in 1996. Data are 15 min mean surface temperature (°C) measured by thermocouple on north- and south-facing facets at M1 and U1, and west- and east-facing facets at M1 and M3.

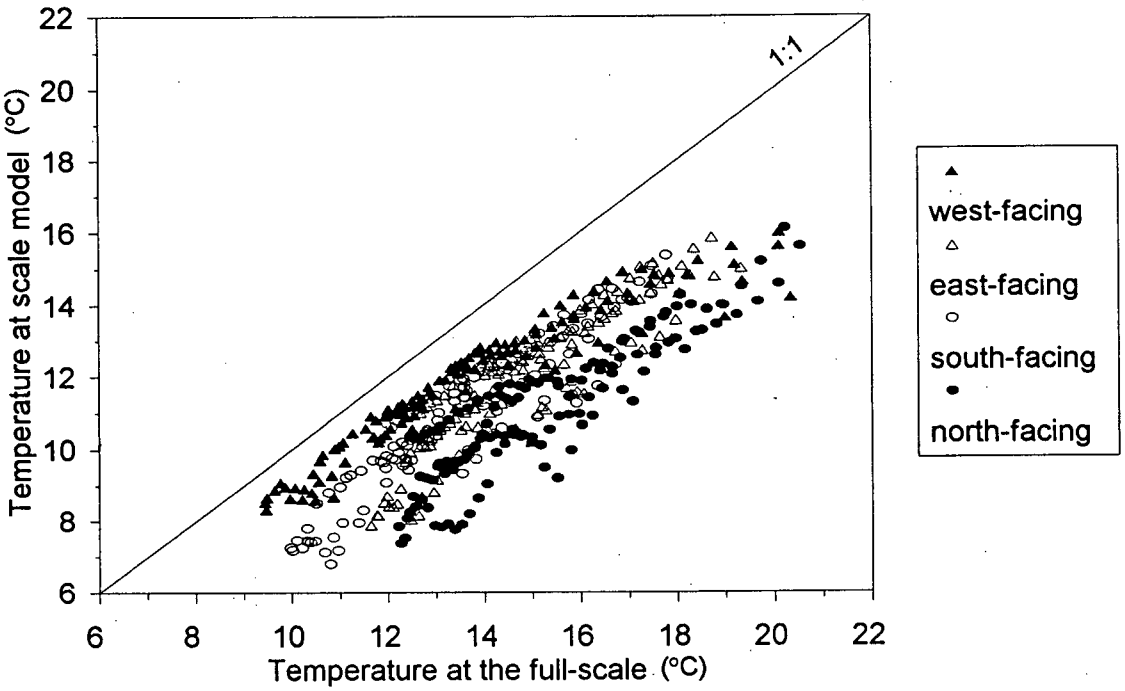

Figure 6.7 Agreement between observed nocturnal surface temperature for full-scale and scaled walls for four nights in 1996. Data are 15 min mean surface temperature (°C) measured by thermocouple for north-, south-, west- and east-facing facets at M1 and M3.

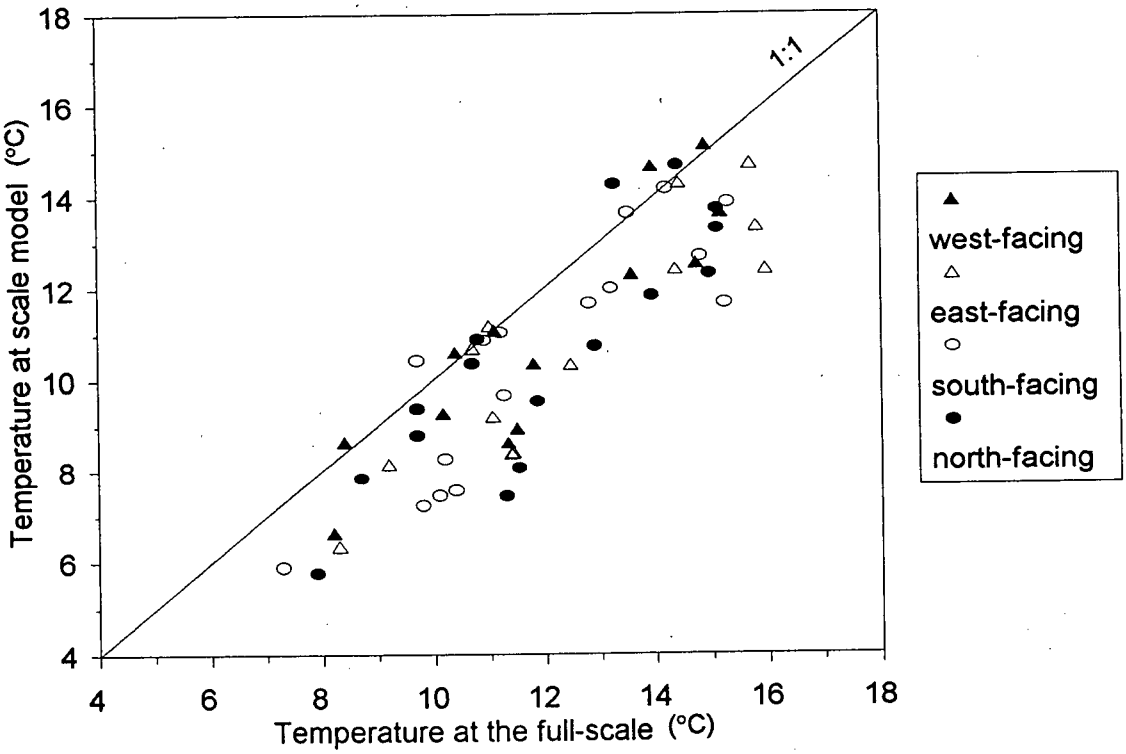

Figure 6.8 Agreement between observed surface temperature at dawn for full-scale and scaled walls for 16 nights in 1996. Data are surface temperature (°C) measured using a hand-held infrared thermometer at U1 and at M1 thermocouples attached to the north-, south-, west- and east-facing walls of the central house in the model.

For convenience, data are stratified according to wall orientation:

- on the four nights studied, data collected using thermocouples show that the model walls ($\overline{T} = 11.4$) are always cooler than the full-scale walls at M3 ($\overline{T} = 14.3$) (Figure 6.7). The differences are ordered: closest west-facing (~2°C), south-facing, east-facing, least similar north-facing (~4°C). This order is the reverse of the order of irradiation through the day,
- a small residual effect, similar to that seen for roofs, appears to be present in Figure 6.7 in the early evening, especially for the west-facing wall. This is attributed to the fact that the west-facing wall in the model is in shadow at dusk, whereas that at M3 is in full sun,
- model walls tend to be cooler than those at U1 (Figure 6.8). However, the differences are smaller (<2°C) than with M3 and there is no obvious ordering of wall differences, and
- there is no evidence to suggest that Q_F greatly affects wall temperature at dawn at U1.

Model: full-scale wall temperatures are systematically different. Some of this seems to be linked to contrasts in site configuration. For example, the north-facing wall at M3—which is relatively warm—is close to another building, whereas the north-facing wall in the model is openly exposed. Part of these differences relate to real differences in siding materials and, again, surface albedo.

Data for full-scale and scaled lawns, tree canopies and pavement were also compared using 15 min and/or instantaneous data:

- on average, grassed surfaces in the model are cooler at night than the lawn at U1 ($\overline{T} = 10.9°C$) (Figure 6.9). This is true for data from both the model park ($\overline{T} = 10.0°C$) and lawn ($\overline{T} = 10.3°C$) (Table 6.3). The difference is attributed to the greater sky view and, therefore, increased longwave radiative cooling at M1 compared to U1. There is also a location effect present because the UCL UHI will tend to be better developed at the more built-up site, which is U1,
- at dawn the trees in the model ($\overline{T} = 11.1°C$) tend to be slightly warmer than those at U1 ($\overline{T} = 10.4°C$) (Figure 6.10 and Table 6.3). There is no strong difference between the deciduous and coniferous trees, and
- on all occasions at dawn the model pavement ($\overline{T} = 11.7°C$) is considerably cooler than the full-scale pavement at U1 ($\overline{T} = 15.2°C$). The offset is about 4°C (MD = 3.5°C, RMSD = 4.5°C) but the difference is non-critical because observations show that neither the model nor the full-scale pavement cool sufficiently to accumulate dew.

(c) Surface moisture and dewfall

Reasonable agreement is found between moisture accumulation in the model and at the full-scale (Table 6.4):

- spatial patterns of surface moisture (dew + guttation) measured by blotting on grass agree with observations made at the full-scale at P1 and U2 (Chapter 3). Spatial patterns which are seen in the scale model (such as in Figures 6.16–6.17) bear strong resemblance to those at the full-scale, for example

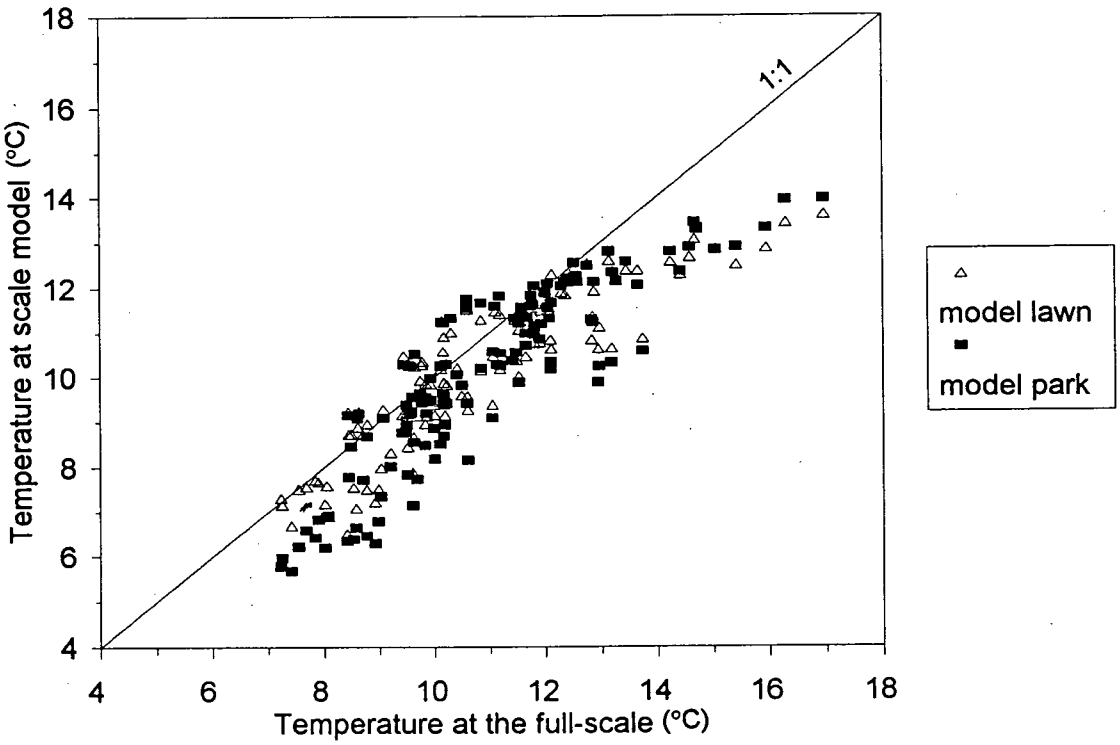

Figure 6.9 Agreement between observed nocturnal surface temperature for grassed surfaces at full-scale and scaled sites for four nights in 1996. Data are surface temperature (°C) measured synchronously using *Everest* infrared thermometers mounted over the model park and lawn at U1.

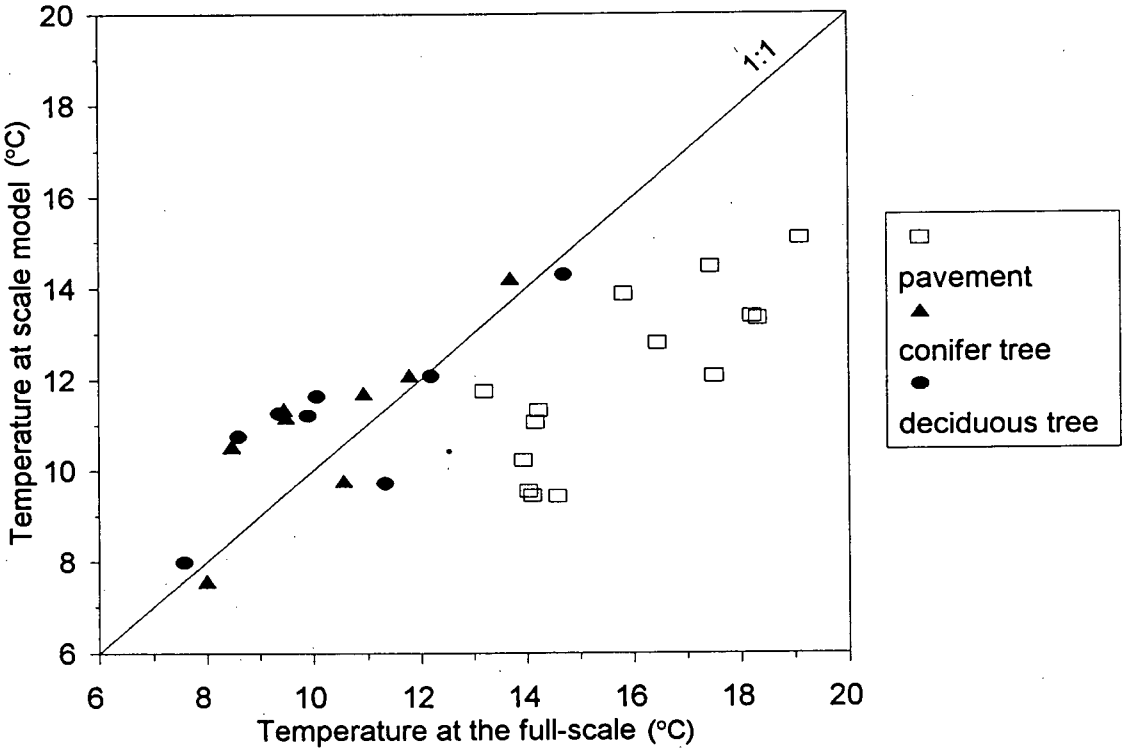

Figure 6.10 Agreement between surface temperature at dawn for deciduous and conifer trees, and pavement in the model and at U1, for 8 and 14 nights in 1996, respectively.

Table 6.4 Summary of statistical indices used to test the similarity in surface moisture conditions between the model (M1) and at the full-scale site at U1.

		Scale model		**Full-scale**			
	n	*Mean*	*SD*	*Mean*	*SD*	*MD*	*RMSD*
•*Surface moisture (mm per night)*							
Grass: M1 *vs* U1[1]	18	0.05	0.03	0.03	0.03	0.03	0.04
•*Dewfall (mm per night)*							
Grass: M1 *vs* U1[1]	14	0.05	0.04	0.07	0.05	0.05	0.06
Roof: M1 *vs* U1	15	0.10	0.06	0.13	0.04	0.03	0.04

1. Open park at M1 (Ψ_{sky} = 0.98) and back yard at U1 (Ψ_{sky} = 0.57).

in Figures 3.28–3.29, but absolute dimensions and amounts differ. In general, more dew is seen at open sites and less close to trees and buildings where sky view is reduced, and

- on any particular night, synchronous measurements at M1 and U1 show that the amount of surface moisture on grass in the model park (Ψ_{sky} = 0.98) at dawn tends to be greater than that seen on the back yard lawn at U1 (Ψ_{sky} = 0.57) (Figure 6.11). However, the average difference between the sets is relatively small (MD = 0.03 mm; RMSD = 0.04 mm).

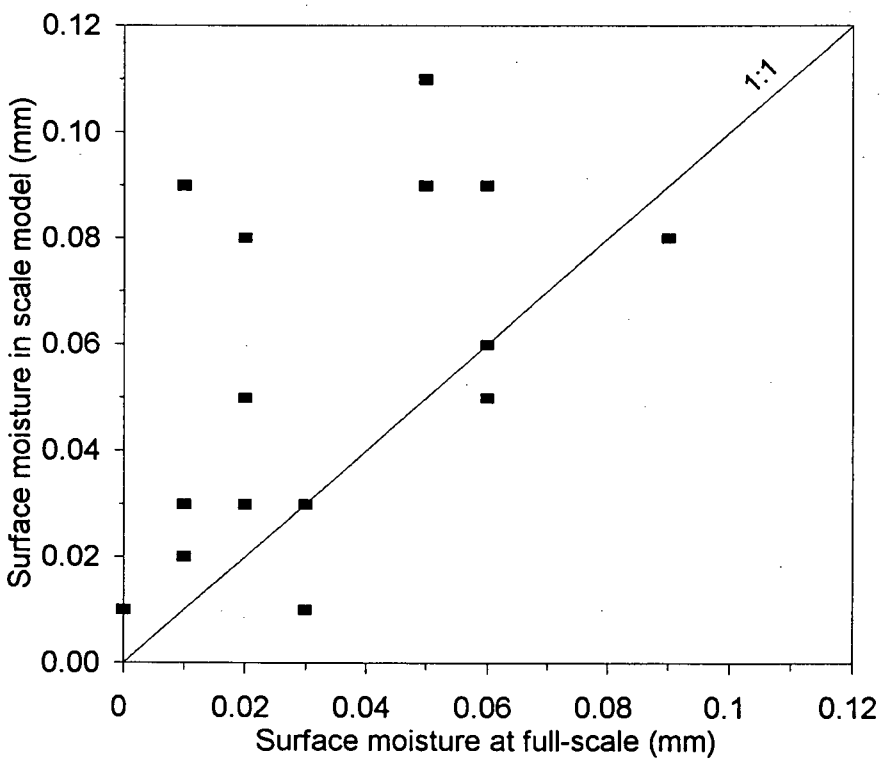

Figure 6.11 Agreement between the observed nocturnal amount of surface moisture accumulated on grass at the full-scale and model sites, for 18 nights in 1996. Data are the maximum amount (mm) measured by blotting at dawn at M1 and U1.

When dewfall data measured using mini-lysimeters are compared:

- on most nights, dewfall on the model lawn ($\overline{E}$ = 0.05 mm) is generally less than that on the lawn at U1 ($\overline{E}$ = 0.07 mm), and
- on most nights, there is remarkably close agreement between the amount of dewfall on the model roof at M1 ($\overline{E}$ = 0.10 mm) and the full-scale roof at U1 ($\overline{E}$ = 0.13 mm), but the full-scale roof tends to accumulates more water when dewfall at the model is <0.05 mm per night (Figure 6.12).

(d) Validation summary

On the whole, ambient conditions at the site of the model (M1) and at M3 and U1 are fairly similar:

- air temperature at the model site measured at 1.5 m tends to be slightly greater than values measured at the same height in the back yard at U1, but air temperature and humidity values at roof-level are remarkably close,
- surface temperatures of roofs, walls and pavement in the model (M1) tend to be less than those seen at the full-scale. The exception is, perhaps, tree canopies which are slightly warmer in the model than at the full-scale. These differences may contribute to a slight enhancement of dew deposition on the model roof, walls and paving, and a slight reduction on trees,
- the greatest difference in model: full-scale temperatures are with the walls and pavement and, since neither cool sufficiently to accumulate dewfall, the effect is of little significance in the present study, and

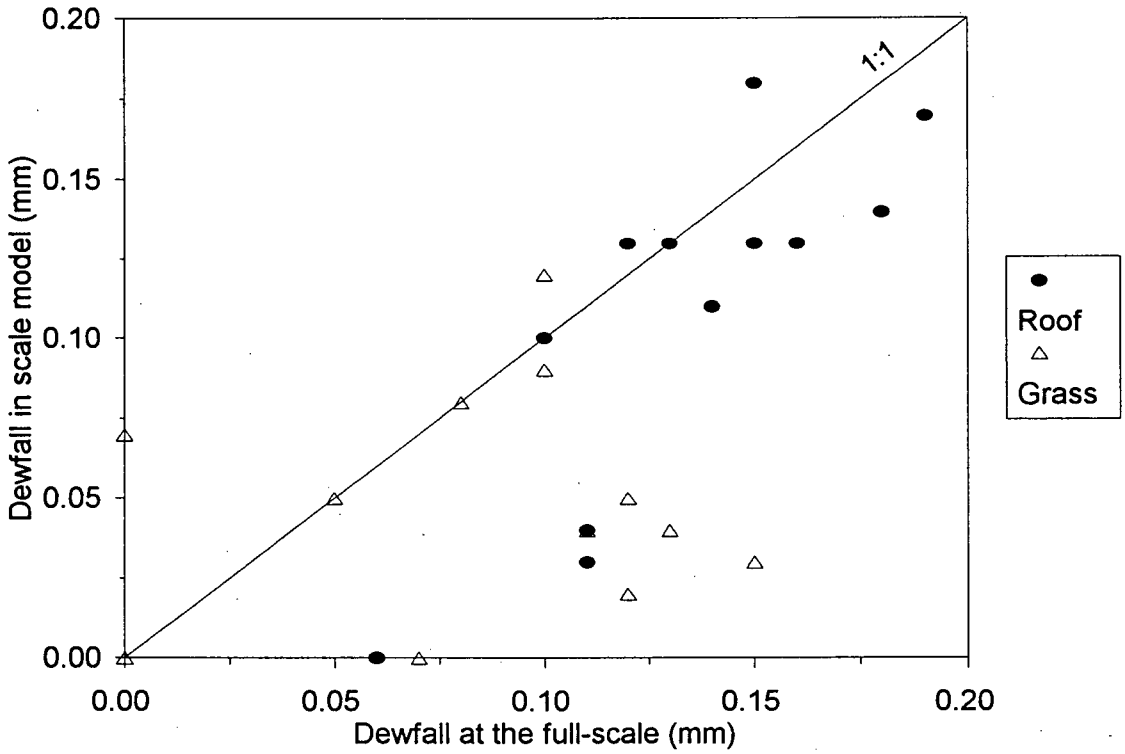

Figure 6.12 Agreement between the observed amount of dewfall measured by mini-lysimeters in the model and at the full-scale during the summer of 1996. Two comparisons are made: firstly, dewfall for the roof at M1 and U1(15 nights), and secondly, dewfall for the most open locations at M1 (park) and U1 (centre of lawn) (14 nights). Data are the maximum accumulated dewfall per night (mm).

- grassed surfaces in the model tend to accumulate greater amounts of surface moisture but less dewfall compared to the lawn at U1. The model roof, on the other hand, accumulates similar, or slightly greater amounts of dewfall than the roof at U1.

As stated, this validation procedure did not seek to find a one-to-one correlation between these data. The relatively close similarity which is seen is therefore encouraging. The absolute differences are small and probably explicable in terms of the physical differences which exist between the full-scale and scaled sites. Hence, it is concluded that the surface conditions in the scale model are 'realistic' and, therefore, the model can be used to gain insight into the patterns and relative magnitudes of surface moisture and dewfall in urban environments.

6.3 Results of the scale model

The following discussion focuses on the primary modelling season conducted at M1 during 1996. Some findings are presented from the 1994 trial at M2 to illustrate a particular feature of interest. These 1994 instances are noted, otherwise data are from 1996. The observations include selected aspects of temporal (mostly daily) and spatial variations of: surface temperature, surface moisture (dewfall + distillation + guttation) measured by blotting, and dewfall measured by mini-lysimetry.

6.3.1 Surface temperature in the model

(a) Variation in surface temperature of the substrate at dawn

Day-to-day variations in the surface temperature of scale model components observed at dawn are: wall surface temperature ~6°C to ~15°C (Figure 6.8), tree foliage ~7°C to ~14°C (Figure 6.10), pavement from ~9°C to ~15°C (Figure 6.10) and roof from ~6°C to ~14°C (not shown).

At open sites with large Ψ_{sky}, surface temperature varies depending on the intrinsic thermal and radiative characteristics of surfaces and whether they are isolated from significant sources of sensible heat (Q_G). In the model at M1, only the model park has Ψ_{sky} approaching unity. However, each of the elemental surfaces (roof, paving, tree, grass) has areas with $\Psi_{sky} \geq 0.70$. The most open areas for these are: the model roof, upper canopy of the central maple tree, the grass of the open park, and the model pavement when trees are absent (Table 6.5). These surfaces are assumed to have sufficiently small horizon obstruction that they are 'open' and therefore comparable.

Temperature contrasts in the model at dawn are greater when the prevailing weather conditions (expressed as Φ_w) favour radiative cooling. Weather conditions for nights used in the following discussion are summarised in Table 6.6 (for clarity, certain data from Table 6.1 are repeated). Observations on high Φ_w nights show that:

- on YD 171/172, 1996 (Φ_w = 1.00), the coldest sites are the grass of the model park (5.7°C) and the roof (6.3°C) (Table 6.5),

- similarly, on YD 187/188, 1996 (Φ_w = 0.82), with no trees in the model, the coolest surfaces are again the grass (6.0°C) and roof (6.7°C). Both the shingle roof and the grass canopy are physically separated from potential sources of sensible heat (Q_G), i.e., the ground and house interior, respectively, and on YD 187/188 when trees are absent the model pavement is warm (8.9°C). This is because the concrete has a relatively large heat storage capacity and is in direct contact with the ground heat source, and
- leaves on the upper surface of the maple canopy are 2.5 to 3 degrees warmer than the roof and grass on YD 171/172 (Table 6.5).

Theory dictates that convective sensible heat transfer from the air to a leaf, and *vice versa*, increases with increased wind speed and decreased leaf size (the relationship is formalised in Equation 7.14 as part of the numerical model in Chapter 7). In practice this means that nocturnal leaf temperature is closer to air temperature—that is, warmer—at sites with greater wind speed. This applies to the maple canopy (1.5 m in height), whereas at grass-level wind speed is close to zero and convective heat transfer is inhibited. At grass-level, therefore, the radiative heat loss from the blades is not offset by convective warming. Hence they are typically colder.

On nights with greater wind speeds and smaller Φ_w, temperatures across the model are closer to air temperature (Table 6.5) but substrate effects are still evident, e.g., at dawn on YD 173/174 and 191/192, 1996, with Φ_w = 0.51 and Φ_w = 0.31, respectively (Table 6.6).

Table 6.5 Apparent surface temperature (°C) observed at dawn in the scale model at M1, showing data for selected sites with relatively open exposure ($\Psi \geq 0.70$). Data are apparent surface temperatures measured using a hand-held *Omega* infrared thermometer (see Table 5.2 for a more detailed description of the instrument).

YD	Substrate temperature				Air Temperature
	Roof	Paving	Tree leaf	Grassed park	(at 1.5 m)
•*Temperature (°C)*					
171/172[1]	6.3	-	8.7	5.7	11.4
173/174[1]	8.6	-	10.1	8.8	12.0
187/188[2]	6.7	8.9	-	6.0	11.3
191/192[2]	8.6	10.5	-	8.1	12.1
•*Sky view factor*[3]					
Trees in model	~0.70[4]	-	~0.98[4]	0.98	
Trees removed	~0.73[4]	0.96	-	0.98	

1. Trees present in the model; 2. Trees absent; 3. Determined using fish-eye lens photography and/or site geometry; and 4. Approximate value.

Table 6.6 Summary of average weather conditions on selected nights in 1996.

YD	*Wind speed at 10 m*[1] *(m s*$^{-1}$*)*	*Cloud Cover*[2]	*Cloud Height*[2]	ρ_{vd}[1] *(g m*$^{-3}$*)*	Φ_w[1,2]	*Surface moisture*[3] *(mm)*
•*Trees present in model*						
164/165	1.5	0.7	low	2.9	0.46	0.05
171/172	1.0	0.0	-	3.6	1.00	0.08
173/174	3.5	0.2	mid	4.7	0.51	0.01
•*No trees in model*						
187/188	1.5	0.0	-	4.7	0.82	0.08
189/190	0.5	0.1	high	6.8	1.41	0.06
191/192	2.0	0.8	low	4.3	0.31	0.03
193/194	3.5	0.0	-	4.8	0.53	0.03

Source: 1. UBC; 2. VIA; and 3. P2 (=M1).

Thus, overall, the surface temperatures in the model at dawn relative to air temperature for sites with open exposure are ordered: grass and roof surfaces (~3.5–5.5°C below T_a), maple tree leaves, pavement (~1.5–2.5°C below T_a), where the greater value is for nights with high Φ_w and T_a is air temperature measured at 1.5 m.

(b) Variation in grass canopy temperature at dawn

For a given substrate, on nights that favour radiative cooling, spatial patterns of nocturnal temperature appear to be strongly related to site geometry, expressed using sky view factor, Ψ_{sky}. In near-calm air, grass canopy temperature is lowest at sites with open exposure (high Ψ_{sky}) and higher where Ψ_{sky} is relatively low. At greater wind speeds, the maximum observed temperature difference ($\Delta T = T_{Max} - T_{Min}$) across the surface is smaller and patterns related to Ψ_{sky} are less obvious.

These generalisations are illustrated in Figures 6.13 and 6.14. The data are apparent grass canopy temperature measured along the central transect in the model using a hand-held infrared thermometer. On the two nights shown (YD 171/172 and 173/174) trees are present in the model (see Table 6.6 for weather conditions).

On YD 171/172, 1996 ($\Phi_w = 1.00$), temperature variation along the transect is relatively large ($\Delta T = 4.3$°C). Further:

- grass canopy temperature is lowest ($T_{Min} = 5.4$°C) in the model park where $\Psi_{sky} > 0.95$,

- the grass canopy is cool (6.5°C) at the relatively open centre (Ψ_{sky} = 0.89) of the model lawn, and
- the warmest sites, with temperature values of up to 9.7°C, are where Ψ_{sky} is relatively small, i.e., immediately adjacent to wall of the model building (Ψ_{sky} = 0.49) and under the maple trees (Ψ_{sky} = 0.70).

On YD 173/174, 1996 (Φ_w = 0.51; Table 6.6), spatial variations are more muted (ΔT = 1.8°C) but similar patterns related to site geometry are present (Figure 6.13).

When trees are removed from the model the typical shape of the temperature distribution on the grass at dawn is less complicated (Figure 6.14). This is expected because site geometry is simpler. Grass surface temperature patterns observed at dawn on three nights with contrasting weather are shown in Figure 6.14. On YD 187/188, 1996, Φ_w = 0.82 and ΔT is relatively large (4.3°C). Observations show that:

- grass temperature is highest (9.5°C) adjacent to the model building where Ψ_{sky} is reduced (0.50),
- temperature decreases rapidly away from the model wall and reaches a value of 6.5°C at the centre of the model lawn, and
- the lowest temperatures (~6.0°C to 5.2°C) are seen in the open park where Ψ_{sky} is large (>0.95).

On YD 191/192, 1996, Φ_w = 0.31. The shape of the temperature curve is close to that observed on YD 187/188 but its magnitude is less (ΔT = 3.3°C). The

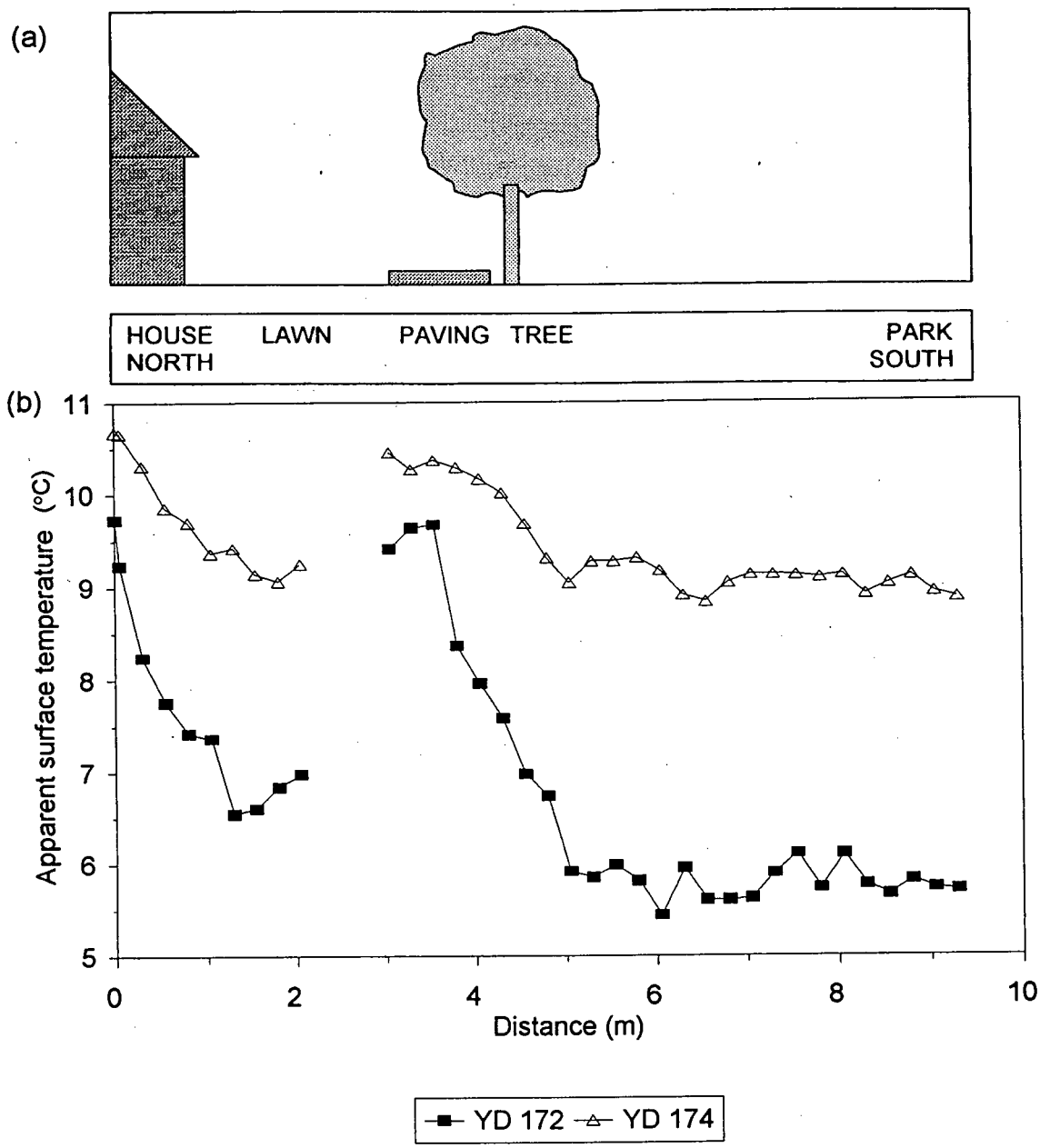

Figure 6.13 Surface temperature (°C) in the model at dawn on two days, both with trees present but contrasting weather: YD 172 (Φ_w = 1.00) and YD 174 (Φ_w = 0.51), 1996. (a) Schematic cross-section of the transect sampled, and (b) spatial trends of surface temperature (°C).

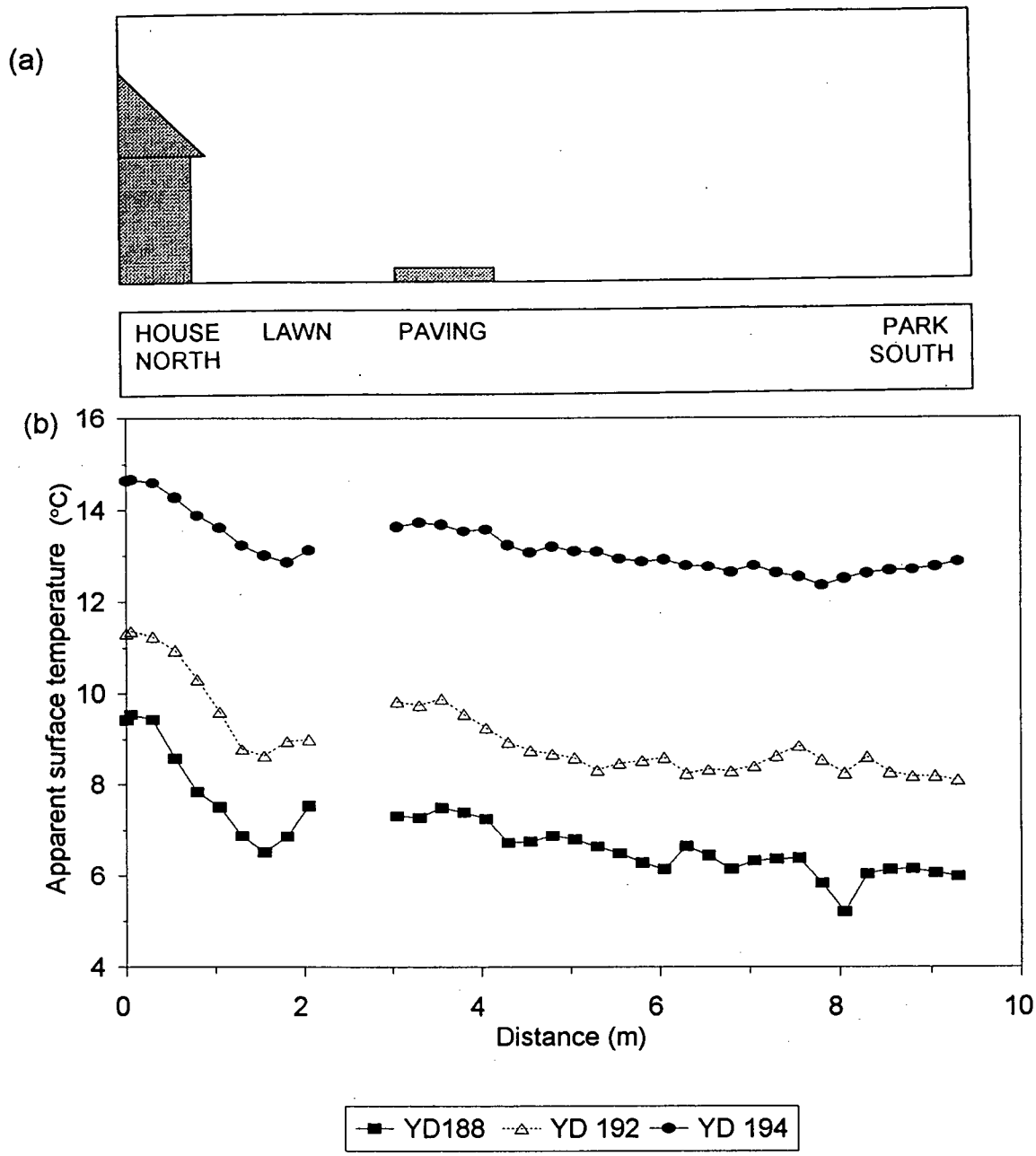

Figure 6.14 Data as in Figure 6.13, but for three days with no model trees: YD 188 (Φ_w = 0.82), 192 (Φ_w = 0.31) and 194 (Φ_w = 0.53), 1996.

homogenising effect of windy weather on surface temperature is even stronger on YD 193/194, 1996, when ΔT is only 2.3°C. On this night, average wind speed at UBC is 3.5 m s^{-1} at 10 m height (the associated Φ_w is high (0.53) because the night is cloudless).

A warm anomaly seems to be present for grass adjacent to the model pavement. The feature is most evident on YD 187/188, 1996, with high Φ_w and no trees in the model (Figure 6.14) but it is also present on nights with relatively low Φ_w values (YD 191/192 and 193/194, 1996). Its presence or absence is masked in Figure 6.13 because its potential location coincides with the higher temperature associated with the presence of street trees. This feature was not observed in site surveys undertaken prior to the installation of the model (Section 5.2.3) and cannot be explained using Ψ_{sky}. It may be a pavement effect created by the lateral transfer of sensible heat (Q_G) from the relatively warm paving to adjacent soil. This may buffer the radiative heat loss of the grass canopy at this location.

6.3.2 Surface moisture and dewfall in the model

(a) Temporal patterns of surface moisture on grass

The amount of water on grass in the model (M1) at dawn was measured by blotting on 22 occasions (Figure 6.15) over a period of about two months. A variety of weather is included but the data-set is biased toward nights with fine weather. Measurements are made at the most open site in the model, i.e., the open park. On

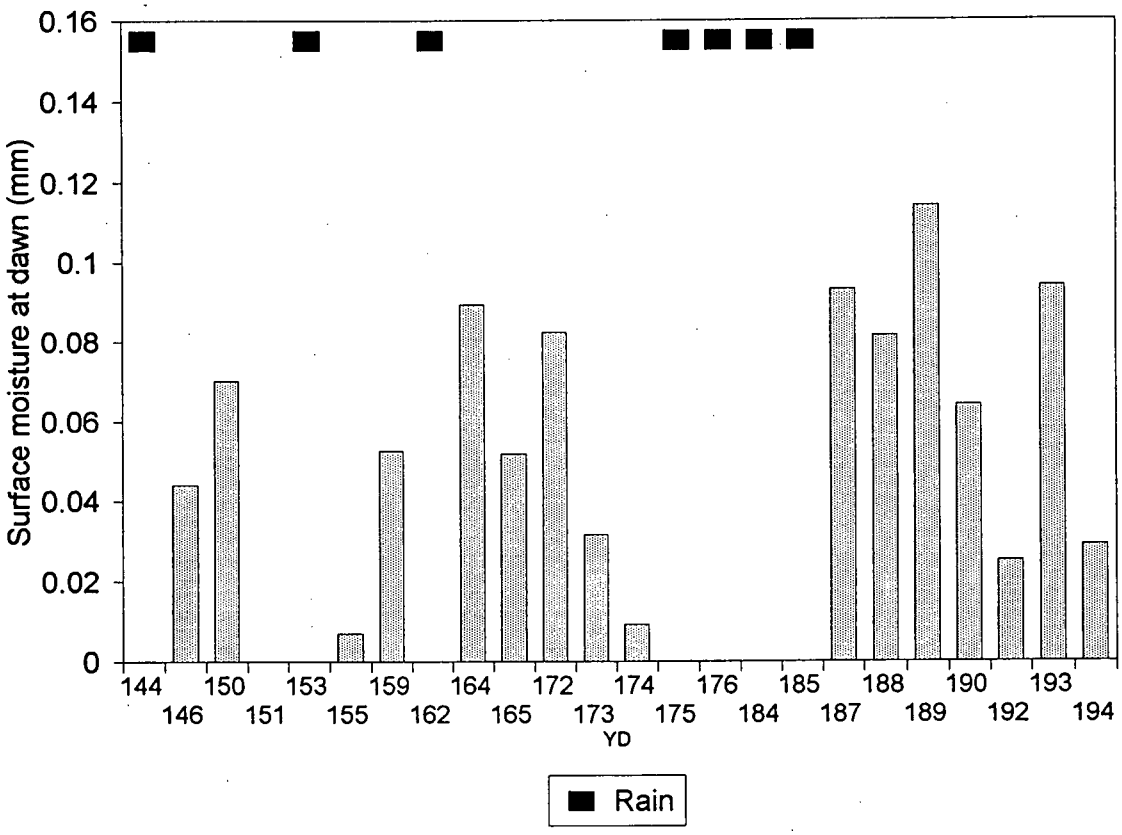

Figure 6.15 Amounts of surface moisture (mm) collected by blotting at dawn at the open model park (M1 which coincides with P2) during the summer of 1996. No bar means zero surface moisture (note that the sequence of days is discontinuous).

most of the days studied (18 nights or 82% of the total) surface moisture is present at dawn (Figure 6.15). The amount typically varies from 0.12–0.13 mm when skies are clear and winds light, to 0.00–0.01 mm per night in windy and/or overcast weather. As shown earlier (Chapter 3), much of the day-to-day variation in surface moisture in the open park at M1 (which coincides with P2; see Chapter 3) seems to be accounted for by Φ_w.

(b) Spatial variation of surface moisture on grass at dawn

Observations such as those presented in Figure 6.16 show that, at open sites in the model with high Ψ_{sky} (>0.95), the amount of surface moisture measured at dawn may vary by up to 0.05 mm over short distances (~1 m). However, a strong central tendancy is present. Standard deviation for such data are ~0.01–0.02 mm, where the higher value is for nights with greater moisture accumulation. A measure of periodicity seems to be present. The feature is also evident at full-scale locations (P1 and U2; Figures 3.28–3.30) and in the model at M2. It seems to be independent of the exact blotting method used, and it is difficult to suggest a cause with any degree of certainty.

On nights with abundant surface moisture, spatial patterns of moisture accumulation on grass are well explained by site geometry expressed as Ψ_{sky}. This location effect is best seen during weather strongly favouring dew (large Φ_w) when longwave radiation cooling is the dominant mechanism of surficial heat loss. However, consistent patterns are also present in less than ideal conditions.

A good example of the relationship between surface moisture and sky view factor is illustrated in Figure 6.16 for YD 171/172, 1996, with Φ_w = 1.00 (see Table 6.6 for a description of weather conditions) when trees were present in the model. It is apparent that:

- there is more surface moisture (0.07–0.11 mm per night) on grass at sites with large sky view factor such as the model park (Ψ_{sky} = 0.98) and the relatively open centre of the model lawn (Ψ_{sky} = 0.89), and
- less surface moisture accumulates where Ψ_{sky} is reduced, i.e., under model trees (Ψ_{sky} = 0.70) and close to the model building (Ψ_{sky} = 0.49) where the moisture accumulation is 0.03–0.05 mm and 0.02 mm per night, respectively.

When the street trees are removed from the model, spatial trends of Ψ_{sky} are less complicated and so, too, are patterns of moisture accumulation. For example, on YD 187/188 with Φ_w = 0.82 (Figure 6.17):

- little moisture (0.01 mm per night) is sensed immediately next to the base of the model wall where Ψ_{sky} is small (0.50),
- moisture accumulation increases rapidly across the model lawn (up to 0.08 mm) in agreement with Ψ_{sky}, and
- larger amounts (0.06–0.13 mm) are deposited on grass in the model park which has large Ψ_{sky} (up to 0.98).

The underlying mechanism is interpreted to be the systematic reduction in longwave radiation loss that occurs when a proportion of the cold night sky is obscured by relatively warm objects (trees and buildings). Hence, surface temperature tends to be greater when terrain view factor (Ψ_{ter}) is greater.

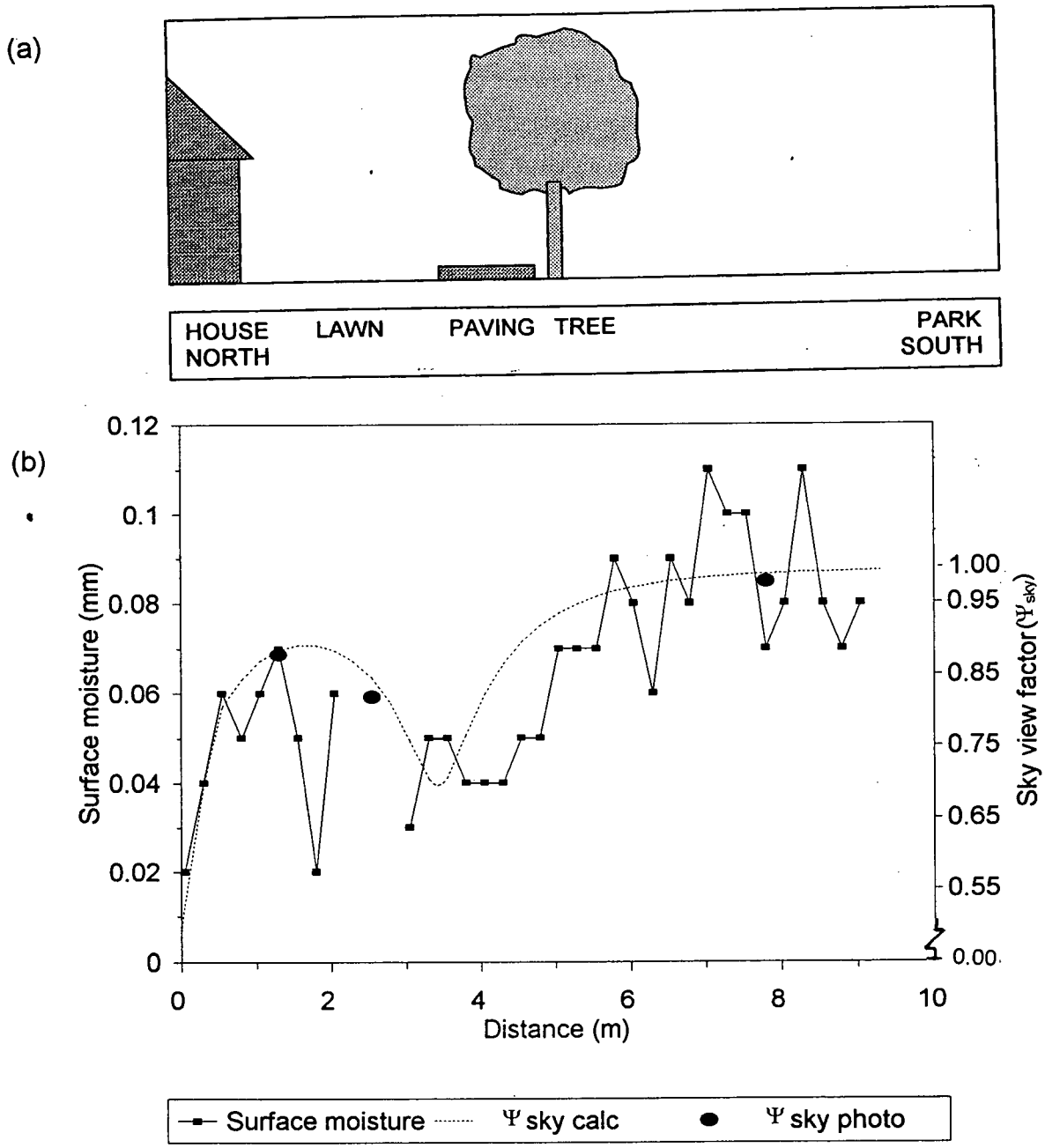

Figure 6.16 Relationship between the amount of surface moisture (mm) present on grass in the model at dawn and micro-scale location. Data for YD 172, 1996, with clear skies, light winds, and trees present in the model. (a) Schematic cross-section of the transect sampled, and (b) spatial trends of surface moisture amount (mm) and Ψ_{sky} (subscripts photo and calc indicate Ψ_{sky} determined using fish-eye lens photography and site geometry, respectively).

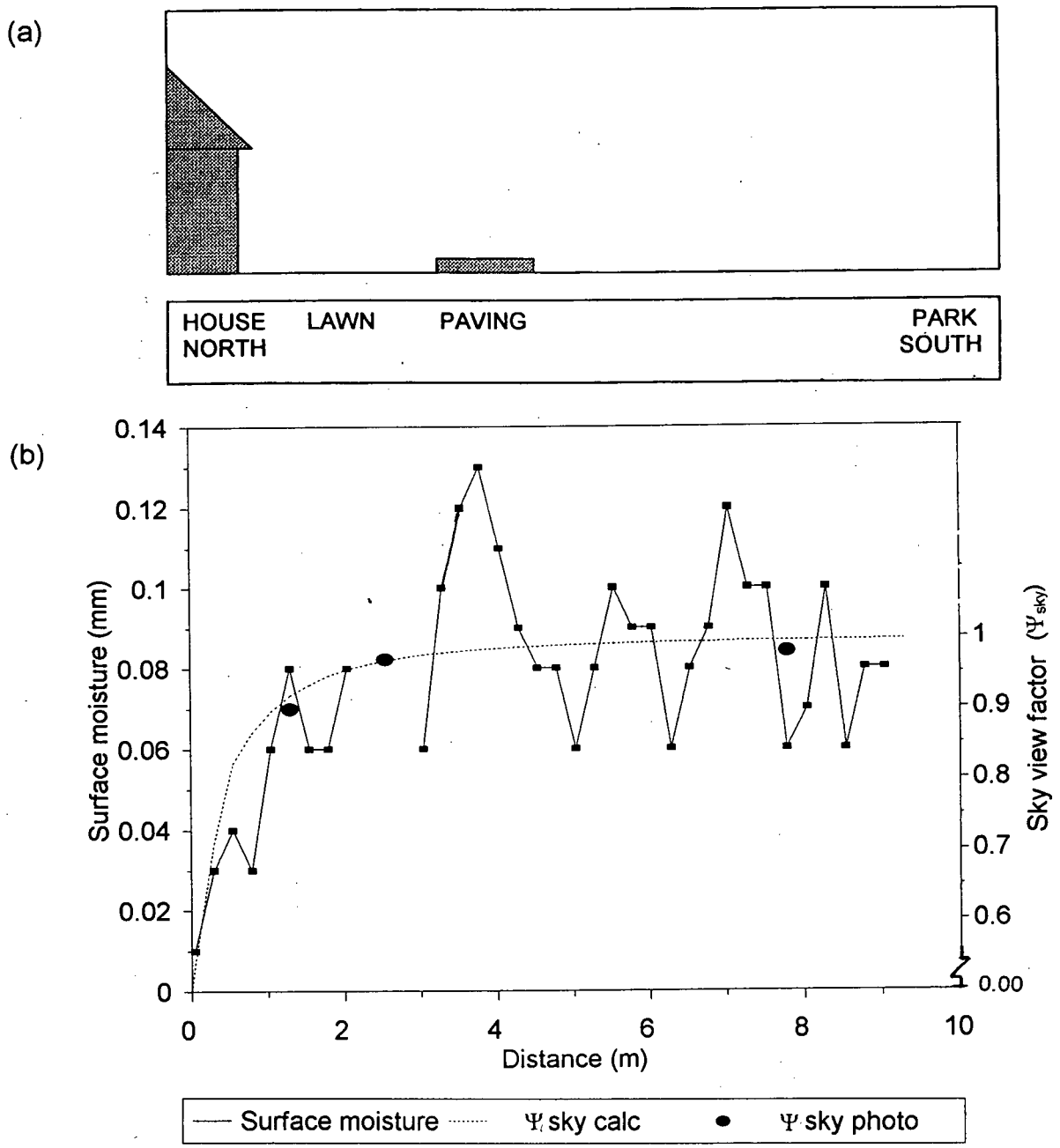

Figure 6.17 As for Figure 6.13, but for YD 188, 1996, with clear skies, light winds and no trees present in the model.

In the scale model, the combined effect of weather and location agrees with that seen at the full-scale, e.g., for the lawn at U2 (Figure 3.30). On nights when street trees are present in the model (Figure 6.18):

- spatial patterns related to Ψ_{sky} are most evident when the night favours dew, e.g., YD 171/172 with clear skies, light winds and Φ_w = 1.00 (Table 6.6),
- spatial patterns are clearly present when the weather is less than ideal, e.g., YD 164/165. On this night, abundant low cloud (n = 0.7) and light wind give a Φ_w of 0.46, and
- on YD 173/174 with windy weather (Φ_w = 0.51; Table 6.6) the maximum amount of surface moisture is small and patterns related to Ψ_{sky} are less obvious.

Similarly, on nights with no trees in the model (Figure 6.19):

- moisture patterns related to Ψ_{sky} are more obvious on nights with large Φ_w e.g., YD 187/188 (Φ_w = 0.82), and
- patterns are muted in less favourable conditions, e.g., YD 191/192 (Φ_w = 0.31) and YD 189/190. In the latter case, the unusually high vapour density deficit (6.8 g m^{-3}) overrides otherwise positive indicators, i.e., only a few high clouds, light winds and a Φ_w of 1.41 (Table 6.6).

In theory, surface moisture which accumulates on grass in the model may include water from guttation (i.e., exuded from the plant). Visual observations at dawn suggest that some guttation is present on grass in the model on most nights with dew. Moisture from the two processes—guttation and condensation—are readily distinguished by visual inspection because guttation forms large droplets on the tips

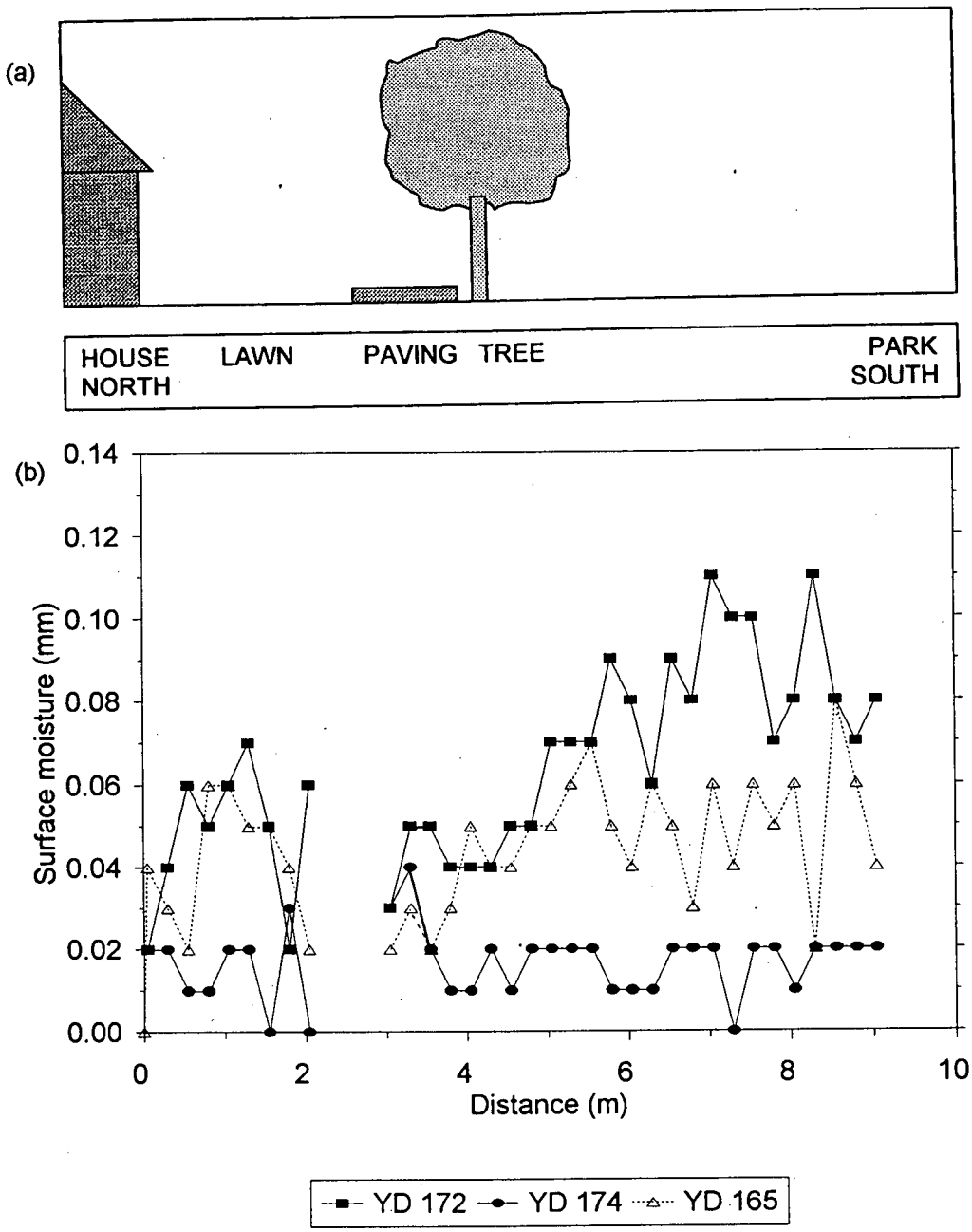

Figure 6.18 Relationship between the amount of surface moisture (mm) present on grass in the model at dawn and micro-scale location with trees present in the model. Days are differentiated by the weather of the preceding night (see text).

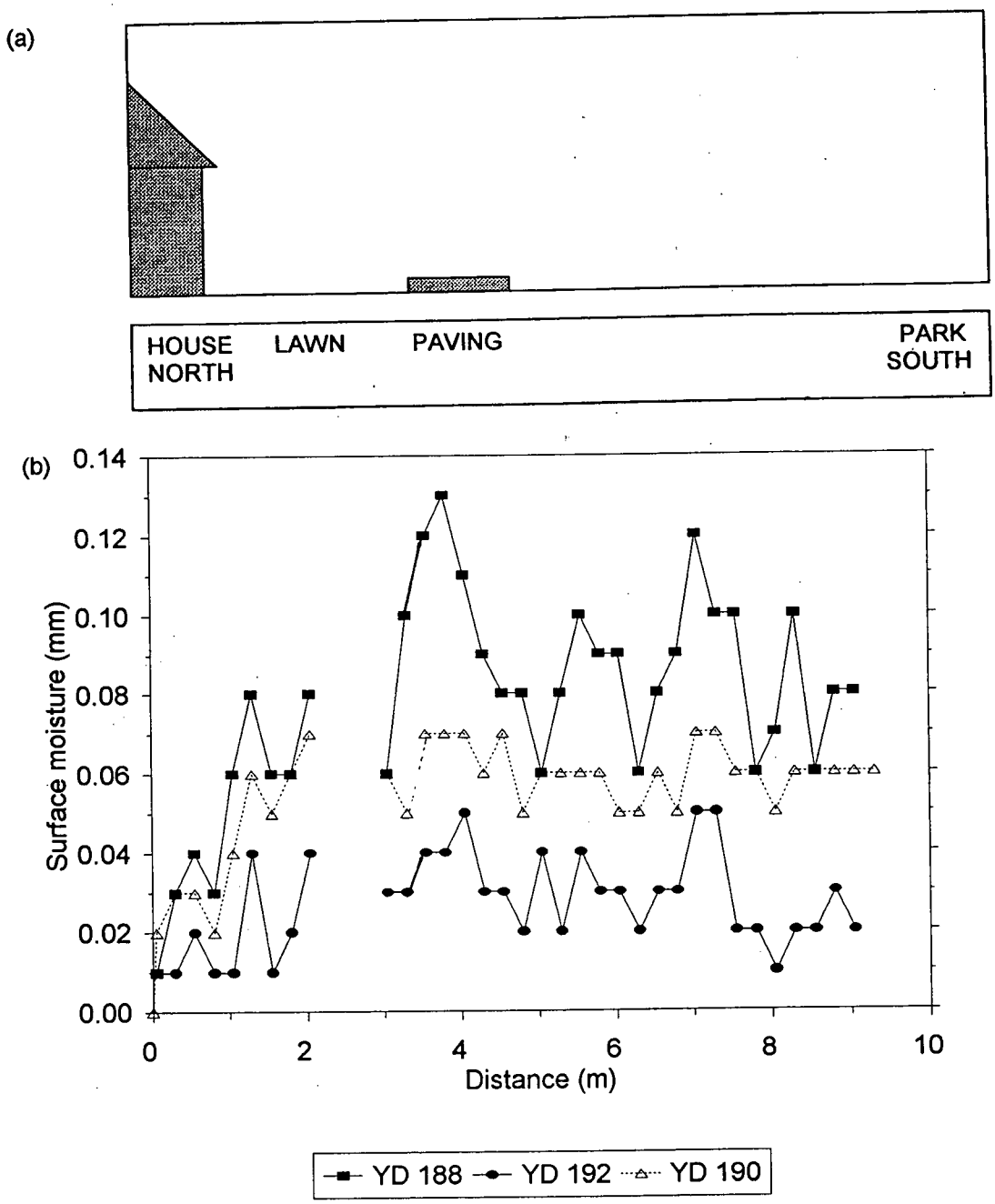

Figure 6.19 As for Figure 6.18, but for nights with no trees present in the model.

of grass blades. At dawn, guttation droplets are not evenly distributed. Often, there is a relative excess of guttation on grass close to the model pavement. When model trees are present their location coincides with this area of excess guttation. So it could be argued that the extra guttation is linked to an excess of soil moisture created by tree-shade and watering. However, the feature is also seen when no trees are present so it may be related to the presence of the concrete paving. Alternatively, a residual tree effect may be present such as excess soil moisture for distillation.

In general, the area of excess guttation coincides with the warm anomaly on several occasions, e.g., YD 187/188 (Figure 6.14). This suggests a common mechanism for both the excess temperature and guttation, such as higher soil moisture and temperature, associated with the concrete paving. Regardless of the underlying cause of this feature, the extra water from guttation helps to explain the larger-than-expected amounts of surface moisture seen on some nights, e.g., on YD 187/188, 1996, near the north edge of the model park (Figure 6.17).

Surface moisture observations collected at full-scale sites and in the scale model during fine weather conditions are presented in Figures 3.28–3.29 and 6.16–6.17, respectively. In these graphs, the y-axes are arbitrarily scaled to maximise the visual fit of spatial patterns of Ψ_{sky} and surface moisture. The two measures have different units so a quantitative analysis of agreement is not straightforward. However, if the data are appropriately normalised, then the sets are potentially comparable.

In the present study, the greatest precision in view factor is seen for the scale model where site geometry is relatively simple and Ψ_{sky} can be more easily computed from this. Observations from the model, rather than full-scale sites, are therefore used to test the quantitative fit between Ψ_{sky} and surface moisture (SM).

In the present study, surface moisture (SM) is normalised by sky view factor to create:

$$\widetilde{SM} = \left(\frac{SM_{Max} - SM_{Min}}{\Psi_{sky\,Max} - \Psi_{sky\,Min}} \right) \times \left(\Psi_{sky} - \Psi_{sky\,Min} \right) \qquad [6.1]$$

where $\widetilde{SM}$ has units of mm per night and SM is the amount of surface moisture on grass at dawn [mm per night]. The subscripts Max and Min indicate maximum and minimum values such that $\Psi_{sky\ Min}$ and $\Psi_{sky\ Max}$ are values at the base of the house wall and the south edge of the park, respectively, SM_{Min} equals zero, and SM_{Max} is arbitrarily scaled by eye to provide the best possible match with the observed moisture. That is, SM_{Max} is a weighted mean accumulation for the most open area of park (between about 7 m and 9 m away from the house wall). The method is essentially similar to that used to construct Figures 3.28–3.29 and 6.16–6.17, but it is possible to compare data directly because they are in the same units [mm].

The outcome of the normalisation exercise for two days with trees in the model is shown in Figures 6.20 and 6.21. On YD 172, 1996 (Figures 6.20a), surface moisture in the model at dawn was abundant (up to 0.12 mm), whereas on YD 174 only 0.04 mm of moisture accumulated (Figure 6.20b). Comparisons between the moisture data and normalised surface moisture show that (Table 6.7):

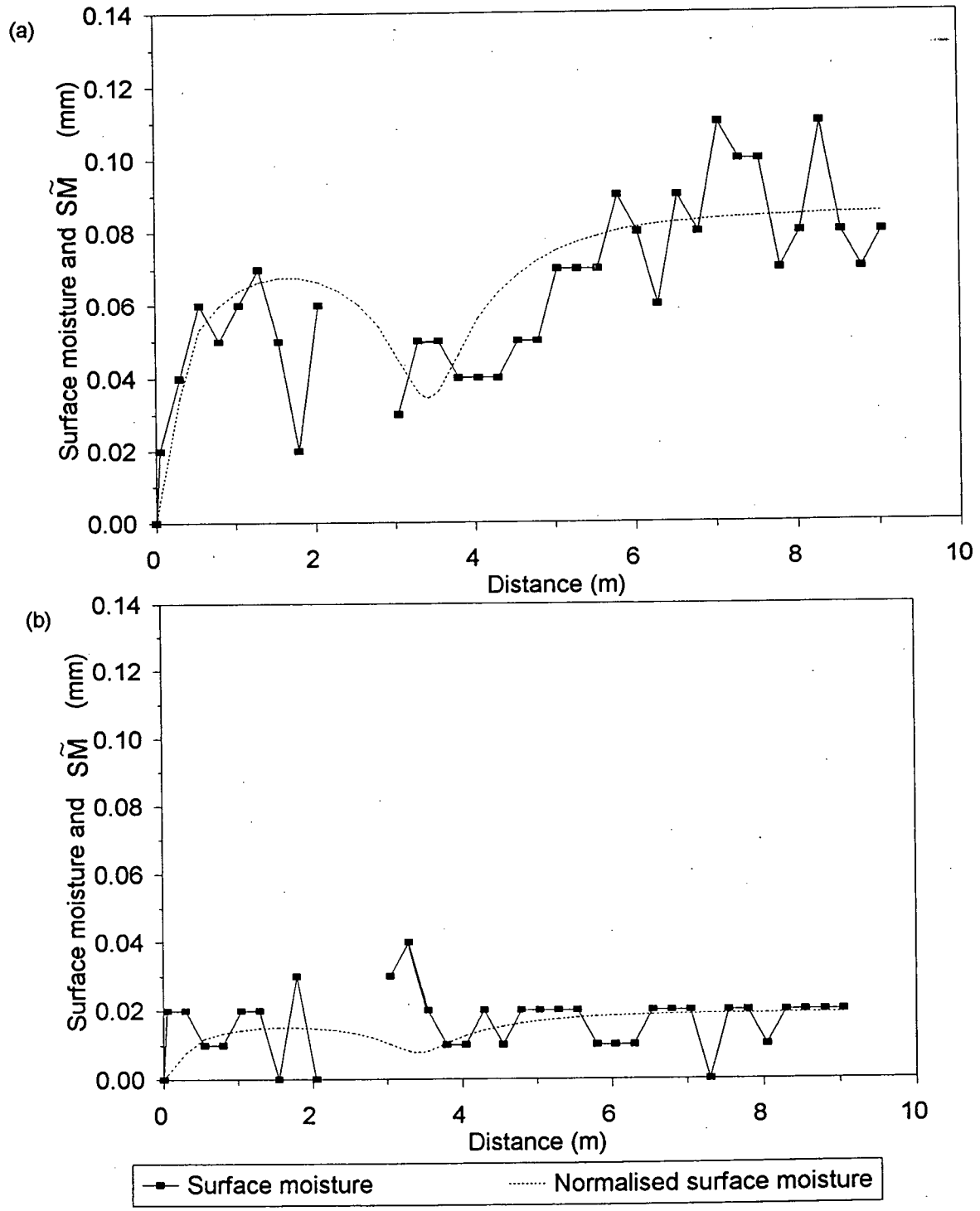

Figure 6.20 Agreement between surface moisture normalised by sky view factor ($\tilde{SM}$ with units mm; see text for explanation), and the measured surface moisture (mm) on grass at dawn in the model. Data are for two days with trees in the model: (a) YD 172 (Φ_W = 1.00) and (b) YD 174 (Φ_W = 0.51), 1996.

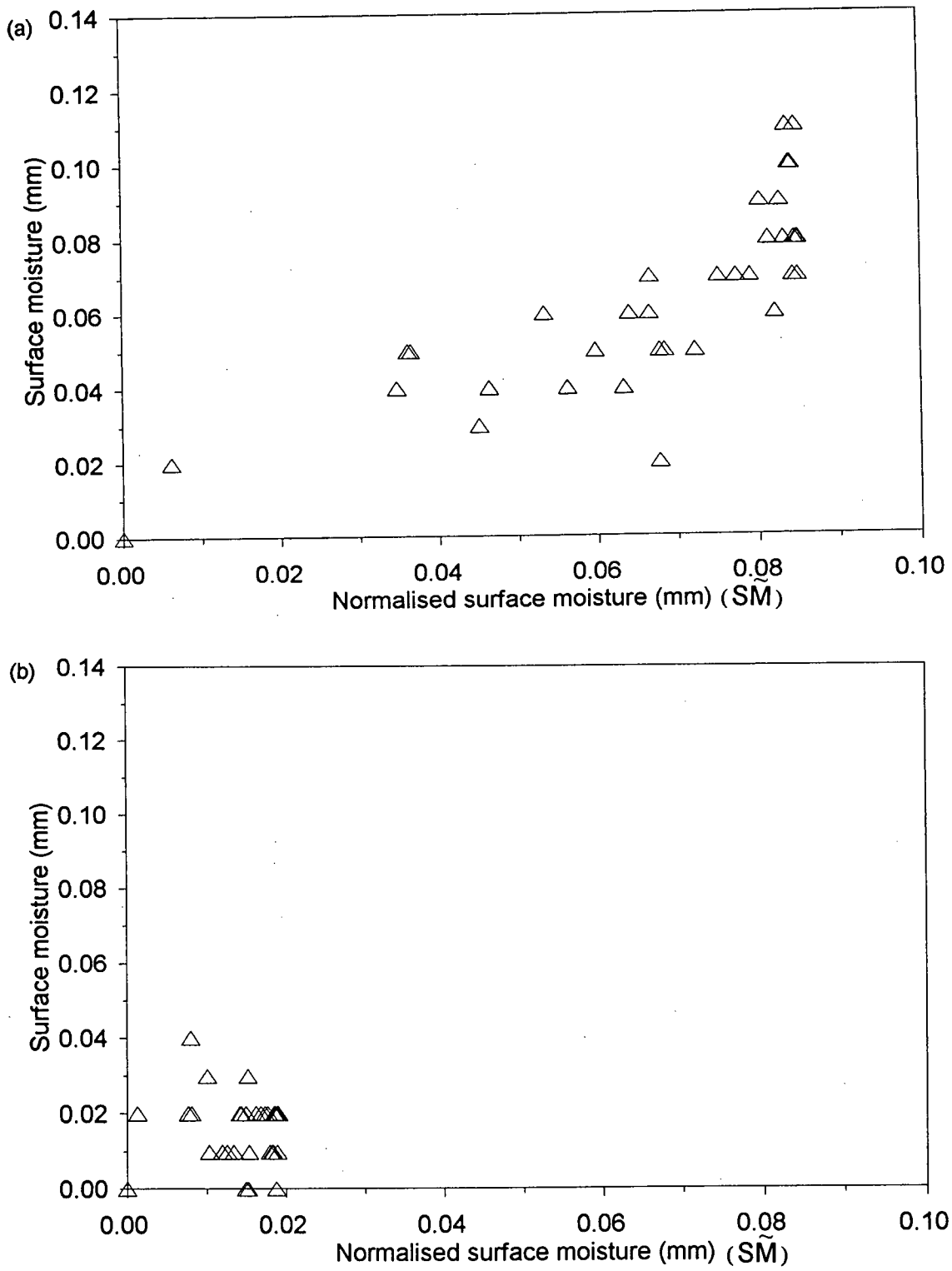

Figure 6.21 Surface moisture data for (a) YD 172 and (b) YD 174, 1996, as shown in Figure 6.20 but with $\tilde{SM}$ plotted against SM (see text for explanation of terms).

Table 6.7 Statistics used to compare measured surface moisture (SM) on grass and normalised surface moisture ($\widetilde{SM}$) from the central transect in the scale model (see also Figures 6.20–6.23).

			Surface moisture		**Normalised surface moisture**				
	n	Φ_w	*mean (mm)*	*SD (mm)*	*mean (mm)*	*SD (mm)*	*MD (mm)*	*RMSD (mm)*	*ID*
YD172	35	1.00	0.06	0.03	0.07	0.02	0.01	0.02	0.87
YD174	35	0.51	0.02	0.01	0.02	0.01	0.01	0.01	0.36
YD188	35	0.82	0.08	0.03	0.08	0.02	0.02	0.02	0.85
YD192	35	0.31	0.03	0.01	0.03	0.01	0.01	0.01	0.67

- on YD 172, there is close agreement between the means for the surface moisture (SM = 0.06 mm) and $\widetilde{SM}$ (0.07 mm),
- differences between the sets are small (MD = 0.01 mm, RMSD = 0.02 mm), and
- the agreement between SM and $\widetilde{SM}$ is relatively strong (ID = 0.87) (Figure 6.21a).

On YD 174, SM and $\widetilde{SM}$ are small everywhere in the model. This leads to means for both of 0.02 mm, but there is no real agreement between the spatial patterns of SM and $\widetilde{SM}$ (ID = 0.36) (Figure 6.21b).

Similarly, for days with no trees present in the model (Table 6.7 and Figures 6.22 and 6.23):

- on YD 188, the mean for both the surface moisture and view factor sets is 0.08 mm (Figure 6.22a),

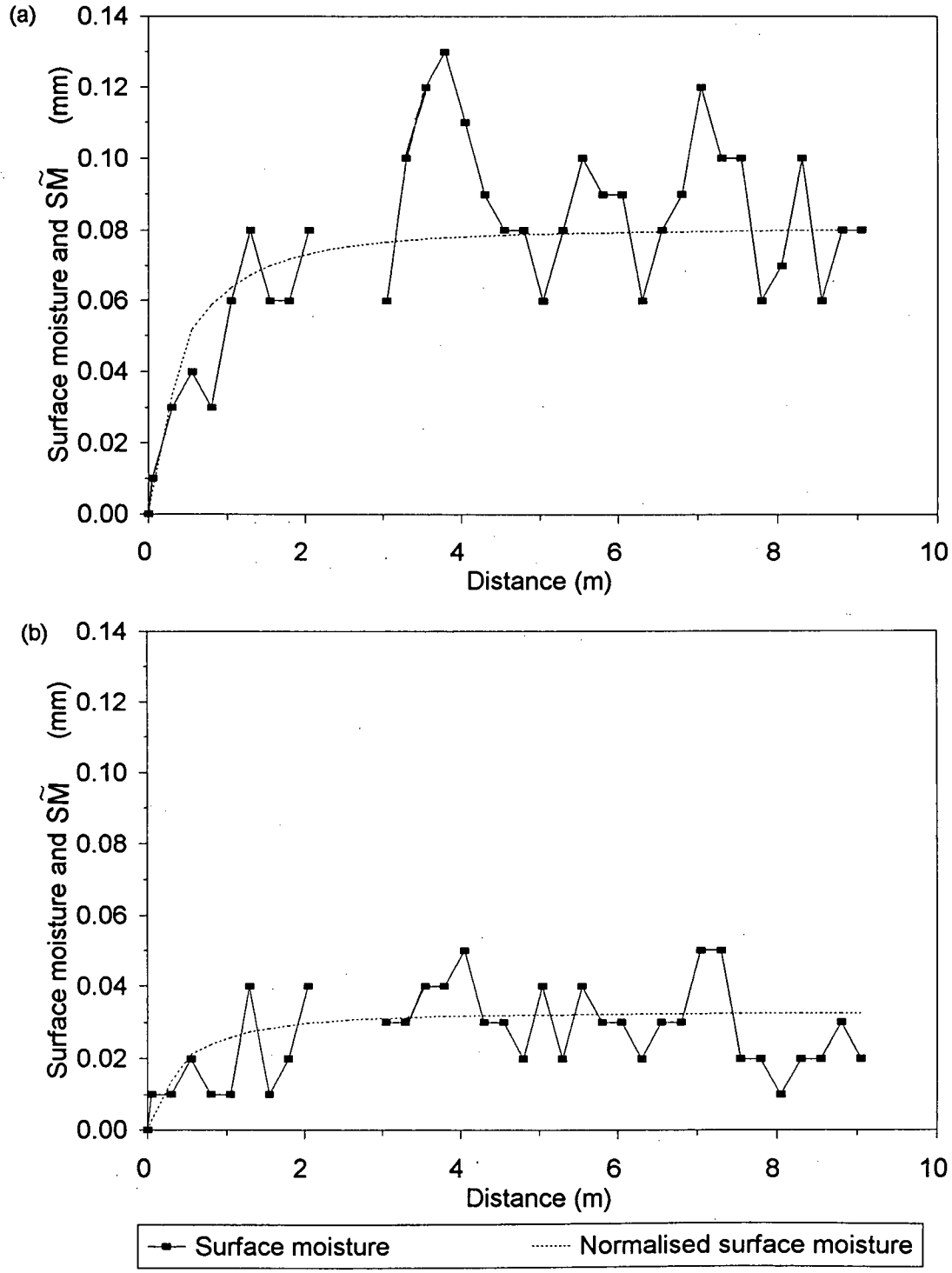

Figure 6.22 Data as in Figure 6.20, but for two days with model trees absent: (a) YD 188 and (b) YD 192, 1996.

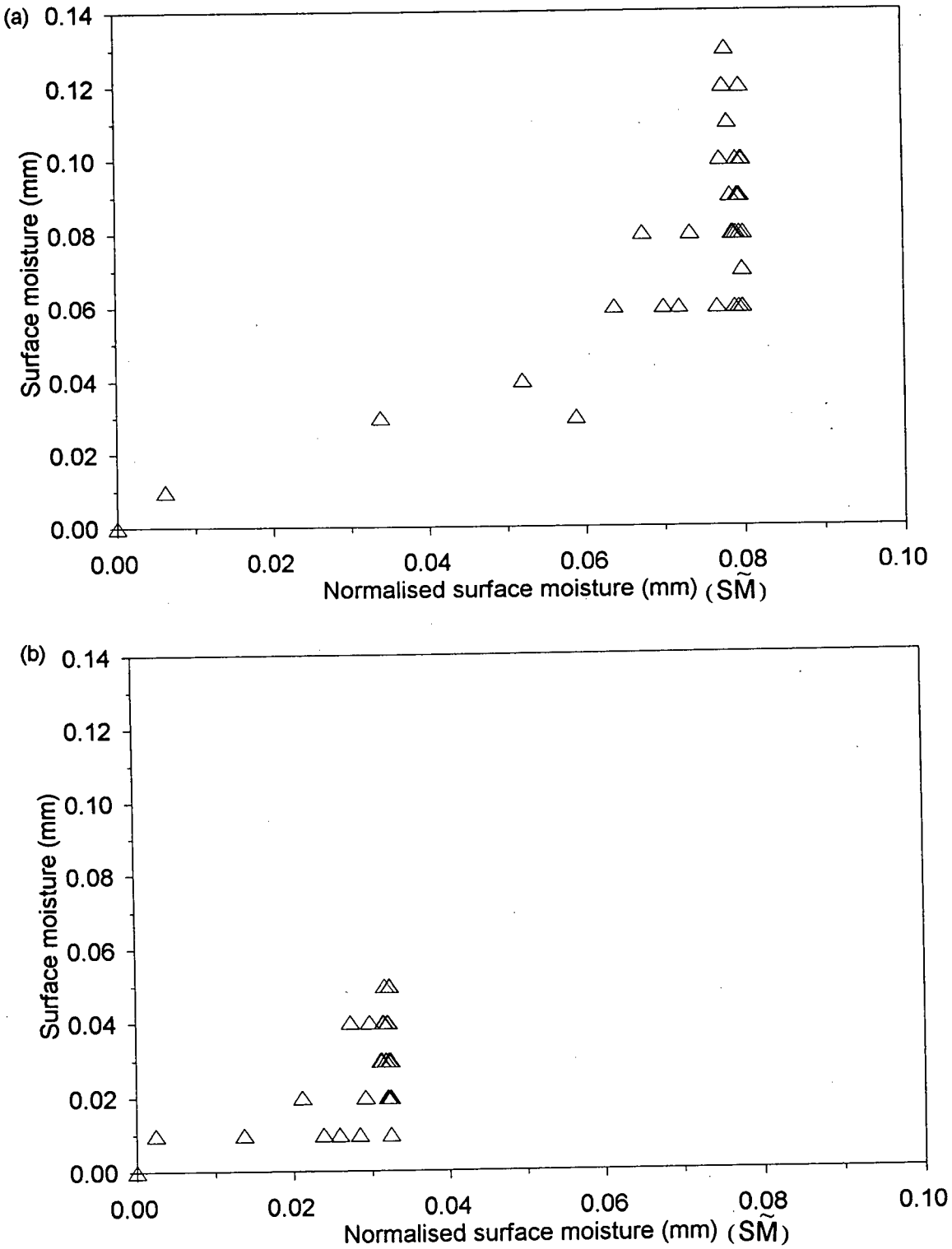

Figure 6.23 Surface moisture data for (a) YD 188 and (b) YD 192, 1996, as shown in Figure 6.22 but with $\tilde{SM}$ plotted against SM (see text for explanation of terms).

- differences between the data are small (MD = 0.02 mm, RMSD = 0.02 mm),
- good agreement exists between SM and $\widetilde{SM}$ (ID = 0.85) (Figure 6.23a), and
- on YD 192, all the statistical indicators (mean, SD, MD and RMSD) have small, and therefore similar, values but agreement between the data is poor (ID = 0.67) (Figures 6.22b and 6.23b).

These results suggest that surface moisture in the model is well described by $\widetilde{SM}$, provided the amount of moisture which accumulates is large. When dew is light, correlations are weak. This, in turn, suggests that the spatial distribution of moisture on ideal nights is predictable using sky view factor and an appropriately weighted mean moisture accumulation determined for an open site.

(c) Variation of dewfall in the model

Observations show that the amount of dewfall in the model varies considerably from day-to-day. Table 6.8 summarises the dewfall observations made during the summer of 1996 using mini-lysimeters installed in several surfaces in the model (see Figure 5.5). Dewfall is sensed by the 'roof' mini-lysimeter on 13 (81%) of the 16 nights studied, on grass in the model park on 67% of nights (12 out of a possible 18), and on grass on the model lawn on 50% (9) of nights. No dewfall is sensed by the mini-lysimeters installed under a maple tree or the model pavement.

Observations for three surfaces in the model (park grass, lawn and roof) for selected days in the period YD 155–195, 1996, are show in Figure 6.24. Only days with complete data are shown, so the absence of a bar means no dewfall was observed. In the period up to YD 174 trees are present in the model, after that they

Table 6.8 Statistics of the presence and amount of dewfall in the model at M1 during 1996, measured using mini-lysimeters for days selected for study in 1996 (dates as for Figure 6.15).

	Nocturnal accumulation of dewfall					
	n (d)	*Present* (d)	*Absent* (d)	*Maximum* (mm)	*Mean* (mm)	*SD* (mm)
Grass in park	18	12	6	0.12	0.04	0.04
Grass in lawn	18	9	9	0.29	0.06	0.08
Shingle roof	16	13	3	0.18	0.09	0.06
Pavement	18	0	18	-	-	-
Maple tree	8	0	8	-	-	-

are absent. By chance, the change in configuration on YD 182/183 (July 1, 1996) coincides with a change in weather from condition close to the average for June, to those more favourable for dew (higher dew-point temperature and less cloud) in July (see discussed in Chapter 3). For the purposes of dewfall analysis in the scale model, this is interpreted to mean that some features which coincide with the change in model configuration are actually attributed to weather differences.

For the roof and model park, the variation of dewfall in the model (Figure 6.24) bears a remarkable similarity to patterns seen in Figure 3.20, wherein rural and urban dewfall are compared, i.e., using data for the full-scale sites at R1 and U1. That is:

- in the period YD 155–174, dewfall in the model never exceeds 0.13 mm per night on either surface,
- from YD 187 to 195 dewfall is present on both surfaces on each night, and amounts are often large (>0.13 mm per night), and

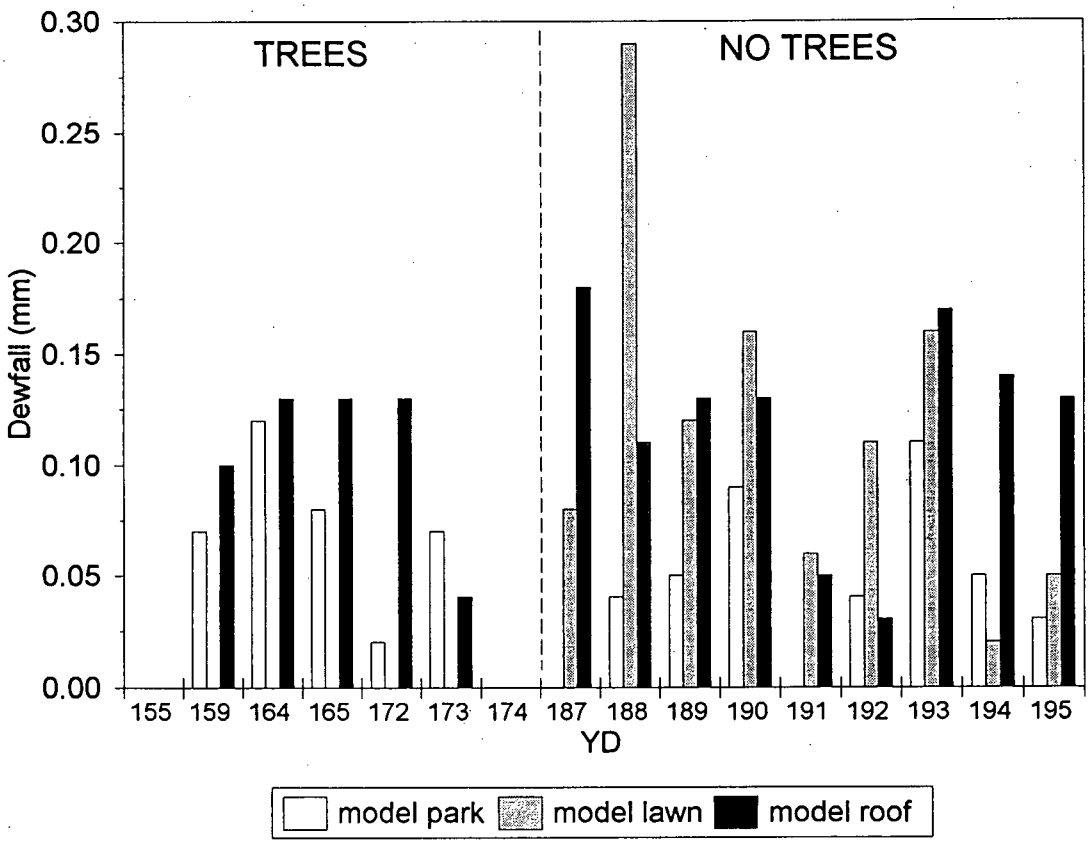

Figure 6.24 Dewfall data measured by mini-lysimeter in the model for selected days during the period YD 155–195, 1996. Data are the maximum accumulated dewfall per night (mm) on grass in the model park and lawn, and on the roof of the model house (no bar means zero dewfall). The dashed line indicates periods with trees present in the model (YD 155–174) and without model trees (YD 187–195).

- for both the full-scale and the scale model data, the largest dewfall is on the grass on YD 188, i.e., 0.27 mm at R1 and 0.29 mm at the model park.

These results strongly suggest that dewfall patterns on the model roof and park are controlled by regional weather and that any tree effect at M1 is weak. This is reasonable since trees provide only a small fraction of the horizon obstruction for the model park and roof. In addition, this suggests that the potential aerodynamic effects of trees on moisture delivery to the surface (associated with wind direction, wind speed and turbulence) are weak.

The model roof seems to be a preferred site for dewfall accumulation. This agrees with patterns seen at the full-scale (Chapter 3):

- on almost all nights with dewfall the amount deposited on the model roof exceeds that sensed on grass in the model park,
- prior to YD 187, dewfall is often abundant on the model roof (up to 0.13 mm per night), whereas dewfall on grass in the model park is typically less (up to 0.12 mm),
- from YD 187 onwards, dewfall is deposited on all nights on the model roof but it is absent in the park on two occasion,
- mean dewfall is 0.09 mm on the roof but only 0.04 mm in the park, and
- the maximum dewfall event is 0.18 mm for the model roof but only 0.09 mm for grass in the model park.

In sharp contrast to the observations for the park and roof, the change in model configuration has a dramatic effect on dewfall on the model lawn (Figure 6.24):

- when trees are present no dewfall is sensed on the model lawn even though up to 0.13 mm is present elsewhere in the model. Although it is difficult to rule out the effects of weather differences, the temporal shift to greater dewfall after YD 174 is interpreted to be largely due to increased sky view factor and/or greater efficiency of vapour transport to the lawn surface because shelter is decreased,
- from YD 187 onwards with no model trees, dewfall is sensed on the model lawn on all nights studied, and
- dewfall of up to 0.16 mm per night and, on one occasion (YD 188), 0.29 mm is sensed on the model lawn.

Dewfall is absent on walls on all nights. This is probably because they have negligible Ψ_{sky} and are in contact with a heat source, the residual heat reserves of the interior of the house, and so remain warm during the night. But when the same material (wood) is used to shingle a roof (as was done in the 1994 trial at M2) dewfall is observed, i.e., when its Ψ_{sky} is high, and the surface is insulated from heat sources.

No dewfall was evident on maple and conifer foliage in the model at M1 in 1996, and leaves were observed to be dry every day at dawn. It is difficult to absolutely exclude the presence of small amounts of dew, on some maple leaves, for limited periods. However, measured leaf temperatures suggest that leaves at this site seldom cooled far below the ambient air temperature. In such cases, dew is not strongly favoured. In contrast, at M2 in 1994, trees in the prototype model were often wet at dawn. On some nights the observed leaf wetness at M2 was due to fog

impact (see Figure 1.1a), but on other occasions dewfall was almost certainly the cause of surface moisture. The difference between the sites may be due to the preponderance of near-calm ($\leq$0.2 m s^{-1} at 1.5 m) conditions at M2. In contrast, air movement at M1 appears to have been sufficiently consistent throughout the night as to inhibit dewfall on the maple canopy.

6.4 Summary

The main findings of the modelling programme can be summarised:

- in environments possessing complex geometry, such as a three-dimensional model, spatial patterns are also complex,
- the presence and amount of surface moisture and dewfall in the model is ultimately controlled by weather and the nature of the substrate, but
- weather and substrate effects are modified by effects relating to the net radiation balance of the surface, which is strongly linked to site geometry (Ψ_{sky}) and whether surfaces are isolated from heat sources (Q_G or ΔQ_S),
- significant amounts of dewfall are deposited to grass at open sites in the model and on asphalt shingle roofs which cool rapidly after sunset, and no water is deposited on the concrete paving and tree leaves which remain warmer than other surfaces throughout the night, and
- for nights with moderate to heavy dew, patterns of surface moisture seem to be well explained by the distribution of sky view factors, but when the amount of moisture is small this has less explanatory power.

The model performs well. It provides significant information about the behaviour of several artificial materials (wood, asphalt shingle and concrete), and confirms that amounts of dewfall deposited to an asphalt shingle roof may be significant when weather is favourable for dewfall. The model helps to build an intuitive understanding of the controls on surface moisture at urban sites with complex configuration. The outcome is satisfactory and encouraging, especially because the scaling approach has not previously been tried to simulate moisture conditions. Results suggest that maps of site geometry expressed as sky view factor and knowledge of dew at an open site could potentially be used to create maps of dew distribution in urban environments.

Some relations in the model are difficult to interpret because of spatial complexity, due in part to juxtaposition of elements (trees, buildings, grass and concrete paving) and the potential effects of guttation. Later in this study (Chapter 7) I investigate the alternative of simulating dewfall using a numerical model. In the numerical model the configuration of the urban environment to be simulated is reduced even more.

PART III MODELLING

Chapter 7: Numerical modelling of urban dewfall

7.1 Context

In environments with complex physical configuration, such as cities, modelling is often a viable alternative to measurement. A hardware model to simulate urban dew is described in Chapters 4–6. The model performs well, however, some relationships are masked by spatial complexity. Here I investigate the alternative of using a physically-based numerical model. In the approach taken, the urban environment to be simulated is reduced to very simple generic elements (a leaf or roof) and dew deposition on these surfaces is viewed in isolation. In theory, accumulation on individual elements could later be linked and amalgamated to give an areal estimate of the total amount of surface water present in an urban area. There are no existing numerical models to predict urban dew. Several types of existing model offer approaches of potential value, but in practice the list of likely candidates is relatively narrow (Section 2.5.2).

7.2 Objectives

The aim of the numerical modelling here is to investigate the physical processes and temporal patterns of dewfall at the micro-scale for typical urban materials. These are exploratory simulations to predict dewfall accumulation on certain surfaces which are present in significant proportions in cities, especially in residential areas. While it is ultimately desirable to develop a comprehensive and detailed urban model which predicts dew for urban areas and incorporates the

heterogeneity and three-dimensional nature of the urban surface, this task lies beyond the scope of this thesis.

The amount of dewfall deposited overnight on the following isolated surfaces are simulated:

- deciduous tree leaves, and
- asphalt shingle roofs.

Other surfaces, such as walls and paving are also present in significant proportion in cities but, as observations in Chapters 3 and 6 show, these are less important. They are less likely to accumulate significant amounts of dew, compared to leaves and roofs, because of reduced Ψ_{sky}, anthropogenic heating and/or a strong sub-surface heat flux. Grassed surfaces are not addressed because, in the model, leaves are assumed to be horizontal, and this is not true for grass blades.

In this chapter, a micrometeorological model to predict dewfall on crop leaves (Pedro, 1980) is modified and extended to predict dewfall on urban surfaces. Underlying theory concerning the model is discussed in Section 7.3 and Appendix A2; details of its implementation are given in Section 7.4; Section 7.5 presents results (these are summarised in Section 7.6); and potential approaches towards developing an areally-integrated urban dew model are forwarded in Section 7.6.

7.3 An urban dewfall model

7.3.1 Context

In general, the most successful rural models are those which predict dewfall on leaves using a rigorous, time-dependent methodology and micrometeorological

concepts. A 'single-layer' scheme generally works well: energy balances are calculated for the upper and lower sides of the leaf, and the presence of dewfall is inferred from the latent heat flux. Computations are often based on the Penman equation (Equation 1.1). In theory, such a model can be extended to predict dewfall on leaves and other surfaces in a city.

In the present study, it was decided that the leaf-wetness model of Pedro (1980) was a suitable candidate for modification to urban uses. The model accounts for the downward flux of atmospheric water vapour by turbulent transfer (dewfall), but not for the upward flux of moisture from the soil, which may occur on very short vegetation (Scherm and van Bruggen, 1993), and potential guttation is ignored. Wittich (1995) tested the performance of three single-layer models in predicting leaf wetness duration, and found that the model of Pedro (1980) performed best. Pedro's model has proven reliable and transferable, having been validated for a number of different crops (corn, soybean, apple and lettuce) and locations (Pedro, 1980; Gillespie and Barr, 1984; Scherm and van Bruggen, 1993; Wittich, 1995). While Pedro's model was originally designed to predict leaf wetness duration on broad-leafed crops, the methodology is rigorous and has been applied with success to cylindrical leaves (onion) (Gillespie and Barr, 1984). In theory, Pedro's model also predicts dewfall amount, because wetness duration is computed from a latent heat flux budget, in which moisture amount is implicit, but this is seldom done; Heusinkveld *et al.* (1998) is the rare exception.

The model developed here follows the micro-meteorological approach developed by Pedro (1980; Pedro and Gillespie, 1982a), with the following

modifications: (a) it explicitly computes dewfall amount (mm), (b) dewfall is simulated for maple tree leaves, i.e., a leaf type which differs from those in Pedro's original simulations, and (c) more importantly, dewfall is simulated for built surfaces (roof shingles). Pedro's model predicts dewfall on leaves but there is no fundamental reason why the essential method contained in the model cannot be applied to surfaces other than leaves. The approach is rigorous and so the model can readily be modified to taken into account the intrinsic characteristics of a new type of leaf or, even, a built surface (roof). Aspects of theory underlying the model are discussed by McAdams (1954), Ede (1967), Mintah (1977), Pedro (1980), and Pedro and Gillespie (1982a; 1982b).

7.3.2 Theory and structure

In this section, topics of discussion and numerical formulae which relate specifically to the example of a generic two-sided leaf are closely based on existing ideas and previously developed formulae presented by Pedro (1980) and summarised in Pedro and Gillespie (1982a). The portions of the following discussion which address a generic roof surface, however, are developed by me. The concepts contained in these portions are derived from first principles or based on the findings of several modelling and thermal engineering publications.

It is often useful to describe the climatology of a physical system as a balance between inputs, outputs and changes in storage of energy or mass. In theory, in the absence of rain and irrigation, the change in surface water storage (ΔS_{wa}) on an isolated leaf, for example, is expressed (see Section 1.2.3):

$$\Delta S_{wa} = M_{in} - M_{out} = C + G - E_e - R - D_i \quad [7.1]$$

where M is mass of water (kg), and subscripts in and out indicate transfers to and from the leaf surface, respectively (the other terms are described in Section 1.2.3). In the approach discussed here, two types of systems are addressed, i.e., energy balances and surface water budgets of a leaf (broad-leaved deciduous tree), and those of an extensive roof surface. On the one hand, a leaf is a three-dimensional object, albeit of small thickness. Energy and water vapour are transferred through its surfaces, dew is stored on it, but it is assumed that liquid water is not absorbed by, or exuded (guttated) from, leaf tissue, and distillation is absent. Further, being thin, it is assumed to have negligible heat storage potential. A roof, on the other hand, is essentially an impermeable surface plane through which energy but not water is transferred, but upon which liquid water accumulates. It is sufficiently connected to underlying materials that heat fluxes to and from underlying structures are relevant. The energy balance of a two-sided leaf is expressed:

$$Q^* = Q_H + Q_E + Q_M = aK_{in1} + aK_{in2} + \varepsilon L_{in1} + \varepsilon L_{in2} - \varepsilon\sigma T_{l1}^4 - \varepsilon\sigma T_{l2}^4 \quad [7.2]$$

and, for a roof surface:

$$Q^* = Q_H + Q_E + Q_G = aK_{in1} + \varepsilon L_{in1} - \varepsilon\sigma T_r^4 \quad [7.3]$$

where Q_H is convective sensible heat, Q_E is convective latent heat, Q_G is sub-surface sensible heat, Q_M is metabolic heat, Q^* is net all-wave radiation, and K_{in} and L_{in} are incoming shortwave and longwave radiation, respectively. All terms are expressed as flux densities with units W m^{-2}. The coefficients are the absorptivity of the surface (leaf or roof) for shortwave radiation (a), surface emissivity (leaf or roof) for longwave radiation (ε), the Stefan-Bolzmann constant (σ = 5.67x10^{-8} W m^{-2} K^{-4}),

and temperature (T) in kelvins; subscripts l, r, 1 and 2 refer to leaf, roof, upper, and lower surfaces, respectively.

Equations 7.2 and 7.3 describe the balance of energy and the budget of radiation for a leaf and a roof surface, respectively (Figure 7.1). If all other terms were known these equations could be solved for Q_E—a positive value indicating evaporation, a negative value indicating condensation or dewfall. The individual component radiative fluxes which are integral to solving these equations are not always straightforward to measure or to estimate numerically with sufficient accuracy to resolve fluxes of dewfall. This is even more true when seeking to evaluate the turbulent and conductive fluxes of heat, Q_H and Q_G. It is, therefore, useful if Q_E is determined using an alternate numerical method that does not require solution of all the individual terms shown in Equations 7.2 and 7.3. In overview, the approach taken here is to redefine all terms in Equations 7.2 and 7.3 using relatively easily measured parameters, and to solve the resulting energy balances for surface temperature. It is assumed that the surface is wet so, by definition, surface humidity is at saturation and depends solely on surface temperature. Thus, when surface temperature is known so is surface humidity, and hence Q_E is found using:

$$Q_E = h_v\left(q_l^* - q_a\right) = h_v \Delta q \qquad [7.4]$$

where h_v is the convective water vapour transfer coefficient [W m^{-2} K^{-1}], and Δq is the specific humidity difference between the leaf (q^*_l) or roof (q_r) surface and the overlying air (q_a) [kg kg^{-1}]. Numerical simulation is aided if two simplifications are made: (i) the surface of interest is located at the top of the vegetation/urban canopy

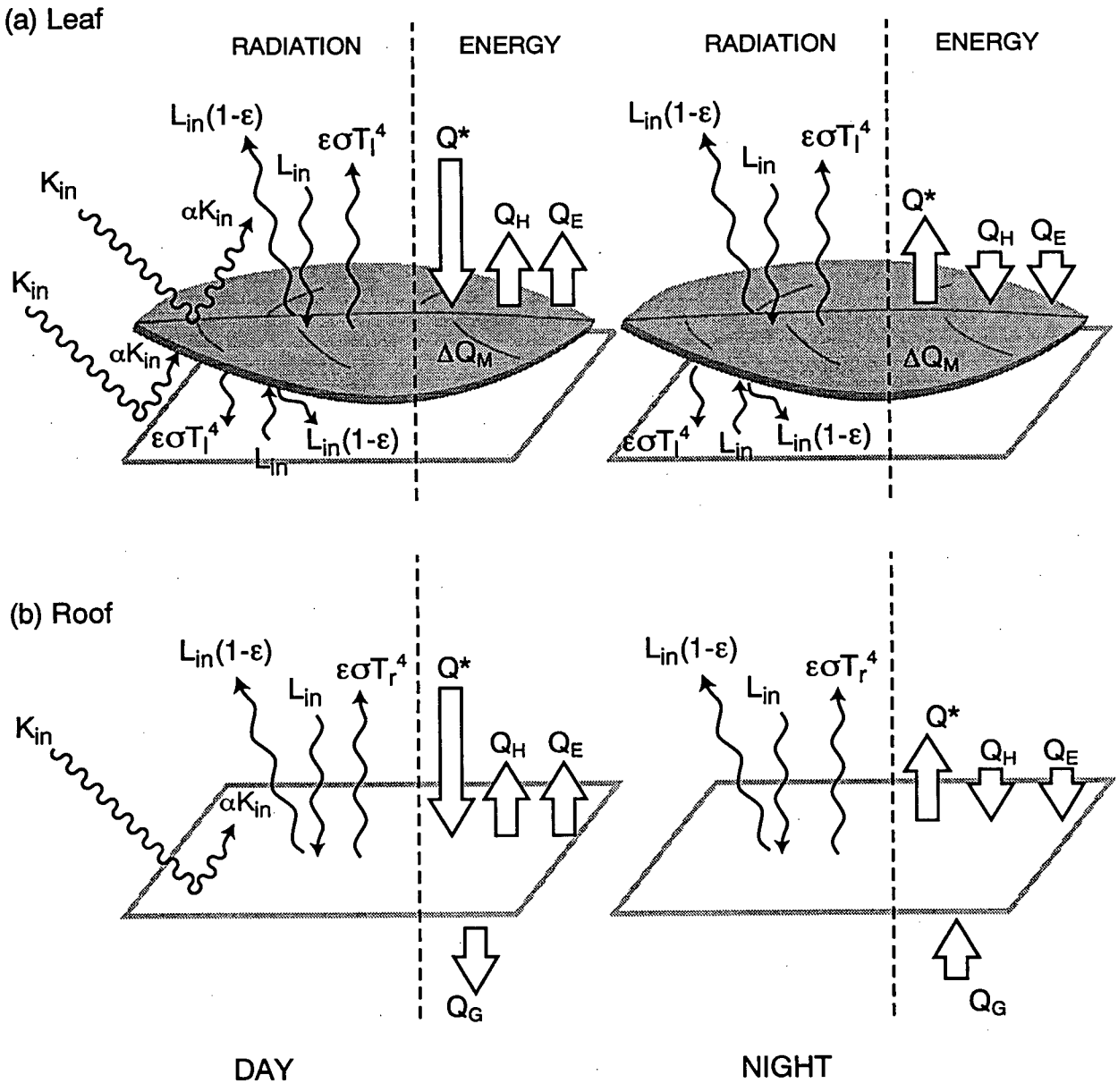

Figure 7.1 Schematic summary of the fluxes involved in the radiation budget and energy balance of (a) a leaf underlain by continuous canopy, and (b) the surface of a horizontal roof, for typical day and night conditions.

and is horizontal, and (ii) the leaf and the underlying canopy are of relatively similar temperature and emissivity. Thus, for the leaf, radiative gains are the absorbed fractions of K_{in1} and K_{in2}. The latter is the absorbed fraction of the shortwave radiation reflected from the underlying canopy and can be rewritten $\alpha_c a K_{in1}$, where α_c is the apparent shortwave reflectivity for the underlying canopy (leaves, branches and soil). For computational purposes, it is assumed that longwave radiation exchanges between the leaf and underlying canopy are sufficiently similar that they cancel, and that Q_M is negligible (Pedro, 1980). In reality, the underlying canopy may be warmer at night than the leaf which is openly exposed to the sky, i.e., $\varepsilon L_{in2} - \varepsilon\sigma T_{l2}^4$ may be greater than zero.

Taken together, this means, for a two-sided leaf:

$$Q_H + Q_E = aK_{in1} + \alpha_c aK_{in1} + \varepsilon L_{in1} - \varepsilon\sigma T_{l1}^4 \qquad [7.5]$$

and, for leaf and roof, no reflected shortwave radiation is received by upper surfaces. All radiative parameters are defined in terms of fluxes from above, so subscripts 1 and 2 are omitted hereafter. As a second step, those energy flux terms in Equations 7.3 and 7.5 that can be are redefined as functions of an appropriate temperature or humidity gradient and a transfer coefficient. By convention, the latter is expressed for a single surface. It is assumed that conditions on each side of the leaf are sufficiently similar that transfer coefficients are the same for both sides of the leaf (Pedro, 1980; Wittich, 1995). Thus, for a two sided-leaf:

$$Q_H = 2h_c(T_l - T_a) \qquad [7.6]$$

$$Q_E = 2h_v(q_l - q_a) \qquad [7.7]$$

where T_a and q_a are measured at a standard height above the surface and T_l is leaf surface temperature. For the surface of a roof:

$$Q_H = h_c(T_r - T_a) \quad [7.8]$$

$$Q_E = h_v(q_r - q_a) \quad [7.9]$$

$$Q_G = h_k(T_r - T_u) \quad [7.10]$$

where h_c is the convective, and h_k the conductive sensible heat transfer coefficients [all with units W m^{-2} K^{-1}], and the subscript u indicates the roof substrate. Substituting Equations 7.6–7.10 into Equations 7.3 and 7.5, the energy balances are expressed, for a two-sided leaf:

$$2h_c(T_l - T_a) + 2h_v(q_l - q_a) = aK_{in} + \alpha_c aK_{in} + \varepsilon L_{in} - \varepsilon\sigma T_l^4 \quad [7.11]$$

and, for a roof surface:

$$h_c(T_r - T_a) + h_v(q_r - q_a) + h_k(T_r - T_u) = aK_{in} + \varepsilon L_{in} - \varepsilon\sigma T_r^4 \quad [7.12]$$

Rather than calculate convective transfer coefficients from first principles, their value is determined empirically, based on experiments conducted in wind tunnels under conditions of controlled flow. Because h_c is more easily determined, h_v is commonly derived from:

$$h_v = 1.07\left(\frac{L_v}{c_{wa}}\right)h_c \quad [7.13]$$

where L_v is the latent heat of vaporisation [J kg^{-1} K^{-1}], c_{wa} is the specific heat of water [J kg^{-1} K^{-1}], and 1.07 is a dimensionless ratio derived, in part, from rates of molecular diffusion (Section A2.2). When natural or forced convection dominates over free convection (air movement caused by air density differences), then for leaves:

$$h_c = 4.0\left(\frac{u}{d}\right)^{0.5} \qquad [7.14]$$

where 4.0 [W m^{-2} K^{-1} $s^{0.5}$] is the numeric value for a ratio derived from thermodynamic variables (Section A2.1), u is wind speed [m s^{-1}] measured at a standard height above the surface, and d is the effective length of the leaf [m]. Values for d are most easily derived for theoretical leaves of perfect rectangular shape. But real leaves are of many different shapes so d, the effective leaf length, reflects leaf size and shape. Typical values for d have been derived for several plants as a function of maximum leaf length (d_{max}) and a non-dimensional conversion ratio which accounts for leaf shape (Parkhurst *et al.*, 1968). For leaves with deeply indented margins (such as maples) a reasonable estimate of the conversion ratio is found using the ratio of 'leaf blade' area to 'overall leaf area', where the latter is the minimum rectangular area required to enclose the leaf silhouette.

Relationships determined for leaves are inappropriate for flat surfaces larger than about leaf size, e.g., building walls or roofs. In such cases empirical relationships formalised by McAdams (1954) are more suitable, i.e., in conditions when dewfall commonly forms (u <5 m s^{-1}) the :

$$h_c = 5.9 + 4.1\hat{u} \qquad [7.15]$$

where $\hat{u} = u \times \left(\frac{511+294}{511+T_a}\right)$ is the wind speed [m s^{-1}] at a standard height above the surface, adjusted for air temperature in excess/deficit of a standard value (294 K); remaining values are empirical coefficients (McAdams, 1954).

Pedro's original model does not include Q_G, but substrate conductivity is addressed in the thermal engineering literature, and h_k can be derived from first principles. For a roof (or other solid) h_k depends on the nature of underlying materials, i.e., layers of shingles, wood and still air. If it is assumed that adjacent layers are in perfect thermal contact:

$$h_k = \left(\frac{x_i}{k_i} + \frac{x_{ii}}{k_{ii}} + \cdots + \frac{x_n}{k_n} \right)^{-1} \qquad [7.16]$$

where k is thermal conductivity [W m^{-1} K^{-1}], x is thickness [m], and subscripts i to n indicate individual layers. In the present study, the gradient of interest is from the outer surface of the roof to its under-surface. However, in the literature the underlying attic air space, insulation and floor are typically factored in. Still air and insulation layers have very low k, so when these are included the overall h_k is small. Hence, h_k values computed in the present study exceed those published in the literature for 'shingle roofs' by ~300% (Szokolay, 1980; McPherson *et al.*, 1989).

Fewer observations are needed to solve Equations 7.11 and 7.12 if it is assumed that surfaces are wet so that q_l and q_r are at saturation, and are solely a function of surface temperature. However, obstacles remain: surface temperature is difficult to measure with accuracy, especially for leaves. In the approach described here, T_l and T_r are estimated numerically, based on an extended series of substitutions and mathematical manipulations (given in detail in Section A2.3); so there is no need to measure surface temperature. To achieve this, Equations 7.11 and 7.12 are redefined in terms of the difference (ΔT) between surface temperature

and air temperature measured at a standard height above the surface. Ultimately, the resulting relationship is written, for a two-sided leaf:

$$\Delta T = \frac{aK_{in} + \alpha_c aK_{in} + \varepsilon L_{in} - \varepsilon\sigma T_a^{\,4} - 2h_v\left(q^*_a - q_a\right)}{2h_v\left(c_a/1.07L_v\right) + 2h_v s + 4\varepsilon\sigma\overline{T}^3} \qquad [7.17]$$

and, for a roof surface:

$$\Delta T = \frac{aK_{in} + \varepsilon L_{in} - \varepsilon\sigma T_a^{\,4} - h_v\left(q^*_a - q_a\right) - h_k\left(T_r - T_u\right)}{h_v\left(c_a/1.07L_v\right) + h_v s + 4\varepsilon\sigma\overline{T}^3} \qquad [7.18]$$

where $\overline{T}$ is the mean of surface and air temperatures [K], s is the slope of the saturation specific humidity *vs* temperature curve [K^{-1}] evaluated at $\overline{T}$, and q^*_a is the saturation humidity at air temperature. Since Equations 7.17 and 7.18 are derived from surface energy balances, and solution of the energy balance governs surface temperature, values for ΔT can be estimated by solving these equations iteratively. Initially it is assumed that all T terms are equal; q^* and s values are calculated from the relevant temperature, using the method of Lowe (1977) (Section A1.4). Other numerical methods are available, but lack the accuracy and elegance of Lowe's approach. Convergence (to ±0.1 °C) for T_l and T_r is often reached after only a few iterations (Pedro, 1980). When suitable T and q^* terms are produced, the latent heat flux is calculated using Equations 7.7 and 7.9, expressed as: $Q_E = 2h_v\left(q^*_l - q_a\right)$ and $Q_E = h_v\left(q^*_r - q_a\right)$, where h_v is found using Equations 7.13–7.14. This provides values for Q_E but, to determine wetness duration or the amount of water present at a given time, a time-dependent water budget is necessary. Onset of dewfall is inferred when Q_E becomes negative and deposition ceases when Q_E turns positive. Surface

wetness persists until Q_E has been positive for sufficient time such that all water accumulated on the leaf or roof has evaporated. The evaporation rate is given by:

$$E = \frac{Q_E}{L_v} \qquad [7.19]$$

where E is the mass flux rate of water [kg s^{-1}], or, alternatively by:

$$E = \frac{Q_E}{680 \times I} \qquad [7.20]$$

where E is an equivalent depth of water per unit area, as if the water present were distributed in a film of constant thickness [mm], 680 [m^3 J^{-1}] is the appropriate conversion factor to convert W m^{-2} to mm h^{-1} (Section A1.1), and I is the step rate of the model [h^{-1}].

7.3.3 Assumptions

Several assumptions are contained in the model. It is assumed that:

- the surface of interest is flat, elevated and horizontal. In reality, most roofs and leaves are tilted. Reduced Ψ_{sky} means the model tends to under-estimate L_{in}, and the model may over- or under-estimate K_{in}, depending on Sun-Earth geometry and surface orientation,
- transfer coefficients are similar on both sides of the leaf. While this may be true for thin leaves, at night, in canopies with adequate air flow, this assumption will not always be valid,
- the surface acts as if saturated. This is reasonable for a freely transpiring leaf, or dewy surface, but is less valid when stomata close or surfaces are

dry. This means the model will be less accurate in predicting T_l and T_r when dew is absent (Pedro, 1980),

- surfaces neither absorb nor release liquid water. The small amount of water directly absorbed by certain leaves can be ignored. Guttation is not present on the maples used in the study but may be present on other plants. Distillation may be present on very low vegetation but this is not factored into the model. Therefore in reality the model tends to under-estimate total amounts of surface moisture for certain surfaces, and
- no runoff occurs. In reality, runoff is likely for leaves and inclined roofs, especially when dewfall is moderate or heavy. This means the model may over-estimate the amount of water on surfaces at particular times.

7.4 Implementation

7.4.1 Overview

The final version of the model was written in FORTRAN and run on an IBM-compatible personal computer using a WATFOR compiler. The simulations presented here follow, in essence, the approach described in Section 7.3. Two versions of a 'core' model were developed, to deal with two specific surfaces of interest: (a) a deciduous tree leaf and (b) an extensive roof surface covered with asphalt shingles. (a) is therefore closely similar to Pedro's original model to predict dewfall on a crop-leaf, but (b) has been modified specifically for the present study. The methods contained in the model are general, and the approaches taken could

readily be applied to other surfaces, e.g., a leaf of another species, a wooden roof, or pavement.

The model requires relatively few inputs and is simple to run. Input data are 15 min mean values of measured environmental data (T_a, q, u, K_{in}, L_{in} and T_u), measured or derived surface characteristics (d, x and materials), and values from the published literature (Table 7.1). Output from the model are 15 min values for T_l and T_r (expressed as °C), E [mm], Q^*, Q_H, Q_G, Q_{Eq} [these in units W m^{-2}], and Q_E; the latter in units W m^{-2} and as a fraction of computed Q_{Eq} values. Energy balance components are calculated using Equations 7.2–7.3, 7.7 and 7.9–7.10, excepting Q_H which is found by residual. To determine Q_{Eq} (Equation 1.2), Γ is estimated as a simple function (Section A2.4) of its published value (Oke, 1987) at temperatures when dew commonly forms.

Each simulation is initialised by assuming the surface of interest is dry. The model is then run at time steps of 15 minutes, from 1 hour prior to sunset (typically ~1900 LAT during summer in Vancouver) to sunrise (~400 LAT). For each time step, a surface energy budget is solved for surface temperature (Equations 7.17 and 7.18), the latent heat flux is inferred (Equations 7.7 and 7.9), and $-Q_E$ is converted to E (Equation 7.20). Linkage between time steps is provided by a cumulative water (dewfall) budget, which is carried forward from each interval to the next. If at dawn, dewfall is present (E>0) then the simulation continues until the surface of interest is dry. It is assumed that the leaf is freely transpiring, and that evaporation can occur from it at all times. For the roof, evaporation can only take place when water is present, so Q_E is set to zero whenever dewfall is absent.

Table 7.1 Input and output data for the numerical model to predict dewfall on urban surfaces, and data used to validate its results.

Parameter	*Symbol*	*Units*
Input Data		
• *Measured environmental data*		
Wind speed at surface[1]	u	$m\ s^{-1}$
Ambient specific humidity[1]	q	$kg\ kg^{-1}$
Ambient air temperature[1]	T_a	K
Incoming longwave radiation[1]	K_{in}	$W\ m^{-2}$
Incoming shortwave radiation[1]	L_{in}	$W\ m^{-2}$
Roof substrate temperature[2]	T_u	K
• *Observed surface characteristics*		
Effective leaf length	d	m
Roof substrate materials[2]	x, type	m, -
• *Values from the published literature*		
Radiative characteristics	a, ε, α_c	-
Roof thermal characteristics[2]	k	$W\ m^{-1}\ K^{-1}$
Stefan-Boltzmann constant	σ	$5.67 \times 10^{-8}\ W\ m^{-2}\ K^{-1}$
Specific heat of air	c_a	$1010\ J\ kg^{-1}\ K^{-1}$
Latent heat of vaporisation	L_v	$2.464 \times 10^{6}\ J\ kg^{-1}$
Output data		
Times of onset and drying of dewfall		h
Dewfall duration		h
Dewfall amount	E	mm
Potential dewfall	Q_{Eq}	$W\ m^{-2}$
Dewfall fraction	Q_E/Q_{Eq}	-
Energy balance terms	Q^*, Q_E, Q_H[3], Q_G[2]	$W\ m^{-2}$
Data to validate model		
Times of onset and drying of dewfall (lysimeter)[1]		h
Dewfall amount and duration (lysimeter)[1]		mm, h
Surface temperature (thermocouples)[1]		°C

1. Described in Table 5.1; 2. Roof only; 3. Found by residual.

The model was run using data I collected during 1996, at the Fairground site (M1), the site of the scale model (Chapter 5), and validated using independent data measured from the scale model itself (Section 7.4.3). This site was chosen because of its relatively simple geometry, the availability of leaf and roof surfaces, and because suitable data-sets were available both to run the model and to provide a first order validation of its results. In the scale-model, surface temperatures and moisture accumulations mimic those for equivalent full-scale objects (the reasoning underlying this assertion is given in detail in Chapter 4–6), so the success (or otherwise) of the numerical model signals its potential skill if it were implemented at a full-scale site, possessing similar geometry and ambient conditions.

7.4.2 Input data

All the instruments used to measure the input data were described in Tables 3.1 (background climate data) and 5.2 (instrumentation at M1). Briefly, K_{in} was measured at UBC; L_{in} was measured at the hardware model (southwest corner); u, T_a and RH were measured at 1.5 m (southeast corner at M1); and T_u was measured using a thermocouple attached to the underside of a model roof. Data were sampled electronically at 60 s intervals, and recorded as 15 min averages. RH data were later converted to q (Section A1.4).

Values for a, ε, α_c and k are from the published literature (Table 7.2). Values for x were measured; these include the thickness of a thin air layer, lying between

Table 7.2 Values for radiative and thermal parameters used in the model, for Japanese maple leaves and an asphalt shingle roof, as present at M1. For the roof, these data and Equation 7.17 provide an h_k value of 5.72 W m^{-2} K^{-1}.

Parameter	a	ε	α_c	d (m)	x (m)	k (W m^{-1} K^{-1})
• **Maple leaf**	0.50[1]	0.95[1]	0.25[1]	0.03	-	-
• **Roof**						
Asphalt shingle[2]	0.87[1]	0.92[1]	-	-	0.007	0.43
Plastic film[3]	-	-	-	-	negligible	
Air (still)[1]	-	-	-	-	0.0005	0.025
Cedar[3]	-	-	-	-	0.018	0.13

Sources: 1. Oke, 1987 (sealed air layer, i.e., between solid layers); 2. Szokolay, 1980; 3. ASHRAE, 1993

the wood and plastic layers of the roof. For Japanese maples at M1, d was estimated using: $d = 0.5d_{max} = 0.03$ m, where $d_{max} = 0.06$ m for a typical leaf at M1.

7.4.3 Data to validate the model

Instruments and methods used to collect data to validate the numerical model are described in Table 5.2. Data for Japanese maple leaves and the south-facing roof facet at M1 were used to validate the 'leaf' and 'roof' models, respectively. Briefly, dewfall amount and duration were measured using electronic weighing mini-lysimeters (leaf and roof), and surface temperature was measured using attached thermocouples (leaf and roof). Electronic instrument signals were sampled each 60 s using a *Campbell Scientific* logger and stored as 15 min averages.

Ideally, validation requires close correspondence between the theoretical surface simulated by the model and the actual surface used to validate the model. In the present study, the physical correspondence is not ideal. The model simulates dewfall to horizontal surfaces—in reality roof and leaves are tilted; the roof is assumed to be extensive—in reality the roof has a maximum width of 1.2 m. The differences have implications for incident radiation, runoff and the thermal-dynamic behaviour of surfaces.

The differences between simulated and real surfaces probably result in more scatter when observed and predicted data are compared. However, there is sufficient similarity that the numerical model can be validated to a first approximation. The success of the model was tested using a combination of simple skill scores—how often the model correctly predicts the nightly presence of dewfall and its maximum amount (to within arbitrary bounds of ±0.02 and ±0.05 mm)—and several statistical descriptors: mean, standard deviation (SD), mean absolute difference (MD), root mean square difference (RMSD) and Willmott's index of agreement (ID) (Section A2.5). The numerical model predicts dewfall accumulation, and this is what the mini-lysimeter gives for each surface.

7.5 Results

Simulations were undertaken for selected nights from YD 154 to 196, 1996. Days were chosen to include a variety of weather conditions; days with missing input data or lacking suitable data to validate the model were excluded. Overall, the 'roof' model was run for 16 nights and the 'leaf' model for 8 nights. The latter simulation is

of smaller size because trees were present at M1 for only one of the possible two months of study. In the present study, measured data show that dew sometimes forms prior to 1900 LAT. However, tests indicate that it is appropriate to begin simulations at ~1900 LAT, because predicted dewfall events consistently began after this time.

7.5.1 Energy balances

Typical mean nightly values computed by the model for Q^*, Q_E, Q_H and, for the roof Q_G are summarised in Table 7.3, for the example of a night (YD 171/172) with favourable weather (clear with light winds) for dew. Derived values are the total dewfall accumulation (mm per night) and the mean $-Q_E$, (W m^{-2}) i.e., the average value of Q_E for periods only when its value is negative. For the roof, the mean Q_E for the entire night has a negative value, more dew is deposited than evaporates, and surface moisture is inferred to be present at dawn. Leaf surfaces, on the other hand, show an overall evaporative loss during the night. Condensation does occur. Dewfall is predicted on leaf surfaces (0.02 mm), but the gains are masked by the evapotranspiration losses predicted by the model. Results show that during conditions favourable for dew, Q_{Eq} potentially utilises about 0.30–0.50 of the net radiation, but the fraction of Q^* involved in actual dewfall is typically less. Here, 15 min mean values (not shown) for roof surfaces on YD 171/172 show Q_E to be about 0.50–0.80 of Q_{Eq}, and 0.15–0.30 of Q^* during periods of dewfall. These fractions approach zero when weather and/or surface conditions are unfavourable for dew, e.g., for maple leaves on this night.

Table 7.3 Energy balance components for a roof and leaf surfaces, as computed by the model, for the example of YD 171/172 with nocturnal weather favourable for dewfall (clear with light winds). Data are nightly mean (W m^{-2}) or nightly total (mm per night) values. Q_H is found by residual.

	Roof	**Maple leaf**
• *Energy Balance (W m^{-2})*		
Q^*	-74.4	-84.9
Q_H	61.2	50.8
Q_G	21.9	-
Q_E	-8.7	34.1
• *Derived terms*		
Mean $-Q_E$ (W m^{-2})	-24.0	-12.0
Dewfall (mm per night)	0.12	0.02

7.5.2 Predicted surface temperature

The model typically under-estimates roof temperature in the first hour or so of the simulation, sometimes by 6–10°C (see sequences in Figure 7.2). However, within an hour after sunset, predicted and observed surface temperatures converge, and similarity is often to within ±1–2°C. After sunrise, observed and predicted temperatures again diverge, with the model over-estimating surface temperature by perhaps 10°C by the time the dewfall predicted by the model dries. This suggests that the model may be able to predict nocturnal dewfall amount, but is perhaps less skillful at predicting time of onset and drying.

At night and during morning hours when dewfall is present, modelled and simulated tree leaf temperature are reasonably similar, but the model tends to under-estimate observed leaf temperature by ~1–3°C. Leaf temperature is very

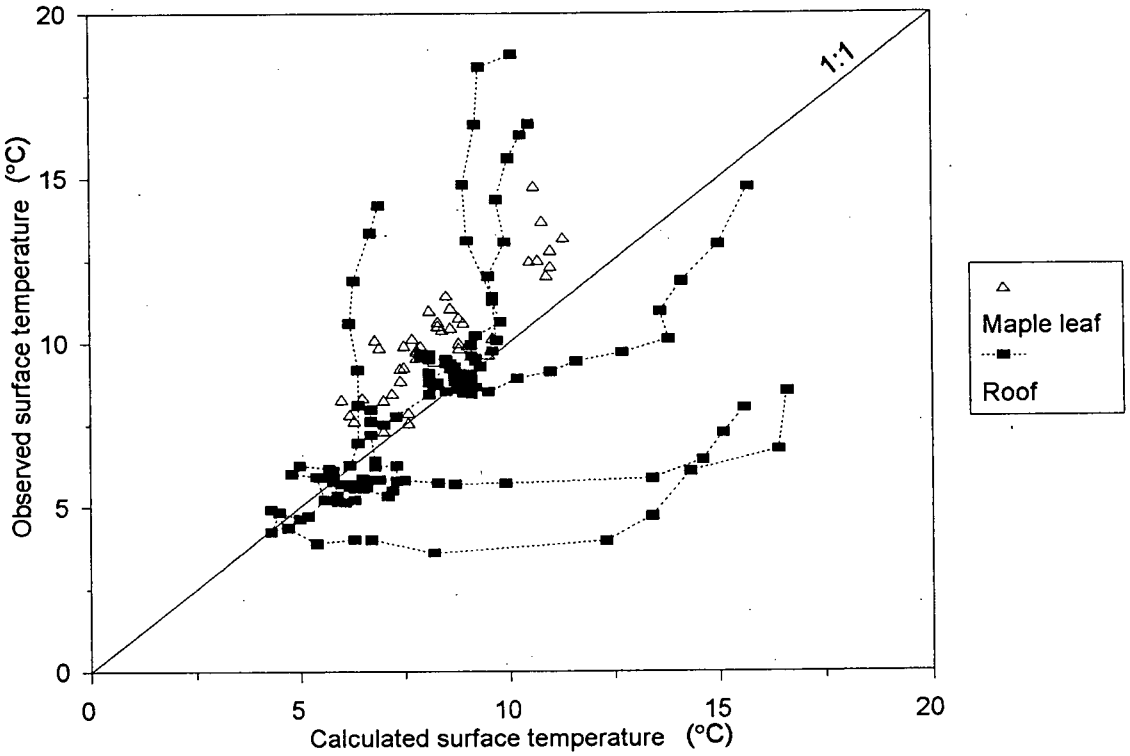

Figure 7.2 Agreement between observed and computed surface temperature for roof (■) and maple leaf (Δ) surfaces, for periods when the model predicts the presence of dewfall. Three days are shown (YD 163/164, 164/165 and 171/172). The dotted line indicates temporal sequences, and shows how the model under-estimates roof surface temperature in early evening and over-estimates this after sunrise.

difficult to measure with accuracy but, assuming the data here are reasonable, the model may tend to over-predict dewfall.

7.5.3 Simulation of dewfall for an asphalt shingle roof

The 'roof' model correctly predicts the presence of dewfall on the 13 nights when it occurred. It also correctly predicts its absence on two nights (Table 7.4 and Figure 7.3). On one night the model predicts a trace of dewfall (0.01 mm) when none is present. Thus, on presence-absence data alone, the model is successful 94% of the time. Since the expected frequency of events in each of the four possible categories of outcome—successfully predicting dewfall and also its absence, predicting dewfall when none was observed, and *vice versa*—is less than five for a data-set of <20, statistical tests such as the Chi-squared test cannot be used. However, the results appear to differ from those expected by chance alone, i.e., an even distribution of errors and successes.

Comparison of predicted and observed amounts (Table 7.4) shows that on 62% of nights (10 nights) predicted amounts are accurate to ±0.02 mm per night, compared to observed values, and on 81% of nights (13) estimates are accurate to ±0.05 mm per night. The latter error is exceeded on only three nights, when the model under-estimates the amount of dewfall by 0.06–0.10 mm. Absolute differences between the predicted and observed mean and SD values (Table 7.5) are small (≤0.01 mm), and the model yields a MD and RMSD of 0.03 and 0.04 mm, respectively. The ID value of 0.87 shows that the model predicts the maximum dewfall accumulation (mm) with a high level of skill.

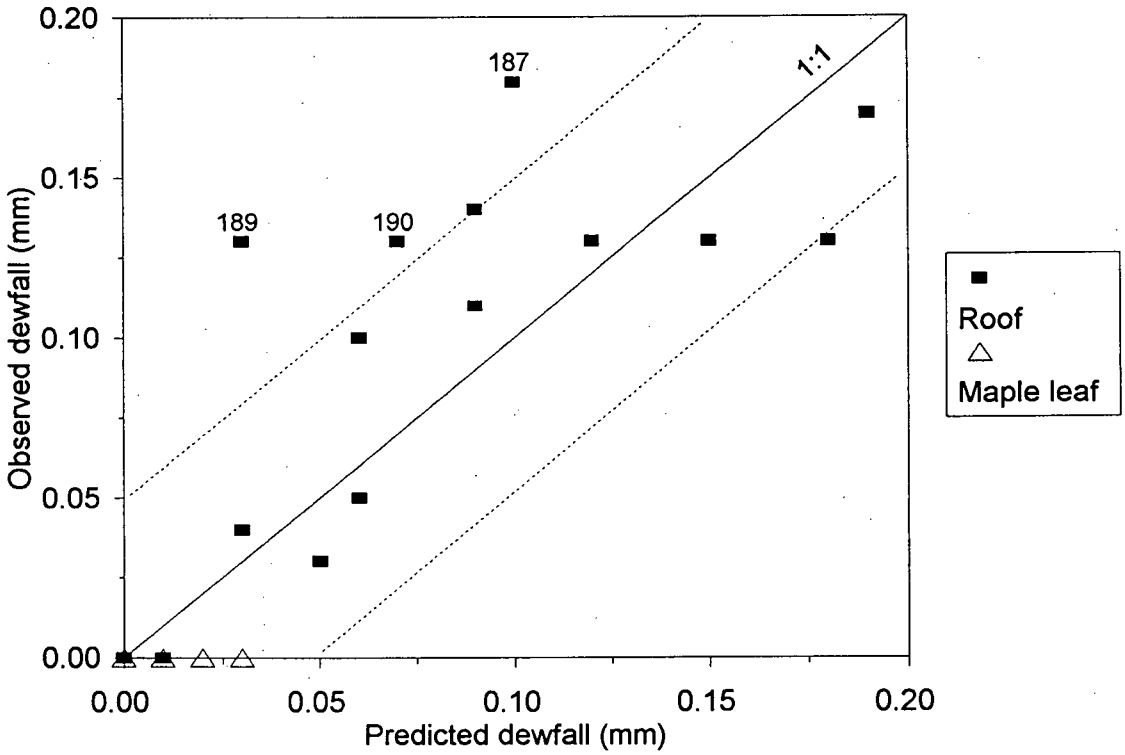

Figure 7.3 Agreement between the amount of dewfall predicted by the model and that measured, for a roof (■) and a maple leaf (Δ). Lines shown are for a 1:1 correlation (__) and its ±0.05 mm per night envelope (....). Outliers (labelled by YD) are discussed in the text. Note that some data points represent more than one outcome.

Table 7.4 Observed and predicted dewfall values (mm), and the difference ($\Delta E_{Pr\text{-}Ob}$) between these, for roof and leaf surfaces.

YD 1996	Roof simulations Obser. (mm)	Pred. (mm)	$\Delta E_{Pr\text{-}Ob}$ (mm)	Leaf simulations Obser. (mm)	Pred. (mm)	$\Delta E_{Pr\text{-}Ob}$ (mm)
155	0.00	0.01	0.01	0.00	0.00	0.00
158	0.00	0.00	0.00	0.00	0.00	0.00
159	0.10	0.06	-0.04	0.00	0.01	0.01
164	0.13	0.18	0.05	0.00	0.03	0.03
165	0.13	0.15	0.02	0.00	0.02	0.02
172	0.13	0.12	-0.01	0.00	0.02	0.02
173	0.04	0.03	-0.01	0.00	0.00	0.00
174	0.00	0.00	0.00	0.00	0.00	0.00
187	0.18	0.10	-0.08	-	-	-
188	0.11	0.09	-0.02	-	-	-
189	0.13	0.03	-0.10	-	-	-
190	0.13	0.07	-0.06	-	-	-
191	0.05	0.06	0.01	-	-	-
192	0.03	0.05	0.02	-	-	-
193	0.17	0.19	0.02	-	-	-
194	0.14	0.09	-0.05	-	-	-
195	-	-	-	-	-	-
196	-	-	-	-	-	-
Mean	0.09	0.08	-0.02	0.00	0.01	0.01
SD	0.06	0.06	0.04	0.00	0.01	0.01

Table 7.5 Summary of statistical indices used to test the skill of the 'roof' and 'leaf' dewfall models (see text for definitions).

	n (*d*)	**Predicted** *Mean* (mm)	*SD* (mm)	**Observed** *Mean* (mm)	*SD* (mm)	**MD** (mm)	**RMSD** (mm)	**ID**
Roof	16	0.08	0.06	0.09	0.06	0.03	0.04	0.87
Maple leaf	8	0.01	0.01	0.00	0.00	0.01	0.02	-

Examination of the 15 min data shows that at night the correspondence between the course of the predicted and observed amounts is remarkably good. This is especially true on clear, calm nights which are 'ideal' for dewfall accumulation, as illustrated in Figure 7.4. The model shows some skill in identifying the time of onset of dewfall, often to within ±1.0–2.0 h. Even better skill (±0.25–1.0 h) is shown in identifying the time of the daily dewfall maximum, which is typically seen soon after dawn, e.g., at 0515 h on YD 172 (Figure 7.4a). Good skill is also shown in detecting nocturnal points of inflection, when dewfall amount decreases for a short period, for example at 2200 h on YD 171.

The model shows little skill in simulating the course of daytime drying on the roof at M1. The model roof dries rapidly (in 1.0–1.5 h), and typically is dry 4.0–6.0 h, or even 11.0 h before the roof shingles at M1. The premature drying is almost exclusively a daytime feature, it is seen on only one occasion during night, and seems to be linked to the warmer-than-actual surface temperatures predicted by the model after dawn (Figure 7.2). It is possible that the error is caused by absolute differences between the modelled and observed environments. The modelled roof may, for example, have relatively less thermal inertia than that of the roof of the (scaled) house at M1. The latter is an integral part of a entire building, and this may inhibit the rate of warming of its roof after dawn. This would help to explain temperature patterns seen in Figure 7.2. Alternatively, the simulation may be poor because there is a surface resistance to evaporation present in reality for asphalt shingles, caused by water being absorbed by, or 'trapped' in crevices on shingles. Studies conducted in sand show that significant surface resistance is present when

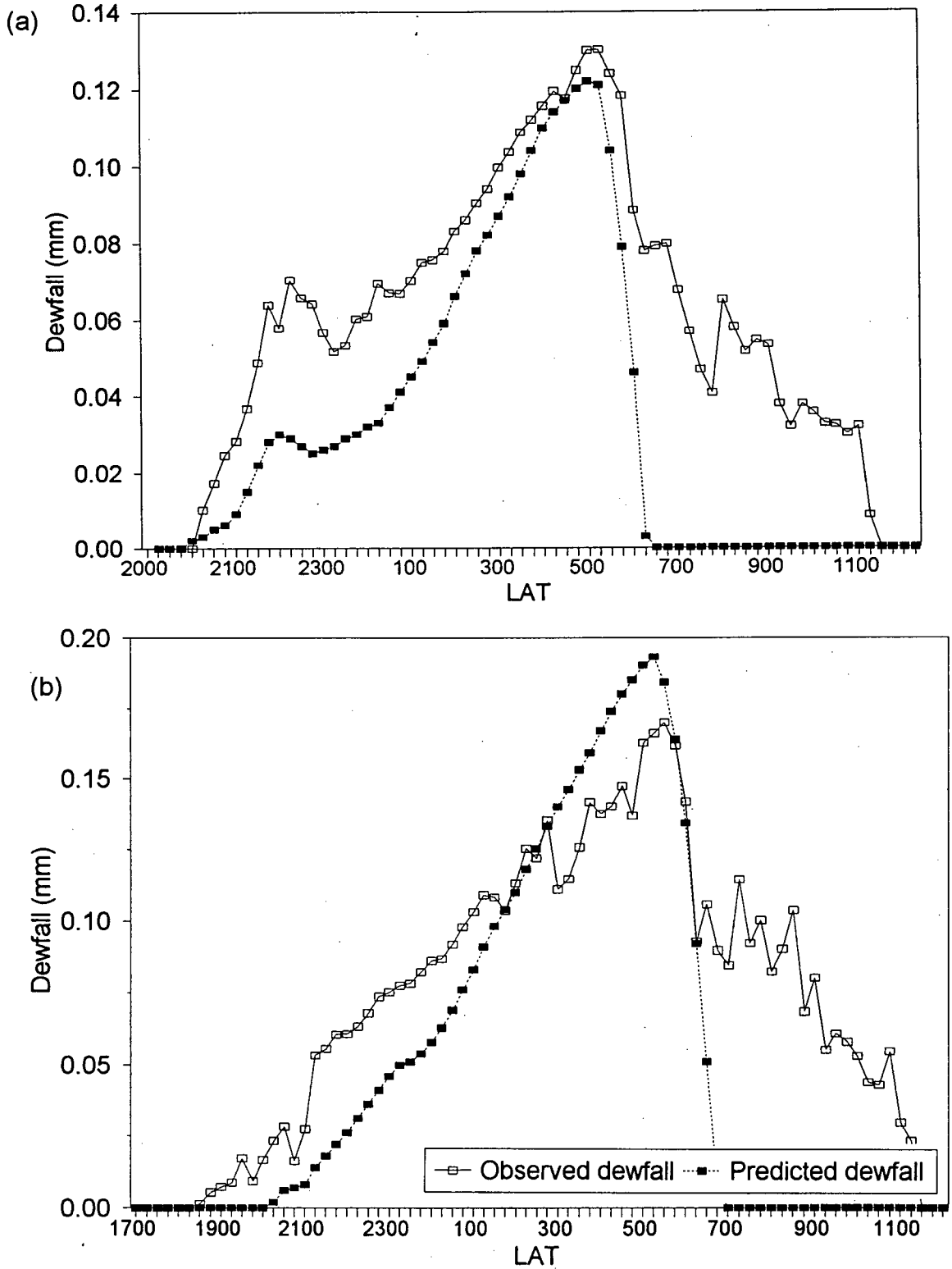

Figure 7.4 Examples of the agreement between the amount of dewfall predicted (■) by the model for a roof, and that measured (□) using a mini-lysimeter at M1, for (a) YD 171/172 and (b) 192/193, 1996.

dewfall is drying because some dewfall penetrates the surface, and that this resistance may exceed aerodynamic resistance (Jacobs *et al.,* 1998). By extension, an additional transfer coefficient may need to be considered, linked to the transfer of water to and from the roof materials. However, in general the error is non-critical because the primary aim of the model is to predict the maximum dewfall accumulation and its timing, tasks which the model does to a high level of skill.

7.5.4 Simulation of dewfall for a Japanese maple leaf

Accurate assessment of the skill of the 'leaf' model is difficult. At this site, no dewfall is evident in the measured data, and leaves were dry to the touch at dawn on each day studied. The model predicts small amounts (0.01–0.03 mm per night) of dewfall on four nights (Figure 7.3), for short periods (0.5–3.0 h). It is possible that dewfall was present in reality on some nights in small amounts which were not detected by the observations.

7.6 Summary

The numerical model shows skill in predicting dewfall accumulation on roof surfaces. Too few data were available to test the 'leaf' version. The main findings are summarised:

- During weather favourable for dew, Q_{Eq} potentially utilises 0.30–0.50 of the net radiation, but typically only 0.15–0.30Q^* is involved in dewfall, because Q_E tends to equal 0.50–0.80 Q_{Eq}.

- On average, the model under-estimates nocturnal surface temperature for maple leaves (by ~1–3°C). Nocturnal roof surface temperature is predicted to ±1–2°C, but the model consistently under-estimates this parameter around dusk, and over-estimates it after dawn, by up to 6–10°C.
- The presence-absence of dewfall on roof surfaces is successfully predicted on 94% of nights. Dewfall amount is successfully predicted on 62–81% of nights for the roof (to ±0.02 and ±0.05 mm per night, respectively).
- The skill of the model is confirmed by several statistical indices (see Table 7.5). For roof surfaces, absolute differences between predicted and observed values are small, and a high level of agreement exists for the sets (ID = 0.87).
- The model shows considerable skill in identifying the time of onset of dewfall (±1.0–2.0 h), and the amount and timing of its daily maximum, especially on the roof, but it cannot predict the time of drying.

These preliminary simulations suggest that it is feasible to model dewfall accumulation on urban surfaces using Pedro's approach, with modifications for building materials. The model seems robust. It performs well despite physical differences between, on the one hand the simple surfaces modelled, and on the other, the actual surfaces used to validate its results. The 'core' model is general and has potential to simulate dewfall to new materials (concrete, wood, metal) and sloped surfaces. More importantly, the model is technically a first step towards a more comprehensive model to predict urban dew.

North American urban residential landscapes are characterised by complicated three-dimensional mosaics of built materials and vegetation, whereas the model described here deals with only a few materials with very simple geometry and hydrology. Further, each surface is treated in isolation with the exception that, for leaves, reflected shortwave radiation ($\alpha_c a K_{in}$) is factored in. A more realistic urban model needs to address both the intrinsic characteristics of materials (as done here) and interactions caused by geometry and juxtaposition of surfaces and objects. When dewfall patterns on simple surfaces are integrated with a spatial model then realistic areal estimates of dewfall accumulation may be made.

A detailed model which incorporates a three-dimensional and patchy surface is beyond the scope of this thesis. One potential approach, however, is to grid the three-dimensional potentially active surface for dew accumulation, and to calculate E for each grid point (Fulton, *unpubl.*). An alternative may be to simulate dewfall accumulation along a vertical cross-section similar to that modelled in my hardware model (Chapters 4–6). Topics which such a model may need to address include:

- a wider range of built materials and vegetation types including grass,
- spatially complex view factors and longwave radiative exchange with surrounding objects (Pedro, 1980),
- Sun-Earth relations, site geometry and shading (Fulton, *unpubl.*),
- sloping surfaces, and effects on incident shortwave radiation,
- wind fields around buildings and trees,
- surface orientation with respect to wind direction and vapour sources,

- runoff of dew and the maximum holding capacity for the surface (Fulton, *unpubl.*), and
- distillation and guttation, which are potential sources of additional water on the surface (Equation 1.3).

Several of the effects in this list are independent of the presence of dew, and are governed by site geometry, surface temperature and radiation processes. Thus, an existing model to simulate urban surface conditions (temperature fields, incident short- and long-wave radiation) may prove to be a suitable candidate on which to base an urban dew model. Regardless, the simple model presented here is a good first step towards a more comprehensive model to predict spatial and temporal patterns of dew in urban environments.

PART IV CONCLUSION

Chapter 8: A measurement protocol and conclusions

8.1 Summary

The overall objectives of the thesis were to investigate methods appropriate to measuring dew in urban environments, to implement these for a particular urban area, and to investigate the feasibility of modelling urban dew. These goals were implemented using observational surveys of surface and near-surface moisture and temperature conditions in Vancouver, and by developing and testing a scale model and a numerical model to predict moisture accumulation on a range of surface materials in a generic urban environment. Much of the work is exploratory because there has been very little previous research on urban dew, methods to measure dew are not standardised, and there are no existing hardware or numerical models to predict urban dew.

In this chapter, a protocol for measuring surface moisture and dewfall in urban environments is presented in Section 8.2, the main findings of the thesis are summarised in Section 8.3, and Section 8.4 contains suggestions for future work.

8.2 A protocol for measuring urban surface wetness

The accumulation of surface moisture at urban sites cannot be measured using standard weather station equipment, nor using micro-meteorological techniques such as eddy correlation, flux-profile and energy balance-Bowen ratio approaches. An exception is mini-lysimetry but this measures only the dewfall component of surface moisture, and installation may not always be practical. Even at rural sites

where there is a long history of research on dew, there is no universal protocol for measuring surface moisture.

The observational exercises undertaken in the present study at the full-scale and in the hardware model aided the development of a set of practical guidelines—a measurement protocol—for use in studies of surface moisture conditions in urban environments. It is forwarded that an observational programme should include:

- visual and/or tactile assessment to confirm the presence of surface moisture and times of onset and drying,
- blotting to measure the total amount of surface moisture accumulated on grass, using a standardised method such as that described in Section A1.3,
- electronic wetness sensors to record the duration of surface moisture,
- electronic weighing mini-lysimeters to measure dewfall accumulation on built and grassed surfaces, and
- local hourly precipitation and wind speed data to identify periods of rain wetting and windiness.

For more simple studies, a researcher may wish to reduce this array of methods and instruments. This may result in loss of information and/or ambiguity in the data, but ultimately the suite of methods chosen must reflect the observational objectives, i.e., whether wetness duration, surface moisture amount, or solely dewfall is the parameter of interest.

It is often useful to measure more than one surface moisture parameter, but measured parameters (surface moisture duration and/or amount, and dewfall duration and/or amount) cannot be directly compared, because they sense different

phenomena. Care is needed to ensure that the surface water which is measured is correctly identified. Terms such as 'dew' must be used with precision and it is strongly suggested that carefully defined, unambiguous terms such as 'dewfall', 'distillation' and 'surface moisture' be adopted.

8.3 Conclusions

Individual chapters provide detailed summaries of findings from the present study. These include conclusions from the surveys of moisture and temperature conditions at the full-scale in Vancouver and its rural surrounds; surveys of surface moisture and temperature conditions in a scaled, generic urban environment (the scale model); and results from the numerical model to predict dew on urban surfaces. In view of the overall objectives of the present study (Chapter 1), the main conclusions of this thesis are as follows:

- urban environments are spatially complex and this creates complicated patterns of surface moisture and dewfall. This leads to different issues of interest in cities compared to rural sites, such as spatial inhomogeneity of dew at dawn, but the underlying processes are the same everywhere and patterns are therefore potentially predictable,
- certain methods used at rural sites to measure surface moisture and dewfall can be transferred to urban sites: wetness sensors, mini-lysimeters and blotting,
- at the meso-scale, spatial contrasts in canopy layer conditions (T_a, ρ_v, ρ_{vd}) at rural and urban sites are most evident on clear nights with light winds which

favour longwave radiative cooling at the surface. On such nights, urban residential sites are warmer, more moist, but have higher ρ_{vd}, compared to the surrounding countryside. In Vancouver during summer urban dew seems to be as frequent as rural dew but accumulation on grass at urban sites tends to be less than that at rural sites on the same night. On the other hand, urban roofs may rival rural grassed surfaces as favoured locations for dewfall accumulation,

- at the micro-scale, surface moisture amount at urban sites is controlled by weather, substrate type, position relative to potential sources of sensible heat (Q_G and Q_F), and site geometry expressed as Ψ_{sky}. The latter relates to the effect of horizon obstruction on the net longwave radiation balance of the surface. It is useful to express the combined effects of cloud and wind as Φ_W, but high vapour density deficits may also need to be taken into account,
- surface moisture and temperature conditions in the scale model are similar to those seen at the full-scale for sites with approximately similar configuration and ambient weather conditions. Thus, the scale model fulfills its initial goal to mimic the surface temperatures seen at the full-scale. This shows that the Internal Thermal Mass (ITM) approach to scaling is useful for modelling patterns of dew deposition as well as nocturnal surface temperature,
- observations in the scale model show the main controls on surface moisture and dewfall to be weather, substrate type, sources of sensible heat (Q_G), and site geometry expressed as view factor (Ψ). Guttation is another source of water on grass. In general, preferred sites for surface moisture accumulation

are on grass at open sites and roofs which cool rapidly after sunset. Moisture accumulation may be absent on relatively warm surfaces such as pavement and tree leaves, and

- numerical modelling appears to be a feasible method to predict dewfall on urban surfaces possessing simple geometry. This approach has potential to be expanded to include more surfaces and different configurations.

8.4 Suggestions for future research

The results of this thesis indicate the potential for further research in several areas. There remains a clear need for observations of dew in cities and their rural surrounds. The observations in Vancouver should be replicated elsewhere and observations should be expanded to include new surfaces and seasons. The feasibility of using the weather factor, Φ_W, to predict dew in the city could be investigated further. The success of the hardware model suggests that further scale modelling could be used to experiment with different site configurations and building materials. The exploratory numerical modelling shows that it is feasible to simulate dew on urban materials using an approach adapted from rural research. The model could be extended to include more realistic surface configurations, interaction between surfaces and a wider range of materials (see Section 7.6). Existing models of, for example, shortwave radiation loading, could be incorporated into the new model. Alternatively, the model could be tailored to become a subroutine in an existing model to predict urban evaporation or temperature.

REFERENCES

Ackerman, B. 1987: Notes. Climatology of Chicago area urban-rural differences in humidity. *Journal of Climate and Applied Meteorology* **26**: 427–430.

Aida, M. 1982: Urban albedo as a function of the urban structure. A model experiment (Part I). *Boundary-Layer Meteorology* **23**: 405–413.

Angus, D.E. 1958: Measurements of dew. *Proceedings of the Canberrra Symposium of Climatology and Micrometeorology, UNESCO Arid Zone Research* **2**: 301–303.

Anon. 1993: Environmental Matters. Plastic Forests. *Reader's Digest* (New Zealand), Auckland. June: 157.

Anon. 1995: A brush with a lawn. *Country Living*: 64–65.

Arends, B.G. and Eenkhoorn, S. 1989: The influence of manganese on the oxidation of sulfite in dew water. In Georgii, H.-W. (ed.). 1989: *Mechanisms and Effects of Pollutant-transfer into Forests.* Kluwer Academic Publishers, Dordrecht: 231–238.

Ari, N.N., Zangvil, A. and Berliner, P.R. 1998: The contribution of dew to the water balance of bare soil in a desert area. *Proceedings of the Conference on Fog and Fog Collection.* Vancouver, Canada, 19-24 July, 1998: 265–268.

Arnfield, A.J. 1976: Numerical modelling of urban surface radiative parameters. In Davies, J.A. (ed.). 1976: *Papers in Climatology: The Cam Allen Memorial Volume.* Department of Geography, McMaster University: 1–28.

ASHRAE 1993: *1993 ASHRAE Fundamentals Handbook, SI Edition.* American Society of Heating, Refrigeration and Air-Conditioning Engineers, Atlanta.

Atkinson, B.W. 1985: *Update. The Urban Atmosphere.* Cambridge University Press, Cambridge.

Baier, W. 1966: Studies on dew formation under semi-arid conditions. *Agricultural Meteorology* **3**: 103–112.

Barozzi, G.S., Imbabi, M.S.E., Nobile, E., and Sousa, A.C.M. 1992: Physical and numerical modelling of a solar chimney-based ventilation system for buildings. *Building and Environment* **27**: 433–445.

Barr, A.G. and Brown, D.M. 1995: Estimating forage yield and quality changes during field drying for hay. 2. Model of forage drying. *Agricultural and Forest Meteorology* **76**: 107–127.

Bornstein, R.D., Lorenzen, H. and Johnson, D. 1972: Recent observations of urban effects on wind and temperatures in and around New York City. *Preprints of the Conference on Urban Environment, 2nd Conference Biometeorology, American Meteorology Society*: 28–33.

Bourque, C.P.-A. and Arp, P.A. 1994: Dawn-to-dusk evolution of air turbulence, temperature and sensible and latent heat fluxes above a forest canopy: Concepts, model and field comparisons. *Atmosphere-Ocean* **32**: 299–334.

Brimblecombe, P. 1978: "Dew" as a sink for sulphur dioxide. *Tellus* **30**: 151–157.

Brimblecombe, P. and Todd, I.J. 1977: Short communications. Sodium and potassium in dew. *Atmospheric Environment* **11**: 649–650.

Brooks, F.A. and Pruitt, W.O. 1966: *Investigation of Energy, Momentum and Mass Transfers Near the Ground.* Final Report 1965, June 1966. USAECASL Contract No. DA-AMC-28-043-65-G12. University of California, Davis, California.

Budagovskii, A.I. and Nasonova, O.N. 1991: The role of condensation in the soil water balance. *Soviet Meteorology and Hydrology* **9**: 72–78.

Buiuc, M. 1990: Estimări ale depunerilor de rouă în România. *Studii şi Cercetări Meteorologie (Bucharest)* **4**: 107–120.

Burrage, S.W. 1972: Dew on wheat. *Agricultural Meteorology* **10**: 3–12.

Butler, D.R. 1980: Dew and thermal lag: Measurements and an estimate of wetness duration on cocoa pods. *Quarterly Journal of the Royal Meteorological Society* **106**: 539–550.

Campbell, D. 1994: Letter to author. June 1994.

Campbell, G.S. 1977: *An Introduction to Environmental Physics.* Springer-Verlag, New York.

Chameides, W.L. 1987: Acid dew and the role of chemistry in the dry deposition of reactive gases to wetted surfaces. *Journal of Geophysical Research* **92**: 11895–11908.

Chandler, T.J. 1967: Absolute and relative humidities in towns. *Bulletin of the American Meteorological Society* **48**: 394–399.

Chapman, A.J. 1984: *Heat Transfer.* Macmillan, New York.

Chen, W.J. and Novak, M.D. 1997: An improved tension-plate system for measuring first-stage evaporation under straw mulch. *Agricultural and Forest Meteorology* **85**: 1–17.

Chowdhury, A., Idas, H.P., and Mukhopadhyay, R.K. 1990: Distribution of dew and its importance in moisture balance for rabi crops in India. *Mausam* **41**: 547–554.

Cleugh, H. and Oke, T.R. 1986: Suburban-rural energy balance comparisons in summer for Vancouver, B.C. *Boundary-Layer Meteorology* **36**: 351–369.

Collins, B.G. 1961: A standing dew meter. *Meteorological Magazine* **90**: 114–117.

Collins, B.G. and Taylor, R.J. 1961: Conditions governing the onset of dew on large leaves. *Australian Journal of Applied Science* **12**: 23–29.

Corliss, W.R. 1984: *Rare Halos, Mirages, Anomalous Rainbows and Related Electromagnetic Phenomena. A Catalog of Geophysical Anomalies.* The Sourcebook Project, Glen Arm, MD.

Crowe, M.J., Coakley, S.M. and Emge, R.G. 1978: Forecasting dew duration at Pendleton, Oregon, using simple weather observations. *Journal of Applied Meteorology* **17**: 1482–1487.

Cuesta Santos, O., González González, M. and Ananias Degado, G. 1990: Comunicaciones Breves. El rocío en Casablanca y su relación con la contaminación atmosférica. *Revista Cubana de Meteorologia* **3**: 101–104.

Daamen, C.C., Simmonds, L.P., Wallace, J.S., Laryea, K.B. and Sivakumar, M.V.K. 1993: Use of microlysimeters to measure evaporation from sandy soils. *Agricultural and Forest Meteorology* **65**: 159–173.

Davis, M.L. and Pearson, J.E. 1970: Modeling urban atmospheric temperature profiles. *Atmospheric Environment* **4**: 277–288.

Dirks, R.A. 1974: Urban atmosphere: warm dry envelope over St. Louis. *Journal of Geophysical Research* **79**: 3473–3475.

Douglas, I. 1983: *The Urban Environment.* Edward Arnold, London.

Dröscher, F., Nickel, J. and Mikisch, E. 1989: Measurement of dew and fogwater deposition in forest stands. In Georgii, H.-W. (ed.). 1989: *Mechanisms and Effects of Pollutant-transfer into Forests.* Kluwer Academic Publishers, Dordrecht: 239–247.

Dzurisin, G. 1978: Average dew points. *Summary of METROMEX, Volume 2, Illinois State Water Survey Bulletin* **63**: 43–62.

Eckert, E.R.G. and Drake, R.M. 1972: *Analysis of Heat and Mass Transfer.* McGraw-Hill Book Company, New York.

Ede, A.J. 1967: *An Introduction to Heat Transfer Principles and Calculations.* Pergamon Press, London.

Eliasson, I. 1990/91: Urban geometry, surface temperature and air temperature. *Energy and Buildings* **15-16**: 141–145.

Eliasson, I. 1992: Infrared thermography and urban temperature patterns. *International Journal of Remote Sensing* **13**: 869–879.

Eliasson, I. and Holmer, B. 1996: Urban-rural vapour pressure differences and the urban heat island formation. *Preprints International Conference on Urban Climatology.* June 10-14, 1996, Essen: 16–17.

Fitzharris, B.B. 1998: Conversation with author. July, 1998. University of Otago, Dunedin.

Fowler, D. 1980: Removal of sulphur and nitrogen compounds from the atmosphere in rain and by dry deposition. In Drablos, D. and Tollan, A. (eds.). 1980: *Ecological Impact of Acid Precipitation.* The Norwegian Interdisciplinary Research Programme, Oslo: 22–32.

Fowler, D. 1992: Air pollution transport, deposition, and exposure to ecosystems. In Barker, J.R. and Tingey, D.T. (eds.). 1992: *Air Pollution Effects on Biodiversity.* Van Nostrand Reinhold, New York: 31–51.

Fraser, A.B. 1994: The sylvanshine: Retroreflection from dew-covered trees. *Applied Optics* **33**: 4539–4547.

Fritschen, L.J. and Doraiswamy, P. 1973: Dew: An addition to the hydrological balance of a Douglas fir. *Water Resources Research* **9**: 891–894.

Fuentes, J.D. and Gillespie, T.J. 1992: A gas exchange system to study the effects of leaf surface wetness on the deposition of ozone. *Atmospheric Environment* **26A**: 1165–1173.

Fulton, D. Unpublished: Prediction of potential for disease of turfgrass shaded by trees. University of Guelph, Guelph. 15pp.

Garrard, S. and Griffiths, J.F. 1996: Preliminary results on the forecast of dew. *Preprints 22nd Conference on Agricultural and Forest Meteorology.* Atlanta, Georgia, Jan 28-Feb 2 1996: 373–375.

Garratt, J.R. 1992: *The Atmospheric Boundary Layer.* Cambridge University Press, Cambridge.

Garratt, J.R. and Segal, M. 1988: On the contribution of atmospheric moisture to dew formation. *Boundary-Layer Meteorology* **45**: 209–236.

Getz, R.R. 1978: Dew-monitoring network in the Southeast. *Bulletin American Meteorology Society* **5**: 1150–1158.

Getz, R.R. and Harker, K.S. 1996: An approach for modeling leaf wetness. *Preprints 22nd Conference on Agricultural and Forest Meteorology.* Atlanta, Georgia, Jan 28-Feb 2 1996: 373–375.

Gillespie, T.J. and Barr, A. 1984: Adaptation of a dew estimation scheme to a new crop and site. *Agricultural and Forest Meteorology* **31**: 289–295.

Gillespie, T.J. and Duan, R.-X. 1987: A comparison of cylindrical and flat plate sensors for surface wetness duration. *Agricultural and Forest Meteorology* **40**: 61–70.

Goldreich, Y. 1974: Observations on the urban humidity island of Johannesburg. *Israel Journal of Earth Science* **23**: 39–46.

Grimmond, C.S.B. 1983: The suburban water balance: Daily, monthly and annual results from Vancouver, B.C. M.Sc. thesis. University of British Columbia, Vancouver.

Grimmond, C.S.B. 1988: An Evapotranspiration-interception Model for Urban Areas. Ph.D. thesis. University of British Columbia, Vancouver.

Grimmond, C.S.B. and Oke, T.R. 1991: An evapotranspiration-interception model for urban areas. *Water Resources Research* **27**: 1739–1755.

Grimmond, C.S.B. and Oke, T.R. 1995: Comparison of heat fluxes from summertime observations in the suburbs of four North American cities. *Journal of Applied Meteorology* **34**: 873–889.

Grimmond, C.S.B., Isard, S.A. and Belding, M.J. 1992: Development and evaluation of continuously weighing mini-lysimeters. *Agricultural and Forest Meteorology* **62**: 205–218.

Hage, K.D. 1975: Urban-rural humidity differences. *Journal of Applied Meteorology* **14**: 1277–1283.

Haines, D.A. 1979: Dew measurement and forest fuels. *Preprints 14th Conference on Agriculture and Forest Meteorology and 4th Conference on Biometeorology.* Minneapolis, MINN., April 2-6, 1979: 25–29.

Haines, D.A. 1980: The adjective classification for dew: What does it mean? *National Weather Digest* **5**: 47–50.

Hall, C. and Kalimeris, A.N. 1984: Rain absorption and runoff on porous building surfaces. *Canadian Journal of Civil Engineering* **11**:108–111.

Harter, P. 1986: *Acidic Deposition—Materials and Health Effects.* ICTIS/TR36. IEA Coal Research, London.

Heusinkveld, B.G., Jacobs, A.F.G. and Berkowicz, S. 1998: Dew and dew collection in the Negev desert. *Proceedings of the Conference on Fog and Fog Collection.* Vancouver, Canada, 19-24 July, 1998: 257–260.

Hewson, T.D. and Gait, N.J. 1992: Hoar-frost deposition on roads. *The Meteorological Magazine* **121**: 1–21.

Hicks, B.B. 1981: *An analysis of Wangara micrometeorology: Surface stress, sensible heat, evaporation, and dewfall.* NOAA Technical Memorandum ERL ARL-104. NOAA/ERL Air Resources Laboratory, Maryland.

Hilberg, S.D. 1978: Diurnal temperature and moisture cycles. *Summary of METROMEX, Volume 2, Illinois State Water Survey Bulletin* **63**: 25–42.

Hofmann, G. 1955: Zur thermodynamik der taubildung. *Ber. dtsch. Wetterdienstes* **3.** Cited in Geiger, R. 1965: Harvard University Press, Cambridge, Massachusetts.

Holtslag, A.A.M. and de Bruin, H.A.R. 1988: Applied modeling of the nighttime surface energy balance over land. *Journal of Applied Meteorology* **27**: 689–704.

Hoogenboom, G. 1996: The Georgia automated environmental monitoring network. *Preprints 22nd Conference of Agricultural and Forest Meteorology*: 343–346.

Howell, J.R. 1982: *A Catalog of Radiation Configuration Factors.* McGraw-Hill, New York.

Hoydysh, W.G. and Dabberdt, W.F. 1988: Kinematics and dispersion characteristics of flows in asymmetric street canyons. *Atmospheric Environment* **22**: 2677–2689.

Hsu, S.-H. and Sakanoue, T. 1980: Studies on dew.I. On the dewy time and dew amount in southwest area of Taiwan. *Journal of Agricultural Meteorology (Tokyo)* **36**: 95–101.

Huber, L. and Gillespie, T.J. 1992: Modelling leaf wetness in relation to plant disease epidemiology. *Annual Review Phytopathology* **30**: 553–577.

Hughes, R.N. and Brimblecombe, P. 1994: Dew and guttation: Formation and environmental significance. *Agricultural and Forest Meteorology* **67**:173–190.

Hutorowicz, H. 1981: Próba oszacowania wysokości osadu rosy na podstawie temperatury powietrza przy powierzchni gruntu, zachmurzenia i predkości wiatru. *Przeglad Geofizyczny, Warsaw*, **26**: 189–193.

Imbabi, M.S. 1990a: A general procedure for the small-scale modelling of buildings. *International Journal of Energy Research* **14**: 311–321.

Imbabi, M.S. 1990b: Computer validation of scale model tests for building energy simulation. *International Journal of Energy Research* **14**: 727–736.

Imbabi, M.S. 1991: Scale modelling of the built environment. *Energy and Building* **17**: 7–12.

Jacobs, A.F.G., Heusinkveld, B.G. and Berkowicz, S. 1998: Dew deposition in the Negev desert: The biological crust. *Proceedings of the Conference on Fog and Fog Collection.* Vancouver, Canada, 19-24 July, 1998: 261–264.

Jacobs, A.F.G., van Pul, A. and El-Kilani, R.M.M. 1994: Dew formation and the drying process within a maize canopy. *Boundary Layer Meteorology* **69**: 367–378.

Jacobs, A.F.G., van Pul, W.A.J. and van Dijken, A. 1990: Similarity moisture dew profiles within a corn canopy. *Journal of Applied Meteorology* **29**: 1300–1306.

Janssen, L.H.J.M. and Römer, F.G. 1991: The frequency and duration of dew occurrences over a year. *Tellus* **43B**: 408–419.

Johnson, S. 1964: *Gay Bulgaria*. The Travel Book Club, London.

Jones, A.L. 1986: Role of wet periods in predicting foliar diseases. In Leonard, K.J. and Fry, W.E. (ed.). 1986: *Plant Disease Epidemiology.* Collier MacMillan, New York: 87–100.

Jumikis, A.R. 1965: Aerial wells: Secondary sources of water. *Soil Science* **100**: 83–95.

Kerr, J. P. and Beardsell, M. F. 1975: Effect of dew on leaf water potentials and crop resistances in a paspalum pasture. *Agronomy Journal* **67**: 596–599.

Kopec, R.J. 1973: Daily spatial and secular variations of atmospheric humidity in a small city. *Journal of Applied Meteorology* **12**: 639–648.

Kratzer, A. 1956: *Das Stadklima*. Die Wissenschaft, 90. Vieweg and Sohn, Braunschweig. Cited in Geiger, R. 1965: *The Climate Near the Ground*. Harvard University Press, Cambridge, Massachusetts.

Kreith, F. and Black, W.Z. 1980: *Basic Heat Transfer*. Harper and Row Publishers, New York.

Landsberg, H.E. 1981: *The Urban Climate*. Academic Press, New York.

Landsberg, H.E. and Maisel, T.N. 1972: Micrometeorological observations in an area of urban growth. *Boundary-Layer Meteorology* **2**: 365–370.

Lee, D.O. 1991: Urban-rural humidity differences in London. *International Journal of Climatology* **11**: 577–582.

Lettau, H.H. 1967: Problems of micrometeorological measurements. In Bradley, E.F. and Denmead, O.T. (eds.). 1967: *The Collection and Processing of Field Data*. Wiley-Interscience, New York: 3–40.

Lloyd, M.G. 1961: The contribution of dew to the summer water budget of Northern Idaho. *Bulletin of the American Meteorological Society* **42**: 572–580.

Lowe, P.R. 1977: Notes and correspondence. An approximating polynomial for the computation of saturation vapor pressure. *Journal of Applied Meteorology* **16**: 100–103.

Lowry, W.P. 1977: Empirical estimation of urban effects on climate: A problem analysis. *Journal of Applied Meteorology* **16**: 129–135.

Malek, E. 1998: Detecting and quantifying dew in semi-arid irrigated and desert valleys. *Proceedings of the Conference on Fog and Fog Collection*. Vancouver, Canada, 19-24 July, 1998: 253–256.

Marlatt, W.E. 1971: Short Communication. A note on the variation of dew amount with elevation. *Agricultural Meteorology* **8**: 151–154.

Mattsson, J.O. 1962: A simple dew recorder. *Weather* **17**: 268–272.

Mattsson, J.O. 1971: Dagg som klimatindikator. *Svensk Geografisk Årsbok* **47**: 29–52.

Mattsson, J.O. 1979: *Introduktion till mikro-och lokalklimatologin*. Liber Läromedel, Malmö.

Mattsson, J.O. 1998: Letter to T.R. Oke and author. 2 Jan, 1998.

Mattsson, J.O. and Cavallin, C. 1972: Retroreflection of light from drop-covered surfaces and an image-producing device for registration of this light. *Oikos* **23**: 285–294.

Mattsson, J.O., Nordbeck, S. and Rystedt, B. 1971*: Dewbows and fogbows in divergent light.* Lund Studies in Geography, Series C, No.11. Royal University of Lund, Sweden.

McAdams, W.H. 1954: *Heat Transmission.* McGraw-Hill, New York.

McAneney, K.J., Prendergast, P.T., Judd, M.J. and Green, A.E. 1992: Observations of equilibrium evaporation from a windbreak-sheltered kiwifruit orchard. *Agricultural and Forest Meteorology* **57**: 253–264.

McClean, M.A. 1993: The evaluation and modification of a prediction model for road surface temperatures. M.Sc. thesis. University of British Columbia.

McCowan, R.L. and Wall, B.H. 1981: The influence of weather on the quality of tropical legume pasture during the dry season in Northern Australia. II. Moulding of standing hay in relation to rain and dew. *Australian Journal of Agricultural Research* **32**: 589–598.

McPherson, E.G. 1980: The Use of Plant Materials for Solar Control. Master of Landscape Architecture thesis. Utah State University, Utah.

McPherson, E.G., Simpson, J.R., and Livingston, M. 1989: Effects of three landscape treatments on residential energy and water use in Tucson, Arizona. *Energy and Buildings* **13**: 127–138.

Mills, G. 1997: Letter to author. 7 May, 1997.

Mintah, C.N. 1977: A numerical model to estimate leaf wetness duration. M.Sc. thesis. University of Guelph, Guelph.

Monteith, J.L. 1957: Dew. *Quarterly Journal of the Royal Meteorological Society* **83**: 322–341.

Monteith, J.L. 1963: Dew: Facts and fallacies. In Rutter, A.J. and Whitehead, F.H. (eds.). 1963: *The Water Relations of Plants.* John Wiley and Sons, New York: 37–56.

Monteith, J.L. and Butler, D.R. 1979: Dew and thermal lag: a model for cocoa pods. *Quarterly Journal of the Royal Meteorological Society* **105**: 207–215.

Monteith, J.L. and Unsworth, M.H. 1990: *Principles of Environmental Physics.* Edward Arnold, London.

Moomen, S.E. and Barney, C.W. 1981: A modern technique to halt desertification in the Libyan Jamahiriya. *Agricultural Meteorology* **23**: 131–136.

Mooney, H.A., Gulmon, S.L., Ehleringer, J. and Rundel, P.W. 1980: Reports. Atmospheric water uptake by an Atacama Desert shrub. *Science* **209**: 693–694.

Mulawa, P.A., Cadle, S.H., Lipari, F., Ang, C.C. and Vandervennet, R.T. 1986: Urban dew: Its composition and influence on dry deposition rates. *Atmospheric Environment* **20**: 1389–1396.

Myers, T. M. 1974: Dew as a visual indicator of the urban heat island of Washington, D.C. M.Sc. thesis. University of Maryland, Maryland.

Myers, T.M. 1997: Letter to author. 25 June, 1997.

Nagel, J.F. 1962: On the measurement of dew. *Archiv für Meteorologie, Geophysik und Bioklimatologie, Serie B* **11**: 403–423.

Nakamura, Y. and Oke, T.R. 1988: Wind, temperature and stability conditions in an east-west orientated urban canyon. *Atmospheric Environment* **22**: 2691–2700.

Newton, O.H. and Riley, J.A. 1964: Dew in the Mississippi Delta in the fall. *Monthly Weather Review* **92**: 369–373.

Nikolayev, V.S., Beysens, D., Gioda, A., Milimouk, I., Katiushin, E. and Morel, J.-P., 1996: Water recovery from dew. *Journal of Hydrology* **182**: 19–35.

Noffsinger, T.L. 1965: Survey of techniques for measuring dew. In Wexler, A. (ed.). 1965: *Humidity and Moisture Control in Science and Industry*. Reinhold, New York: 523–530.

Nunez, M. 1974: The energy balance of an urban canyon. Ph.D. thesis. University of British Columbia, Vancouver.

Oke T.R. 1987: *Boundary Layer Climates*. Routledge, London.

Oke, T.R. 1974: *Review of Urban Climatology 1968-1973*. WMO publication No. 383, Technical Note No. 134. World Meteorological Organization, Geneva.

Oke, T.R. 1979: *Review of Urban Climatology 1973-1976*. WMO publication No. 539, Technical Note No. 169. World Meteorological Organization, Geneva.

Oke, T.R. 1981: Canyon geometry and the nocturnal urban heat island: comparison of scale model and field observations. *Journal of Climatology* **1**: 237–254.

Oke, T.R. 1982: The energetic basis of the urban heat island. *Quarterly Journal of the Royal Society* **108**: 1–24.

Oke, T.R. 1988: The urban energy balance. *Progress in Physical Geography* **12**: 471–508.

Oke, T.R. 1992: Conversation with author. January 1992. University of British Columbia, Vancouver.

Oke, T.R. 1998: An algorithmic scheme to estimate hourly heat island magnitude. *Preprints 2nd Urban Environment Symposium.* Albuquerque, New Mexico: Paper 6.1.

Oke, T.R. 1998: Conversation with author. November, 1998.

Oke, T.R. and Hay, J. 1994: *The Climate of Vancouver.* (2nd edition). B.C. Geographical Series, No. 50. University of British Columbia, Vancouver.

Oke, T.R. and Maxwell, G.B. 1975: Urban heat island dynamics in Montreal and Vancouver. *Atmospheric Environment* **9**: 191–200.

Oke, T.R., Grimmond, C.S.B. and Spronken-Smith, R.A. 1998: On the confounding role of rural wetness in assessing urban effects on climate. *Preprints 2nd Urban Environment Symposium.* Albuquerque, New Mexico: Paper 5.1.

Okochi, H., Takeuchi, M. and Igawa, M. 1998: Effect of acid deposition on urban dew chemistry in Yokohama, Japan. *Proceedings of the Conference on Fog and Fog Collection.* Vancouver, Canada, 19-24 July, 1998: 301–304.

Padmanabhamurty, B. and Subrahmanyam, V.P. 1960: Dew observations at Waltair. *Journal of Scientific and Industrial Research* **19A**: 82–84.

Padro, J. 1994: Observed characteristics of the dry deposition velocity of O_3 and SO_2 above a wet deciduous forest. *The Science of the Total Environment* **146/147**: 395–400.

Parczewski, K.I. and Renzi, P.N. 1963: Scale model studies of temperature distributions in internally heated enclosures. Technical Paper. *ASHRAE Journal* **5**: 60–68.

Parkhurst, D.F., Duncan, P.R., Gates, D.M. and Kreith, F. 1968: Wind-tunnel modelling of convection of heat between air and broad leaves of plants. *Agricultural Meteorology* **5**: 33–47.

Parks, N. 1996: Bounty from the sea. *Earth. The Science of Our Planet* **5**: 50–55.

Pedro, M.J. 1980: Relation of leaf surface wetness duration to meteorological parameters. Ph.D. thesis. University of Guelph, Guelph.

Pedro, M.J. and Gillespie, T.J. 1982a: Estimating dew duration. I. Utilizing micrometeorological data. *Agricultural Meteorology* **25**: 283–296.

Pedro, M.J. and Gillespie, T.J. 1982b: Estimating dew duration. II. Utilizing standard weather station data. *Agricultural Meteorology* **25**: 297–310.

Pereira, H.C. 1973: *Land Use and Water Resources in Temperate and Tropical Climates.* Cambridge University Press, Cambridge.

Pickering, K.E. and Jiusto, J.E. 1978: Observations of the relationship between dew and radiation fog. *Journal of Geophysical Research* **83**: 2430–2436.

Pindják, P. 1980: Výsledky merania rosy rosografom M-35. *Meteorologické Zprávy (Prague)* **33**: 48–53.

Pinter, P.J. 1986: Effect of dew on canopy reflectance and temperature. *Remote Sensing of Environment* **19**: 187–205.

Plauborg, F. 1995: Evaporation from bare soil in a temperate humid climate—measurement using micro-lysimeters and time domain reflectometry. *Agricultural and Forest Meteorology* **76**: 1–17.

Potts, D.F. and Herrington, L.P. 1979: Modeling and measurement of evapotranspiration from urban trees. *Preprints 14th Conference on Agriculture and Forest Meteorology and 4th Conference on Biometeorology.* Minneapolis, MINN., April 2-6, 1979: 188–189.

Price, D. 1967: *Silent Flowers. A Collection of Japanse Haiku.* Hokuseido Press, Tokyo.

Rajvanshi, A.K. 1981: Large scale dew collection as a source of fresh water supply. *Desalination* **36**: 299–306.

Richards, K. 1991: Modelling incidence of a weather associated disease: Black spot of apples. M.Sc. thesis. University of Otago, Dunedin.

Rodda, J.C., Downing, R.A. and Law, F.M. 1976: *Systematic Hydrology.* Newnes-Butterworths, London.

Roth, M. 1988: Spectral analysis of turbulence in an unstable suburban atmosphere. M.Sc. thesis. University of British Columbia, Vancouver.

Roth, M., Oke, T.R. and Emery, W.J. 1989: Satellite-derived urban heat islands from three coastal cities and the utility of such data in urban climatology. *International Journal of Remote Sensing* **10**: 1699–1720.

Runnalls, K.E. 1995: Temporal dynamics of Vancouver's urban heat island. M.Sc. thesis. University of British Columbia, Vancouver.

Sadler, E.J. 1996: Considerations for determining leaf wetness using infrared thermometry in humid regions. *Preprints 22nd Conference on Agricultural and Forest Meteorology.* Atlanta, Georgia, Jan 28-Feb 2 1996, Joint Session: J6-J7.

Salau, O.A. and Lawson, T.L. 1986: Dewfall features of a tropical station: The case of Onne (Port Hartcourt), Nigeria. *Theoretical and Applied Climatolology* **37**: 233–240.

Samways, M.J. 1989: Insect conservation and the disturbance landscape. *Agriculture, Ecosystems and Environment* **27**: 183–194.

Scherm, H. and van Bruggen, A.H.C. 1993: Sensitivity of simulated dew duration to meteorological variations in different climatic regions of California. *Agricultural and Forest Meteorology* **66**: 229–245.

Scherm, H., Koike, S.T., Laemmlen, F.F., and van Bruggen, A.H.C. 1995: Field evaluation of fungicide spray advisories against lettuce downy mildew (Bremia lactucae) based on measured or forecast morning wetness. *Plant Disease* **79**: 511–516.

Schmid, H.-P.E. 1988: Spatial scales of sensible heat flux variability. Ph.D. thesis. University of British Columbia, Vancouver.

Schroder, L.J., Willoughby, T.C., See, R.B. and Malo, B.A. 1989: The chemical composition of precipitation, dew and frost, and fog in Denver, Colorado. In Delleur, J.W (ed.). 1989: *Atmospheric Deposition.* IAHS Publication No. 179: 83–90.

Sharma, M.L. 1976: Contribution of dew to the hydrologic balance of a semi-arid grassland. *Agricultural Meteorology* **17**: 321–331.

Shea, D.M. and Auer A.H. 1978: Thermodynamic properties and aerosol patterns in the plume downwind of St. Louis. *Journal of Applied Meteorology* **17**: 689–698.

Simpson, G.C. 1929: Letters to the editor. Dew: Does it rise or fall? *Nature* **124 (3128)**: 578.

Sisterson, D.L. and Dirks, B.A. 1978: Structure of the daytime urban moisture field. *Atmospheric Environment* **12**: 1943–1949.

Skvarenina, J. and Mindas, J. 1998: Dew in Carpathian Mountain forests—micrometeorology and hydrochemistry. *Proceedings of the Conference on Fog and Fog Collection.* Vancouver, Canada, 19-24 July, 1998: 293–296.

Slatyer, R.O. and McIlroy, I.C. 1961: *Practical Microclimatology.* UNESCO. CSIRO Australia, Aspendale.

Spronken-Smith, R.A. 1994: Energetics and cooling in urban parks. Ph.D. thesis. University of British Columbia, Vancouver.

Spronken-Smith, R.A. Unpublished: Field data for an urban park in Vancouver. University of Canterbury, Christchurch.

Steubing, L. 1952: Der tau und seine beeinflussung durch windschutzanlagen. *Biolog. Zentralbl.* **71**: 282–313. Cited in Geiger, R. 1965: *The Climate Near the Ground.* Harvard University Press, Cambridge, Massachusetts.

Steyn, D.G. 1980: Research Note. The calculation of view factors from fisheye-lens photographs. *Atmosphere-Ocean* **18**: 254–258.

Steyn, D.G. and Lyons, T.J. 1985: Comments on the determination of view factors in urban canyons. *Journal of Climate and Applied Meteorology* **24**: 383–385.

Stull, R.B. 1988: *An Introduction to Boundary Layer Meteorology.* Kluwer Academic, Dordrecht.

Stull, R.B. 1996: Conversation with author. November 1996. University of British Columbia, Vancouver.

Subramaniam, A.R. and Kesava Rao, A.V.R. 1983: Dew fall in sand dune areas of India. *International Journal of Biometeorology* **27**: 271–280.

Sudmeyer, R.A., Nulsen, R.A. and Scott, W.D. 1994: Measured dewfall and potential condensation on grazed pasture in the Collic River basin, southwestern Australia. *Journal of Hydrology* **154**: 225–269.

Szokolay, S.V. 1980: *Environmental Science Handbook for Architects and Builders.* The Construction Press, London.

Thompson, N. 1981: The duration of leaf wetness. *The Meteorological Magazine* **110 (1302)**: 1–12.

Tuller, S.E. and Chilton, R. 1973: The role of dew in the seasonal moisture balance of a summer-dry climate. *Agricultural Meteorology* **11**: 135–142.

van Eimern, J. 1953/54: Beeinflussung meteorologischer größen durch ein engmaschiges heckensystem. *Annalen der Meteorologie* **6**: 213–219. Cited in Geiger, R. 1965: *The Climate Near the Ground.* Harvard University Press, Cambridge, Massachusetts.

van Eimern, J. 1985: Fühler zur bestimmung der blattnäse und der regendauer—Meßergebnisse aus einem buchenwald während zweier sommer. *Archives for Meteorology, Geophysics, and Bioclimatology. Series B. Theoretical and Applied Climatology* **36**: 99–113.

Voogt, J.A. 1989: Validation of an urban canyon radiation model for nocturnal long-wave radiative fluxes and the effect of surface geometry on cooling in urban canyons. M.Sc. thesis. University of British Columbia, Vancouver.

Voogt, J.A. 1995: Thermal remote sensing of urban surface temperatures. Ph.D. thesis. University of British Columbia, Vancouver.

Wagner, G.H., Steele, K.F. and Peden, M.E. 1992: Dew and frost chemistry at a midcontinent site, United States. *Journal of Geophysical Research* **97 (D18)**: 20591–20597.

Wales-Smith, B.G. 1983: An inexpensive device for measuring net dewfall. *Weather* **38**: 54–56.

Wallin, J.R. 1967: Agrometeorological aspects of dew. *Agricultural Meteorology* **4**: 85–102.

Wegner, D., Hassid, S. and Poreh, M. 1988: Investigation of the thermal performance of passive solar popular apartments in Israel using small-scale physical models. *Energy and Buildings* **11**: 301–308.

Weiss A. and Lukens, D.L. 1981: Electronic circuit for detecting leaf wetness and comparison of two sensors. *Plant Disease* **65**: 41–43.

Weiss, A. and Norman, J.M. 1987: Comparison of field measurements and numerical simulations of leaf wetness durations in a dry bean crop. *Preprints 18th Conference Agricultural and Forest Meteorology.* W. Lafayette, Indiana, Sep 15-18, 1987: 52–53.

Willmott, C.J. 1984: On the evaluation of model performance in physical geography. In Gaile, G.L. and Willmott, C.J. (eds.). 1984: *Spatial Statistics and Models*: 443–460.

Wisniewski, J. 1982: The potential acidity associated with dews, frosts, and fogs. *Water, Air, and Soil Pollution* **17**: 361–377.

Wittich, K.-P. 1995: Some remarks on dew duration on top of an orchard. *Agricultural and Forest Meteorology* **72**: 167–180.

Wolff, G.T., Rodgers, W.R., Collins, D.C., Verma, M.H. and Wong, C.A. 1990: Spotting of automotive finishes from the interactions between dry deposition of crustal material and wet deposition of sulfate. *Journal of the Air Waste Management Association* **40**: 1638–1648.

Woodhouse, A.E. 1959: *Guthrie-Smith of Tutira*. Whitcombe and Tombs, Christchurch.

APPENDICES

Appendix A1: Common definitions and derivations

A1.1 Converting latent heat flux to an equivalent depth water

Q_E [W m^{-2}] can be expressed in hydrologic terms as a depth of water per unit area per unit time $(\Delta h_w/\Delta t)$, i.e., the equivalent depth which would be seen if the water involved were present as a film of even thickness (mm). Conversion is achieved:

$$\frac{\Delta h_w}{\Delta t} = \frac{Q_E}{L_v \rho_w} \qquad [A1.1]$$

so at 20°C when $L_v \approx 2.45$ MJ kg^{-1}:

$$\frac{1 \text{ mm}}{h} = \frac{680 \text{ W m}^{-2}}{2.45 \text{ MJ kg}^{-1} \times 1000 \text{ kg m}^{-3}} \qquad [A1.2]$$

A1.2 Corrections to mobile survey data

Measured data (χ_m) which could be temperature or humidity are adjusted spatially by assuming a constant rate of travel between pre-selected sites along the route, at which travel time was recorded, manually or using a voice-activated tape recorder. Temporal corrections are based on data (X) measured at the point of origin (A) and end-point (B) of the survey, using instruments installed at 1.5 m at R1 and U1, respectively. Corrections address temporal changes at the point of origin of the survey $(X_{A2} - X_{A1})$, where the subscripts 1 and 2 are the start and end times, and changes seen at the end-point that are in excess of this $(X_{A1} - X_{B1} + X_{B2} - X_{A2})$ (Figure A1.1). The maximum correction is applied to data at the end of the survey, so resulting data are equivalent to an instantaneous

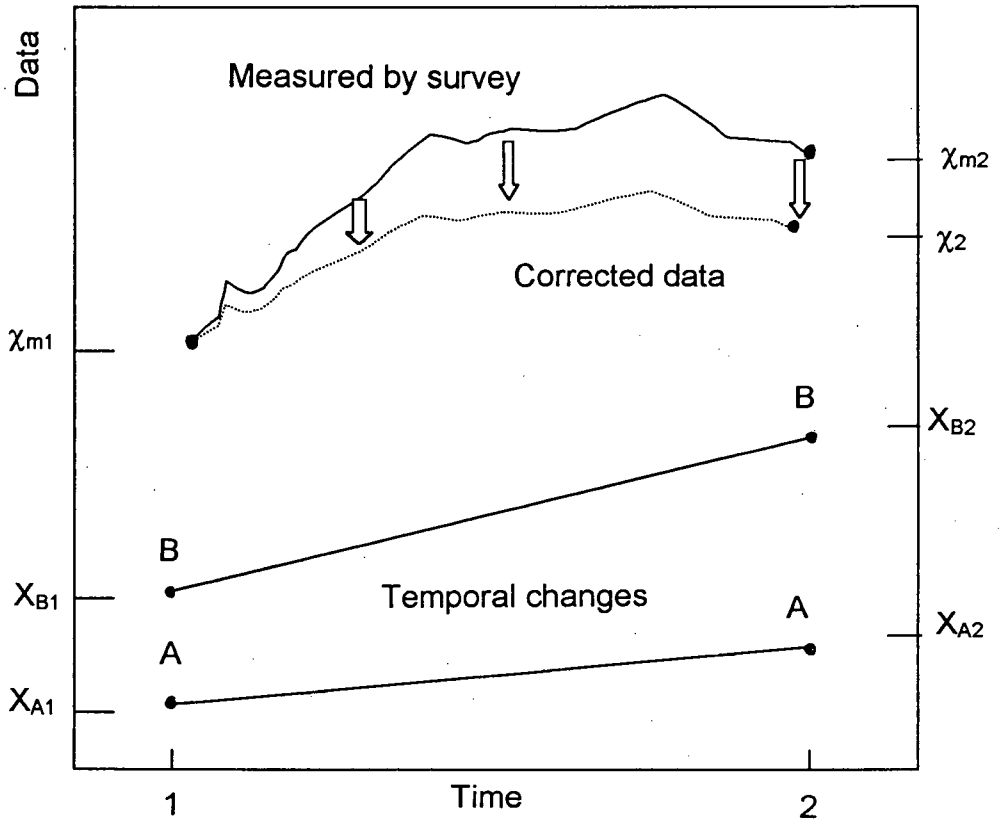

Figure A1.1 Schematic depiction of the geometry used to derive temporal corrections for data measured along the mobile survey (see text).

'snap-shot' taken at the start time of the survey. The full correction is derived (after Stull, *pers. comm.*):

$$\chi = \chi_m - (X_{A2} - X_{A1}) - (X_{A1} - X_{B1} + X_{B2} - X_{A2}) = X + X_{B1} - X_{B2} \qquad [A1.3]$$

where χ is the corrected value for mobile survey data, χ_m is the value measured by mobile instruments, X is data measured at fixed sites, and subscripts A, B, 1 and 2 indicate the start and end locations and times of the survey, respectively. Temporal change is assumed to be linear, so a 100% correction is applied at A (U1) and zero correction at B (R1).

A1.3 Method of blotting

A pad of three sheets of blotting paper (0.2 x 0.2 m) are used to blot surface water from mown grass. During the preceding day, sheets are dried at room temperature, then re-weighed to determine their dry mass. Dry pads are sealed in plastic bags overnight. The pad is pressed onto the wet grass—lightly at first (by hand or using small weights), then harder—for approximately one minute. In heavy dew, the lowest sheet often becomes saturated. Hence, after one minute a final 'blot' is undertaken using the upper (dry) sheet of the pad. At dawn, after blotting, 'wet' pads are immediately sealed in individual *Ziploc* plastic bags, the mass of which is known (to 0.01 g). Samples remain bagged until after weighing, which takes place at a nearby laboratory. Surface moisture amount is found:

$$\text{Surface moisture [mm]} = \frac{M_{wet+bag} - M_{dry} - M_{bag}}{A} \times 100 \qquad \text{[A1.4]}$$

where M is mass [kg], A is area blotted, effectively pad area [m^2], 100 is the appropriate conversion factor to give moisture amount in units of mm equivalent depth, and subscripts dry, wet and bag indicate pad mass prior to, and after blotting, and the mass of plastic bag in which the 'wet' pad is stored.

Blotting is labour intensive, on average two minutes are required to collect each sample. At dawn, sampling must be completed quickly, because by one hour after sunrise dew typically begins to dry. Sealing pads in plastic bags prior to, and after the act of blotting reduces errors associated with 'dry' and 'wet' weights to a negligible mass (<0.001 mm equivalent depth of water per sample). In theory, pads with area 0.02–0.04 m^2 weighed with a precision of 0.1 g give a resolution of 0.005–

0.0025 mm per sample. In practice, an operational accuracy of ±0.01 mm of water is realistic.

A1.4 Humidity relations

Humidity values can be converted from RH [%] to ρ_v [kg m^{-3}] and vapour pressure, e [Pa] using:

$$\rho_v = \frac{RH.\rho^*_v}{100} \text{ and } e = \frac{RH.e^*}{100}, \text{ respectively,} \qquad [A1.5]$$

and from q [kg kg^{-1}] to vapour pressures, e [Pa], and *vice versa*, using:

$$q = \frac{0.622e}{P} \qquad [A1.6]$$

where, P is measured barometric pressure [Pa]. Dew-point temperature, T_d [K] is found using :

$$T_d = \frac{T^*}{1 - \left(\frac{\ln \frac{e}{e^*}}{\frac{L_v M_{wa}}{RT^*}} \right)} \qquad [A1.7]$$

where e* is evaluated at T^* [273 K], M_{wa} is the molecular mass of water (18 g mol^{-1}), R is the gas constant [8.31 J mol^{-1} K^{-1}], and L_v [J kg^{-1} K^{-1}] is found using:

$$L_v = 1.91846 \times 10^6 \left(\frac{T}{T - 33.91} \right)^2 \qquad [A1.8]$$

Vapour density deficit, ρ_{vd} [kg m^{-3}], is expressed:

$$\rho_{vd} = \rho^*_v - \rho_v \qquad [A1.9]$$

Using the method of Lowe (1977), for temperatures greater than 0°C, saturation vapour pressure, e^* [Pa] is given:

$$e^* = 100 \times \left(a_1 + T\left(a_2 + T\left(a_3 + T\left(a_4 + T\left(a_5 + T\left(a_6 + a_7\right)\right)\right)\right)\right)\right) \qquad [A1.10]$$

where T is temperature in units °C, a_1 = 6.10779961, a_2 = 4.436518521 x 10^{-1}, a_3 = 1.428945805 x 10^{-2}, a_4 = 2.650648471 x 10^{-4}, a_5 = 3.031240396 x 10^{-6}, a_6 = 2.034080948 x 10^{-8}, and a_7 = 6.136820929 x 10^{-11}.

Similarly, for temperatures greater than 0°C, the slope (s) of the saturation vapour pressure *vs* temperature curve is given by the nested polynomial (Lowe, 1977):

$$s = 100 \times \left(a_8 + T\left(a_9 + T\left(a_{10} + T\left(a_{11} + T\left(a_{12} + T\left(a_{13} + a_{14}\right)\right)\right)\right)\right)\right) \qquad [A1.11]$$

where s has units Pa $°C^{-1}$, a_8 = 4.438099984 x 10^{-1}, a_9 = 2.857002636 x 10^{-2}, a_{10} = 7.938054040 x 10^{-4}, a_{11} = 1.215215065 x 10^{-5}, a_{12} = 1.036561403 x 10^{-7}, a_{13} = 3.532421810 x 10^{-10}, and a_{14} = -7.090244804 x 10^{-13}.

A1.5 Statistics of comparison

Data from the model and full-scale sites are compared using the mean ($\overline{m}$, $\overline{h}$) and standard deviation (SD_m, SD_h) for model and full-scale data-sets, respectively, and by computing the mean absolute difference (MD):

$$MD = \frac{\sum_{i=1}^{n} |m_i - h_i|}{n} \qquad [A1.12]$$

and the root mean square difference (RMSD):

$$RMSD = \left[\frac{\sum_{i=1}^{n} (m_i - h_i)^2}{n} \right]^{0.5} \quad [A1.13]$$

between two sets. The agreement between the two sets is described using Willmott's index of agreement, ID index of agreement (Willmott, 1984):

$$ID = 1 - \frac{n(RMSD)^2}{\sum \left(|m - \bar{h}| + |h - \bar{h}| \right)^2} \quad [A1.14]$$

Similarly, the long-term weather data-set from VIA and weather data from 1996 are compared using formulae equivalent to Equations A1.12–A1.14, i.e., substituting '1996' for 'm' and 'long-term' for 'h'.

A1.6 Estimating sky view factor using site geometry

A simplified geometry is used to estimate Ψ_{ter} at points on lawn and park surfaces: (a) For lawns of approximately rectangular shape, the geometry of surrounding buildings, fences and trees is approximated using four walls. So site geometry is reduced to an orthogonal box which is open to the sky. For a given point on the box floor (lawn), the Ψ_{ter} for an indivudual vertical wall is calculated using a formula derived from Steyn and Lyons (1985):

$$\Psi_{sky} = \frac{\pi}{2} \left(\tan^{-1}\left(\frac{\frac{b}{2} - x}{y} \right) + \tan^{-1}\left(\frac{\frac{b}{2} + x}{y} \right) - \frac{y}{\sqrt{h^2+y^2}} \left(\tan^{-1}\left(\frac{\frac{b}{2} - x}{\sqrt{h^2+y^2}} \right) + \tan^{-1}\left(\frac{\frac{b}{2} + x}{\sqrt{h^2+y^2}} \right) \right) \right) \quad [A1.15]$$

where b is wall length, h is wall height, and x and y define the location of P; all these have units m (Figure A1.2a).

(b) Where the horizon obstruction is approximated by a sphere (deciduous tree), Ψ_{ter} for a given point on the park surface is found using (Howell, 1982):

$$\Psi_{ter} = \frac{\frac{x}{l}}{2\left(1+\left(\frac{y}{l}\right)^2\right)}\left\{\frac{\left(\frac{r}{l}\right)^2+\left(\frac{y}{l}\right)^2+\left(\frac{x}{l}\right)^2+1}{\left[\left(\left(\frac{r}{l}\right)^2+\left(\frac{y}{l}\right)^2+\left(\frac{x}{l}\right)^2\right)^2-4\left(\frac{r}{l}\right)^2\left(1+\left(\frac{y}{l}\right)^2\right)\right]^{0.5}}-1\right\} \qquad [A1.16]$$

where x, y, l and r are lengths [m] as shown in Figure A1.2b.

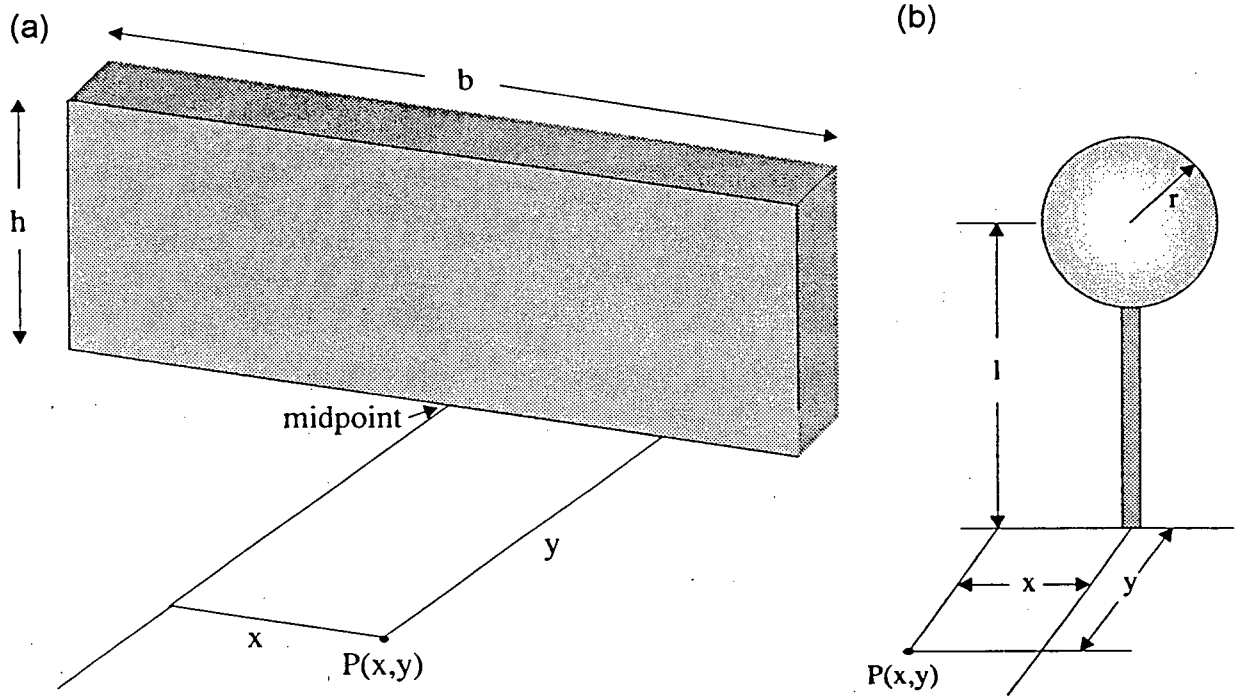

Figure A1.2 Geometry used to compute terrain view factor for an individual (a) wall and (b) sphere for a given point (P) on the surface. *Source:* Spronken-Smith (1994).

A1.7 Ratio of wind speed at two heights

In neutral conditions, the ratio of wind speed for two heights of measurement are determined using the log profile approach. That is:

$$\frac{u_z}{\ln(z/z_0)} = \frac{u_*}{k} \qquad [A1.17]$$

where u_z is the wind speed [m s^{-1}] at height z [m], u_* is the friction velocity [m s^{-1}], a measure of surface roughness, and k is the von Karman constant [0.4]. For example, in neutral atmospheric conditions and over a short grass surface with $z_0 = 0.01$ (Oke, 1987) and z_1 and z_2 of 1.5 m and 3.6 m, respectively, the ratio u_1: u_2 is found:

$$\frac{u_1}{u_2} \propto \frac{\ln(z_2/z_0)}{\ln(z_1/z_0)} \qquad [A1.18]$$

Hence:

$$\frac{u_{1.5}}{u_{3.6}} = \frac{\ln(3.6/0.01)}{\ln(1.5/0.01)} = 0.85 \qquad [A1.19]$$

Appendix A2: Derivations in the numerical model

A2.1 Derivation of the sensible heat flux

The role of the turbulent state of the atmosphere in the transfer of sensible heat from a surface can be expressed as a function of a resistance (r_h) or a heat transfer coefficient (h_c). If it is assumed that conditions are similar on both sides of the leaf, for a two-sided leaf, this means we can write:

$$Q_H = 2\rho_a c_a \frac{T_l - T_a}{r_h} = 2h_c(T_l - T_a) = 2h_c \Delta T \qquad [A2.1]$$

$$\text{thus:} \quad h_c = \frac{\rho_a c_a}{r_h} \qquad [A2.2]$$

where r_h is the convective resistance to heat transfer [s m^{-1}] and ρ_a is the density of air [kg m^{-3}]. Values for h_c are derived from experiments conducted in conditions of controlled airflow. In conditions of forced convection, heat transfer from a flat plate can be described by three non-dimensional groups: Nu, Re and Pr. For leaves or artificial plates which have low conductivity and relatively small size, the appropriate form is:

$$Nu = 0.68 Re^{0.50} Pr^{0.33} = \frac{h_c d}{k_a} \qquad [A2.3]$$

$$\text{and,} \quad Re = \frac{ud}{\nu} \qquad [A2.4]$$

where k_a is the thermal conductivity of air [W m^{-1} K^{-1}] and ν is the kinematic viscosity of air [m^2 s^{-1}]. If one assumes that air temperature is 15°C then values can be assigned to Pr (0.7019), k_a (0.0253 W m^{-1} K^{-1}), and ν (1.46 x 10^{-5} m^2 s^{-1}). By substitution, an empirically-based solution can then be defined for h_c. That is:

$$h_c = \frac{0.0253}{d} 0.68 \left(\frac{ud}{1.46 \times 10^{-5}} \right)^{0.5} 0.7019^{0.33} = 4.0 \left(\frac{u}{d} \right)^{0.5} \quad [A2.5]$$

where the resulting 4.0 has units W m^{-2} K^{-1} $s^{0.5}$.

A2.2 Derivation of the latent heat flux

Q_E can be expressed as a function of a convective resistance (r_v) or a convective water vapour transfer coefficient (h_v). If the surface is wet, then surface humidity is, by definition, saturated. So, for a two-sided wet leaf:

$$Q_E = 2\rho_{wa} L_v \frac{\left(q^*_l - q_a \right)}{r_v} = 2h_v \left(q^*_l - q_a \right) \quad [A2.6]$$

$$\text{where } h_v = \frac{\rho_{wa} L_v}{r_v} \quad [A2.7]$$

and r_v is resistance to water vapour transfer [s m^{-1}]. h_w is often determined as an empirical function of h_c. In conditions of forced convection, vapour transfer from a flat plate is described by Re, Sherwood Number (Sh) and Schimdt Number (Sc). In conditions of laminar flow (i.e., right at the surface), the relationships of interest are:

$$Nu = 0.68 Re^{0.5} Pr^{0.33} = \frac{\delta}{D_h r_h} \quad [A2.8]$$

$$Sh = 0.68 Re^{0.5} Sc^{0.33} = \frac{\delta}{D_v r_v} \quad [A2.9]$$

$$Pr = \frac{D_h}{\nu}, \text{ and} \quad [A2.10]$$

$$Sc = \frac{D_v}{\nu} \quad [A2.11]$$

where δ is the thickness of the laminar boundary layer [m], and D_h and D_v are the rates of molecular diffusion in the laminar boundary layer for heat and water vapour [$m^2\ s^{-1}$], respectively. By substituting Equations A2.8 to A2.11 into Equations A2.2 and A2.7, the non-dimensional ratio h_v:h_c can be shown to be a function of rates of molecular diffusion. The ratio D_v:D_h is conservative, and has a value close to 1.107 for temperatures when dew forms, i.e., 0°C to 20°C. Thus, if it is assumed that δ is the same for heat and vapour, and that Re and ν are constant, it can be shown that

$$\frac{h_w}{h_c} = \frac{\rho L_v r_h}{\rho c r_v} = \frac{\rho L_v D_v 0.68 Re^{0.5} (\nu/D_v)^{0.33} d}{\rho c D_h 0.68 Re^{0.5} (\nu/D_h)^{0.33} d} = \frac{L_v}{c}\left(\frac{D_v}{D_h}\right)^{0.67} \qquad [A2.12]$$

$$\text{and, } h_v = h_c\left(\frac{L_v}{c_a}\right)1.07 \qquad [A2.13]$$

where 1.07 is non-dimensional. It is assumed that this relationship holds for leaves and also for building surfaces, in conditions when dew forms. It is well established that h_v and h_c are enhanced by turbulence, for leaves in natural air flow. A factor of β (0.0 to 2.5) can be introduced into Equation A2.13 to account for this effect. However, for the conditions typical of dew formation, when turbulence is minimal, research indicates that β equals one (Mintah, 1977; Pedro, 1980).

A2.3 Estimating surface temperature

If surface temperature is unknown, then appropriately simplified energy balances can be used to estimate its value, i.e., for a two-sided leaf:

$$Q_H + Q_E = aK_{in} + \alpha_c aK_{in} + \varepsilon L_{in} - \varepsilon\sigma T_l^4 \qquad [A2.14]$$

and, for a roof surface:

$$Q_H + Q_E + Q_G = aK_{in} + \varepsilon L_{in} - \varepsilon\sigma T_r^4 \qquad [A2.15]$$

Solution is possible when terms that can be are restated in terms of ΔT, the surface-air temperature difference. Two manipulations are required; (a) derivation of the longwave radiation flux term, and (b) linearisation of the saturation vapour curve:

(a) According to the Stefan-Bolzmann Law, longwave emission is proportional to surface temperature raised to the fourth power, i.e., $L_{in} = \varepsilon\sigma T^4$. Derivation of this relationship leads to $dL_{in} = 4\varepsilon\sigma T^3 dT$ or, in finite difference form, for the example of a leaf:

$$\varepsilon\sigma T_l^4 - \varepsilon\sigma T_a^4 = 4\varepsilon\sigma \overline{T}^3 \Delta T \qquad [A2.16]$$

where $\overline{T}$ is the mean of T_a and T_l. Thus:

$$\varepsilon\sigma T_l^4 = 4\varepsilon\sigma \overline{T}^3 \Delta T + \varepsilon\sigma T_a^4 \qquad [A2.17]$$

(b) To continue the example of a leaf, at a wet surface, humidity is assumed to be at saturation, i.e., q^*_l. q^* is a non-linear function of temperature, however, linearisation of the relationship over small intervals of T is useful and allows more simple computation. The difference of interest is between q^*_l and q (see Figure A2.1) and can be expressed:

$$q^*_l - q = q^*_l - q^*_a + q^*_a - q \qquad [A2.18]$$

The mean of air and surface temperature is defined as $\overline{T}$ and if a line is drawn between q^*_l and q^*_a, it can be assumed that its slope is equal to the slope (s) of the saturation specific humidity curve at $\overline{T}$. The relationship can be defined:

$$s = \frac{q^*_l - q^*_a}{T_l - T_a}, \text{ and } q^*_l - q^*_a = s(T_l - T_a) = s\Delta T \qquad [A2.19]$$

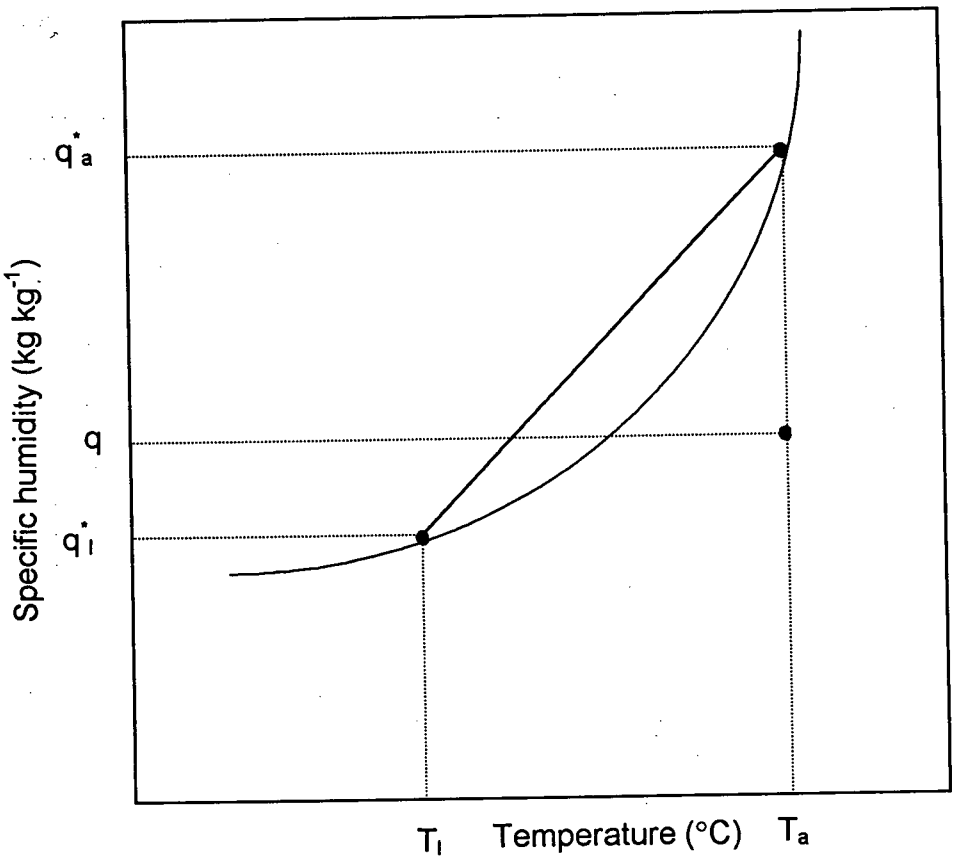

Figure A2.1 The saturation specific humidity vs temperature curve, illustrating the geometry used to linearise the slope of the curve at mean temperature ($\overline{T} = \frac{T_a + T_l}{2}$) for the case of a leaf.

Thus, substituting Equation A2.19 into Equation A2.18, gives, for a wet leaf:

$$q^*_l - q = s\Delta T + q^*_a - q \qquad [A2.20]$$

and similarly for a wet roof: $q^*_r - q = s\Delta T + q^*_a - q$. [A2.21]

For a leaf, if Equations A2.1, A2.6, A2.17, and A2.21 are substituted into the energy balance equation (A2.14), it can be shown that, for a two sided leaf:

$$2h_c\Delta T + 2h_v s\Delta T + 2h_v(q^*_a - q) = aK_{in} + \alpha_c aK_{in} + \varepsilon L_{in} - 4\varepsilon\sigma\overline{T}^3\Delta T - \varepsilon\sigma T_a^4 \qquad [A2.22]$$

Similarly, for a roof substitution of an analogous set of equations into Equations A2.15 gives, for a one sided roof:

$$h_c\Delta T + h_v s\Delta T + h_v\left(q^*_a - q\right) + h_k\left(T_r - T_u\right) = aK_{in} + \varepsilon L_{in} - 4\varepsilon\sigma\overline{T}^3\Delta T - \varepsilon\sigma T_a{}^4 \qquad [A2.23]$$

Equations A2.22 and A2.23 can be manipulated so that both relationships can be solved for ΔT: if terms containing ΔT are isolated on the left hand side (lhs) of the equation and both sides are divided by ΔT, then ΔT will be eliminated from the lhs. Then, if both sides of the equation are divided by the resultant lhs numerator and multiplied by ΔT, the final form of the equation is derived. So, for a two sided leaf:

$$\Delta T = \frac{aK_{in} + \alpha_c aK_{in} + \varepsilon L_{in} - \varepsilon\sigma T_a{}^4 - 2h_v\left(q^*_a - q\right)}{2h_c + 2h_v s + 4\varepsilon\sigma\overline{T}^3} \qquad [A2.24]$$

and, for a roof surface:

$$\Delta T = \frac{aK\downarrow + \varepsilon L\downarrow - \varepsilon\sigma T_a{}^4 - (0.622/P)h_w\left(e^*_a - e\right) - h_k\left(T_s - T_u\right)}{h_c + (0.622/P)h_v s + 4\varepsilon\sigma\overline{T}^3} \qquad [A2.25]$$

h_c can be removed by defining it as a function of h_v (using Equation A2.13; see Equations 7.18 and 7.19). The resulting versions of Equations A2.24 and A2.25 can be solved iteratively, by initially assuming that ΔT, T_a and surface temperature (T_l or T_r) are equal. When stable values ($\pm 0.1°C$) for T_l and T_r are reached, values for q^*_l and q^*_r are determined, and the equations are solved for ΔT.

A2.4 Estimating Γ

Γ (the fraction $\frac{s}{s+\gamma}$) is a non-linear function of temperature, however, its value can be linearised over small intervals of T, to allow more simple computation. In temperate climates, dew commonly forms when temperature is 0–20°C, and a linear fit between published values for Γ at 0°C (0.39) and 20°C (0.67) (Table A3.1; Oke, 1987) gives:

$$\Gamma=0.4+0.014 \qquad [A2.26]$$

The error associated with this step is small (±0.01) in this temperature range.

A2.5 Statistics of model performance

General skill [mm dew] is tested using the absolute error between the predicted and observed means ($\overline{Pr}-\overline{Ob}$) and standard deviations ($SD_{Pr}-SD_{Ob}$). A skill score [%] is computed using:

$$\text{Skill score (\%)} = \frac{\text{Number of hits}}{\text{Number of predictions}} \times 100 \qquad [A2.27]$$

where a 'hit' means a successful prediction, i.e., $Ob - X \le Pr \le Ob + X$, and X is the acceptable margin of error. Here I used arbitrary values of 0.02 and 0.05 mm of dew per night. MD, RMSD and ID for the sets are computed using formulae equivalent to those presented in Equations A1.12–A1.14, i.e., substituting '*Pr*' for 'm' and '*Ob*' for 'h'.

Appendix A3: Dew and the Fine Arts

A3.1 Illustrative examples of dew in art and literature

Figure A3.1 Dew sculpture by Chris Parsons, Shropshire, created in dew on a lawn at dawn, using a wide broom. *Source*: Anon. (1995).

A small garden
Brimming with dew, —
Half a gallon of it.

Haiku by Shiki, no date. *Source*: Price (1967).